

Design of an adaptive Congestion Control Protocol for reliable Vehicle Safety Communication

Von der Fakultät für Elektrotechnik und Informatik
der Gottfried Wilhelm Leibniz Universität Hannover
zur Erlangung des akademischen Grades

Doktor-Ingenieur

genehmigte

Dissertation

von

M. Sc. Torsten Lorenzen
geboren am 30. Oktober 1988 in Flensburg

2017

1. Referent : Prof. Dr.-Ing. Markus Fidler
2. Referent : Prof. Dr. Jörg P. Müller
Tag der Promotion : 20. Dezember 2017

Torsten Lorenzen: *Design of an adaptive Congestion Control Protocol for reliable Vehicle Safety Communication*, Dissertation, © 2017

ABSTRACT

The progressive development in the area of automation no longer takes place only in the industry, but also in road traffic. By the development of modern Advanced Driver Assistance Systems (ADAS), more and more responsibilities are transferred from the driver to the vehicle. This development culminates in the vision of fully autonomous vehicles which significantly increase efficiency, safety, and comfort. Although ever more sophisticated sensor technologies help to break down complex situations, these systems are limited in the provision of complete and accurate environmental information. A key technology providing this awareness, which is necessary for future ADAS, is the communication between the stakeholders on the road.

Vehicles periodically share information among each other and the environment that is used to enhance the awareness. The communication medium thereby needs to meet various requirements so that for Vehicle-to-Vehicle (V2V) communication special technologies must be designed. Today, more than ever, two different approaches are discussed: Wireless Local Area Network (WLAN)-based communication and cellular networks. While the former is a mature system, which has been developed, standardized, and evaluated in the recent years, the use of cellular networks becomes more and more popular among car companies, especially in Europe. For them, the major issue of the WLAN-based ITS-G5 named architecture is the low throughput, communication range, and market penetration. Subsequently, they promote the advantages of cellular networks.

The spread of cooperative driver assistance systems will grow rapidly with the introduction of communication technology so that the available resources will reach channel capacity limits. The resultant congestion provokes a reduction in the communication quality for all traffic participants, which can result in the loss of critical messages. Particularly, in the case of high traffic volumes (e.g. traffic-jam, rush-hour, etc.), congestion can lead to considerable problems which significantly reduce the performance of ADAS. In order to prevent this, methods are needed that at best prevent congestion or, at the very least, mitigate the effects of congestion for all participants. Irrespective of the technology used, no adequate solution has yet been found despite intensive research work.

Various approaches are used to avoid congestion with specific advantages and disadvantages each. While some approaches attempt to reduce the throughput within a region, for example by reducing the message generation rate, other approaches proactively suppress redundant information. Doing so, many Congestion Control (CC) schemes fail to ensure basic properties such as fairness, stability, and scalability.

A further problem of CC algorithms is the question of the effect on the ADASs themselves. In many cases, the decisive optimization criterion is the avoidance of congestion under all circumstances and the resulting reduction in the performance of the ADAS is not considered. However, it is important to check whether the performance reduction due to interference is less strong than the reduction in the throughput by a CC algorithm. This thesis presents the algorithm Semi-Cooperative

Weighted Rate Control (SWeRC), which is an enhancement of two known approaches. SWeRC allows a decentralized, adaptive adjustment of the message rate of a vehicle, resulting in a density independent stability and maximum efficiency combined with fast response time. In the first step, the detailed numerical analysis investigates the properties of SWeRC. In addition to verifying the functionality of SWeRC's modules, it contains a detailed theoretical and numerical optimization of the convergence parameters. Based on the optimized parameters, the performance of the protocol is determined both under static conditions and in various realistic dynamic scenarios and compared with state-of-the-art protocols, i.e. LIMERIC and PULSAR.

In a second step, the effect of congestion control on specific ADAS is evaluated. For this purpose, various awareness metrics are examined and adapted to allow a quantification of the reliability of ADASs. Among others, an analysis is conducted on how the algorithm affects the reliability of a collision avoidance system in the various reaction zones, i.e. information, warning, and emergency braking. We show that CC has a positive effect on the reliability and SWeRC achieves the best reliability. The analysis also reveals the indispensability of a fair distribution of resources in urban areas. At the same time, we demonstrate that the achieved awareness range under high vehicle densities is significantly reduced, and thus the requirements regarding the warning time of an application, even under ideal conditions, can in part no longer be fulfilled.

Keywords: V2V, VANET, Vehicle Safety Communication, Congestion Control, Cooperative Awareness

ZUSAMMENFASSUNG

Die fortschreitende Entwicklung im Bereich der Automatisierung findet sich längst nicht mehr nur in der Industrie, sondern hält auch im Straßenverkehr Einzug. Durch die Entwicklung moderner Fahrerassistenzsysteme werden immer häufiger Kompetenzen vom Fahrer auf das Fahrzeug übertragen. Diese Entwicklung gipfelt in der Vision völlig autonomer Fahrzeuge, welche die Effizienz, Sicherheit aber auch den Komfort im Straßenverkehr deutlich erhöhen. Obgleich immer ausgeklügeltere Sensortechnologien dazu beitragen komplexe Situationen aufzuschlüsseln, sind diesen Systemen doch Grenzen hinsichtlich der vollständigen und akkuraten Umgebungserfassung gesetzt. Ein Schlüsselbaustein für zukünftige Fahrerassistenzsysteme ist die Kommunikation zwischen den Verkehrsteilnehmern.

Fahrzeuge teilen in regelmäßigen Abständen Statusinformationen, welche zur erweiterten Umgebungswahrnehmung beitragen, mit ihrer Umgebung. Dabei muss das Kommunikationsmedium diversen Anforderungen gerecht werden, so dass für die Fahrzeugkommunikation spezielle Technologien entworfen werden müssen. Dabei werden heute mehr denn je zwei grundsätzlich unterschiedliche Ansätze diskutiert: WLAN basierte Kommunikation und zellulare Netzwerke. Während ersteres bereits ein ausgereiftes System darstellt, welches in den vergangenen Jahren entwickelt, standardisiert und erforscht wurde, findet die Nutzung zellulärer Netze insbesondere in Europa immer mehr Anhänger unter den Automobilunternehmen. Diese schrecken bei der WLAN basierten ITS-G5 genannten Architektur insbesondere vor der niedrigen Bandbreite, Reichweite und Marktdurchdringungen zurück und bewerben die Vorteile zellulärer Netze.

Die Verbreitung kooperativer Fahrerassistenzsysteme wird mit Einführung der Kommunikationstechnologie Prognosen zufolge rasant ansteigen, so dass die verfügbaren Kanalressourcen an ihre Kapazitätsgrenzen stoßen. Die dadurch entstehende Überlast auf dem Kommunikationsmedium sorgt bei allen Verkehrsteilnehmern für eine Minderung der Kommunikationsqualität, wodurch kritische Nachrichten verloren gehen können. Insbesondere bei hohem Verkehrsaufkommen (z.B. Stau, Rush-Hour, etc.) kann eine Überlast zu erheblichen Problemen führen, wodurch die Leistungsfähigkeit der Assistenzsysteme stark gemindert wird. Um dies zu verhindern, werden Methoden benötigt, die im besten Falle die Überlast verhindern oder zumindest die Auswirkungen jener für alle Teilnehmer mildern.

Dabei werden verschiedene Ansätze mit spezifischen Vor- und Nachteilen verfolgt, um die Überlastung des Kanals zu vermeiden. Während einige Ansätze versuchen, den regionspezifischen Durchsatz zu vermindern, indem sie beispielsweise die Übertragungsleistung oder die Nachrichtenrate herab regeln, versuchen andere proaktiv redundante Informationen zu reduzieren. Viele verfehlen es dabei, grundsätzliche Eigenschaften wie Fairness, Stabilität und Skalierbarkeit zu gewährleisten.

Ein weiteres Problem bei vielen Algorithmen zur Überlastkontrolle ist die Frage nach der Auswirkung auf die Fahrerassistenzsysteme selbst. Da das maßgebliche Optimierungskriterium in vielen Fällen die Überlastvermeidung unter allen Umständen ist, wird die aus den Aktionen des Algorithmus resultierende Reduzierung

der Leistungsfähigkeit der Fahrerassistenzsysteme oft außer Acht gelassen. Es gilt jedoch zu prüfen, ob gegebenenfalls die Auswirkung einer Überlast auf die Leistungsfähigkeit durch zufällige Paketkollisionen weniger ins Gewicht fällt, als die Reduzierung des Durchsatzes durch einen Algorithmus.

Im Rahmen dieser Arbeit wird der auf zwei bekannten Ansätzen basierende Algorithmus SWeRC vorgestellt. SWeRC ermöglicht eine dezentrale, adaptive Anpassung der Nachrichtenrate eines Fahrzeugs, die zu einer Verkehrsdichte unabhängigen Stabilität und maximaler Effizienz bei gleichzeitig schneller Reaktionszeit führt. Die detaillierte numerische Analyse zeigt die kommunikationstechnischen Eigenschaften von SWeRC. Dazu gehört neben der Verifikation der Funktionalität der in SWeRC enthaltenen Module auch eine ausführliche theoretische und numerische Optimierung der Parameter. Basierend auf den optimierten Parametern wird die Leistung des Protokolls sowohl unter statischen Bedingungen, als auch in realitätsnahen dynamischen Szenarien ermittelt und mit *LIMERIC* und *PULSAR* verglichen.

In einem zweiten Schritt wird die Auswirkung der Staukontrolle auf spezifische Fahrerassistenzsysteme ermittelt. Hierfür werden verschiedene Metriken untersucht und adaptiert, um eine Quantifizierung der Zuverlässigkeit dieser Assistenzsystems zu ermöglichen. Unter anderem wird dabei analysiert, wie sich der Algorithmus auf die Zuverlässigkeit eines Kollisionsvermeidungssystems in den verschiedenen Reaktionszonen auswirkt. In der Arbeit wird gezeigt, dass die Überlastkontrolle sich positiv auf die Zuverlässigkeit auswirkt und SWeRC die beste Verlässlichkeit erreicht. Dabei zeigt sich auch die Unabdingbarkeit einer fairen Verteilung der Ressourcen im urbanen Bereich. Gleichzeitig wird verdeutlicht, dass die verlässliche Kommunikationsreichweite bei hohen Fahrzeugdichten erheblich eingeschränkt wird und somit die Anforderungen bezüglich der Vorwarnzeit einer Anwendung selbst unter idealen Bedingungen zum Teil nicht mehr erfüllbar sind.

Schlagwörter: Fahrzeugkommunikation, Überlastkontrolle, Kooperative Wahrnehmung

CONTENTS

1	INTRODUCTION	1
1.1	Motivation	3
1.2	Main Contribution	4
1.3	Outline of the thesis	6
2	CONCEPT OF NEIGHBORHOOD AWARENESS	9
2.1	Local Dynamic Map (LDM)	9
2.2	Positioning	11
2.3	Sensors	14
2.4	Cooperative Intelligent Transportation Systems (C-ITS)	18
2.4.1	Vehicular Communication (V2X)	18
2.4.2	Cellular-V2X	30
3	AWARENESS AND CONGESTION CONTROL IN VANETS	37
3.1	Basic Concepts	37
3.1.1	Congestion Control and Avoidance	37
3.1.2	Congestion Control in Networks	39
3.1.3	Input Variables	42
3.2	Discussion of Awareness, Fairness and Efficiency	44
3.3	Classification based on controlled parameter	47
3.3.1	Packet Size Control (PSC)	47
3.3.2	Data Rate Control (DRC)	48
3.3.3	Contention Window Control (CW)	50
3.3.4	Carrier Sense Threshold Adaption (CS)	52
3.3.5	Transmit Power Control (TPC)	53
3.3.6	Transmit Rate Control (TRC)	58
3.3.7	Joint Control of Multiple Parameters	66
3.3.8	Summary	70
4	INVESTIGATION OF CONGESTION AND AWARENESS CONTROL	73
4.1	Addressed Problems	73
4.1.1	Dynamic CAM generation	73
4.1.2	Fairness / Environment Dependency	75
4.1.3	Stability and Scalability	77
4.1.4	Channel Smoothing	79
4.2	Summary	82
5	DESIGN AND DESCRIPTION OF THE ADAPTIVE PROTOCOL	83
5.1	Protocol architecture	83
5.2	CBR Volatility Suppression	84
5.3	Transmission Rate Adaption	86
5.3.1	Target Rate Mechanism	88
5.3.2	Message Rescheduling	90
5.4	Aggregation and Exchange of Information	95
5.4.1	One-Hop Piggybacking	95
5.4.2	Fairness Range Extension	97
5.4.3	Cooperative Target Rate	98

5.5	Parameter Discussion	99
5.5.1	Convergence Parameters	99
5.5.2	Channel Monitoring and Decision Interval (CMDI)	102
5.6	Summary	105
6	SIMULATION BASED EVALUATION OF THE ALGORITHM	107
6.1	Description of used Metrics	107
6.2	Verification and validation	110
6.2.1	Dynamic CAM generation	110
6.2.2	Rescheduling	112
6.2.3	Transmission rate adaption	113
6.2.4	Information Exchange	117
6.3	Numeric Parameter Evaluation	120
6.3.1	Target resource utilization	120
6.3.2	Convergence Parameters	122
6.4	Convergence in a Static NLOS Scenario	130
6.5	Performance under dynamic conditions	136
6.5.1	Highway	136
6.5.2	Urban	140
6.6	Discussion and Comparison with Related-Work	143
6.7	Summary	150
7	RELIABILITY ANALYSIS OF CAM BASED VSC	151
7.1	Awareness Metrics	151
7.1.1	Awareness evaluation	153
7.2	Evaluation for different Applications and Scenarios	156
7.2.1	Calculation of the Awareness Probability	156
7.2.2	Reliability of VSC	158
7.3	Summary	162
8	CONCLUSION AND OUTLOOK	165
A	SIMULATION ENVIRONMENT AND CONFIGURATION	169
A.1	Simulation Environment	170
A.2	Detailed Scenario Description	175
B	CHANNEL BUSY RATIO MEASUREMENT SETUP	181
B.1	Experiment Setup	181
B.2	Theoretical Analysis of Channel Load	182
B.3	Testbed Verification	183
B.4	Evaluation Method	184
	BIBLIOGRAPHY	187
	PUBLICATIONS	207
	SCIENTIFIC CAREER	208

LIST OF FIGURES

Figure 1	History of reported crashes in Germany	2
Figure 2	LDM Architecture	10
Figure 3	DSRC and ITS-G5 protocol stacks	19
Figure 4	ITS-G5 frequencies and channels	20
Figure 5	Sequential process of the medium access using CSMA	22
Figure 6	CSMA Flowchart	23
Figure 7	Access times for EDCA	24
Figure 8	Hidden (H) and exposed (E) terminal problem	25
Figure 9	Packets collision types using CSMA	26
Figure 10	ITS facilities	27
Figure 11	ETSI application time horizon	30
Figure 12	Congestion avoidance and control	38
Figure 13	Illustration of open- and closed-Loop controllers	39
Figure 14	DCC states with up to n active sub-states	68
Figure 15	Impact of dynamic CAM generation on the observed CL	74
Figure 16	Information freshness under AC in urban areas	74
Figure 17	Divergence of the message rate on the highway	75
Figure 18	Unfair resource allocation using <i>LIMERIC</i>	76
Figure 19	Convergence to unfair message rates	77
Figure 20	Performance of <i>LIMERIC</i> with <i>gain saturation</i>	78
Figure 21	Impact of filtering techniques on the observed CBR	80
Figure 22	Environmental influence on channel smoothing	82
Figure 23	Illustration of the protocol stack	84
Figure 24	Dynamic load smoothing weights	85
Figure 25	Convergence behavior of SWeRC	88
Figure 26	Illustration of rescheduling for a rate decrement	91
Figure 27	Illustration of rescheduling for a rate increment	92
Figure 28	Effect of initialization and rescheduling	92
Figure 29	Distribution of the CAM generation times	93
Figure 30	Impact of initialization and synchronization	93
Figure 31	Illustration of jitter for CAM generation	94
Figure 32	Illustration of the position for the nodes using cooperation.	95
Figure 33	Illustration of the exchange via 1-hop piggybacking.	96
Figure 34	Illustration of the exchange for multi-hop piggybacking	97
Figure 35	Convergence of the parameter optimized SWeRC	101
Figure 36	Impact of measuring interval on CL_{est}	102
Figure 37	Impact of measuring interval on the CBR for time invariant load	103
Figure 38	Correlation between invariant and CBT accuracy	104
Figure 39	Active modules for verification of dynamic CAM generation	110
Figure 40	CBR using dynamic CAM generation	111
Figure 41	Average message rate for dynamic CAM generation on highway	111
Figure 42	Selected message rates for dynamic CAM generation on highway	111

Figure 43	Active modules for verification of rescheduling	113
Figure 44	Distribution of initial CAM generation trigger	114
Figure 45	Rescheduling process for selected nodes over time	114
Figure 46	Active modules for verification of rate adjustment scheme . . .	115
Figure 47	Validation of convergence behavior for SWeRC	116
Figure 48	Impact of interference on rate adjustment	116
Figure 49	Validation of the SWeRCs convergence for lower target utilization	117
Figure 50	Active modules for verification of information exchange	118
Figure 51	Validation of the channel status exchange	119
Figure 52	Fairness range achieved by the information exchange	119
Figure 53	Relation between offered load, goodput and CBR	121
Figure 54	Relation between offered load and blackout probability	122
Figure 55	Active modules for the evaluation of SWeRC	123
Figure 56	Boxplots of message rate for selected convergence parameters .	124
Figure 57	Stability analysis of SWeRC	124
Figure 58	Illustration of SWeRCs convergence for selected parameters . .	125
Figure 59	Convergence speed analysis of SWeRC	126
Figure 60	Illustration of the best convergence parameters for SWeRC . . .	126
Figure 61	Convergence analysis for SWeRC with higher target utilization .	129
Figure 62	Performance without cooperation under NLOS conditions . . .	131
Figure 63	Performance of 1-hop cooperation under NLOS conditions . . .	131
Figure 64	Performance of 2-hop cooperation under NLOS conditions . . .	133
Figure 65	Illustration of cooperation range border instability for FGC . . .	134
Figure 66	Average results for SWeRC w. WGC for Non Line-of-Sight (NLOS)	135
Figure 67	Using WGC for cooperation border range instability	135
Figure 68	Vehicle density within the highway scenario	137
Figure 69	Key parameters for SWeRC on the highway	138
Figure 70	Key-parameters over time for SWeRC on the highway	139
Figure 71	Performance indicators for SWeRC on the highway	140
Figure 72	Vehicle density in the urban scenario	141
Figure 73	Key parameters for SWeRC on the highway	141
Figure 74	Key-parameters over time for different algorithms (highway) .	141
Figure 75	Performance indicators for SWeRC in urban scenario	143
Figure 76	Stability and conv. speed of different protocols	144
Figure 77	Comparison of performance for protocols on the highway . . .	145
Figure 78	Key-parameters over time for different algorithms (highway) .	145
Figure 79	Comparison of Fairness and Stability (highway)	146
Figure 80	Comparison of performance for protocols on the highway . . .	147
Figure 81	Comparison of performance for protocols in urban	148
Figure 82	Key-parameters over time for different algorithms (highway) .	148
Figure 83	Performance comparison in the urban scenario	149
Figure 84	Awareness probability	155
Figure 85	Ideal awareness probability of SWeRC	156
Figure 86	Awareness probability for FCW	158
Figure 87	Awareness probability for ICW	160
Figure 88	Awareness probability for ICW (varied speed)	161
Figure 89	Hybrid simulation set-up	169

Figure 90	Parameterization of timings and regions	170
Figure 91	Path-loss used for urban LOS propagation	173
Figure 92	Path-loss used for urban NLOS propagation	174
Figure 93	Path-loss used for highway propagation	175
Figure 94	Ideal PDR for the different scenarios	176
Figure 95	NLOS intersection scenario	176
Figure 96	Illustration of the dynamic highway scenario	177
Figure 97	Speed distribution on the highway	177
Figure 98	End of tailback prediction method	178
Figure 99	Illustration of the generic urban scenario	179
Figure 100	CBR measurement set-up	182
Figure 101	A sample of a measured received signal power S	183
Figure 102	Measured distribution of the transmission time B	183
Figure 103	Distribution of estimated CL	185

LIST OF TABLES

Table 1	Requirements of the localization accuracy for VANET application	12
Table 2	Comparison of localization techniques	13
Table 3	Illustration of the key features of selected sensors	16
Table 4	List of ADAS and their sensor data requirements	17
Table 5	Comparison between 802.11a and 802.11p	20
Table 6	Modulation schemes, data rates and SNIR for IEEE 802.11p	21
Table 7	Channel access timing parameters for IEEE 802.11p	22
Table 8	Default EDCA parameter set	22
Table 9	Description of safety applications	29
Table 10	Application class requirements	31
Table 11	Wireless communication technologies	34
Table 12	Access technologies for application classes	34
Table 13	Excerpt of parameters for basic DCC-G5CC config.	68
Table 14	Default state configuration for DCC-G5CC	69
Table 15	Overview of CC and AC algorithms for VANETs	72
Table 16	Verification of used AC	111
Table 17	Simulated and calculated CAM trigger for Node 1	114
Table 18	Impact of interference on the CBR	116
Table 19	Validation of the 1-hop information exchange	119
Table 20	Validation of the 2-hop information exchange	120
Table 21	Convergence values for minimum and maximum rel. deviation	125
Table 22	Summary of convergence values for conv. speed	127
Table 23	Suitable values for the convergence parameters	127
Table 24	Convergence speed and stability for exemplary parameters	128
Table 25	Good convergence parameters for higher target utilization	130
Table 26	Convergence values for different protocols	144
Table 27	Awareness metrics	152
Table 28	Blackout probability for different protocols	153
Table 29	System age [s]	154
Table 30	Reliability of SWeRC for FCW	159
Table 31	Simulation parameters	172

ABKÜRZUNGSVERZEICHNIS

AC	Awareness Control
ACK	Acknowledgement
ADAS	Advanced Driver Assistance Systems
AIFS	Arbitration Interframe Space
AIAD	Additive Increase Additive Decrease
AIMD	Additive Increase Multiplicative Decrease
AP	Access Point
API	Application Programming Interface
ARF	Auto Rate Fallback
BL	Beacon Load
BS	Base Station
BSA	Basic Set of Applications
BSS	Basic Service Set
BTP	Basic Transport Protocol
CA	Cooperative Awareness
CC	Congestion Control
CL	Channel Load
CS	Carrier Sense
CAM	Cooperative Awareness Message
CBR	Channel Busy Ratio
CCBR	Cooperative Channel Busy Ratio
CCA	Clear Channel Assessment
CCH	Control Channel
CDF	Cumulative Density Function
C-ITS	Cooperative Intelligent Transport Systems
C-V2X	Cellular Vehicle-to-X
CMDI	Channel Monitoring and Decision Interval
CSMA	Carrier Sense Multiple Access
CTS	Clear To Send
CW	Contention Window
D2D	Device-to-Device
DCC	Decentralized Congestion Control
DCF	Distributed Coordination Function
DEN	Decentralized Environment Notification
DENM	Decentralized Environment Notification Message
DGPS	Differential Global Positioning System
DIFS	DCF Interframe Space
DRC	Data Rate Control
DSRC	Dedicated Short Range Communication
EDCA	Enhanced Distributed Coordination Access
EIRP	Equivalent Isotropically Radiated Power
eMBMS	evolved Multimedia Broadcast Multicast Service
ETSI	European Telecommunications Standards Institute
EWMA	Exponentially Weighted Moving Average
FCW	Forward Collision Warning
FGC	Full Global Cooperation
GIS	Geographic Information System

GPS	Global Positioning System
GPSR	Greedy Parameter Stateless Routing
HCF	Hybrid Coordination Function
HMI	Human Machine Interface
HSPA	High Speed Packet Access
ICRW	Intersection Collision Risk Warning
ICW	Intersection Collision Warning
IFS	Interframe Space
IoT	Internet of Things
IF	Information Freshness
IP	Internet Protocol
IPv6	Internet Protocol version 6
IRT	Packet Inter-Reception Time
ITS	Intelligent Transport Systems
LCRW	Longitudinal Collision Risk Warning
LDM	Local Dynamic Map
LLC	Logical Link Control
LOS	Line-of-Sight
LTE	Long Term Evolution
MAC	Medium Access Control
MBMS	Multimedia Broadcast Multicast Service
MIMD	Multiplicative Increase Multiplicative Decrease
MSS	Maximum Segment Size
NLOS	Non Line-of-Sight
NUM	Network Utility Maximization
OCB	Outside the Context of a BSS
OFDM	Orthogonal Frequency Division Multiplexing
QoS	Quality of Service
PDR	Packet Delivery Ratio
PER	Packet Error Rate
PLCP	Physical Layer Convergence Protocol
PSC	Packet Size Control
RHS	Road Hazard Signaling
RoI	Region of Interest
RSSI	Received Signal Strength Indicator
RSU	Road Side Unit
RTO	Retransmission Timeout
RTS	Ready To Send
RTT	Round Trip Time
SIFS	Short Interframe Space
SINR	Signal to Interference plus Noise Ratio
SMA	Simple Moving Average
SNR	Signal to Noise Ratio
SQL	Structured Query Language
SWeRC	Semi-Cooperative Weighted Rate Control
TCP	Transmission Control Protocol
TDMA	Time Division Multiple Access
TP	Transmission Power
TPC	Transmit Power Control
TRC	Transmit Rate Control
TTA	Time to Avoidance
TTC	Time to Collision

UDP	User Datagram Protocol
UMTS	Universal Mobile Telecommunications System
VANET	Vehicular Ad-Hoc Network
VSC	Vehicular Safety Communication
V2I	Vehicle-to-Infrastructure
V2V	Vehicle-to-Vehicle
V2X	Vehicle-to-X
WAAS	Wide Area Augmentation System
WGC	Weighted Global Cooperation
Wi-Fi	Wireless Fidelity
WLAN	Wireless Local Area Network
WSN	Wireless Sensor Network

INTRODUCTION

Mobility was and still is a key factor for the wealth of a modern society. People which suffer from insufficient mobility due to missing infrastructure or vehicles can hardly compete and participate in this society. The development of modern vehicles, like trains, ships, planes and cars was a milestone for the mobility offering new possibilities for the people.

However, new technologies are hard to control and a continuous optimization process is needed to eliminate threats. Due to its comparable high speed and people which were not aware of it, the first cars were involved in many critical accidents. Restrictions and regulations by the government, acceptance and knowledge in the society and technological progress lead to the comparable safe mobility observed nowadays. Obviously, the total amount of reported crashes is significantly increasing over time (cf. figure 1). The major reason for this is that the total number of cars is increasing due to the increase in the wealth of the nation. However, this total number also includes minor accidents without casualties. The figure also reveals the ratio of reported crashes with injuries to people, which has a decreasing tendency, but progress is stagnating in the recent past.

Nowadays, the major reason for accidents with casualties is the driver of the vehicle itself. While failure of the technology is responsible for 1% of the accidents and obstacles for 8%, the driver of the vehicle is responsible for 88% of all accidents¹. In order to further decrease the number of accidents, car manufacturers are focusing on new technologies for enhanced driving. Advanced Driver Assistance Systems (ADAS) are designed to assist the driver with information, warnings and if necessary direct actions are taken. To do so, vehicles are equipped with sensors having different specializations each. In Line-of-Sight (LOS) those sensors can detect an obstacle, calculate the distance and velocity to it and report this to the various ADAS which take appropriate actions. If all vehicles would be equipped with the available sensors and ADAS the amount of accidents can be decreased by up to 28% [1]. While simple sensor techniques are widely available for at a low price, complex sensor systems like surround cameras are more expensive and they are mostly deployed in high priced vehicles.

In order to increase the safety of the vehicles, responsibility from the driver needs to be taken and given to a reliable system. This is the road to fully autonomous vehicles. Currently systems are under testing, which do already provide (fully) autonomous driving^{1,2} based on sensor technology. However, the first step is that the vehicle takes control in situation which are easily controllable for the system (e.g. highways) [2]. Based on this partial automation, conditional and highly automatic systems will follow, where the systems can perform complex tasks without the control of a driver [1], like lateral and longitudinal maneuvers on the highway.

0 Statistisches Bundesamt, 06/12/17: <https://www.destatis.de/>

1 Google Labs, 06/20/2017: <https://waymo.com/>

2 Tesla, 06/20/2017: <https://www.tesla.com>

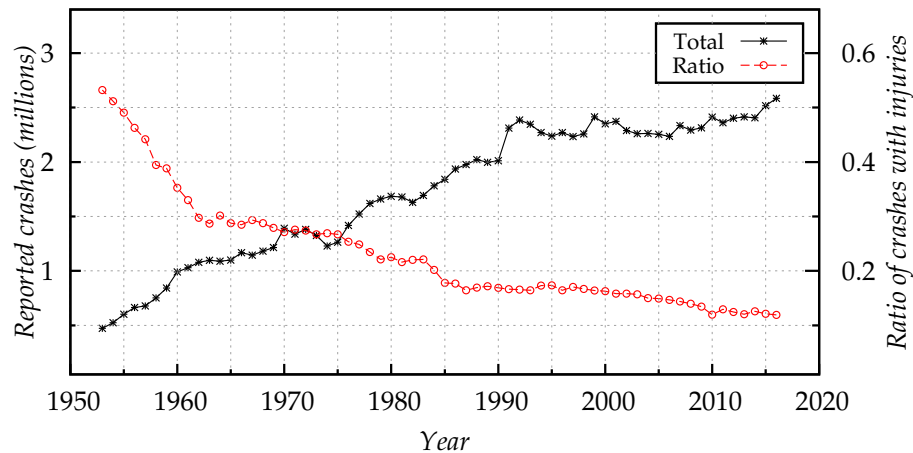


Figure 1: History of reported crashes in Germany¹

Considering this, almost all accidents caused due to driver imperfection can be omitted if the responsibility is given to an autonomous system. Besides traffic violations done by the driver, like speed or priority violations, which will be omitted by a (semi-) autonomous system, there are systems for obstacle detection to avoid crashes with animals or other obstacles [3] and there are also systems to prevent driving under the influence of drugs³. Furthermore, efficiency can be significantly increased. Efficiency means a reduction of emissions due to a reduction of the total travel time. Considering fully autonomous vehicles, cooperation at intersections is applied, such that vehicles do not need to stop at traffic lights, but rather use the intersection as a shared space with cooperation based rules⁴ [4]. However, fully autonomous driving is not expected before 2030 [1, 2] and some questions are still open.

Besides the legal and ethical aspects of the system design and responsibilities, technological standardization is necessary to allow cooperation between the different brands of the vehicles. Indeed, cooperation is a precondition for complex ADAS which can only be provided by a communicative exchange of information between the vehicles. Unlike sensors, information provided by communication is not limited and it enables cooperative planning and maneuvers. For fully autonomous driving, a decentralized list of maneuvers planned in the environment is necessary for efficient, safe and reliable mobility. Unfortunately, neither the government nor the car manufacturers could agree on underlying technology for the communication, yet.

While in the past, there was an agreement to use WLAN based decentralized communication among the vehicles to share information and coordinate actions⁵, nowadays car manufactures prefer to use widely available cellular networks for this purpose [5]. ITS-G5 is the name of the standardized architecture that was proposed for WLAN based communication between Cooperative Intelligent Transport Systems (C-ITS) stations in the European Union [6]. It relies on the IEEE 802.11p protocol developed for Vehicular Ad-Hoc Networks (VANETs) and is also used within

³ DADSS, 06/20/2017: <http://www.dadss.org/>

⁴ light traffic (MIT), 06/20/2017: <http://senseable.mit.edu/light-traffic/>

⁵ C2C-CC, 06/20/2017: <https://www.car-2-car.org>

a similar protocol stack in the US [7]. ITS-G5 is a mature technique, which has been analyzed, evaluated and standardized for many years and within several studies. However, due to its limitations in the communication range, bandwidth and the chicken-egg-problem, manufactures are currently focusing on the upcoming 5th generation of mobile networks, which is said to fulfill the requirements of VANETs [8]. Unfortunately, development is still in progress, standardization is not yet finished and studies for the current generation show, that Cellular Vehicle-to-X (C-V2X) does not provide a reliable service. A suitable alternative is also discussed by several studies and suggested by the European Commission [9]: the hybrid usage of both techniques. Recently, a Memorandum of Understanding has been signed between the Car-2-Car Communication Consortium and the C-Roads Platform⁶ enabling a close cooperation between the different stake holders (industry, road authorities and operators) for preparing the deployment of initial C-ITS services across Europe by 2019 based on the complementary usage of ITS-G5 and cellular networks.

1.1 MOTIVATION

In order to create and maintain neighborhood awareness, vehicles periodically need to broadcast their position and status information. These information need to be exchanged independently of the underlying transmission technology. So it does not matter, whether ITS-G5, cellular networks or future 5G Device-to-Device (D2D) communication is used. Considering the ITS-G5 architecture, those messages are referred to as Cooperative Awareness Message (CAM). The typical size of a CAM can vary depending on the amount of status information carried, but is typically in the range of a few hundreds of bytes [10]. With the deployment of these technologies, a significant increase of the market penetration of connected cars is predicted [2]. However, the CAMs need to be disseminated on a common channel, which capacity is naturally limited. In case of ITS-G5, the maximum would be 2000 msg/s for the default capacity of $C = 6 \text{ Mbit/s}$ and a size of 300 bytes [11]. At this rate, the communication will be significantly degraded due to occurring interference. A realistic amount of messages supported is lower in the region of 1000 to 1200 msg/s. Thus, the channel would support 120 vehicles transmitting at a rate of 10 Hz within the communication range. In situations, where there is dense traffic, higher rates are required or higher packet size is necessary, the channel can easily get congested considering the increase in the market penetration. A congested channel leads to interference, which leads to subsequent message loss and in consequence the functionality of ADAS relying on accurate neighborhood awareness is influenced.

Congestion on a communication channel has already been investigated under certain conditions. It has been necessary to use Congestion Control (CC) in order to avoid the collapse of the Internet in the early phase of development [12], and still is used to guarantee stability. The Transmission Control Protocol (TCP) includes a congestion control protocol, which has undergone several iterations of improvement. Still there is research analyzing the performance of TCP in order to improve the functionality. VANETs have special characteristics, which makes it difficult to directly apply congestion control used so far for Vehicular Safety Communication (VSC).

⁶ C-Roads, 06/21/2017: <https://www.c-roads.eu>

Instead schemes need to be developed, which are suited for the special requirements of VSC.

Congestion control algorithms in VANETs are either used to prevent the channel from congestion by pro-actively reducing the amount of load generated in a certain area or rely on closed-loop control, where an input parameter like the resource utilization is used to control one or multiple transmission parameters. These parameters can either be the rate of the CAMs, the transmission power, the size of the Contention Window (CW), or others. However, they focus on reducing the injected load to a certain region and have to satisfy the requirements for VSC. The characteristics of a congestion control algorithm need to guarantee awareness, scalability, stability and fairness among the nodes. Awareness is the reason for disseminating messages at all and must be maintained at all costs. An algorithm therefore has to be scalable, i.e. awareness is guaranteed independently of the number of nodes in the region. Furthermore, it must have a predictable and steady behavior, which is offered due to stability within the operating area. Lastly, the algorithm also needs to work on a fair basis, such that each node is treated equally considering a certain set of rules.

State-of-the-art algorithms for VANETs can achieve some of the paradigms, but most of them have restriction for at least one characteristics. *LIMERIC* [13], which is a reactive algorithm regulating the message rate, is an outstanding contribution to this field. It achieves a stable and fair allocation of the available resources, if all nodes perceive the same load and the number of contending nodes is within the operating range. The stability of the algorithm is dependent on the scalability and unfairness can be observed due to environmental influence. *PULSAR* [14] is another outstanding algorithm that rather focuses on the fairness aspects of the resource sharing problem. It allocates an environment independent, fair share of the resources to each node using Additive Increase Multiplicative Decrease (AIMD) based binary control for a transmission rate adaption.

The major purpose of CC algorithms is to provide a reliable communication between the vehicles, such that the functionality of any ADAS depending on this information can be maintained. If the transmission power or message rate is decreased, this might help in reducing the congestion, but on the other hand it significantly reduces robustness of the ADAS. However, if no action is taken, interferences will lead to a decrease of the communication quality as well. It needs to be shown, that applying congestion control in certain situations outperforms uncontrolled message dissemination. Awareness metrics are designed to evaluate different aspects of awareness and can be modified to quantify the reliability of an ADAS.

1.2 MAIN CONTRIBUTION

The main contributions of this thesis can be summarized in different parts:

Provide a profound and detailed overview of Awareness Control (AC) and CC algorithms. Due to the non-clearly defined optimization criteria and the many degrees of freedom, a number of algorithms have been proposed for AC and CC in VANETs. In order to analyze the problems of the state-of-the-art protocols, an overview of the algorithms needs to be provided. This overview includes the input values for reactive algorithms and gives a categorization based on the parameters controlled

by the individual algorithms. A brief description of the parameters including the influence on the communication is also given.

Analysis of the problems of state-of-the-art protocols. Although some CC protocols seem to perform well in creating suitable awareness among the vehicles also under congested conditions, there is still room for optimization. This room is analyzed regarding the stability, fairness and scalability provided by state-of-the-art protocols.

Design of an adaptive CC protocol, that fulfills the characteristics of stability, scalability and fairness and maintains awareness. Based on the problems identified within the analysis, we optimize a state-of-the-art algorithm, such that it can fulfill the requirements regarding stability and scalability. We introduce an entire reactive protocol stack that includes multiple modules. The heart of this architecture is the rate control itself. The adaptation is achieved by the dynamic setting of parameters based on provided information. The input information itself is obtained from local measurements and cooperative exchange.

Theoretic and numeric parameter optimization. Protocols usually use a set of parameters, through which the functionality is specified. In various studies, these parameters are not investigated, but rather chosen based on empirical evaluation. Although a theoretical investigation of the parameters is given for others, optimization and numerical analysis as well as conclusion of best-effort parameters is left open. However, the parameters specify the operating range, stability, efficiency or reaction time such that an optimized parameter set-up is crucial for a reliable and efficient CC protocol. We provide this optimization based on a two-step approach. First, we give a theoretical analysis of the parameters used including an investigation of the effect on the algorithm and conclude this analysis with a parameter optimized protocol. In a second step, based on a numerical evaluation, the convergence parameters of the previously parameter optimized SWeRC is conducted. Through it, parameters offering the best trade-off between convergence speed and stability are quantified which are subsequently used for the later evaluation of the protocol.

In-depth investigation of the performance and comparison with state-of-the-art algorithms. We provide a detailed analysis of the protocols performance under realistic conditions using a hybrid simulation set-up with measurement based, validated propagation models. We investigate the environmental influence of buildings in an urban scenario and different motorway scenarios with and without traffic-jam. In order to investigate the performance, we use common metrics like the Packet Delivery Ratio (PDR) or Packet Inter-Reception Time (IRT) and compare the results with other state-of-the-art protocols. Furthermore, we verify the individual modules in the protocol stack which grants further insights into the protocol. Nevertheless, we investigate the protocols capabilities in satisfying the criteria mentioned above: stability, scalability, efficiency, fairness and awareness.

Analyzing the awareness under congested conditions. Awareness is not the official optimization criteria, however it is the key factor which each protocol should maximize. Awareness describes the ability of a vehicle to know its environment.

For the communication, it describes the completeness and freshness of the list of neighboring nodes. Dedicated metrics can estimate this awareness and express it based on the freshness achieved, the maximal range or the awareness probability. However, ADAS do not always need these information e.g. from vehicles which are not involved in a potential collisions. We evaluate the awareness by exemplary quantifying the reliability of collision warning and avoidance systems. Therefore, a metric is adopted, which quantifies the reliability of the information exchanged for different distances. If used for the Time to Collision (TTC), the reliability of the ADAS for giving advices, warnings or take control can be quantified for different CC algorithms used.

1.3 OUTLINE OF THE THESIS

The structure of the thesis is as follows:

Chapter 2 on page 9ff. gives an overview of the technological background of this thesis. It describes the different components used to create and maintain environmental awareness for ADAS. Besides a brief overview of sensors and positioning techniques used, it gives a detailed overview of the ITS-G5 communication protocol stack used within the European Union for C-ITS. Furthermore, the advantages and disadvantages of cellular networks for vehicular communication are discussed.

Chapter 3 on page 37ff. reviews the state-of-the-art congestion control and awareness control approaches available. Therefore, the basic concepts of congestion control are explained under the aspects of VANETs, possible input parameters are examined and a classification of the protocols is done. We discuss the difference between awareness and congestion control and separate these protocols. We explain and classify the congestion parameters based on the controlled parameter and illustrate the concept of the controlled parameter.

Chapter 4 on page 73ff. investigates the related work based on characteristics necessary for stable congestion control. Therefore, we identify the problems still available in the state-of-the-art based on theoretical and numerical analysis.

In **Chapter 5 on page 83ff.** we introduce an adaptive algorithm used for congestion control based on the investigation conducted in the previous chapter. The general protocol architecture with all responsible elements is illustrated and the individual modules are described. We focus on the transmission rate control, which is the heart of the protocol structure which is surrounded by modules for awareness control, channel load smoothing and information aggregation. We describe the necessity of message rescheduling and asynchronous message dissemination, and illustrate the cooperative exchange of information between the nodes. A theoretical parameter analysis conducted reveals optimized parameter settings which are used in advance to ensure highest efficiency, while maintaining stability and fast convergence.

In **Chapter 6 on page 107ff.** the numerical analysis of the proposed protocol architecture is conducted. It includes a detailed description of common metrics used for

the investigation of communication performance in VANETs, followed by an in-depth verification of the individual protocol components revealing insights into the numerical functionality. We evaluate the parameters for the rate-control algorithm and derive an optimal set-up to guarantee fast and stable convergence and steady-state behavior. The numerical analysis is used to show, if a fair resource allocation will be achieved through the usage of cooperation between the nodes. Furthermore, the performance of the protocol is investigated for different environments using a hybrid simulation set-up with accurate propagation and traffic models for different scenarios. We conclude the numerical evaluation by comparing the performance of the proposed architecture with state-of-the-art protocols.

Chapter 7 on page 151ff. provides an analysis of the communication performance for different ADASs. This chapter investigates the reliability of exemplary ADAS under harsh communication condition in order to quantify the impact of congestion control on the traffic safety. We summarize available metrics to quantify the environmental awareness of a vehicle, from which we derive a metric used to analyze the reliability under exemplary conditions.

In **Chapter 8 on page 165f.** we conclude the theses and discuss potential directions for future research.

CONCEPT OF NEIGHBORHOOD AWARENESS

This chapter gives an overview of core technologies used to provide an enhanced awareness for a vehicle and its driver. Therefore, various core technologies used for the different Advanced Driver Assistance Systems (ADAS) are explained focusing on the future cooperative aspects which are part of this thesis. However, communication itself relies on information retrieved from other sources like the positioning of the ego-vehicle or data retrieved from the sensors. Neighborhood awareness describes the capability to know the objects and events within the neighborhood completely. This awareness can be provided to the individual ADAS by a commonly used database called Local Dynamic Map (LDM) which is described in section 2.1. Besides the ADASs which are consumers of the granted awareness, the major part are the data providers like the sensors (cf. section 2.3), the positioning system (cf. section 2.2), and the communication (cf. section 2.4.1).

2.1 LOCAL DYNAMIC MAP (LDM)

Nowadays, sensors deployed in a vehicle deliver specific information for single ADAS which can be retrieved via the Controller Area Network (CAN). With the increasing complexity of future ADAS, it will be necessary to retrieve more data from different sensors and sources in order to guarantee a robust functionality. Furthermore, different sensors and sources can perceive a completely different view of the same situation such that a suitable validation and classification of every situation is mandatory. Aggregation and integration of the data received from the different sources are reasonable steps in order to provide a robust and reliable database for all applications. In the context of C-ITS, this idea is realized by the *SAFESPOT* project via the so called Local Dynamic Map (LDM). The LDM is a database which is used to combine static information with dynamic environment dependent objects like Geographic Information System (GIS) maps. The LDM is represented by the following four layers:

PERMANENT STATIC: This layer consists of static information like the GIS map which can either be stored for a whole region or provided dynamically. It also includes detailed information about roads, intersections, and points-of-interest.

TRANSIENT STATIC: The second layer extends the static map by adding semi-static information like ITS stations, landmarks, long term constructions, and more detailed traffic related data (e.g. road signs).

TRANSIENT DYNAMIC: This layer provides temporary objects like fog-areas, road-works, obstacles, and traffic conditions (e.g. traffic-jam).

HIGHLY DYNAMIC: The fourth layer contains highly dynamic information about the environment and is responsible for providing accurate neighborhood awareness. It includes the positions of all relevant vehicles with detailed status

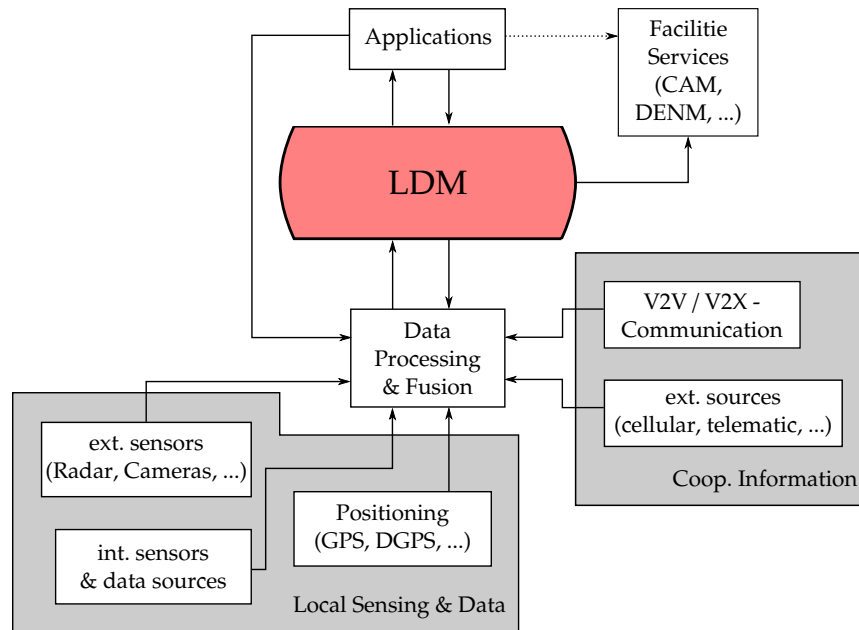


Figure 2: Illustration of the architecture used for providing and receiving information from a LDM [15, 16].

information within a certain area, which is retrieved by sensor data (Radar, GPS, cameras,...), and the exchange of information via V2X Communication.

Based on the *SAFESPOT* study [15], standardization of this key technology has already started. Both the European Telecommunications Standards Institute (ETSI) [16, 17] and the ISO [18] released standards describing the architecture and key features of the LDM. Due to this standardization, the common understanding is that the LDM should include a high level Application Programming Interface (API) and a GIS database which is accessed via Structured Query Language (SQL). Figure 2 shows a simplified architecture of a LDM, its data providers, and consumers.

Both data-providers and consumers need to register to the LDM in order to get access. This ensures the integrity and security of the system. The LDM receives its data based on the local perspective of the vehicle itself provided by the external and internal sensors of the vehicle, the positioning system, and further data sources connected to the LDM. Further knowledge about the environment will be provided by the cooperation between different vehicles using communication technologies. In that way, periodic status updates (via Cooperative Awareness Messages (CAMs)), individual notifications (via Decentralized Environment Notification Messages (DENMs)), map data, and traffic light information will be available for a vehicle. Further centralized information (e.g. from traffic management) can be retrieved via cellular networks, close field communication, and so on. The raw data retrieved from individual sources will be validated and processed based on knowledge patterns and crowd sensing approaches such that each object and event will be given a level of confidence based on the common agreement of the different data providers.

Typically, the data consumers are applications running on top of each Intelligent Transport Systems (ITS) station, i.e. the Advanced Driver Assistance Systems (ADAS). An application can retrieve all necessary information about the environment from the LDM using the specific SQL requests. However, the data still has to be processed

and decisions as well as selections based on the confidence of retrieved data need to be conducted. For example, a Forward Collision Warning (FCW) application might realize the vehicles and obstacles which are in front of the ego-vehicle, including the specific information (speed, distance, heading, etc.) and will react based on the calculated Time to Collisions (TTCs). Registration of other facility services like the Cooperative Awareness (CA) service shall be supported. A CAM will subsequently include the aggregated and validated information about a vehicle based on the LDM, but it can also retrieve further information like the neighborhood perception or fused sensor data.

2.2 POSITIONING

Accurate localization services are an important precondition for the functionality of ADAS. Especially for communication based cooperative ADAS used in VANETs, the precise acquisition of absolute and relative position information is necessary for each vehicle in order to create and maintain neighborhood awareness. The Global Positioning System (GPS) is a robust and easy to install module that provides services for absolute positioning based on satellite techniques. However, with the increasing complexity of ADAS and the progress towards highly automatic driving, problems with GPS based localization begin to arise, including local unavailability and lack of accuracy.

Table 1 gives an overview of the required positioning accuracy for exemplary applications used in VANETs. Some future applications may profit from accurate localization, but they do not need a high precision for the functionality. In this context, low accuracy implies a maximal error between 10 m and 30 m. For example, *Routing* profits from localization in terms of finding a good forwarder for a message on the path, but due to fall-back methods, failures because of imprecise localization can be minimized. *Data Dissemination* relies on local information about the nodes in the neighborhood rather than on accurate position information of close and far nodes. Most *infotainment* applications do not need highly accurate position information.

Higher accuracy of about 1 m – 5 m is required by applications where cooperation between the nodes is applied. Messages containing the absolute locations will be exchanged in order to cooperatively share a common space. Part of these applications are either efficiency or safety related ADAS. Vehicles using C-ACC try to maintain a user defined speed by cooperating with each other. Accurate localization is required in order to avoid overtaking errors or speed miscalculations which would lead to accidents or at least instable algorithm behavior. Almost the same applies to *Platooning*, where accurate localization is important to decrease the gap between the individual vehicles in order to increase the efficiency. More critical applications like *Coop. Intersection Safety* or *Blind Crossing* will need accurate positioning in order to give accurate warnings to the driver or allow precise cooperative sharing of an intersection.

Accuracy of 1 m or less is required by most of the road safety applications which are used to provide real-time information of the environment to the driver and the system. The system can use this information to calculate possible hazards or risky situations and warn the driver or perform automatic breaking. *Collision Warning Systems* are part of these safety applications. They need accurate, robust, and reliable information about the positioning of the ego vehicle and surrounding vehicles in

Table 1: Requirements of the localization accuracy for exemplary VANET applications [19, 20].

Technique	Localization Accuracy		
	Low	Medium	High
Routing	X	-	-
Data Dissemination	X	-	-
Map Localization	X	-	-
Coop. Adapt. Cruise Control	-	X	-
Coop. Intersection Safety	-	X	-
Blind Crossing	-	X	-
Platooning	-	X	-
Vehicle Col. Warn. System	-	-	X
Vision Enhancement	-	-	X
Automatic Parking	-	-	X

- = not required, x = required

order to give a correct warning about possible collisions. In case vision is not suitable, *Vision enhancement* techniques can be used to guide the driver through the area.

Although the precision, availability, and robustness have significantly increased by new satellites, the performance of stand-alone GPS can still not fulfill the accuracy requirements of most safety applications. GPS has a horizontal localization error of ± 10 m up to 30 m [21]. There are several causes for this imprecision, for example disturbance of the signal by obstacles, electromagnetic interference, and so on. Especially in urban environments, where precise localization is required for e.g. collision avoidance applications, buildings can lead to multi-path propagation evoking interference. These interferences can cause huge inaccuracies or even the unavailability of GPS positioning due to lack of satellite signals. In these urban canyons, tunnels, indoor parking lots, or underground roads GPS availability is often not guaranteed or accuracy is below suitable values. However, VANET application always need robust information to guarantee functionality.

The Federal Aviation Administration conducts evaluations of the GPS performance which are published on a regular basis. The requirements for the accuracy are formulated in such a way that 95% of the measured signals should have a horizontal error of ≤ 9 m [22]. However, they evaluate a Wide Area Augmentation System (WAAS) called enhancement for GPS available in the United States. For this technique, additional satellites send correcting signals to a GPS receiver at a different frequency in order to overcome ionospheric interferences. Measurements show that 95% of the horizontal errors are less than 1.891 m [22] on average and within the 99.99% interval they are below ≤ 4.4 m. In Europe a similar system called *EGNOS*¹ is used to increase the accuracy of GPS. The gain in accuracy is significant, but still not sufficient on a submeter range level [23].

Another way to reduce the position error is to use Differential Global Positioning System (DGPS). In general nearby nodes receive the same positioning error such that if a station knows its accurate position, it can calculate the difference between the

¹ EGNOS, 03/23/2017: <https://www.egnos-portal.eu/>

Table 2: Comparison of localization techniques [19, 20, 24].

Technique	Infra-structure	Availa-bility	Accuracy	Syn-chroni-zation
Global Positioning System (GPS)	x	-	-	x
Differential GPS (DGPS)	x	-	x	x
Map Matching	-	x	-	-
Dead Reckoning	-	x	-	-
Cellular Localization	x	-	-	x
Image/Video Localization	x	-	x	-
Localization Services	x	-	x	-
Ad hoc Localization	-	x	x	-
Coop. Positioning Localization	x	x	x	-

- = not provided, x = provided

received GPS signal and its position and broadcast this difference. Receiving nodes can correct their received GPS position based on the received differential information. For DGPS, fixed stations are deployed which broadcast this difference in order to increase the accuracy. The use of DGPS can lead to submeter precision which is suitable for most VANET applications, but the precision depends on the distance to the reference station and thus a huge network of stations has to be deployed.

In order to overcome the problem of imprecise localization in VANETs, studies have focused on the development of different absolute and relative localization techniques enhancing stand-alone GPS positioning. Table 2 gives a summary of the proposed methods and their characteristics in terms of accuracy, availability, synchronization possibility, and necessity of infrastructure. Besides GPS and the more cost-intensive, but accurate DGPS, localization via cellular networks only offers the ability of time synchronization. Cellular localization approximates the distance to several cellular Base Stations (BSs) using the Received Signal Strength Indicator (RSSI). Coverage of multiple cells is necessary for a good triangulation which, however, is less accurate than GPS. Cellular localization is used in mobile devices, because it is more energy-efficient than GPS.

Map matching enhances the accuracy of GPS localization by aligning a sequence of observed vehicle positions to the road network retrieved from a locally stored map. This method can be applied on the fly and is already widely available. Almost every modern navigation system uses map matching algorithms in order to map the retrieved GPS coordinates to the street layout. However, if no map is available or there is no street layout given, map matching cannot be applied.

Dead Reckoning is used whenever localization services like GPS are not available. Based on the last localization, the current position will be calculated based on movement information like distance, speed, direction, time, and so on. If a map is available, the calculated positions are mapped to the street layout, such that localization is possible. However, the longer it is used, the higher its calculation error. Thus, once a GPS signal is available, an update of the calculated position will be conducted.

Image processing can be used from a centralized perspective to retrieve accurate positions of cars which are used to feed a real-time representation of the environment. The responsible area has to be covered with cameras and the location as well as a reference point within the view must be known in order to calculate the correct position based on the image data. However, this method does not guarantee a localization service for a single vehicle.

Infrastructure based localization services work very much like cellular localization. In case a GPS signal is not available due to urban canyons or tunnels, different techniques can be used to determine the position of a node. Radio frequency-based systems use triangulation of the RSSI and appropriate propagation models to determine a nodes position.

A local relative positioning is achieved by using ad hoc localization techniques. All nodes exchange their positions such that relative distances between communicating vehicles can be calculated. Thus a vehicle can locate itself relative to the neighboring vehicles. This relative positioning is accurate, because there is a strong correlation of the GPS measurement error for nearby nodes. This method can also be used to transmit absolute coordinates to a vehicle which is equipped with communication techniques without having a GPS signal. Another approach is to use the RSSI of the Wireless Fidelity (Wi-Fi) signal retrieved by a node in order to estimate the relative distance and thus improve the initial GPS position.

In VANETs, vehicles can cooperate and share their local information about the environment to provide a more accurate view. Basically, the nodes can share absolute positions, sensor information, or whole dynamic maps. Based on this information and the locally assessed localization, an algorithm is used to fuse all the incoming information and reduce the positioning error.

As illustrated in table 2, none of the methods can work on a stand-alone basis. Most of them are used to enhance the accuracy of GPS by utilizing additional information. In order to guarantee robust and accurate localization, data fusion techniques are considered which utilize different techniques. Highly accurate localization that is necessary for safety critical cooperative ADAS can be ensured by a fine-grained localization system comprising all of these techniques.

2.3 SENSORS

This chapter gives a brief overview on sensors used for ADAS. Since this work focusses on communication, we refer to specific literature for a detailed description of the functionality and parameters of the sensors.

Current and next-generation ADAS rely on information retrieved from their environment. Autonomous systems must have at least the amount of information recognized by a human driver itself. The capabilities of the latter to sense his environment is thus replaced by a set of sensors deployed in the vehicle. Each of them is designed to obtain certain information at high resolution and reliability. A short description of sensors is given below based on [25, 3]. Further detailed information about the functionality of the individual sensors can also be found in [3].

RADAR Radio Detection and Ranging (Radar) is used to detect objects and measure their relative position and velocity. The major purpose of radar sensors is the

detection of longitudinal objects. Thus, the sensors are aligned in the front and the back of the vehicle. The used technique is based on pulse compression modulation meaning that pulsed electromagnetic waves at the speed of light are emitted. These waves will be reflected by obstacles and are subsequently recognized by the sensor. The size, shape, and material of an object influences the reflection. Special antennas allow bundling of the electromagnetic waves in a particular direction. In this way, it is possible to calculate the exact angular coordinates of the object. The velocity and position of the object is determined by measuring the time between transmission and sensing of the reflected wave using the Doppler effect. The combined signals are clustered according to their position and movement and stored in a Cartesian coordinate system. Radars can measure the distance, velocity and angle of multiple objects in the sensing range simultaneous in real-time.

There are two types of radars: long and short range. The major difference between both types is the maximal distance in which objects can be detected, influenced by the used frequency. While long range radars operate at a frequency of 77 GHz with a maximal distance of 250 m, short range radars operate at 24 GHz. The resolution of a radar sensor is 0.1 m for the distance and 0.2 m/s for the velocity for a relative speed of up to 35 m/s [25].

LIDAR The Light detection and ranging (lidar) is a radar operating in the infrared spectrum such that it achieves much shorter wavelength typically in the ultraviolet, visible or near infrared spectrum. Metallic objects produce significant reflections for radar waves, but non-metallic objects produce much weaker reflections and thus are hardly recognized by a radar. Because of the low wavelength, a lidar can detect these objects at a much higher resolution.

A lidar can be used to measure the relative speed and distance of a longitudinal vehicle with an accuracy of 0.1 m and 2 km/h. Therefore, it does not rely on the Doppler effect, instead the *time-of-flight* principle is used to determine these values. Typically, the used wavelengths are in the near infrared spectrum between 850 nm and 1 μm . Short range lidar is used for object detection up to 10 m and long range lidar covers a range of up to 150 m, which is slightly smaller than today's radar ranges [3].

CAMERAS A vision sensor collects light and represents it as multi-dimensional measurement signals. Based on these signals, time-dependent images will be created. The most important aspect of the image is its resolution. However, the core of machine vision is the image processing from where the raw data is processed in order to gain secondary information like position, velocity, and the type of an object. Image processing describes the preparation, analysis, and interpretation of visual information. To reduce the computational complexity of image processing, pre-processing and characteristics extraction are applied to generate specific input for single tasks like object classification or pedestrian detection.

Machine vision outperforms usual sensors due to its potential features. The sensor is completely passive such that no radiation is emitted and provides a high information content and the principle used to measure the environment is closely linked to human perception of the traffic environment. However, it is limited to the image processing software and fails under adverse conditions, e.g. rain or night.

Table 3: Illustration of the key features of selected sensors [25, 3, 26].

	Radar	Lidar	Cameras (Mono/Stereo)
Prov. Information:			
Position	y	y	n
Velocity	y	n	n
Performance:			
Range	++	-	+/+
Longitudinal Perf.	++	+	-/+
Lateral Perf.	-	-	++/++
Weather Dependency	+	-	-/-
Low Visibility	++	++	-/-
Application Performance:			
Object detection	+	+	++/++
Stationary Objects	-	++	++/++
Object classification	o	+	+/++
Lane detection	-	-	+/+
Costs:	o	+	++/+

- = poor, o = average, + = good, ++ = very good
y = provided, n = not provided

Camera systems deployed in the vehicle can be separated into three major categories. A mono-system consists of one single camera deployed in the front and/or in the back of the car for longitudinal and semi-lateral measurements. A stereo-system consists of two closely placed cameras. It benefits from redundancy in the information retrieved and the effect of stereo-vision allowing a more precise image processing. Besides these, surround-cameras can be installed at the sides of the vehicle to grant lateral vision.

NIR / FIR Near Infrared (NIR) and Far Infrared (FIR) sensors are sensitive to heat radiation of objects. While NIR sensors also illuminate infrared light and measure the reflection at a wavelength of 800 nm, the FIR sensor consists of a single detector for wavelengths of 7 – 14 μm . The major purpose of these sensors is to detect stationary objects. Due to the detection using infrared waves, they are suited to provide vision during the night.

ULTRASONIC Ultrasonic sensors send pulsed waves at 40 kHz and detect objects by the reflection of the sound waves. Due to its limited range and resolution, they are mainly used for longitudinal and lateral parking assistance in range of up to 3 m. In order to overcome the drawback of the low resolution which can lead to inaccuracies of up to 20 cm, multiple sensors are used. By applying beam-forwarding technologies, the ability of measuring target angles is achieved. It can be applied by the fusion of sensor data and control of multiple sensors.

Table 4: List of ADAS and their sensor data requirements [3].

ADAS	Radar	Lidar	Camera	others	V2V	
					repl.	opt.
Adaptive Cruise Control	x	(x)	(x)	-	x	x
Stop & Go	-	x	-	-	x	x
Platooning	-	-	x	infrared	x	x
Lane Departure Warning	-	-	x	-	x	x
Lane Keeping Assistance	-	-	x	-	x	x
Lane Change Assistance	x	(x)	x	-	x	x
Forward Coll. Warning	x	-	-	-	x	x
Near Field Coll. Warning	x	(x)	(x)	-	-	x
Pre-Crash Coll. and Mitigation System	x	-	x	ultrasonic, infrared	-	x
Intersection Assistance	(x)	(x)	x	-	-	x
Enhanced Vision	(x)	(x)	x	infrared	-	x
Parking Assistance	x	-	(x)	ultrasonic	-	x
Side Obstacle Warning	x	-	(x)	-	-	-

- = not used, x = used, (x) = beneficial

Table 3 gives an overview of selected key parameters of exemplary sensor solutions. While *Radar* sensors conduct precise distance and velocity measurements at high longitudinal range and robustness against adverse weather conditions and visibility, they offer a poor lateral performance at medium costs. An application can perform reliable obstacle detection based on the *Radar* technology, but classification of the obstacles and more complex processing options are not possible based on the retrieved sensor data. *Lidar* sensors offer almost the same longitudinal performance at a lower range, but with the same precision at least for the distance detection. However, their performance depends on the weather conditions and the lateral performance is as poor as for *Radar*. Based on the retrieved data, smaller objects can be detected and classified and the performance for the detection of stationary objects is increased at low costs. An outstanding application performance can be achieved by the use of cameras. They fail to provide accurate distance and velocity measurements, but based on the image processing that is done for the raw data, the performance of cameras in the detection and classification of objects is high and more complex tasks like sign or lane detection are possible.

Obviously, none of the sensor achieves the full support needed for current and future ADAS on its own. However, integrating all possible sensors into the vehicle will lead to increased costs and weight without a significant increase of the performance. The basic concept which is discussed at this point is *sensor fusion* which is used to aggregate, validate, and classify the data received from individual sensors to obtain a reliable and robust situational awareness. A combination of *Radar* with *Mono-Cameras* can already provide precise measurements and good application performance for lateral and longitudinal awareness at low costs. However, further cost-efficient and easy to integrate sensors like ultrasonic or infrared sensors are necessary for short

range lateral detection and can contribute to the situational awareness. Another sensor which is not considered at the moment achieves highly precise awareness in terms of position, distance, velocity, object class, and so on. This sensor has not been deployed yet and is still under development, but future ADAS will significantly profit from the information and it is a precondition for (semi-)autonomous driving. The mentioned sensor is known as Vehicle-to-Vehicle (V2V) communication and its technique is further described in section 2.4.1.

In table 4 we summarize the requirements for exemplary ADAS in terms of necessary sensors. Reliability and functionality of these ADAS can be increased significantly by the usage of communication, and in some cases the usage of sensors can be neglected by it. However, for certain applications like parking, vehicles still have to be equipped with sensors.

2.4 COOPERATIVE INTELLIGENT TRANSPORTATION SYSTEMS (C-ITS)

C-ITS provides the next step towards highly complex ADAS and is the enabling technology for highly autonomous driving. Although the perception of a vehicle can be significantly enhanced by complex sensor systems, processing, and computation of the data, it is still limited to the limited awareness about the neighboring vehicles. Plans can be guessed based on predicted movements and analysis of possible situations, but real cooperation is not possible. As a result, the efficiency and operating area of ADASs is reduced. Complex maneuvers like crossing a frequently used unregulated urban intersection without a significant reduction of individual speeds is not possible without cooperation. Furthermore, information of the traffic management like signal phases of traffic lights cannot be achieved without communication. Cooperation between vehicles will allow these advanced maneuvers, enable enhanced vision, and increase the integrity of perceived data. This section gives a detailed description of the technology dedicated for this purpose based on the standards published by the ETSI in Europe. The section focuses on the description of the different communication layers used for VSC (cf. section 2.4.1) and also gives a short overview of the impact of the cellular technology on different areas of C-ITS (cf. section 2.4.2).

2.4.1 *Vehicular Communication (V2X)*

Due to the ongoing research in C-ITS, different protocol stacks for the communication between the stations have been developed. The leading institutes are the Institute of Electrical and Electronics Engineering (IEEE) and Society for Automotive Engineers (SAE) in the United States and the ETSI within the European Union. Apart from that, there are standardization tendencies in other countries (like Japan or China), but they are far behind the progress of the leading institutes.

An overview of the standards and the protocol stacks currently available is provided in figure 3. Both protocol stacks follow the ISO/OSI reference structure with slightly different abstractions between the layers. In the United States, the lower four layers are standardized under one major architecture called Wireless Access in Vehicular Environments (WAVE). On top of WAVE, the application layer summarizes the upper three layers of the ISO/OSI reference model. Besides the

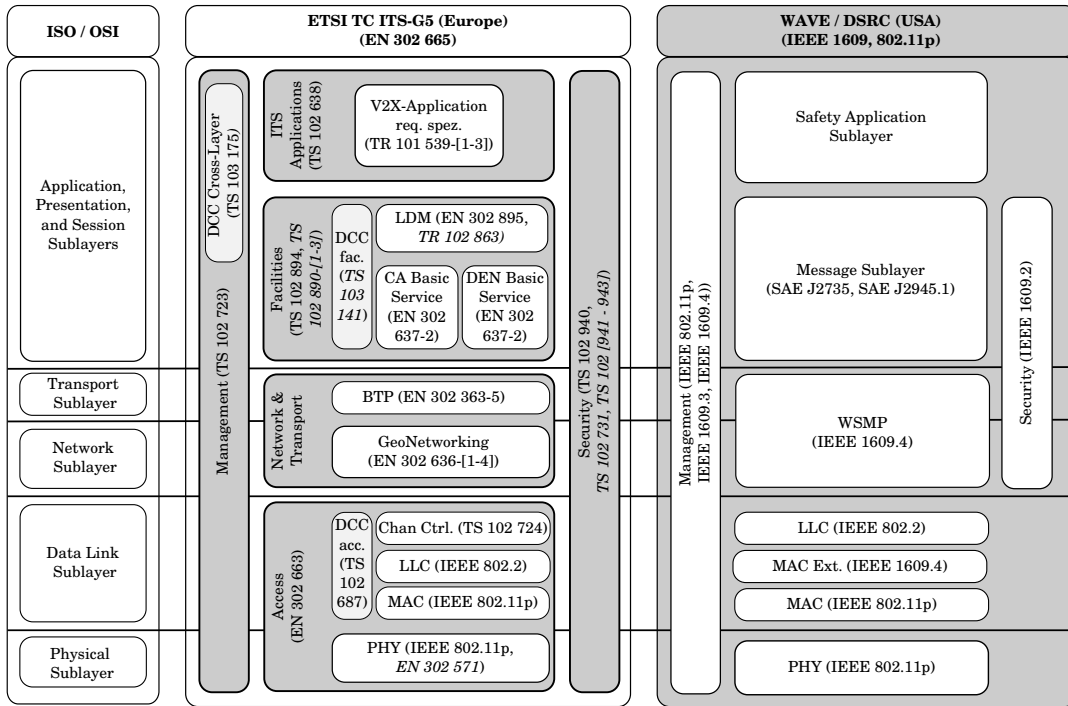


Figure 3: Overview of the protocol stacks and the corresponding standards for VSC in Europe [6] and US [7].

horizontal layers, both protocol stacks use a horizontal cross-layer architecture for management and security operations. The European architecture as proposed by the ETSI can be summarized by four major layers, namely *Access*, *Networking*, *Facilities*, and *Applications*. For each of these major layers, there are individual standards describing the functionality, structure, interfaces, and submodules included in this layer. Although the proposed method in this thesis is independent of the used protocol stack, we focus on the description of the European protocol stack. In the following subsection, the architecture is described in detail starting from bottom to top.

2.4.1.1 Access Layer

The access layer represents the lowest layer in the protocol stack consisting of the physical and data link layer. In general, the access layer supports different communication modes like cellular (GPRS/UMTS/LTE), Bluetooth and Wi-Fi (IEEE 802.11a/b/g/n). Besides that, the IEEE 802.11p protocol designed for VSC is of major interest.

PHY LAYER Communication between ITS stations is enabled by the usage of IEEE 802.11p protocol. This protocol is an adopted version of IEEE 802.11a with certain parameter changes to meet the requirements of VANETs, such as severe multipath propagation and high relative speeds. IEEE 802.11p [27] is included in the latest revision of IEEE 802.11 [11] from 2012.

In Europe the frequencies between 5.875 Mhz and 5.925 Mhz are allocated [30] and used for VSC. Additionally, it is recommended to allocate frequencies between

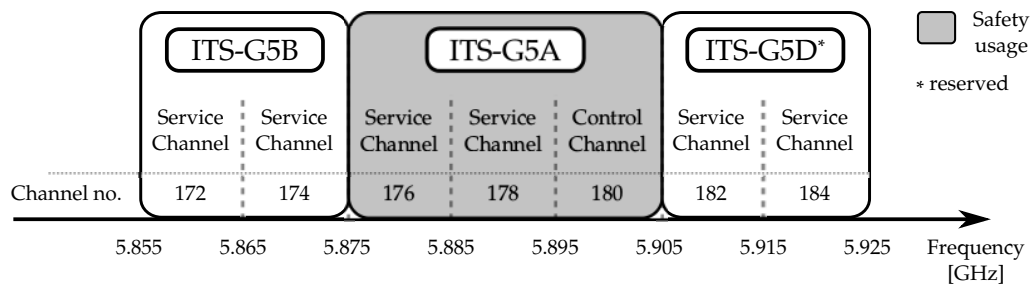


Figure 4: Frequency and channel allocation for ITS-G5 in the EU [28, 29].

Table 5: Comparison of selected timing parameters between 802.11a and 802.11p (cf. table 18.5 [11])

Parameter	802.11a (20 MHz channel spacing)	802.11p (10 MHz channel spacing)
N_{ST} : Number of subcarriers	52	52
T_{FFT} : FFT period	3.2 μ s	6.4 μ s
$T_{PREAMBLE}$: Preamble duration	16 μ s	32 μ s
T_{SIGNAL} : OFDM symbol duration	4 μ s	8 μ s
T_{GI} : Guard interval duration	0.8 μ s	1.6 μ s
T_{SYM} : Symbol duration	16 μ s	32 μ s

5.855 Mhz and 5.875 Mhz for non-safety related communication between ITS stations [31]. These frequencies are divided into seven distinct channels with a bandwidth of 10 Mhz each (cf. figure 4), six service channels, and one control channel. Channels 176 to 180 are referred to as *ITS-G5A* and used for time critical safety related communication. *ITS-G5B* is used for non-safety related communication and allocates the channels 172 to 174. The remaining channels 182 to 184 are referred to as *ITS-G5D* and reserved for future usage. Since the ITS stations cannot listen to all seven channels at the same time, the stations have to listen to the control channel for arrangements. For communication on the service channels (in the context of a safety related ITS station), a separate receiver is required. This channel is used for the periodic safety messages (CAM) [32].

While the IEEE 802.11a operates at a 20 MHz bandwidth, IEEE 802.11p is designed to use *half-clocked* operation. Changing the channel width leads to a doubling of all relevant timing parameters (cf. table 5). The basic motivation is to overcome the multi-path propagation effect leading to higher delay spreads.

IEEE 802.11p is based on the Orthogonal Frequency Division Multiplexing (OFDM) modulation scheme. This scheme subdivides the total bandwidth of 10 MHz into 52 small sub-carriers from which 48 are data and 4 are pilot sub-carriers which are transmitted in parallel. Each sub-carrier is modulated using binary or quadrature phase shift keying (BPSK, QPSK) or using 16- or 64-quadrature amplitude modulation (16-, 64-QAM). For each modulation scheme there are two coding rates of either 1/2, 3/4 or 2/3 resulting in 8 different possible data rates (cf. table 6). The coding rate represents the ratio of data bits and the total amount of bits of which the rest is used for data correction in case of data corruption. A more complex modulation scheme and higher coding rate allows to transfer more data bits per OFDM symbol,

but loses robustness. This implies that for higher data rates, the minimum sensitivity required drops significantly to achieve the required Signal to Interference plus Noise Ratio (SINR) for a successful reception. It means in effect a reduction of the effective transmission range for higher data rates. Under relaxed conditions a data rate of 6 Mbit/s is found to be optimal for VSC [33]. The SINR values shown in table 6 are acquired from measurements according to Jiang et al. [33], while the minimum sensitivity is specified in the IEEE 802.11 standard [11].

MAC LAYER Several changes have been made to the IEEE 802.11a Medium Access Control (MAC) layer to suite the specific requirements of VSC. IEEE 802.11p introduces the so-called Outside the Context of a BSS (OCB) communication mode which reduces latencies and communication overhead by allowing a direct communication without establishing or joining a Basic Service Set (BSS) first. This mode is suited for safety application with strict timing requirements and fits for the rapidly changing topology of a VANET. The MAC of the IEEE 802.11p is based on the Distributed Coordination Function (DCF) included in IEEE 802.11 [11]. It offers the possibility of a decentralized coordinated access to the channel. DCF uses the Carrier Sense Multiple Access (CSMA) mechanism to allow randomized channel access based on the *listen-before-talk* principle called carrier sensing. IEEE 802.11p uses an augmentation called Enhanced Distributed Coordination Access (EDCA) which adds different access categories and thus channel access timings [29]. The detailed functionality of EDCA is explained later on.

CSMA

Figure 6 shows the flowchart of CSMA for broadcast transmissions using EDCA, where there are no acknowledgements. Whenever a station tries to access the channel in order to transmit a frame, it has to wait for a free channel and afterwards the channel needs to be idle for a certain time period called DCF Interframe Space (DIFS) (cf. figure 5). If the channel is idle during the DIFS, immediate access to the channel is granted. To prevent simultaneous transmissions of several stations, a random backoff mechanism is introduced. Each station draws a random number out of

Table 6: Data rates in a 10 MHz channel using IEEE 802.11p, their required minimum sensitivity [11, 28], and SINR values for reception [33]

Modulation	Coding rate	Data bits per OFDM symbol (N_{DBPS})	Data rate [Mbit/s]	Minimum sensitivity [dBm]	SINR [dB]
BPSK	1/2	24	3	-85	5
BPSK	3/4	36	4.5	-84	6
QPSK	1/2	48	6	-82	8
QPSK	3/4	72	9	-80	11
16-QAM	1/2	96	12	-77	15
16-QAM	3/4	144	18	-73	20
64-QAM	2/3	192	24	-69	25
64-QAM	3/4	216	27	-68	N/A

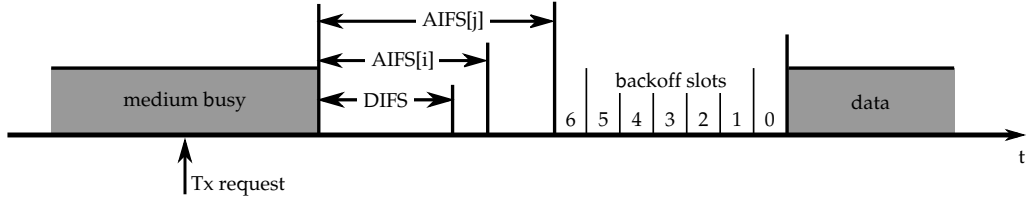


Figure 5: Sequential process of the medium access using CSMA [11].

$[0, CW_{min}]$. This backoff is also known as CW. The CW is decremented by one as long as the channel is idle for T_{slot} and the transmission is started if the CW is zero. If the channel is indicated as busy during the CW, the mechanisms start decrementing after the channel is indicated as idle during one DIFS.

The CW can have a major influence on the channel access time, whenever a station is required to initiate deferred access. If the CW is too small, the probability of packet collisions increases, because stations have a higher probability to draw the same backoff. If on the other hand the parameter is too big, the efficiency of the mechanism is decreased and stations need to wait longer to access the channel.

Since VSC relies on broadcast messages, *binary exponential offset* cannot be applied, because no Acknowledgements (ACKs) are sent. *Binary exponential offset* would double the CW each time an ACK is not received due to a frame collision such that the probability of collisions will be decreased.

In section 3.3.3 the usage of this parameter for congestion control is further explained. One step to adjust this parameter is to use different access categories which is done by EDCA.

EDCA

EDCA is based on the IEEE 802.11e amendment and is introduced to prioritize different message types. While in the original version it differentiated between eight categories, it is used within the IEEE 802.11p with four different access categories, namely background (AC_BK), best effort (AC_BE), video (AC_VI), and voice (AC_VO). The main difference between DCF and EDCA is that the DIFS is replaced

Table 7: Selected channel access timing parameters for IEEE 802.11p [11].

Parameter	Value
aSlotTime	13 μ s
aSIFSTime	32 μ s
aCWmin	15
aCWmax	1023

Table 8: Default EDCA parameter set for ITS-G5 and IEEE 802.11p [27, 11, 29]

Priority	AC	CW_{min}		CW_{max}		AIFSN
Lowest	AC_BK	aCWmin	15	aCWmax	1023	9
	AC_BE	aCWmin	15	aCWmax	1023	6
	AC_VI	$\frac{aCW_{min}+1}{2} - 1$	7	aCWmin	15	3
Highest	AC_VO	$\frac{aCW_{min}+1}{4} - 1$	3	$\frac{aCW_{min}+1}{2} - 1$	7	2

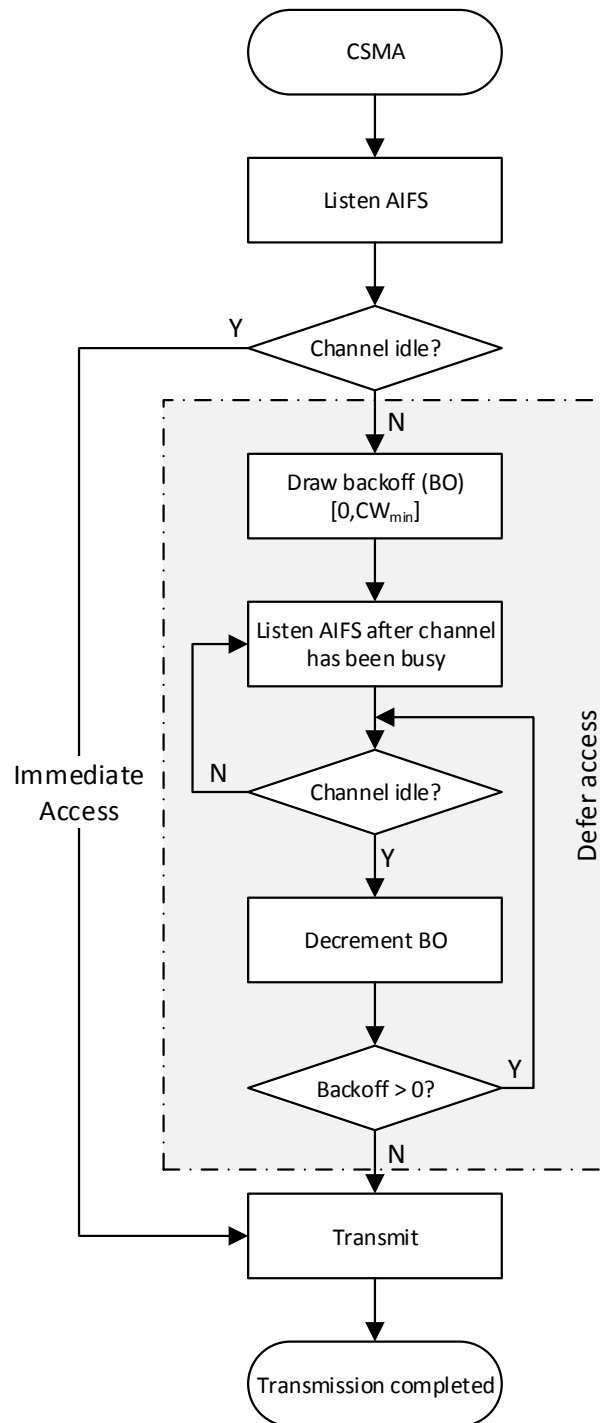


Figure 6: Flowchart of the CSMA mechanism in broadcast mode [11].

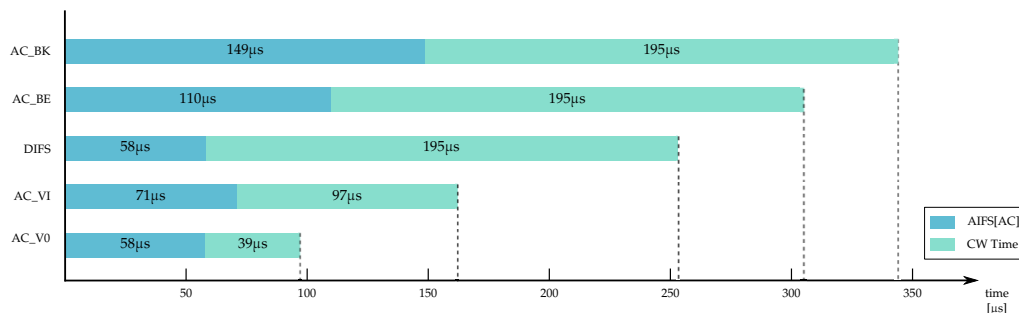


Figure 7: Lower and upper bound of the access time using EDCA for different access categories and the corresponding CW.

by an access category dependent time called Arbitration Interframe Space (AIFS). Each access category has its own message queue and acts as an individual DCF station. The AIFS is calculated based on the sum of Short Interframe Space (SIFS) and a multiple of the slot time:

$$\text{AIFS}[AC] = \text{AIFSN} \cdot T_{\text{slot}} + T_{\text{SIFS}} \quad (2.1)$$

In table 8 the different access categories for IEEE 802.11p are summarized starting with the lowest access priority. The multiplier AIFSN denotes the priority due to the access category, because frames with shorter Interframe Space (IFS) get to access the channel before others. As a result, the access time, i.e. the sum of $\text{AIFS}[AC]$ and $\text{CW}_{\text{min}} \cdot T_{\text{slot}}$ as the upper bound, for AC_VO (97 μs) is nearly 4-times smaller than for AC_BE (344 μs) based on the timing parameters shown in table 7 (cf. figure 7).

Carrier Sensing, Hidden-, and Exposed Terminals

To determine whether a channel is idle or busy, the CSMA mechanism relies on a binary function called Clear Channel Assessment (CCA). If the energy received at the antenna of a station exceeds a certain value, named carrier sense threshold, the channel is indicated as busy. This procedure is called physical carrier sensing and takes place in the PHY layer. Besides that, virtual carrier sensing, located at the MAC layer entity, is triggered if the preamble and header of a frame are received successfully. The channel is considered busy for the duration of the frame as indicated by the frame length in the PHY header. CCA implements these two functions and returns busy if one or both of them indicate a busy channel.

Note that a busy indication of the virtual carrier sensing does not necessarily induce an error-free frame reception. Due to occurring interferences during the frame transmission, a frame might be lost, although the header can be received successfully. It is more likely dependent on the SINR which needs to exceed a data rate dependent threshold (cf. table 6). A simplified calculation of the SINR of a packet is given by

$$\text{SINR} = \frac{P_r}{N + \sum_{i=0}^I P_i}, \quad (2.2)$$

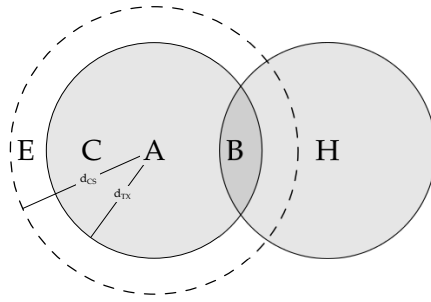


Figure 8: Illustration of the hidden (H) and exposed (E) terminal problem.

where P_r indicates the received power level of a frame, N is the noise level, and P_i is the power level of an interfering frame. If this value exceeds the threshold, the frame can be decoded and received.

The carrier sense threshold, used for the CCA function, is a parameter which determines how aggressive a station accesses the channel. A station's carrier sense range d_{CS} , i.e. the range in which transmissions are recognized, is defined by the parameter. If it is set low, d_{CS} will be increased and thus a station receives transmissions from more distant stations and the access is deferred, because signals with low power from faraway stations are received. In some cases, where the carrier sense range exceeds the transmission range, this leads to the exposed station problem. In contrary, a station ignores other stations' transmissions if the carrier sense threshold is set high. This can lead to packet collisions due to the so-called hidden terminal problem, because the stations do not recognize each other's transmissions.

Figure 8 illustrates the spatial distribution of nodes with equal transmission d_{TX} and carrier sense range d_{CS} . H indicates the hidden node, while E indicates the exposed node from A's perspective. If we consider an unicast transmission from A to B, E will refrain its transmission to C due to the ongoing transmission of A, although it will not interfere the transmission at B. C does however receive the signal from A (cf. figure 9) and in a broadcast environment the frame would be of interest for C as well such that E is no exposed station anymore. Considering this, Stanica et al. [34] argue that VANETs are basically exposed-node free. Schmidt et al. [35] define an exposed node as a node which needs to drop packets due to high channel access delays caused by high carrier sense range. If stations are cooperating with each other, an exposed node will also be an altruistic node which refrains from its access to support other nodes [36].

Packet collisions in CSMA networks are inevitable due to its decentralized coordination. There are two major reasons for packet collisions, CSMA based collisions and collisions due to the hidden terminal problem (cf. figure 9). A CSMA collision will occur if stations which are within carrier sense range start transmitting simultaneously, because they draw the same random backoff, their backoff reaches zero at the same slot or immediate access after simultaneous TX requests is granted. However, this collision probability can be decreased by increasing the CW as mentioned before.

To encounter the hidden terminal problem, the IEEE 802.11 specified a reservation based mechanism called RTS/CTS. Whenever a station wants to transmit a frame, it needs to indicate this by sending a Ready To Send (RTS) message which contains the frame duration and the intended receiver. The receiver then replies with a Clear

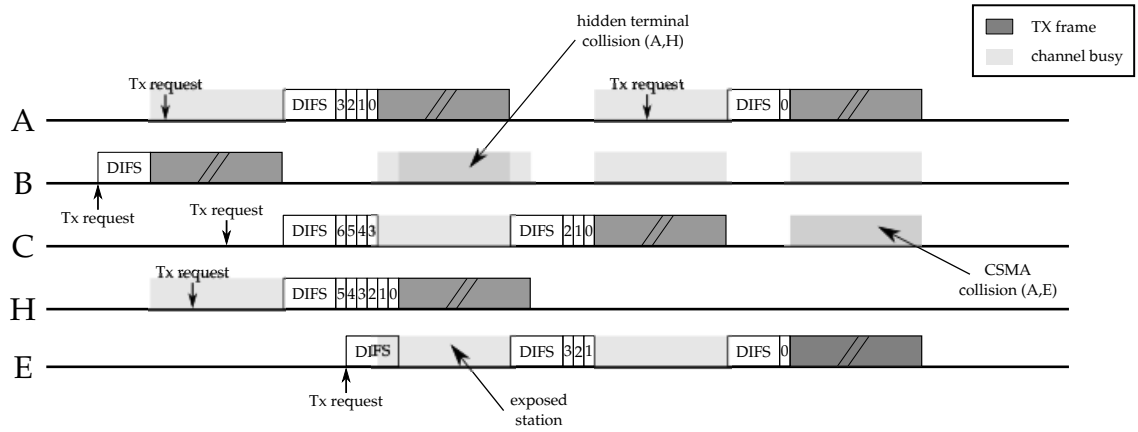


Figure 9: Channel access and state for the nodes illustrated in figure 8.

To Send (CTS) message repeating the frame duration. In this way, all surrounding stations which receive the CTS, but not the RTS, know that they are hidden stations and refrain from their transmission during the frame duration. A sends a RTS to B, which replies a CTS. The CTS is received by H and A such that A starts its transmission, while H refrains from transmitting for that duration (cf. figure 8). However, due to its overhead, RTS/CTS cannot be applied to broadcast environments and thus it is not used in VANETs.

2.4.1.2 Network Layer

The *GeoNetworking* called network layer of an ITS station is based on a series of standards proposed by the ETSI [37, 38, 39, 40]. It includes Internet Protocol version 6 (IPv6), TCP, and User Datagram Protocol (UDP) support to allow connectivity between an ITS station and the Internet as part of the Internet of Things (IoT). Besides this, a suited solution for direct communication between stations will be introduced. It allows communicating with stations which can be outside the communication range by using *multi-hop* communication by addressing the specific region the stations is in. The idea is that safety-specific information is relevant for all stations in a region rather than for individual stations.

GeoNetworking considers three different addressing schemes, namely *GeoUnicast*, *topological broadcast*, and *GeoBroadcast/GeoAnycast*. If a packet is to be delivered to a certain station (identified through the Internet Protocol (IP) address), *GeoUnicast* will be used. It routes the packet to the position of the station by using *line forwarding*. If the position of the destination is unknown to the source, a centralized location service will be used to map the address to a specific position. In contrary, *topological broadcast* floods the region around the originating station until a specific hop-count is reached. In this way, the number of hops increases the information range of the station. *GeoBroadcast/GeoAnycast* is a combination of these two mechanisms, where a packet will be sent to all (broadcast) or a set of vehicles (anycast) within a destination area. Therefore, the packet is first-line forwarded and afterwards flooded within this *GeoArea* called region. The upper layers shall give the destination.

VANETs are highly dynamic which leads to a fast change of the network topology. Thus, the link state can hardly be maintained or huge overhead is required to

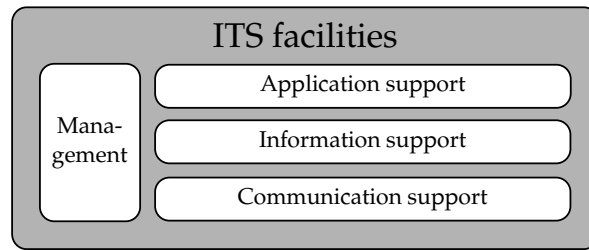


Figure 10: Structure of the ITS facilities [42].

maintain a link between pairs of stations. Position based routing does not need links between the pairs, but instead needs to have accurate position information of the station and its neighbors. By applying the family of Greedy Parameter Stateless Routing (GPSR) protocols to VANETs, an efficient forwarding strategy is considered for *multi-hop* communication. GPSR tries to forward a packet to the neighbor which is closest to the destination position [41]. It is possible to use it for line forwarding, since it incorporates acknowledged unicast transmissions. To obtain the closest neighbor, position updates have to be exchanged periodically or the information can be obtained from the LDM, which considers the CAMs. To overcome the local minimum problem, GPSR employs a repair strategy which is based on the right-hand rule.

In sparse regions a mechanism called *store-and-forward* can be used to maintain connectivity. A station buffers and carries a packet along its way. Whenever the context of the station changes, i.e. a new station is introduced or a station moves to a better position, the stored packet will be forwarded.

On top of the *GeoNetworking* part, the lightweight Basic Transport Protocol (BTP) is employed which provides a connectionless transport service. Through BTP, end-to-end packet transmission between two distinct stations in the VANET is enabled. Furthermore, BTP works as a multiplexer connecting the *GeoNetworking* services to the facility layers.

2.4.1.3 Facility Layer

The main objective of the facility layer is to support the applications with common services and functionality. It is divided into communication, information, and application support (cf. figure 10). The communication support facility includes the selection of addressing modes used by the applications in order to disseminate a message according to the network layer operation. The information facility collects and aggregates all information received by the communication and sensors and stores them in the LDM (cf. section 2.1). Furthermore, it provides location referencing, map matching, and the ITS positioning service. The application support facility offers a data exchange between applications and the driver via the Human Machine Interface (HMI). Besides others, it also includes the Cooperative Awareness (CA) and Decentralized Environment Notification (DEN) basic service which are the heart of cooperative VSC. For further detailed information on the functions implemented in the support facilities, we refer to the corresponding standard [42].

The CA service of the application features the dissemination of the CAM which is a single-hop broadcast message used to create and maintain neighborhood awareness.

Due to the unreliable service and the fast position changes, each ITS station spreads out CAMs at high frequencies. Each CAM includes mandatory information like the position, speed, and heading of an ITS station as part of the High Frequency (HF) container. Long-term information (e.g. vehicle type, size, and so on) is part of the Low Frequency (LF) container and needs to be added to a CAM every 500 ms [10]. The interval between two CAMs is limited to an upper bound of 1 s and a lower bound of 100 ms. The current standard employs a set of trigger rules based on the vehicles dynamics to generate CAMs. In this context, a CAM is generated whenever the change of a vehicles' position, heading, or velocity exceeds predefined thresholds. In case an application is in need of, the functionality of the CA service can be overwritten by reducing the upper bound or limitations for the lower bound due to congestion control, i.e. Decentralized Congestion Control (DCC).

While the CA service pro-actively provides an ITS station with periodic status updates of the local neighborhood, the DEN service can be used by any application to generate a specific DENM. These DENMs are used in the context of the application to inform other ITS stations. They are mainly triggered upon detection of a dangerous situation, e.g. an approaching emergency vehicle [43]. For this purpose, DENMs can use the services of the network layer to inform a specific target area using multi-hop communication. DENMs are repeated based on the application requirements and congestion control limitations until they expire.

2.4.1.4 Application Layer

The application layer of an ITS station is located on top of the facility layer and incorporates the applications specified by the ETSI. The applications are thereby distinguished in three categories: safety, efficiency, and other applications. Three safety applications are specified by the ETSI, i.e., Road Hazard Signaling (RHS) [44], Longitudinal Collision Risk Warning (LCRW) [45], and Intersection Collision Risk Warning (ICRW). Each of them identifies a subset of use cases which are relevant for this application. For example, the RHS specifies use cases like *emergency vehicle approaching*, *slow vehicle*, or *roadwork warnings*. These use cases are also part of the Basic Set of Applications (BSA) [46] together with more than 50 use cases for Vehicle-to-X (V2X)-communication (cf. table 9). The use cases are divided into 7 top-level applications each of which are split into 4 categories: active road safety, cooperative traffic efficiency, cooperative local services, and global Internet services. Table 9 gives a short description of selected safety use cases considered for VSC in Europe. Some of the use cases already specified in [46] will be deployed as part of the *Day 1 C-ITS services*, e.g. Emergency electronic brake light, or *Day 1.5 C-ITS services*, e.g. Cooperative collision risk warning. The European Commission agreed on this *Day 1 C-ITS services* to be the first standardized and deployed cooperative services that shall be supported by an ITS station from 2019 on. Besides that, there is a strong focus on *Day 1.5 C-ITS services* and future services, where standards might not be available until 2019, but are under strong consideration [9].

Figure 11 illustrates the time horizon for an ITS stations safety applications based on the Time to Collision (TTC). In a first stage, information gathered by an ITS station is used in the context of driver assistance. As long as the TTC exceeds a sufficient threshold (>30 s), potentially useful information is displayed to the driver to support the decision making and to avoid safety risks. This information

Table 9: Set of safety applications introduced for deployment in the EU [9] including a short description from [47, 46].

Use-case	Direction	Type	Short description
Emergency electronic brake light	V2V	Day 1	A hard braking vehicle transmits a warning message to vehicles behind in order to avoid rear end collision.
Emergency vehicle approaching	V2V	Day 1	Emergency vehicle transmits a message to other vehicles in its path for them to take appropriate actions.
Slow or Stationary vehicle(s)	V2V	Day 1	Vehicle at low speed or stationary vehicle transmits a message to announce its presence.
Traffic Jam Ahead Warning	V2V	Day 1	Vehicle stuck or aware of traffic jam warns approaching vehicles to avoid rear end collision.
Hazardous Location Notification	V2V/ V2I	Day 1	Vehicles detecting hazardous road conditions transmit a message to oncoming vehicles. This notification can also be sent by infrastructure once detected or in advance from traffic management.
Road Works Warning	V2I	Day 1	Roadwork vehicles or Road Side Units (RSUs) transmit roadwork information as well as relevant speed limit information to oncoming vehicles.
Traffic light violation warning	V2I	Day 1	Warns the driver of a potential traffic light violation if speed is not reduced, by processing the traffic light status information received from a RSU.
Cooperative collision risk warning	V2V	Day 1.5	Will warn the driver if a collision risk with neighbor vehicles is detected by processing the received messages from these vehicles. Includes longitudinal, e.g. Forward Collision Warning (FCW), and lateral, e.g. Intersection Collision Risk Warning (ICRW) or Cross traffic turn collision risk warning use case.
Motorcycle approaching indication	V2V	Day 1.5	Warn driver for arriving motorcycle. This is especially useful in case of reduced visibility.
Lane change warning	V2V	-	Will warn the driver who plans to change lanes if there is a vehicle in the blind spot or an overtaking vehicle
Overtaking vehicle warning	V2V	-	An overtaking (passing) vehicle signals its action to other local vehicles to secure the overtaking situation.
Pre-crash sensing warning	V2V	-	Prepare for imminent and unavoidable collision by exchanging vehicles attributes after unavoidable crash is detected.

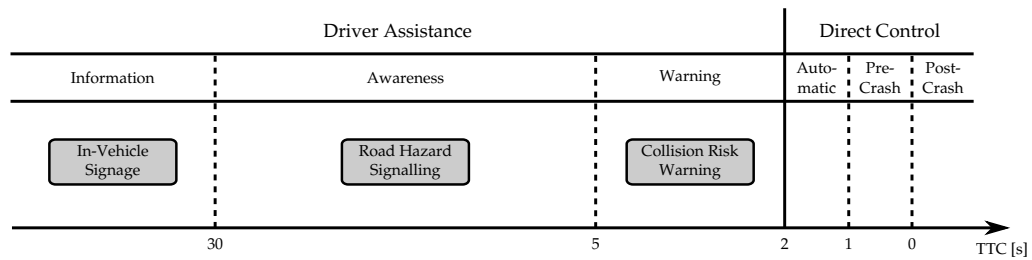


Figure 11: Time horizon of ETSI safety application [44, 45].

can include reminders of traffic rules and road conditions. If the time horizon is progressing ($5\text{ s} < \text{TTC} < 30\text{ s}$), the context is shifted from information to driver awareness. In this context, the driver will be made aware of a potential hazard or risk in the path, but is not forced to react to it immediately. The RHS application is part of the awareness horizon. If the driver does not react in time, a warning will be indicated based on the use case by the ICRW or LCRW application on which the driver has to react.

Direct Control will take over the control of an ITS station by an automatic control system if the time horizon is too small ($\text{TTC} < 2\text{ s}$). If the collision is unavoidable, pre-crash conditions will be evoked to mitigate the collision impact and reduce the damage. Afterwards, post-crash applications will be activated to inform rescue organizations about the accident. The information sent include position and sensor data of the vehicle.

2.4.2 Cellular-V2X

The ITS-G5 [6] architecture as specified by the ETSI provides the ability to use a mixture of different communication technologies to achieve the best possible performance for C-ITS. The European Commission recently suggested to use a "[...] combination of ETSI ITS-G5 and existing cellular networks", because "This ensures the best possible support for deployment of all Day 1 C-ITS services." [9]

The advantages of IEEE 802.11p based short-range communication are easy deployment, low costs, mature technology, and the native ability to support ad-hoc and broadcast communication. With its focus on VSC, Wi-Fi based communication achieves low latencies, but it suffers from its low communication range and lack of infrastructure necessary for Vehicle-to-Infrastructure (V2I) communication. Furthermore, it suffers from scalability issues, penetration rate, unbound delays, and lack of deterministic Quality of Service (QoS) guarantees [47]. Cellular networks can be used to either replace Wi-Fi based communication or to enhance it. Long Term Evolution (LTE) is the most recent deployed wireless broadband technology providing high throughput and low latencies for mobile nodes. It offers a large coverage area and due to its commercial usage, it is already widely deployed. Moreover, it provides high velocity terminal support necessary for communication in VANETs. Since LTE is directly connected to the backbone network, it provides direct access to the Internet without ad-hoc routing schemes and thus is perfectly suited for usage of V2I based *Infotainment* and *traffic efficiency* applications, while its usage for VSC is still under investigation. The main problem of the latter is the centralized infrastructure of

Table 10: Requirements for different application classes as listed in [47].

Application class	Main requirement	Type	Examples
Infotainment	High throughput, medium-to-low latency	V2V, V2I	Web-browsing, VS, file sharing, gaming, e-mail
Comfort	Medium-to-low reliability	V2I	VR, live traffic information, remote software updates
Traffic efficiency	Medium-to-high reliability	V2V, V2I	XFCO, PDAS
Safety	High reliability, low latency	V2V, V2I, V2X	cf. table 9

cellular networks. In order to exchange a safety-critical message between two nearby stations, the whole path through the network via the BS has to be run resulting in high latencies. In dense areas, LTE can also suffer from network congestion due to the high load generated by the periodic update messages which in some cases leads to even higher latencies. Table 10 lists the requirements of the different application classes.

In the context of VSC, cellular-based communication mainly suffers from the lack of broadcast and OCB communication. Since messages are periodically exchanged between neighboring vehicles, each message needs to be first uploaded to a BS via unicast and then unicasted to all the vehicles in the region which may be part of different cells as well. Since all vehicles within this region need to receive the message, Multimedia Broadcast Multicast Service (MBMS) is used to efficiently transmit a signal to multiple stations. Therefore, MBMS data is coordinated among a group of tightly synchronized cells which transmit identical signals at exactly the same time and frequency. This will lead to an increased signal strength which, from a terminal perspective, appears to be a transmission from a single large cell [48]. This technique will be beneficial especially if the density is high, although it can lead to higher latencies due to the MBMS setup time.

2.4.2.1 C-V2X based CA and DEN service

In order to investigate the performance of cellular networks for VSC, the ETSI evaluates different parameters like the vehicle density, broadcast support, or environment on the network performance using either Universal Mobile Telecommunications System (UMTS) or LTE networks in [48]. It shows that cellular networks are not able to fulfill the CAM delivery requirements when using unicasts, even for relatively low vehicle densities. Vinel draws the same conclusion in [49]. He shows that reducing the transmission rate or filtering the messages is sometimes beneficial.

However, cellular networks are useful in addition to Wi-Fi based CA service. The authors in [50] show that the advantage of cells can be used at urban intersections, where the communication between vehicles is shadowed due to obstacles. They propose to disseminate uploaded CAMs to stations close to the intersections, which are not in Wi-Fi communication range, but would benefit from the awareness provided

by the CAM. Tung et al. discuss a similar approach in [51]. Considering the fact of LOS communication, groups of vehicles are treated as a cluster based on their road segment. Each cluster has one cluster head which is responsible to aggregate and upload the received CAMs from neighboring vehicles to a BS which in turn sends it to other NLOS cluster heads to overcome shadowing. The receiving cluster head disseminates the CAM via its Wi-Fi interface to the neighboring vehicles. As a result, the overall delivery rate is improved in comparison to Wi-Fi or LTE communication only. On the other hand, the latency of the forwarded messages is increased.

The reaction-based DEN service typically generates less traffic due to the limited lifetime and number of senders involved in the transmission of DENMs. The main challenge is that multiple stations recognizing an event transmit DENM immediately. Using IEEE 802.11p communication, each message will be treated independently in terms of forwarding and content. The backend server of a cellular network can act as a reflector and aggregator in this case. When doing this, the network load is reduced by filtering the uploaded messages and aggregate similar content to one consolidated message. Furthermore, due to the unicast transmission, the transmitting station receives an acknowledgement and thus does not need to repeat the message. Another benefit is that a cell can cover a huge area, although there are no vehicles nearby, and the message can be routed based on the geographic positions to all designated stations. The use of the LTE-based DEN service results in a much more reliable solution compared to *GeoNetworking*-based communication via IEEE 802.11p as demonstrated in [48, 52]. Kihl et al. evaluate the MBMS service to periodically broadcast DENMs to a cell in [53]. The authors conclude that LTE is well suited for the DEN service, while for the CA service and in dense areas, IEEE 802.11p-based communication clearly outperforms LTE due to its scheduling-based latency.

2.4.2.2 Comparison of IEEE 802.11p and C-V2X

A comparison of different important values for VSC for IEEE 802.11p and C-V2X (UMTS/LTE) is given in table 11. In the following, LTE is considered as the C-V2X access technology, because it offers an overall better performance compared to UMTS and its enhancement High Speed Packet Access (HSPA).

COVERAGE AND MOBILITY The coverage area of usual IEEE 802.11p communication is limited to the communication range of each node. Studies show that the maximum range can vary between 300 m and 1 km under LOS conditions. LTE relies on a cellular deployment of BSs offering a wide area coverage of up to 100 km. Furthermore, LTE offers a suitable mobility support with speeds of up to 350 km/h. Unlike the ad-hoc domain of IEEE 802.11p, LTE does not fully support D2D communication, yet. Thus, the coverage is limited to the amount of BSs deployed. It is increased by taking co-deployed cellular wireless technologies (UMTS) into account. The HSPA coverage and the LTE coverage in the European Union have already been at a very high level of 97.3% and 79.4%, respectively, in 2014 [54]. LTE will also provide a connection between stations if direct V2V communication is not possible due to low vehicle density or obstacles. Because of its coverage and mobility support, LTE can be favorable for V2X-communication. However, backup solutions (e.g. cellular D2D or Dedi-

cated Short Range Communication (DSRC)) for non-covered areas are necessary for a reliable service.

MARKET PENETRATION AND TRANSMISSION COSTS Since LTE and its predecessor UMTS are already under commercial usage, they come up with a high to very high market penetration compared to IEEE 802.11p. The latter suffers from the typical chicken-and-egg deployment problem, i.e. a certain penetration rate is required to support the application effectively, but it will not be deployed without this functionality. LTE is already available in nearly everybody's pocket via a mobile device which also can be used in vehicles as a cellular based ITS station. While IEEE 802.11p frequencies are located in a licensed and free of charge spectrum, LTE relies on the transmission via mobile operators. These operators pursue commercial interest and thus will charge a fee for any transmission.

CAPACITY As depicted in table 11, LTE achieves comparably high bit rates of up to 300 Mbit/s or 1000 Mbit/s for LTE-Advanced (4.5G). With the latest releases, HSPA+ has been developed to use the techniques developed for LTE, like Multiple Input and Multiple Output (MIMO) support and higher bandwidth utilization allowing data rates of up to 672 Mbit/s. These values clearly outperform the maximum bit rate of IEEE 802.11p of 27 Mbit/s. Furthermore, a higher throughput is achieved by a denser LTE network deployment. For applications with a high data transmission rate like video or voice transmissions, LTE is the preferable solution.

LATENCY The Latency is one of the key factors for VSC and needs to be below a critical threshold to fulfill the application requirements. Typical latencies for IEEE 802.11p-based short range communication are in the range of a few ms. Since communication via LTE always needs to run through the whole network path, the latencies are typically higher, but still low (10 ms). A critical part is the connection establishment time between a device in idle mode and the BS which usually takes more than 50 ms. Since vehicles do not need to save energy at this level, the devices should be configured in a way to always stay in the connected mode to avoid connection establishment delays for CAM transmission. However, non-time critical transmissions like DENMs or IP traffic are not heavily distorted by these latencies.

The complementary use of IEEE 802.11p and C-V2X can significantly increase the communication performance and the application support [48]. While IEEE 802.11p is still best suited for the CA service due to its native broadcast and D2D mode, LTE can be efficiently used for other applications like *infotainment*, *comfort*, and *traffic efficiency*, as long as centralized control or information are beneficial or necessary [47, 59]. Cluster-based schemes, which aggregate and upload CAM information, have been investigated and found helpful to enhance IEEE 802.11p communication with a centralized perspective via LTE [60, 61, 62, 63]. Table 12 summarizes the complementary usage of the access technology for V2X communication and its corresponding application class. Considering the results from recent research, CA shall be maintained by IEEE 802.11p via the dedicated control channel at 5.9 GHz, while the other dedicated resources (ITS-G5[A,B,D] service channels) can be used for C-V2X.

Table 11: Comparison of wireless communication technologies considerable for V2X [47, 55, 56, 57].

Feature	802.11p	UMTS	LTE	LTE-A
Channel bandwidth [MHz]	10	5 ¹	1.4, 3, 5, 10, 20	up to 100
Frequency bands [GHz]	5.855 – 5.925	0.7 – 2.6 ¹	0.7 – 2.69	0.45 – 4.99
Bit rate [Mbit/s]	6 – 27	2 ¹	up to 300	up to 1000
Latency [ms]	< 10	> 50	> 10	
Max range [km]	0.3 – 1	10 – 30	100	
Coverage	Intermittent	Ubiquitous		
Capacity	Medium	Low	High	Very high
Mobility support	Medium	High	Very high (up to 350 km/h)	
Broadcast support	Yes	MBMS	eMBMS	
V2I support	Yes			
V2V support	Native (ad-hoc)	No		Yes (D2D)
Market penetration	N/A	High		Potentially high
Transmission costs	Low	High		

1) Higher data rates of up to 672 Mbit/s can be achieved by using the UMTS enhancement HSPA+ [58]

2.4.2.3 5G Features for C-ITS

New technologies are not deployed all of a sudden. Instead a smooth evolution from services that can be operated in today's cellular networks towards more sophisticated services based on future 5G technologies is expected. Thus, 5G communication technologies will provide the basis for developing a huge variety of new applications, including those considered for V2X communication on the one hand, and on the other the requirements for 5G will be defined by the demands that arise.

Recently, the *METIS* project has presented its final report, including the technical goals, requirements, use cases, and much more for 2020 5G cellular networks [8]. Some of the key features [64] compared to LTE Release 8 are

Table 12: Access technologies that fit best to the requirements of an application class for complementary usage of IEEE 802.11p and C-V2X.

Application class	Technology		
	Main	Enhancement	
Infotainment	C-V2X	-	
Comfort			
Traffic efficiency			IEEE 802.11p
Safety	CA service	IEEE 802.11p	C-V2X
	DEN service	C-V2X	IEEE 802.11p

- 1.000 times higher mobile data volume per area
- 10-100 times higher number of connected devices (300.000 per AP)
- 10-100 times higher typical user data rate (10 Gb/s)
- 5 times reduced End-to-End latency (< 5 ms)
- Reliability of 99.999%

with similar costs as today's networks. Stakeholders agree that 5G needs to significantly increase the service requirements in terms of reliability, availability, and latency which current technologies can not provide. Road safety systems, for example, require low latencies and a very high reliability even under poor radio channel conditions (cf. table 10).

Device-to-Device (D2D) Communication

While 5G is handled as an enabler for usage of D2D communication, its predecessor LTE-Advanced already supports this feature. Doppler et al. show that the usage of D2D communication can significantly reduce the latency [65], because the long delay caused by the backbone network will be avoided. Therefore, a logical link between two devices is established which bypasses the cellular infrastructure and enables a direct communication. Fodor et al. reveal that this feature can help to increase throughput, hop gain, and higher spectrum efficiency compared to infrastructure-based cellular communication [66]. The authors of [67] evaluate a self-defined LTE-based D2D-communication scheme for VSC. They further "illustrate that the mechanism's flexibility and extensibility makes LTE-Direct a good complementary technology to DSRC for periodic vehicular safety communications". Khelil et al. [68] investigate recent D2D research efforts and their suitability for V2X applications. They show that current works ignore high mobility and QoS requirements which are critical requirements for VSC.

The main benefit of future 5G communication systems is the potentially high market penetration which allows to overcome the chicken-and-egg deployment problem of IEEE 802.11p. With its included feature of native D2D communication and use cases for VSC, including the consideration of high mobility, latency, and reliability requirements, 5G becomes a considerable solution for V2X [8]. Recently, several commercial partners have founded the 5G Automotive Association (5GAA) with the declared aim to provide non-complimentary Cellular Vehicle-to-X (C-V2X) based on LTE-A and 5G. With the usage of provided D2D communication, they state that C-V2X outperforms IEEE 802.11p and makes it obsolete [5]. Besides that, D2D allows the integration of mobile devices into the vehicle domain such that the safety-relevant information can be directly connected from the mobile device in the context of Vehicle-to-X-to-Device (V2X2D) communication.

Nevertheless, 5G is not yet standardized and further investigation on the suitability of C-V2X needs to prove that it can be used as a stand-alone approach for VSC. IEEE 802.11p to the contrary was evaluated in depth and many of the results have already been considered in recent standards like the DCC. Furthermore, 5G-based ad-hoc D2D communication does not influence the general architecture of the ITS-G5 stack.

Indeed, it can be considered as an enhancement of the old IEEE 802.11p protocol, which has not been updated since 2010 [27].

In this section, we provide an overview of the principles of congestion avoidance and control, and subsequently present algorithms used for congestion and awareness control in VANETs. We briefly explain the principles used in other networks, including TCP, the input parameters for congestion control in VANETs in section 3.1. We discuss the objectives of congestion avoidance and control algorithms under the aspects of fairness and awareness in section 3.2. Finally we present a classification of the algorithms based on the controlled parameter in section 3.3. At the end of section 3.3, we provide a summary of the used techniques for VSC and present the overview of the approaches developed so far.

3.1 BASIC CONCEPTS

3.1.1 Congestion Control and Avoidance

According to Jain et al. [69], there are three categories of control, namely: flow control, congestion control and congestion avoidance. While flow control aims at protecting the destination from being flooded by the source, congestion control is a scheme which "protects the network from being flooded by the users (transport entities at source and destination nodes)" [69]. Congestion avoidance characterizes a control approach which tries to keep the network within the optimal operating area. Flow control prevents the buffer at the receiver from overflow and only concerns one single source-destination pair. Congestion control and avoidance address the input of any node interacting with the network and thus fits better for wireless networks.

In figure 12, the relationship between congestion avoidance and control is illustrated. The figure shows the throughput, response time and power as a function of the offered load within the network, where power quantifies the efficiency denoted by the ratio of throughput and response time [69]. While throughput is first increasing with increasing load, a point of saturation is reached, when the injected load reaches the network capacity. In case of a further increase of the load, the throughput is drastically decreased and drops down to zero: a congestion collapse appears. At this point, buffers overflow throughout the network and no packets will be delivered in consequence. This point is denoted as the *cliff*. Congestion control has the objective to avoid a congestion collapse by preventing the network from passing the cliff on the one hand and if a collapse is unavoidable, help the network to get back to a point before the cliff.

The response time increases with an increase in the load due to increased buffering delay. If the cliff has been passed, the response time reaches infinity, because of the overflowing buffers. One might want to either optimize the throughput and thus have its network work close to the cliff, or optimize the response time. However, the trade-off is denoted by the power curve, where the objective is to minimize response time while maximizing the throughput on the other hand. The power curve has its

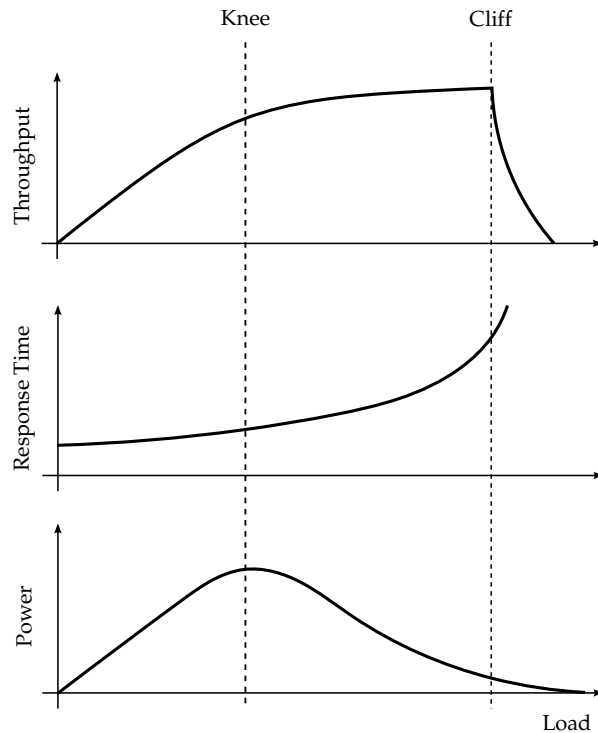


Figure 12: Illustration of the operating area for congestion avoidance and control [69]

maximum before the cliff, where the throughput is stagnating and the response time increases significantly. The maximum in the power curve is denoted as *knee* and the objective of congestion avoidance is to keep the network load near it.

Jain et al. describe the basic components of a congestion avoidance scheme categorized by a feedback and a control part in [69]. The feedback part is responsible for the preprocessing of the measured feedback data from the network and consists of *congestion detection*, a *feedback filter* and a *feedback selector*. The objective of the control part is to take a suitable action based on the received feedback by implementing a *signal filter*, a *decision function* and an *increase/decrease algorithm*.

OPEN- AND CLOSED-LOOP CONTROL In the control theory, there are two major principles of controlling a system, namely open- and closed-loop control.

In an open-loop controlled system, also called non-feedback control, the control action from the controller is independent of the system output. It does not use feedback in order to reach the desired system state, instead accurate models are used. A good example of an open-loop system is a heater, where the aim is to achieve a certain room temperature by turning on the heater for a certain amount of time. Based on the room size, the initial temperature and the heating capability of the heater, an open-loop controlled system can control the heater in order to reach the target temperature. However, open-loop systems can not react to external (unknown) disturbances. In the example, the effect of an open window will not be recognized.

Closed-loop control, also called feedback control, on the other hand utilizes feedback of the controlled parameter as additional input for the control process. If we apply a temperature sensor in the heater example, we can create a closed-loop controlled system, where the temperature is the system output. The objective of a

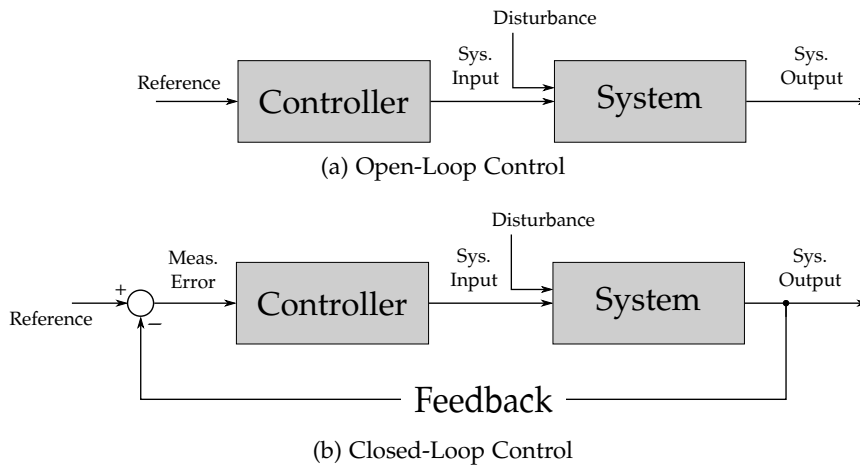


Figure 13: Illustration of open- and closed-Loop controllers

closed-loop control system is to reduce the deviation between the reference and the feedback to zero. Thus, external disturbances are considered in the control process. The afore mentioned congestion avoidance scheme utilizes feedback and can be considered as closed-loop control.

Open-loop control is very stable, easy and cheap to implement, but can not react to external disturbances due to missing feedback. Open-loop control thus can be used for systems, where the controlled variable is not affected by external disturbances and the behavior of the system can be accurately modeled. Closed-loop control is usually complex and in consequence difficult to develop and construct leading to increased costs and maintenance. Furthermore, due to the feedback control and unlimited states, a major issue for closed-loop control is stability. However, closed-loop control benefits from flexibility due to consideration of feedback information.

3.1.2 Congestion Control in Networks

TRANSMISSION CONTROL PROTOCOL Shortly after developing the TCP/IP stack for the internet access, TCP congestion control was introduced in the late 1980s as a host-centric, feedback-based scheme. It was supposed to prevent the congestion collapse, which was expected to occur due to the immediate transmission of data of any source to the network, which was only limited by the receiving hosts *advertised window*. The major idea of TCP congestion control is to determine how much capacity is available in the network for each source, such that the maximum amount of packets which can be transmitted safely is known. This congestion window named amount of packets is the control variable of TCP congestion control and it is measured in the unit of Maximum Segment Size (MSS). For the adaption of the congestion window, a binary scheme called AIMD is used. There are multiple variants of TCP congestion control used nowadays and research in this area is still going on.

Besides flow control, TCP needs to find the bottleneck capacity, which might be at any place within the network path. In order to do so, congestion detection is based on the Round Trip Time (RTT) of a packet, i.e. the time between transmission of the frame and reception of the ACK. This RTT is used to calculate the so called

Retransmission Timeout (RTO), which is used to decide whether a packet has been lost due to missing ACK.

The rate adaption scheme of TCP basically consists of two parts: *slow start* and *additive increase*. Slow start takes place at the beginning of a session or whenever a RTO event occurred. During the slow start, the congestion window is increased exponentially, i.e. it is increased by one MSS for each ACK received. If the slow start threshold is reached, TCP transits to the additive increase phase. During this phase, the congestion window W is increased linearly by adding $MSS * (MSS/W)$ to it after receiving an ACK. This will result in an increase of approximately one MSS when all bytes in the congestion window have been acknowledged. Whenever a congestion is detected based on the RTO, the slow start threshold is set to half of the current congestion window and the current congestion window is reset to one MSS. Afterwards slow start phase is triggered. This scheme of additive increasing and multiplicative decreasing of the congestion window leads to the well known sawtooth pattern over time.

The afore mentioned combination of slow start and additive increase is called TCP *Tahoe*. Besides this, TCP *Reno* implies another mechanism called *fast recovery*. Here it is assumed that the reception of three duplicated ACK indicate that at least some packets still got through the network, although others failed. If this *fast retransmit* called detection triggers, the congestion window is halved and retransmission takes place immediately instead of waiting for RTO to expire. By halving the congestion window instead of setting it to one MSS, slow start phase is avoided and pure AIMD is used instead.

Nowadays, there exists a huge variety of different implementations for the TCP congestion avoidance, which enhance the aforementioned phases in different ways. While the default algorithm for TCP in *LINUX* systems is TCP *Cubic*¹, computers running Windows as operating system rely on *Compound TCP*². However, the detailed implementation is out of the scope of this work.

TCP over Wireless

TCP congestion control is designed for reliable links, where bit errors are unlikely to happen. A failed transmission thus indicated congestion on the channel. However, wireless links are unreliable and bit errors, as well as interference occurs frequently. TCP would indicate this failed transmissions as congestion although the link is not congested resulting in a degradation of performance [70, 71, 72].

In order to engage the problem, different approaches have been described which can be categorized in three categories: *end-to-end protocols*, *link-layer protocols*, and *split-connection protocols* [71]. End-to-end protocols utilize further information provided by a combination of selective ACKs, acknowledging the reception of single packets and explicit congestion notification to distinguish between congestion based transmission failure and bit errors. The link-layer protocols aim at hiding the packet losses on the wireless link from the TCP layer by employing forward error correction and local retransmissions. The TCP layer will perceive a higher delay, but will recognize a channel with good QoS. For the third category, split-connection protocols, the

¹ NC State University, 10/02/2017, <https://research.csc.ncsu.edu/netsrv/?q=content/bic-and-cubic>

² Microsoft, 10/02/2017, <https://www.microsoft.com/en-us/research/project/the-compound-tcp-for-high-speed-and-long-distance-networks>

end-to-end connection between two devices is divided into a wired and wireless part and these segments are controlled separately. However, those approaches encounter individual drawbacks each and require changes to the TCP protocol itself.

WIRELESS NETWORKS Wireless networks utilize congestion control approaches which are specially designed to the characteristics and application requirements. Wireless networks are often affected by small and large scale fading or interference, such that there are more degrees of freedom which can be considered for congestion control. Furthermore, the structures of wireless networks are often highly heterogeneous. Some networks, like cellular networks and typical WLAN are managed centrally via a BS, other networks like Wireless Sensor Network (WSN) and mobile ad-hoc networks are mostly self-organized.

Congestion control in cellular networks is typically based on Transmit Power Control (TPC), where the Transmission Power (TP) is increased or decreased in order to avoid interference or increase the communication range. A major issue for voice traffic is to maintain a significant high SINR to fit the QoS requirements in both directions, where uplink power control is typically more challenging due to the overlapping signals of multiple mobile devices at the BS on the one hand and the restrictions regarding the energy consumption of the mobile device on the other. Possible solutions for TPC in cellular networks are reviewed in [73, 74].

In typical WLAN, mobile devices are connected to an Access Point (AP) in order to get access to the Internet. Due to path loss and fading effects, the link quality can be significantly degraded when the distance to the AP is increased. This can be counteracted by employing TPC or Data Rate Control (DRC). The data rate is adjusted by applying a less complex coding scheme, such that a lower SINR is required for decoding. A commonly used technique for DRC is Auto Rate Fallback (ARF), where the data rate is decreased after a sequence of failed transmissions and vice versa [75]. Unfortunately ARF does also react if transmission fails due to frame collisions, which is counterproductive [76, 77]. Kim et al. propose to use the RTS/CTS scheme to distinguish between frame collisions and fading after a failed transmission. Further reading about DRC in 802.11 wireless networks is provided in [78]. For TPC there are different approaches, which are similar to those used for cellular networks. The objective can be to save energy for the mobile device [79], mitigate interference at neighboring AP [80] or even combine DRC and TPC to maintain link quality even with lower TP [81].

WSN are deployed to collect and monitor environmental data in wide areas. They consists of cheap micro computers with wireless transmission capabilities. The network topology allows to communicate via multi-hop communication with a BS, which will aggregate and forward the collected data. A major issue in WSN is the lifetime of the sensors, because they are powered by batteries and have limited recharge possibilities. Message transmissions are a major contributor to the power demand and thus interference leading to waste of resources needs to be minimized. Several studies have focused on applying CC schemes for WSN focusing on Transmit Rate Control (TRC) based on e.g. binary algorithms like AIMD [82, 83, 84] or others [85, 86]. The control decision is based on either Channel Busy Ratio (CBR) measurements or buffer queue length [85]. Unlike typical WLAN, the nodes have restrictive access to power and thus the major objective is to decrease the TP to the

minimum necessary to maintain network connectivity [87, 88, 89, 90]. However, the BS can have an increased power output for the uplink in order to inform as many nodes as possible and reduce effort of forwarding.

3.1.3 Input Variables

Congestion control algorithms are part of control theory and most of them employ either open- or closed-loop control. In order to allow the functionality, the control module needs to gather valuable input to control the system variable. Depending on the objective of the algorithm, these input variables can differ a lot. A scheme which aims at maintaining awareness will need other input than one, which focuses on a fair resource allocation. However, for congestion control and avoidance the major objective is to keep the injected load below a certain threshold. Due to the system architecture of C-ITS, there are various methods to estimate this load.

CHANNEL LOAD The literature has come up with different approaches to quantify the channel load directly. We will discuss the *communication density* and *beaconing load* metric here and will further focus on the widely used CBR metric allowing a direct estimation of the load on the channel utilizing IEEE 802.11's CCA functionality.

The *communication density* metric is introduced by Jiang et al. in [91]. It describes the number of transmissions, which can be sensed on a road segment within a specific time interval. The communication density can be calculated as

$$CD = \rho \cdot r \cdot d_{TX}, \quad (3.1)$$

where ρ is the vehicle density in vehicles per km, r is the transmission rate in Hz and d_{TX} is the communication range. The communication density can be used to estimate the number of messages per unit of time and thus it quantifies the injected load based on a fixed capacity within the communication range. Furthermore, the authors show that the total communication density for a system is cumulative, i.e. for a highway, the sum of the individual road segments will give the overall communication density within this area.

Another approach similar to the communication density is proposed by Torrent-Moreno in [92] as *beaconing load*. The beaconing load is defined as "the average amount of load offered to the channel within a node's Carrier sense range" and can be calculated as

$$BL = \rho \cdot r \cdot 2d_{cs} \cdot M, \quad (3.2)$$

where d_{cs} denotes the carrier sense range in km and M specifies the message size in bytes. While the communication density quantifies the amount of messages sensed within a certain time, the Beacon Load (BL) quantifies the offered load within this time in bytes.

Channel Busy Ratio (CBR)

In the IEEE 802.11 standard, the CBR is defined as³

$$U = \left\lfloor \frac{t_{\text{busy}}}{t_{\text{total}}} \cdot 255 \right\rfloor$$

where t_{busy} is the time the station sensed the medium is busy and t_{total} is the total time measured [11]. The scaling factor of 255 is used for the over-the-air transmission of channel information in feedback frames. This metric is widely deployed due to its definition in the IEEE 802.11 standard. However, it does not specify how it needs to be implemented.

The ETSI specified a method in [94] which should be implemented by means of channel probing, i.e. the CCA function is evaluated at fixed, uniformly distributed time intervals. The channel is indicated as busy, if

- a detected packets signal level is higher than Thr_{DCC}
- the received signal level is higher than Thr_{CS} ,

where Thr_{DCC} is the default sensitivity threshold value for DCC and Thr_{CS} is the default carrier sensitivity threshold.

The estimation is done using the sampling approach which is defined by the following reference method:

- The received signal is segmented in *busy* and *idle* channel states: The channel is sensed *busy* for the duration of detected packets with $S \geq \text{Thr}_{\text{DCC}}$. Furthermore, the channel is sensed busy if the received signal level is higher than Thr_{CS} .
- N_p probes P of the channel busy signal are taken uniformly distributed within the measuring interval T_m . An estimation of the channel busy time is given by:

$$\text{CBR} = \frac{\sum_{n=1}^{N_p} (1, P_n = \text{busy})}{N_p}$$

where P_n denotes the n -th probe.

The measuring interval T_m shall be chosen long compared to the maximum packet length. The number of probes N_p is determined by the lowest assumed transmission duration given by packet size and the data rate. It should be high enough to grant stochastic evidence. Since used for this work, the CBR is reviewed in section 4.1, section 5.5, and section 6.3.1.

RELATED METRICS Both, communication density and BL can be calculated based on the vehicle density within the carrier sense range. The amount of vehicles within an area directly influences the injected load and thus is a crucial parameter, which can be used as an input for congestion control. Bansal et al. show in [13] that the observed resource utilization within an area is a function of the vehicle density. However, an accurate calculation of the vehicle density is a non trivial problem due to interference, heterogeneous message rates and fading effects.

³ Parts of this chapter are published [93] and are under copyright of the IEEE

In order to realize an approximation of the vehicle density, insights into the beacons need to be provided including the position and the ID of the nodes. The information within the beacons can be further used to determine congestion, if each beacon includes a sequence number [95]. Missing sequence numbers would indicate interference due to congestion and would lead to a reaction of the algorithm. However, the appearing problem is similar to the occurring issues with TCP over wireless. Further reading about vehicle density estimation is provided in [96, 97].

While reactive congestion control protocols objective is to control the channel load and thus implicit or explicit feedback is used, proactive protocols utilize further information from beacons or other sources in order to ensure awareness [98, 99, 100]. Therefore, information from the beacons like the position and the velocity of neighboring vehicles are used to satisfy the application requirements, while globally minimizing the channel load in order to prevent congestion. Furthermore, knowledge about the environmental conditions (urban, highway, street layout, etc.) is used for awareness control [101].

For feedback-based congestion control algorithms, the CBR metric is the most promising metric to quantify the load on the channel. The vehicle density gives analogue information and both metrics can be combined in order to minimize measurement inaccuracy [47].

3.2 DISCUSSION OF AWARENESS, FAIRNESS AND EFFICIENCY

Congestion control in VANETS needs to fulfill various requirements. Two major requirements are to maintain the awareness between the vehicles, which comes along with preventing a congestion collapse and maximizing the efficiency of the disseminated data. The efficiency of a network is often referred to as power of the network [102], which can be quantified by

$$\text{Power} = \text{Throughput}^\alpha / \text{Delay}.$$

This metric is based on infinite queue systems, where due to limited capacity, the delay is increased, if the offered load was increased, while the throughput is stagnating at a certain point. The objective is to maximize this power in order to maximize the efficiency obtained by the resource allocation. According to [102] the power is being maximized at the knee of the delay curve and the efficiency of other allocation can be quantified by [69]

$$\text{Efficiency} = \text{Power} / \text{Power at knee}$$

An optimal allocation however is one, which is fair and efficient. Thus, the available resources at the optimal allocation need to be shared between the participating nodes fairly. However, it is not a simple task to quantify the fairness of a congestion control algorithm, because there are many effects that can occur. Jain et al. [69] proposed

a metric that quantifies the degree of fairness. Given a set of flow throughputs (x_1, x_2, \dots, x_n) , the following function assigns a fairness index to the flows:

$$f(x_1, x_2, \dots, x_n) = \frac{(\sum_{i=1}^n x_i)^2}{n \sum_{i=1}^n x_i^2}$$

This index results in a number between 0 and 1, where 1 indicates the maximal fairness obtained, if all nodes have the same resource share. Considering another example, where just k nodes receive a fair share and the remaining $(n - k)$ nodes have a flow equal to zero, this index would drop to a fairness index of k/n . The same index can be used for non-homogeneous allocation demands. Therefore, x_i is defined as a_i/A_i , where a_i specifies the allocation of node i and A_i is the maximal allocation of the same node. Thus, a fair allocation can also be one, which does not allocate the same amount to each node, but rather a demand based fair amount.

Based on this fairness index, different allocations of the individual maximal share A_i can be defined in order to achieve a certain fairness. One of them is the principle of max-min fairness [103] and another famous principle is called proportional fairness [104]. According to [105], a max-min fair allocation can be defined as one for which "an increase of any rate within the domain of feasible allocations must be at the cost of a decrease of some already smaller rate". In other words, the minimal allocation is maximized. While proportional fairness aims at increasing the total use of the available bandwidth, max-min fairness fits better for VSC, where awareness is a critical requirement and nodes need to have a minimal share.

FAIRNESS AND AWARENESS IN VSC Congestion control can be considered as a resource sharing problem, where each of the participants wants to be treated equally. Thereby equally does not ultimately mean that all participants get the same share. It rather describes a certain level of fairness that needs to be applied. Typically, in computer networks, fairness is expressed in terms of throughput, i.e. the share of bandwidth for each user.

The term of fairness has been defined differently to encounter the special case of VSC by different authors. Based on the considerations of Tielert in [106], there are three principles of fairness: local, global and participation fairness. However, in VSC the aspect of awareness needs to be considered in the context of resource sharing, such that individual nodes can achieve a higher share than others. This principle is described as weighted fairness by Bansal et al. in [107]. An awareness control algorithm can furthermore achieve a share of the resources optimizing the awareness for each participant. In this chapter, we briefly describe the different aspects of fairness and discuss the influence on the awareness of participants.

A certain degree of fairness is always given, if the participants are treated based on a fixed set of rules. Each participant will react equally based on the predefined set. However, depending on the aim of a principle or algorithm, the definition of the rules and its parameters might not lead to the same resource share.

LOCAL FAIRNESS Local fairness is an often used principle among decentralized congestion control methods. For local fairness, it is assumed that nodes which are located close to each other perceive the same channel status. Thus, they observe the same resource utilization, interference level and other distortions. Consequently,

nodes which are closely located should be controlled to the same degree. This leads to a fair share of the available resources for the same region and thus is fair.

PARTICIPATION FAIRNESS In wireless networks, the local fairness principle can lead to a certain degree of unfairness, because nodes which are contributing to a far away congestion do not participate in the control of this congestion. Furthermore, the communication range in wireless networks is not deterministic, such that a node does not know to which degree it is contributing to a congestion at certain locations. However, if a probabilistic propagation is assumed, a threshold based maximal communication range can be determined. A node which is contributing to this congestion should also be aware of the channel status at this location and consequently controlled following the max-min fairness principle.

To achieve this participation fairness [14], cooperation between the nodes is necessary, i.e. the channel status information needs to be shared such that a node contributing to a congestion is aware of the channel status there. To achieve this Tielert et al. [14] suggest to append this information to the CAMs shared among the vehicles, which are aggregating and forwarding these information. In the consequence, a common perception of the same channel status information is achieved within an extended fairness range. Participation fairness follows the local fairness principle, but aggregated information within a certain fairness range is used rather than locally assessed data.

GLOBAL FAIRNESS Both, local and participation fairness are special cases of the global fairness principle. For global fairness, it is assumed that each node contributing to a congestion needs to be controlled. In [108] congestion control in the context of VSC is discussed. Following their discussion, it does not make sense to optimize the overall throughput of CAMs, if single vehicles' communication performance is degraded. Those vehicles which are not able to communicate state a risk for all vehicles and there communication quality should be optimized rather.

Thus, for global fairness max-min fairness should be applied, where each vehicle gets the same share of resources maximizing the minimum throughput and thus the vehicle with the lowest share. Unfortunately, due to unbound and probabilistic propagation true max-min fairness is hard to achieve in wireless networks. Tielert et al. [14] thus suggest to achieve global fairness by a best-effort approach following the participation fairness approach with a certain fairness range. In this thesis, we use this participation fairness approach as part of the global fairness principle. Thus, the term global fairness described the ability of the vehicles to achieve max-min fairness in certain situations.

WEIGHTED FAIRNESS Following the max-min fairness principle, global fairness aims at giving the same share to each participant within the fairness range. However, in VANETS vehicles need to have an accurate neighborhood awareness. A vehicle which is driving at a high speed changes its position more often and is a higher threat to the environment and subsequently communication should be prioritized. Weighted fairness as described by Bansal et al. in [107] joins local fairness with awareness. A higher communication priority can be assigned to individual vehicles or groups by applying predefined weights to them. This leads to different shares of

the same resources, where the shared amount is dependent on the weight given to the participants.

For weighted fairness, the share of resources is not equal and thus might be not fair. However, the decentralized rules are fair and participants with the same status will receive the same share.

AWARENESS Pure awareness describes most of the awareness control algorithms, which focus on controlling the amount of information within a certain region based on the utility of the information itself. Thus, the objective is to maximize the entropy of the channel. Therefore, no explicit fairness principle is used and the share of the resources is completely unconsidered. The algorithms prioritize high entropy (e.g. risky vehicles) and reduce redundancy and thus achieve awareness based fairness. Awareness control is often complimentary used with congestion control [109, 110]. Weighted fairness, where the weights are dynamically set can also be considered as awareness and congestion control [107].

3.3 CLASSIFICATION BASED ON CONTROLLED PARAMETER

For avoidance of congestion in VANETs, there are different degrees of freedom that can be considered. These degrees of freedom are spanned by the adjustable communication parameters. In [111], Weinfeld evaluates the effect of the individual parameters which are TPC, TRC, DRC, Packet Size Control (PSC), Carrier Sense (CS) threshold control, and CW control. He states that each of those parameters can help to mitigate channel congestion. While some like TRC will have a major effect, others like CW control have only marginal effect for congestion avoidance. Weinfeld concludes that applying any congestion control is better, than accepting the overall degradation of the communication due to a congested channel. In the following, we will provide an overview of proposed algorithms for congestion avoidance and control, as well as awareness control in VANETs with a special focus on VSC. The classification thereby is done based on the utilized communication parameters. For a very brief overview of the algorithms reviewed in this thesis, we refer to table 15.

3.3.1 *Packet Size Control (PSC)*

PSC is a method to adjust the packet size of a beacon by attaching or detaching data elements. Basically, the size of a beacon is defined by the safety applications running on top of the C-ITS protocol stack. However, the IEEE 802.11 standard allows a flexible size for a frame between 0 and 2304 bytes [11]. The size of a frame influences the network performance by the transmission time needed for a frame transmission, where a bigger size leads to increased transmission times and consequently higher utilization. In [112], Yin et al. show that the adjustment of a frames size is a trade-off between overhead and frame-loss. While longer frames have a better ratio of overhead to payload, they are more vulnerable to transmission errors and collisions. The authors conclude, that there is an optimal message size for every channel condition. However, CAMs have a fixed structure with mandatory elements that need to be transmitted at any circumstances, such that there is a lower border for the

frame size. On the other hand, long term information and optional data elements can be scheduled such that the transmission of longer CAMs fits the channel conditions.

Robinson et al. introduce a scheme called *message dispatcher* in [113] used to reduce the amount of redundant or unnecessary data elements of a beacon. The idea is to include only data elements, which are useful for the applications running on the vehicle itself or its neighbors. In this way, some data elements might be excluded completely unless used, while others are transmitted less frequently. The *message dispatcher* is extended in [114] by the concept of *predicted coding*. Robinson et al. propose to reduce the frame size of status updates by applying estimation methods and attach only necessary data elements to the beacons, if the estimation error is sufficiently large.

CERTIFICATE OMISSION Another promising focus on frame size reduction is the omission of certificates. Certificates in VSC are used to ensure the authenticity and integrity of the beacons. A proposed strategy is to transmit these certificates less frequently and cache them at the receiver, while a CAM needs to have a signature which can be verified using the afore mentioned certificate. This approach is similar to the transmission of i and p/b frames in video transmission, where the i-frames are needed to utilize the information of the p/b frames. In [115], three different certificate omission schemes are compared:

While Periodic Omission of Certificates (POoC) [116] relies on a periodic dissemination of the certificate in every n th frame, Neighbor based Certificate Omission (NbCO) [117] transmits the certificate whenever there is a change in the neighbor table. Based on the analysis of the aforementioned schemes, the authors of [115] introduce Congestion based Certificate Omission (CbCO), which includes the certificate in every n th CAM, where n depends on the size of the neighbor table. By doing this, they achieve a congestion dependent reduction of the message size

A major issue for certificate omission is the loss of packets due to the reception of CAMs, which signatures can not be verified, because the certificate is not available. This situation can occur, if the CAM including the certificate is lost due to collision, bit errors, or packet drops or the vehicle is new to the neighborhood. Feiri et al [115] show that the amount of frames lost can be significantly reduced by CbCO and it is stated, that up to 70 CAMs can be received in a row without a valid certificate. Those messages are consequently dropped, which if send at a rate of 10 Hz, will lead to an Packet Inter-Reception Time (IRT) of up to 7 s.

3.3.2 Data Rate Control (DRC)

In DRC schemes, the modulation scheme and coding rate can be adjusted to achieve higher or lower data rates. This can have a significant impact on the congestion level. Higher data rates benefit from lower transmission times leading to an increased message capacity for CAMs with a fixed size. On the other hand, the more complex the modulation scheme is, the less is the robustness indicated by the high SINR requirements (cf. table 6). In consequence, the effective transmission range is reduced, while the interference range is maintained. A major benefit is, that DRC can be applied without violating application requirements in terms of transmission rate and communication range.

Jiang et al. [33] show, that the optimal data rate selected for VSC is 6 Mbit/s. While optimizing the PDR under usual conditions, a rate of 9 Mbit/s and 4.5 Mbit/s performs better for congested and unloaded conditions respectively. This simulation based finding is confirmed by measurements conducted by Bai et al. in [118]. They show, that a data rate of 6 Mbit/s clearly outperforms high data rates due to the more robust modulation scheme. Fernandez et al. state in [119] that based on an enhanced scheme for channel estimation, a data rate of 12 Mbit/s optimizes the PDR for packet sizes of up to 600 Bytes. However, the evaluations utilize the PDR as performance indicator which does not reveal the application level performance.

Due to the wide acceptance of the default rate, there is a limited amount of studies focusing on DRC schemes. Yang et al. [120] use a simplified version of the DCC [94] (cf. section 3.3.7) which uses DRC only. The authors argue that the joint adaption of the multiple transmission parameters controlled by DCC will degrade the performance. However, the adaption progress is state-based with only 4 states representing disjunct data rates, where the transitions between the states depend on fixed CBR thresholds. DR-DCC [121] applies this approach, but utilizes all available IEEE 802.11p modulation schemes resulting in 8 different states. Math et al. propose a similar scheme called PDR-DCC in [122] described as packet-count based decentralized data-rate congestion control. Instead of using predefined CBR thresholds for the transitions, the authors propose to use a combination of packets sensed and a target CBR to adjust the data rate. The authors show, that the algorithm leads to a convergence of the CBR to the desired target and state, that their algorithm outperforms state-of-the-art protocols like *LIMERIC*.

Yao et al. introduce a data rate adjustment scheme called LORA in [123]. Unlike DCC the authors propose to use the PDR as indicator for the channel quality and adjust the rate accordingly. Therefore, each node needs to estimate the average packet loss ratio based on the number of nodes within the neighborhood and a pathloss model. This average packet loss ratio can be subdivided into a fading based and interference based loss. The authors suggest to adjust the rate based on this two loss types, i.e. the rate is increased if losses occur due to interference and maintained low otherwise to decrease the necessary SINR for decoding.

In [124], Wischhof et al. propose an utility based congestion control called UBPFCC. An application-specific metric estimating the utility of transmitting an individual data packet at each node (*utility function*) is defined and used in order to prioritize nodes and messages with high entropy. Therefore, the calculated utility is appended to the beacons and shared among the neighbors. Based on this remote information, an average utility value is calculated and each node allocated a share of the available band-width proportional to its utility. The authors state, that UBPFCC avoids the "starvation of individual nodes and significantly increases the efficiency of information dissemination." However, applying this scheme to VSC is problematic, because the 802.11p standard considers 8 distinct data rates only. Furthermore, packet queues as used by UBPFCC are not suited for VSC, because queued packets are replaced by newly arriving ones.

3.3.3 Contention Window Control (CW)

The CSMA algorithm employs a backoff mechanism, where a random number is drawn from the region of possible numbers limited by the Contention Window (CW). While in backoff and the channel is indicated idle, the node has to wait the drawn amount of time slots until access to the channel is granted. The size of the CW has a direct influence on the collision probability on the one hand and the access delay on the other. In [125], Bianchi analyses the performance of the IEEE 802.11 DCF function. It is shown, that assuming greedy nodes, the collision probability depends on the number of contending stations and the CW

$$P_{\text{coll}} = 1 - \left(1 - \frac{2}{\text{CW} + 1}\right)^{(n-1)}, \quad (3.3)$$

if no exponential backoff is considered. Bianchi shows, that the optimal CW in terms of system throughput is given by

$$\text{CW}_{\text{opt}} = n\sqrt{2T_c^*}, \quad (3.4)$$

where T_c^* indicates the average duration of a frame collision measured in time slots.

However, the values that are suggested to be optimal by the afore mentioned equation would lead to high access delay in case of high vehicle density. According to [106], for 40 vehicles in transmission range $\text{CW}_{\text{opt}} = 382$ results in a worst case access delay of 5 ms. It is argued, that this access delay is not acceptable for VSC, where packets are transferred with intervals of 100 ms. On the other hand, it is shown, that the Packet Error Rate (PER) can significantly influence the IRT of CAMs and thus mitigating the effect of frame collisions by adjusting the CW might be desirable. The authors of [126] evaluated the impact of CW adaption on the performance of beaconing in VANETs. While analyzing the effect on PDR, delay and IRT, they concluded that adjustments of the CW as performed in their experiment do not improve beaconing performance.

In the following, we provide an overview of studies focusing on congestion control by the adaption of the CW.

REDUCTION OF THE PACKET ERROR RATE A major aspect of CW adjustment is to reduce the amount of frame collision in order to increase the PDR under saturated conditions. Balon et al. describe a simple scheme in [127], where the CW is adjusted based on the current PDR, estimated based on the sequence number included in the packets. If the PDR has increased by a certain threshold, the channel is assumed to be less congested and the CW is decreased consequently. In [128], Mertens et al. propose a scheme to adjust the CW based on the perceived PER on the one hand and the number of neighbors on the other. The CW therefore is proactively set to the optimal value based on the number of neighbors [125] and subsequently adapted in case the PER threshold is violated using Multiplicative Increase Multiplicative Decrease (MIMD). Stanica et al. propose a similar setting of the CW based on the number of nodes in the neighboring table [129, 130]. An adoption of the CW based on the vehicle density is also suggested by Hsu et al in [131]. In [125], it is shown, that the optimal performance is achieved for a CW where the time the channel is

idle due to back-off procedure equals the time the channel is occupied by collisions. Stanica et al. propose to use this equality and adjust the CW such that it converges to this values by applying MIMD [130]. In [132], Gomez et al. introduce a drop ratio dependent delay, which is added to the MAC layer backoff at the application layer. This delay is calculated as the product of the drop ratio and the CW.

In [133], Rawat et al. introduce a joint scheme utilizing TPC and CW adjustment, where the later one is adjusted based on a collision rate threshold. Zhao et al. also utilize the collision rate in order to set the CW in [134]: If a packet loss is indicated due to a collision, the CW will be increased, while if it is lost due to expiration the CW will be decreased to allow faster access. Stanica et al. also suggest to adopt the CW whenever a CAM is replaced in the queue due to expiration in [135]. They propose a back-off strategy starting with a large initial CW to mitigate packet collisions and half it whenever a CAM is expired. When a CAM was successfully transmitted the CW is reset to the original large value.

Besides the channel quality indicators (CBR, PER,...), there are also a few protocols adjusting the CW based on environmental information. In [136], Wu et al. suggest a dynamic adjustment of the CW which is based on the average speed within the neighborhood. They state, that speed is inversely proportional to the density and thus the collision rate is increased for lower speeds. It is proposed to adjust the CW based on the average speed within the neighborhood, where higher speeds result in lower CW. Kloiber et al. [137] introduce a concept called geo-backoff, which utilizes geographical positions in order to set the backoff counter. Instead of randomly drawing a backoff, they assign position-dependent back-off values drawn from an enlarged CW to each vehicle. Thus, it is guaranteed that vehicles within close vicinity will not have the same backoff value.

Combining multiple input-parameters in order to mitigate estimation errors is applied by Lu et al. in [138]. The authors use functions to set the CW, which are based on the number of neighbors [125], the stopping time and the speed of the vehicle [130]. In a second step, they set the CW based on the weighted sum of the individually calculated CWs.

ADJUSTMENT OF EDCA EDCA grants different access categories for packets arriving to the MAC layer. A packet is queued in one of the AC based on the assigned priority. In [139], Zang et al. propose to freeze all other AC queues, if a safety message is transferred. In order to decrease the load, the authors further suggest to restrict the access by adapting the individual CW of the AC based on CBR thresholds utilizing MIMD. However, CAMs are usually transmitted to the Control Channel (CCH) and no other messages should go there. Sharafkandi et al. [140] introduce a scheme, which utilizes EDCA for CAM dissemination in order to reduce the PER by implementing two schemes: *AC isolation* and *virtual devision*. For AC isolation, the access timings of the different AC are set such that the overlapping slots are eliminated, i.e. a packet with higher priority will safely get transmitted before the packet with lower priority can access the channel. A more sophisticated concept is applied by virtual devision. Although, CAMs usually fall into the same AC, the authors suggest to spread the CAMs across different AC. A CAM is assigned to an AC based on a fixed ratio, which is determined by the PER. By applying these two schemes, the overall PER can be decreased.

A cross-layer architecture using the CBR and the vehicle density as input for a joint TPC, TRC, CW congestion-control protocol is introduced by Puthal et al. in [141]. All transmission parameters are adjusted separately and the CW is multiplicative increased up to the maximum CW based on a predefined threshold until the congestion status indicates relaxed conditions, where the CW is reset to the minimum value. However, this mechanism is applied to the AC responsible for non-safety messages only, while the CW for safety related packets is maintained.

AWARENESS CONTROL Most studies are focused on the reduction of collisions due to insufficiently set CW. However, in some cases, an expired information is more critical than an increased overall PDR. Thus, some approaches focus on increasing application level reliability, or decreasing the congestion by utilizing the utility of a CAM. In [142], a scheme is introduced, which takes into account the utility value of a packet and sets the CW accordingly. A similar approach is described by [143], where the CW is set based on the "emergency" level of a vehicle in order to grant short access times for urgent information. While aforementioned approaches are used for DENMs, the schemes of Stanica et al. [130] can also be applied to CAMs. The authors suggest to adjust the CW proportional to the vehicle status as an estimator of the traffic congestion level. The first idea is to adjust the CW proportional to the time the vehicle has stopped. The authors state, that if this time is small, the vehicle will be in free-flow. A more complex adjustment also utilizes the speed and changes in acceleration (jerk) with the same aim, where the CW is set inversely proportional.

3.3.4 Carrier Sense Threshold Adaption (CS)

The CS threshold is a parameter used by the CCA function of the Physical Layer Convergence Protocol (PLCP) as part of the CSMA algorithm. By determining the energy level present on the channel and comparing it with the CS threshold, a channel is indicated as busy or idle by the CCA function. Assuming fixed propagation conditions, the CS threshold defines the area in which ongoing frame transmissions can be sensed successfully. The threshold plays an important role for the occurrence and detection of hidden terminals. According to [144], the following conclusions regarding the CS threshold can be assumed:

- A too high CS threshold causes strong degradation of the communication range due to hidden stations but keeps the average medium access delay low.
- A too low CS threshold wastes bandwidth by limiting spatial reuse leading to significant medium access delay but few collisions occur on the channel.
- Due to continuously changing network topology and varying channel conditions there is no optimal static CS threshold.

Stanica et al. argue, that "the CS threshold proposed in wireless multi-hop networks tries to find a balance between hidden and exposed stations and therefore they do not fit well with VSC" [145]. In addition it is argued, that the threshold currently defined by the IEEE 802.11p standard [27] is optimized for single-hop infrastructure based WLANs and thus does not suit the special requirements of VANETs.

LINK ASYMMETRY According to [80], TPC can lead to asymmetric links in which a node with a high TP can transmit all the time, while another one does not get access to the channel, if both utilize the same CS threshold. Thus, asymmetric links will increase unfairness and result in the exposed node problem, because it would always sense the channel busy, while the high TP node would always sense the channel idle. Thus, to ensure link symmetry for the usage of TPC, the authors suggest to modify the CS inversely proportional. In other words, a node with a high TP needs to sense the channel more carefully (lower CS threshold) in order to detect nodes utilizing a low TP. The authors find, that applying this algorithm can significantly increase the throughput of the network. Fuemmeler et al [146] have the same finding and suggest to set the product of the TP and CS thresholds to a fixed value. They furthermore describe a dependency of the CS threshold on the number of worst-case interferers k and consequently compute the optimal CS threshold as function of the TP and k .

However, as many other studies considering adopting the CS, the aforementioned studies are conducted for infrastructure based WLAN assuming unicast communication and transmission queues.

CS ADAPTION FOR VSC In [147], Schmidt et al. propose to adjust the CS in order to speed up the access delay. The idea is to trade-off a faster access by a higher collision rate for far away nodes. The CS threshold is adjusted based on the time a CAM is queued in the MAC layer. The CS value therefore is increased by an offset based on exponentially decreasing time intervals, i.e. the CS value will be increased, whenever the CAM is waiting for a fraction of its generation interval ($1/2$, $3/4$, $7/8$, etc.) unless the CAM is transmitted or expired. The exponential timing is necessary, because the likeliness of packet collisions increases with an increased CS threshold and thus a CS threshold should be applied for shorter times.

Stanica et al. [145] show, that an optimal CS value depends on the vehicular density within that area. This is, because a higher density will lead to more stations trying to access the channel using the same CW size and consequently the amount of interference will increase. They suppose to adjust the CS threshold to the vehicle density in order to maintain a certain amount of nodes in the CS range. Therefore, a simple mapping function is used, which maps the vehicle density directly to the CS within predefined limits based on a minimum CS range and the hardware specifications.

In [148], SR-CSMA is introduced by Stanica et al. The goal of SR-CSMA is to "increase the reception probability for safety messages in the immediate neighbourhood and to reduce the update delay between closely situated vehicles" [148]. In order to achieve this, a node can decide to transmit a CAM, although the CCA function indicates a busy channel. The transmission is allowed, if the SINR of the vehicles within the safety range of the already transmitting vehicle still allows reception, if the ego vehicle starts the transmission. For nodes, which are not in the safety-range of the transmitting vehicles, this will lead to a controlled collision.

3.3.5 *Transmit Power Control (TPC)*

Through adjusting the TP, a node can directly adjust the communication range and thus the amount of nodes which will be able to receive the transmission. TPC is used

decentralized in order to adjust the number of nodes in the communication range. However, local adjustment of the TP does not lead to an adjustment of the locally perceived number of neighbors, because the local perception is influenced by the TP of the other nodes on the one hand and on the CS threshold on the other. TPC can significantly influence the congestion state of the channel and thus many works have been focusing on this degree of freedom.

TOPOLOGY CONTROL TPC can be used to maintain connectivity between vehicles by reducing the TP in dense and increasing it in sparse topologies. By doing so a certain topology in terms of vehicle density can be achieved. Topology control is mostly used for multi-hop communication, where the connectivity to only single nodes to forward packets is required.

In [149], Caizzone et al. propose to adjust the TP based on the number of reciprocal neighbors using Additive Increase Additive Decrease (AIAD), i.e. TPC is used to maintain a certain number of reciprocal neighbors. However, the underlying MAC is Time Division Multiple Access (TDMA) and thus the proposed calculation of the amount of reciprocal neighbors needs adjustments in order to work for VSC. Another topology controlling algorithm (*DTRA*) is introduced by Atimy et al. in [150]. The authors propose to use TPC in order to dynamically set the communication range based on the estimated vehicle density. Thereby, the vehicle density is estimated based on the observed traffic-flow, which can be derived either locally or by exchanging this data among the vehicles. However, they assume car-following models, which are not valid for most conditions. Instead of estimating the density locally, Guan et al. [151] propose to attach a list of IDs from the nodes, a message was received within the last period to a newly generated beacon. A node receiving those messages can calculate the number of nodes within the communication range by counting the number of messages containing its ID and subsequently adjust the TP using AIAD to reach the desired amount of neighbors. In order to reduce the huge overhead in dense conditions, the authors further suggest that a node should attach only a subset of the IDs received, e.g. 25% and adjust the target density accordingly.

Although not useful for VSC in terms of beaconing, using TPC to reduce the amount of neighbors to the absolute minimum maintaining connectivity is useful for the exchange of event-driven messages, e.g. DENMs. In [152], Chigan et al. introduce *DB-DIPC*, which aims at achieving minimal connectivity, i.e. the TP is iteratively adjusted until only one neighbor is within the communication range based on periodic probing of the neighborhood. A similar algorithm is proposed by Cheng et al. in [153]. In a first stage, the TP is increased exponentially until connectivity is established. Based on exchanged geographical positions and a path-loss model, a node subsequently uses TPC to set the communication range to only reach the closest neighbor. Due to the probabilist characteristics of the path-loss, it is suggested to set the communication range such that the received power will be larger than the sensitivity either with 95% confidence or on average. However, fading can be hardly modeled for the different environments and thus an accurate calculation of the communication range can not be guaranteed. Another open issue is the question, whether reaching one node is a suitable optimization criteria, i.e. there is just one pair of communicating vehicles, such that multi-hop communication can not be achieved.

PROACTIVE APPROACHES While feedback-based reactive or hybrid protocols target at an optimization of a certain criteria, pro actively adjusting the TP can be applied without any observations. Kloiber et al. [154] propose to randomize the TP over time to reduce the probability of recurring collisions. For each packet, a TP is selected from a given probability distribution. A packet thus will be sometimes transmitted at high power reaching far-away nodes and mostly with low or medium power. The assumption is, that close nodes need a higher information freshness, than nodes far away. By reducing the average communication range far neighbors are sufficiently updated and the number of occurring collisions can be reduced due to decreased overall congestion level. However, probabilistic models can not guarantee the awareness, because a node can select minimum powers for a certain period. Furthermore, the algorithm can not react to dense situations, where the overall communication range should be even lower than achieved by the randomization and consequently congestion will occur. In advance it can be hardly combined with other mechanisms for congestion reduction, because of the non-deterministic behavior.

Instead of randomly selecting the TP, Okamoto et al. introduce a proactive, pattern based design in [155]. Although focusing on the same aim as Kloiber et al. [154], they argue that due to random selection, vehicles can send with low or high TP for a longer time resulting in less awareness or increased interference respectively. The authors suggest, that each vehicle should adjust its TP based on predefined, fixed repetitive patterns, i.e. $P_1, P_2, \dots, P_n, P_1, P_2, \dots$. The authors further suggest, that these patterns can be selected based on the environment, traffic conditions and vehicle maneuvers, i.e. a vehicle doing a left turn has another pattern than a vehicle going straight. Furthermore, it is proposed, that vehicles can coordinate their phases in order to prevent interference. However, coordination as well as adoption to the environmental context is not further explained and no implementation is given.

CONGESTION CONTROL A widely known CC utilizing TPC is proposed by Torrent-Moreno et al. as *D-FPAV* in [156]. The major contribution of the study is a decentralized TPC algorithm which targets at a max-min fair allocation of the available resources in terms of BL. As described beforehand, a major issue of TPC are asymmetric links and the resulting unfair resource allocation. *D-FPAV* is an extension to the previously proposed centralized algorithm *FPAV* [108]. Based on global knowledge, each node is assigned a TPC that minimizes the maximum BL in *FPAV*. Each node increases its TP by a certain offset unless the maximum BL observed within the network is reached. If the maximum BL is exceeded, the TP is reduced by the same offset. In *D-FPAV* semi-global knowledge is achieved by exchanging the TP and positions of the vehicles. A vehicle can locally calculate the maximal TP that does not violate the maximum BL estimated based on locally and remote information. Thus, it is more suitable for VSC, since centralized coordination and global knowledge are hardly achievable. In [157], Torrent-Moreno et al. recapped the *D-FPAV* algorithm with minor changes of the CS threshold, which is adopted "to achieve a lower overhead in areas with high load on the channel". However, exchanging and relaying the exact position information of neighboring vehicles can cause significant overhead and load to the channel. In [158], Mittag et al. subsequently suggest to relay the number of vehicles per road segment only, not their position. Although reducing

the overhead, these aggregated information offers "lower" accuracy and individual nodes can experience BL that exceed the predefined threshold.

Fairness is a severe issue in VANETs and congestion control approaches need to address this issue. Cooperation between the vehicles in terms of sharing information about congestion is a commonly used technique to create global and participation fairness. In [159], Lu et al. propose *ETPC*, a scheme trying to establish a common TP within a certain range. Nodes, which do not recognize a congestion can still contribute to it. The basic idea of *ETPC* is to prevent those nodes from increasing their TP. Therefore, if a node perceives congestion, i.e. a message from more than n nodes was received, a TP advise is disseminated and relayed by the neighboring nodes. Nodes receiving this advise are forced to adjust their TP to the reported value. If no advise is received for a dedicated time, a node will start to increase its TP again. The advised TP shall be calculated such that the affected node is reached by n vehicles only.

Topology control as mentioned before can also be used in order to reduce the level of congestion on the channel, because the load is influenced by the node density within the communication range. In [160], Yang et al. propose to adjust the TP based on a target density and estimation of the PDR. Unless the vehicle density is smaller than a predefined threshold, TP will be increased, if the PDR is above another threshold and vice versa. However, sequence numbers are required in order to calculate the PDR. A similar approach is conducted by Lei et al. in [161]. The authors suggest to calculate the TP based on the number of neighboring nodes and the observed transmission delay, i.e. the time between the generation and transmission of the message, separately. For the vehicle density based TP calculation, a linear convergence towards an optimal value is applied. The transmission delay based TP will be decreased, if the transmission delay exceeds a threshold and vice versa. Finally, the TP of a vehicle is calculated based on the weighted TP based on vehicle density and transmission delay.

A rather simple approach to adjust the TP in order to reach a certain distance is proposed by Nasiriani et al. in [162]. The basic idea of *LMRC* is to decrease the range, if congestion is detected, and increase it if the network is sensed to be empty. Therefore, a linear scaling of the transmission range to the congestion level determined in terms of CBR is suggested. However, the control is only active if the load is within a certain operating range and otherwise fixed minimum and maximum ranges according to safety requirements are proposed. Fallah et al. state in [163], that *LMRC* is under consideration of the industry for standardization and thus proposed an enhancement called *SUPRA*. *SUPRA* adds a configurable gain and one-step memory to *LMRC*, i.e. the load is not linearly scaled to the TP, but instead converges to the desired value within the CBR range. The authors furthermore introduce the piggyback based max-min fairness to *SUPRA*. Instead of using the locally assessed CBR, the maximum observed load within the neighborhood is used to adjust the TP. The authors show, that *SUPRA* achieves stable and fair control. Besides *LMRC*, Nasiriani et al. proposed another scheme called *GRC* in [162]. *GRC* utilizes TPC in order to reach an optimal utilization. The distance is controlled by using an iteration based linear control scheme converging to the optimal CBR.

Shah et al. combine the focus of CC with the requirements of safety applications in [164]. It is assumed, that under congested channel conditions, range requirements

and channel quality are contradictory. The authors suggest, to calculate the TP required for a certain safety range and packet priority and the quality of the channel based on current and expected CBR respectively and use both weighted accordingly for the calculation of the necessary TP. The adjustment of the TP is realized as a linear scaling function.

Egea-Lopez et al. introduce a cooperative congestion control scheme called *SBCC* in [165]. *SBCC* controlled vehicles "locally compute the maximum power needed to comply with a given maximum BL as a function of the channel parameters, average vehicle density, and neighbor TP" [165]. Each vehicle can locally estimate the channel parameters, which are assumed to follow a certain path-loss with fading. Based on these estimated parameters, the TP is explicitly set such that the maximum BL is not exceeded. The maximum BL is thereby either expressed by the estimated vehicle density (*SBCC-N*) or the observed CBR (*SBCC-C*). For a fair regional convergence, the average TP of the neighboring nodes is used as a weighting function. In [166], Egea-Lopez focuses on the problem of optimal TPC and models it as a Network Utility Maximization (NUM) TP allocation problem. A distributed algorithm relying on path-loss model assumption called *FCCP* is proposed that solves the optimization problem. Different levels of fairness can be achieved by the scaling parameter. The author shows that, "*FCCP* converges to the close proximity of the optimal value [...] while keeping the CBR at the desired level" [166].

AWARENESS CONTROL TPC is suited to be used for creating and maintaining awareness between pairs of nodes. In case safety relevant information need to be transferred to nodes far away, the TP will be increased for these packets, while for low priority packets it will be set low in order to reduce congestion.

In [167], Gozalvez et al. introduce an awareness control scheme utilizing TPC called *OPRAM*. The basic idea is, that in case of collision avoidance, an affected vehicle just needs to receive one single message of the other vehicle in order to be informed of a possible collision. Once a collision is detected, *OPRAM* sets the TP to the maximum value one second before the critical distance is reached and decreases it gradually afterwards. The authors propose their protocol for the use-case of ICRW, where buildings are expected to shadow the communication signal. For non-critical information under LOS conditions, the algorithm uses low TP values in order to mitigate congestion. *MINT* is proposed by Sepulcre et al. in [100] and can be seen as a more general version of *OPRAM*. While the basic idea is still the same, *MINT* can be used for different use-cases, i.e. Collision Avoidance and Warning, by calculating the critical distance and adjust the TP as described above. In addition, Sepulcre et al. evaluate information reduction based on contextual information for a lane change warning use-case on a highway in [168]. They show, that if the contextual information about the traffic status is evaluated, single nodes do not need to transmit CAMs at high power or rate, if other vehicles can contribute the same information and in consequence load as well as interference can be reduced.

Jeng et al. [169] show that adjusting the TP based on the vehicular status patterns of neighboring vehicles can help to increase the overall performance of collision avoidance. The authors argue, that emergency messages are only necessary for vehicles within a safe distance to the sender. Applying this safety distance using TPC, the authors show that the amount of interference can be reduced. Javed et al. [170]

introduce a scheme, where the underlying assumption is that a vehicle needs to know its critical neighbors only. Critical neighbors are defined as those possibly affected by a collision (lateral and longitudinal), i.e. the leading, following, and overtaking vehicle. The TP is consequently adjusted to reach all critical neighbors within the safety range, which is the maximal communication range. If a vehicle is missing a critical neighbor, the TP is increased stepwise until either the neighbor is found or safety distance is reached.

DD-FPAV is a scheme introduced by Sattari et al. in [171, 172] which dynamically adjusts the maximum BL threshold defined in [156] based on the estimated traffic-status. Therefore, the algorithm determines, whether there is congestion by calculating the average vehicle speed and if there is traffic, the maximum BL will be set to a lower value, while if there is no traffic, the BL will be large. Furthermore, the authors suggest to adjust the ratio of beacons including piggyback information based on the traffic state. This regulation is finally used for the *D-FPAV* algorithm [156].

3.3.6 *Transmit Rate Control (TRC)*

Transmit Rate Control (TRC) can be used to control the frequency of messages transferred to the channel. While TPC will reduce the number of neighbors and PSC is used to reduce the size of a packet, TRC is used to reduce the load for a given number of vehicles and packet size. Besides TPC, TRC offers the best results in controlling channel congestion and thus a couple of protocols have been proposed in the recent years including some state-of-the-art approaches, which are investigated for standardization. We review both, congestion avoidance in terms of control algorithms and awareness control algorithms. While the CC algorithms focus on adjusting the load, such that the maximal throughput can be achieved, AC algorithms try to adjust the rate based on the environmental and traffic context with the focus of increasing the safety-awareness.⁴

CONGESTION CONTROL

AIMD

Using AIMD for TRC is considered by different approaches and reasonable, because AIMD is a well known scheme whose usage in TCP congestion control makes it very popular and shows the capabilities of the scheme in terms of congestion avoidance.

In [174], He et al. propose to use a TCP like congestion control scheme utilizing AIMD for the control of the traffic rate. Unless a congestion event is detected, the rate will be increased. Whenever a congestion event is detected, the rate will be reduced and dissemination of beacons will be blocked for one interval to allow event-driven safety messages to be transmitted. Afterwards, fast start is applied with subsequent congestion avoidance phase. This scheme was enhanced by Guan et al. in [175]. They specify two different approaches, where either fast recovery (*ARCS-II*) is used, or a combination of fast start and congestion avoidance (*ARCS-I*) as proposed before. However, during the congestion avoidance phase, the time for an increase of the transmission rate depends on the perceived CBR.

⁴ Parts of this chapter are published in [36, 173] and are under copyright of the IEEE or ACM

Threshold based adaption is also frequently used for congestion control. Thus, whenever a certain threshold is exceeded, the rate will be decreased and vice versa. Lv et al. propose *DBFC* in [176], where the threshold is defined in terms of PDR, velocity and vehicle density. An action is only conducted, if congestion in terms of threshold exceeding vehicle density is detected and the PDR is estimated to be below another threshold. An increase/decrease decision is then taken dependent on the velocity of the vehicle only. Kim et al. [177] argue, that unfairness in distributed rate control algorithms is an issue that needs to be addressed. They propose an AIMD based algorithm, which aims at a convergence to a common group rate, e.g. the rate is increased, if the CBR does not exceed the threshold and the individual rate is smaller than the average rate of all neighbors and vice versa. Assuming nodes within the same region will perceive the same load, nodes will take action in order to converge to the average group rate.

PULSAR

In [14] Tielert et al. introduce *PULSAR*, a binary rate adaption using AIMD. At each iteration, the new transmission rate r_{k+1} is calculated based on the previous rate and channel utilization U_k as:

$$r_{k+1} = \begin{cases} r_k + \alpha_I, & \text{if } U_k \leq U_t \\ (1 - \beta_D)r_k, & \text{if } U_k > U_t \end{cases} \quad (3.5)$$

where U_t is the a priori specified target utilization. The parameters α_I and β_D determine the convergence behavior of AIMD.

To overcome the problem of slow convergence, *PULSAR* suggests to add a *target rate* mechanism. Therefore, each vehicle includes its current message rate in the CAMs. Whenever a new transmission rate information r_{new} is received, the target rate is updated using an Exponentially Weighted Moving Average (EWMA):

$$r_t = (1 - \alpha_t) \cdot r_t + \alpha_t \cdot r_{new}. \quad (3.6)$$

where the parameter α_t determines the weight of the new rate. The target rate is then used as a *gravitation pull* when calculating rate adjustments by adding the parameter ω to the AIMD algorithm to fasten convergence (3.10):

$$\omega = \begin{cases} a_c, & \text{if } r_k \leq r_t \\ 1/a_c, & \text{if } r_k > r_t \end{cases} \quad (3.7)$$

where a higher convergence factor a_c accelerates convergence at the cost of decreased smoothness.

PULSAR shares information about the local congestion status of each vehicle using piggyback transmission in order to reach max-min fairness. The fairness range is increased by sharing this information for up to two hops (*2-hop piggyback*), where

each relaying vehicle aggregates the received utilizations of its neighbors $v' \in n(v)$ for one iteration k using the maximum norm:

$$\tilde{U}_k = \max_{v' \in n(v)} U_{k,v'} \quad (3.8)$$

The calculated maximum 1-hop utilization \tilde{U}_k and the local utilization U_k are piggybacked on the next generated CAM. A vehicle calculates the maximum utilization for a 2-hop area at each iteration by applying the maximum norm to the local measurements U_{k-2} , the 1-hop utilization $\tilde{U}_{k-2,1}$ received between $k-1$ and $k-2$ and the 2-hop utilization $\tilde{U}_{k-2,2}$ received between k and $k-2$:

$$\tilde{U}_{k,C} = \max(U_{k-2}, \tilde{U}_{k-2,1}, \tilde{U}_{k-2,2}) \quad (3.9)$$

The algorithm reacts on this cooperative utilization using the modified AIMD with gravitation pull:

$$r_{k+1} = \begin{cases} r_k + \omega\alpha, & \text{if } \tilde{U}_{k,C} \leq U_t \\ (1 - \beta/\omega)r_k, & \text{if } \tilde{U}_{k,C} > U_t \end{cases} \quad (3.10)$$

Zhang et al. propose a modified version of *PULSAR* in [178]. The authors argue, that the algorithm does not reflect the safety requirements in *VSC*. Instead of using the target rate for the gravitation pull, it is suggested to fasten convergence based on QoS requirements in terms of delay constraints. Thus, nodes where the constraints are violated are prioritized in allocating resources.

LIMERIC

Another widely known state-of-the-art congestion control protocol in VANETS is *LIMERIC*. *LIMERIC* is proposed by Bansal et al. in [13] and utilizes linear control of the message rate based on the perceived local CBR. *LIMERIC* achieves local fairness by adjusting the message rate of each vehicle. The underlying function linearly balances the relative percentage of the total channel capacity $r_j(t)$ allocated to each node:

$$r_j(t) = (1 - \alpha)r_j(t-1) + \beta(r_g - r_C(t-1)) \quad (3.11)$$

where $r_C(t-1)$ is the total channel utilization of the previous iteration and r_g determines the cumulative rate that should be allocated to the nodes. The convergence speed and behavior is specified by the parameters α and β .

For a suitable parametrization, the algorithm converges to a steady-state message rate of

$$r_j = \frac{\beta r_g}{\alpha + K\beta}, \quad j = 1, 2, \dots, K \quad (3.12)$$

The convergence strongly depends on the number of nodes K within the transmission range so that the parameters need to be specified to fulfill the convergence criteria

$$\alpha + \beta K < 2 \quad (3.13)$$

Although *LIMERIC* is designed as an unlimited self-regulating system (3.11), the message rate in VANETs is mostly limited to a maximum rate R_{max} . Due to the dependency of an assumed vehicle density K (3.13), the authors propose a modified version of *LIMERIC*, which is more robust to scalability. The modified algorithm benefits from this in terms of convergence speed due to *gain saturation*:

$$r_j(t) = (1 - \alpha)r_j(t-1) + \text{sign}(r_g - r_C(t-1)) \cdot \min[X, \beta|r_g - r_C(t-1)|] \quad (3.14)$$

with

$$X = \alpha \cdot R_{max} \cdot \text{TXTIME} \quad (3.15)$$

where X specifies the maximum gain of the relative message rate r_j and thus limits the message rate based on the transmission delay TXTIME . Assuming constant transmission parameter settings, TXTIME is a function of the packet length [11].

Kennedy et al. show in [179], that *LIMERIC* can be combined with the information sharing scheme, proposed by Tielert et al. in [14] in order to reach a globally fair allocation of the resources. In [180], Ogura et al. propose to use the vehicle density as an input parameter instead of the resource utilization measured in terms of CBR. They argue, that while the CBR tends to be volatility over time, the vehicle density provides robustness in terms of stability and is not affected by several effects. However, in the end both inputs measure are the same and the important fact is how accurately the perceived information can be obtained.

The authors themselves propose some enhancements to *LIMERIC* in order to account for the safety aspects in VSC. In [107], Bansal et al. propose that vehicles within the same environment could use different values for the convergence parameter β in parallel to account for their priority. It is shown, that vehicles using different β values will converge to different steady-state message rates. More precisely, if the β value of a group is half of the default value, it will result in a steady-state message rate, which is half of the message rate allocated by the vehicles using the default β .

Another proposed algorithm assumes, that the vehicles estimate the position of vehicles unless they get fresh position information resulting in a certain tracking error. By estimating this tracking error, a node can decide to schedule extra transmissions or reschedule beacons in order to provide fresh position information to the neighboring vehicles. Bansal et al. introduced this approach in [181] as *EMBARC*. In *EMBARC*, *LIMERIC* is used for congestion avoidance still, but modified in order to take extra transmissions due to exceeding tracking error based on a probability function into account. Thus, the steady-state message rate of *EMBARC* will be lower compared to *LIMERIC*, but the tracking-error will be lower due to better information freshness resulting in increased safety.

Cheng et al. [182] evaluate the effect of mixed topology of vehicles using *LIMERIC* and CAM-DCC⁵. The authors propose a scheme in which *LIMERIC* vehicles adjust their target resource utilization in order to achieve a steady-state resource allocation equal to the allocation expected for the CAM-DCC vehicles. Fairness is further

⁵ vehicles, that use the CAM generation rules as introduced in [10] and state based decentralized congestion control [94]

achieved by sharing this target CBR with surrounding vehicles, where the rate adaption is done by *LIMERIC* according to this CBR.

FABRIC

FABRIC as proposed by Egea-Lopez in [183, 184] is a rate adaption protocol which is modeled and solved as a NUM rate allocation problem. The NUM problem is formulated to maximize the sum of the utility function of each source, while maintaining the link utilization below the capacity. Furthermore, no negative bandwidth shall be assigned to any source. The authors show, that this can be achieved, if the prices reflecting the congestion state at a vehicle are exchanged among the neighbors, where the price is defined by:

$$\pi_v^{k+1} = \pi_v^k - \beta \text{sign}(C - \sum_{v' \in n(v)} r_{v'}), \quad (3.16)$$

where π_v^k is the previous price, C is the target BL and $\sum_{v' \in n(v)} r_{v'}$ is the currently observed BL. The observed BL shall be estimated by piggybacking the current rate, while CBR can also be used for the calculation instead. These prices are shared among the neighbors and the rate shall be adjusted as follow

$$r_v^k = \left(\sum_{v' \in n(v)} \pi_{v'} \right)^{-\frac{1}{\alpha}}, \quad R_v^{\min} \leq r_v^k \leq R_v^{\max}, \quad (3.17)$$

where α defines a fairness related parameter and R_v^{\min} and R_v^{\max} defines a nodes individually assigned minimum and maximum rates respectively. A higher value for α increases the achieved fairness among a region.

Vehicle density based adjustment

Besides *LIMERIC* and *PULSAR*, which are the most recent state-of-the-art CC algorithms providing fair, efficient and stable control, there are some other aspects that can be highlighted.

In [185], Thaina et al. focus on the relation of the vehicle density and the rate and provides two approaches: linear regression and k-nearest neighbor. For TRC schemes based on linear regression, the next rate will be estimated based on the perceived vehicle density. A novel approach is to use k-nearest neighbor, i.e. an instance-based machine learning technique, in order to adjust the rate. Based on a training-set, a vehicle can decide about the rate based on learned knowledge about the vehicle density. The authors show, that both approaches perform better than simple linear adaption, but they do not contribute an implementation of it.

While most algorithms utilize the CBR as an input for the feedback-control due to simple local estimation, the vehicle density is considered to give the same feedback and needs to be provided by the LDM in terms of a neighboring table. Park et al. [186] propose to adjust the rate to optimize the goodput in terms of beacons received based on an application level scheme to estimate the neighboring vehicle density. The idea is, that there is an optimal frequency indicated by the vehicle density, which can indirectly be estimated by the PDR. A similar assumption is conducted by Piao

et al. in [187]. They start with a broadcast rate of 10 Hz and reduce this rate, if the amount of neighbor vehicles increases. *CBA* as proposed by Chaabouni et al. in [188] sets the rate inversely proportional to the number of neighbors detected aiming at a reduction of the collision probability. Sommer et al. [189] propose to set the transmission interval based on the product of neighbors and congestion level to

$$I = I_{des}(1 + rK), \quad (3.18)$$

where I_{des} is the desired maximum packet interval, K is the number of neighbors and $r = b_i/b_{des} - 1$ is the congestion level indicated by the ratio of observed to desired load.

Zhang et al. propose *DTRCS*, a multi-agent based model predictive control scheme, in [190]. Each agent calculates its access probability based on the estimated vehicle density and shares this probability with neighboring agents in order to decide for the rate adjustment. The authors state, that the multi-agent system can achieve a fair resource allocation due to the cooperative exchange of the information.

Safety-aware congestion control

While the vehicle density and the channel status information are reliable indicators for the congestion status, they do not give sufficient information about the safety-related aspects of the vehicle. Sommer et al. [191] propose a scheme, where the transmission interval is adjusted based on a weighted input of channel quality and message utility. The channel quality is quantified in terms of collisions, number of neighbors, and Signal to Noise Ratio (SNR) and the message utility is determined in terms of distance to an event and message age. These input factors are used for a linear scaling of the transmission interval. Liu et al. [192] also utilize multiple weighted input parameters for a linear scaling of the rate. The authors further suggest to use an EWMA in order to smooth the rate adjustment.

Huang et al. [193] propose a scheme, where the transmission of a message is based on a periodically calculated probability to transmit a beacon. Besides scaling parameters, these probability is dependent on the ratio of the suspected tracking error and the channel state observed within the last periods. Thus, within each iteration a beacon can be generated following this probability, where it is more likely with higher tracking error and low channel utilization and vice versa.

AWARENESS CONTROL

Beacon suppression

The estimation of the tracking error is an essential metric for the vehicles to quantify the awareness. Within certain borders, a decent tracking error can be accepted by most safety-related applications and thus reducing the amount of messages in order to provide enough information to prevent a too huge tracking error seems reasonable. In [194], Rezaei et al. propose a scheme in which a beacon is generated, if the estimated longitudinal or lateral tracking error exceeds a predefined threshold. The same focus is used by Nguyen et al. in [195]. Unless the tracking error is expected to fall of a safety-region, no beacon will be generated. If the estimated tracking error is outside of the safety region, a beacon will be generated. Thus, a reduction of the

beacons can be achieved. However, a major issue for the estimation of those tracking errors is, that it is decentralized based on local knowledge and it assumes, that a beacon transmitted will also be received by the nodes. Estimation of the tracking error thus can be seen as an open-loop control, where the loss of a beacon is an external distraction leading to false results.

Proactive reduction of the BL based on traffic related patterns by reducing the beaconing rate thus should include a certain safety margin for packet losses. Implicitly adjusting the rate based on the vehicle dynamics or risk can help in reducing the overall load, while maintaining an individual fair and safe rate. Javed et al [196] propose a scheme, where TRC is used to set the rate of beacons according to the estimated headway of a vehicle. The rate is modeled as a function of the time headway with a maximum and minimum rate at the minimum and maximum headway respectively, e.g. at a minimum headway time of 1 s, a vehicle would use the maximum rate of 10 Hz. Jerk beaconing as introduced by Segeta et al. in [197] is designed for vehicles within a platoon. The idea is, that status information are just necessary, if there is a change of the acceleration (jerk) by a vehicle within the platoon. The authors state, that this will reduce the amount of beacons and can even improve the safety.

ETSI CAM generation rules

Generating CAMs with a fixed packet interval leads to a possible overflow of information which is not urgently needed in certain situations. The approach of dynamic message generation [10] which takes into account the change of transmitting vehicle status is proposed by the ETSI. The generation of a message is triggered by the change in vehicle dynamics such as velocity, position, and heading. This is motivated for example by the observation that stationary vehicles which are waiting at the signal light could diminish the message generation rate which in turn would reduce the channel load.

The time interval between two consecutive message generation periods is limited to an upper and lower threshold leading to a message interval [0.1 s, 1 s] and a corresponding message generation rate of [1 msg/s, 10 msg/s], defined by requirements from safety-based applications which can be found in [46].

The decisive factor for dynamic generation is the change of one or mutual parameters within the following constraints:

- The distance between the current and the previous position exceeds 4 m, e.g. $\Delta\text{POS} \geq 4 \text{ m}$
- The difference between the current and the previous velocity exceeds 0.5 m/s, e.g. $\Delta\text{VEL} \geq 0.5 \text{ m/s}$
- The difference between the current and the previous heading exceeds 4° , e.g. $\Delta\text{HEAD} \geq 4^\circ$

In addition, the interval will be maintained for a number of consecutive CAMs if the dynamics leads to a reduced CAM generation frequency, e.g. when the vehicle is braking.

Fuzzy Logic

Fuzzy logic defines a concept, where the truth value of a variable can be any number between 0 and 1. While in the boolean logic, a variable is either true or false, fuzzy logic quantifies the steps in between and thus can help to quantify relations. As an example, if the temperature of water is described by a boolean variable, it can be either hot or cold, while in fuzzy logic, it can also be a mostly hot and a bit cold. Applied to the vehicle context, multiple input variable, like traffic density or message utility can be used with fuzzy logic in order to set the transmission rate. One benefit of fuzzy logic is, that due to the fuzzyfication, inaccurate and incomplete information are tolerated without degradation of the systems performance.

In [198], Ghafoor et al. propose a fuzzy logic based approach (*ABR*) to tune the beacon rate in response to vehicular traffic characteristics. Therefore, the percentage of neighbors with the same direction and the vehicle status, i.e. emergency or not is used for fuzzyfication. The resulting fuzzy beacon rate is in the range between very high (sparse vehicle with same direction and emergency status) to very low (high density and no emergency). Finally defuzzyfication will map this result to the actually used beacon rate.

Wang et al. use AIMD to map the result of the fuzzy logic to the beacon rate in [199]. The authors use CBR, local density and mobility as input for the fuzzy logic and subsequently adjust the rate based on the quantified beacon rate. In [200], Soleymani et al. propose BRAIN-F a multiple input fuzzy logic based BL control. As input they use traffic density, location, and vehicle status. Using triangular membership functions, the observed value is classified.

Increase application-safety

In [201], Drigo et al. propose *DRCV*, a threshold based resource allocation scheme. *DRCV* assigns a higher priority to event-driven messages (DENM) than to beacons. They assume, that both message types share the same channel and the load induced by beacons shall be within a certain range. It shall further not exceed a threshold, which is based on the ratio of event driven and beacon messages. Another technique called fast drop will reduce the maximum load by beacons to a minimum capacity keeping more space for the event driven message, if an event driven message arrives until the message expires. The authors argue, that in case of an event driven message, applications are aware of a risk and reliable transmission of these messages needs to be ensured.

The major information necessary for collision avoidance applications is the position, speed and heading of neighboring vehicles. Those information are basically included in the CAM. Joerer et al. [202] calculate the probability of a collision based on the information of neighboring vehicles and adjust the beacon rate according to this probability. Therefore, they utilize *DynB* [189] as a default congestion control algorithm, but allow to transmit beacons at very high rates of up to 100 Hz if necessary. If the probability for a collision exceeds a predefined threshold, the beacon rate is increased proportional to the collision probability. Furthermore, they keep track of the vehicles and if a vehicle timed-out due to subsequent packet-loss or fading, a default collision probability will be calculated and used subsequently.

Kaul et al. introduce an awareness metric called system age in [203]. The system age defines the average IRT of a vehicle's neighbors, averaged over all vehicles. The

goal of the adaptive rate algorithm is to minimize this system age. If the system age exceeds twice the average transmission interval of the neighbors, a congestion is assumed and the transmission interval shall be increased. If the current system age is higher than the past system age, the previous decision was not good and reverse action is taken. Furthermore, in order to achieve fairness among the neighbors, the transmission interval is set to the average transmission period of the neighbors, if the spread between the individual and the group rate is to huge.

3.3.7 *Joint Control of Multiple Parameters*

CONGESTION CONTROL Joining multiple parameters to decrease the congestion on the channel is a complex, but effective method. The complexity is given by the fact, that the parameters are correlated and a joint control usually needs to trade-off an increase by decreasing the other one to guarantee the status quo. With the aim of congestion control however, it might be sufficient to adjust the parameters sequentially for congestion reduction.

TPC and TRC

The most promising transmission parameters for congestion avoidance are TPC and TRC. While TPC can adjust the range and thus the number of communicating nodes, TRC is capable of adjusting the BL within that area effectively. In [204], Baldessari et al. propose a joint algorithm, where a maximum transmission rate is calculated for each possible TP. The maximum transmission rate shall be calculated such, that the estimated load under this combination does not exceed the CBR threshold. A node selects a combination from this power-rate curve in the next iteration. The proposed method is recapped in [205], where a performance analysis is conducted.

Tielert et al. propose a rather simple strategy in [206], where the TP is increased, if the observed CBR is below the target threshold and the target power is below a distance and target load based threshold. In case of a detected congestion, i.e. CBR exceeds the target utilization, the rate will be decreased unless it reaches the minimum rate, where power adjustment is conducted consequently. However, the authors do not describe a complete algorithm, instead they argue that rate control can be done e.g. by PULSAR [14]. A simple mapping function of the adjusted rate to the TP is introduced by Lu et al. in [207]. In each iteration, the rate is adjusted using LIMERIC. The resulting rate is subsequently used for power adjustment using a linear scaling function. The authors propose the optional usage of information sharing to reach max-min fairness. However, assuming ideal conditions, LIMERIC would lead to an optimal allocation of the rate in one iteration. Applying further decrease of the power in the same iteration will lead to a lower utilization than adjusted by the rate algorithm. A combined approach needs to consider this to guarantee stability, efficiency and fast convergence.

The same problem can occur in the scheme proposed by Jose et al. in [208]. Similar to FABRIC [184], the authors propose to model TRC as a NUM rate allocation problem. TPC is formulated as an integer programming problem offering a decentralized optimal solution for both transmission parameters. It is shown that, compared to EMBARC, the proposed protocol achieves a better close range performance. Egea-Lopez et al. propose to enhance their FABRIC scheme by an additional power

component. They introduce FABRIC-P [209], where the NUM rate allocation problem is solved decentralized by every vehicle for every possible TP. The optimization variable used in the utility function is the beaconing rate for a selected TP multiplied by the number of neighbors reached at that power.

In [95], Zemouri et al. introduce a joint algorithm called SuRPA, which is based on collision rate and CBR observations. If both values are below a predefined threshold, an increase of the transmission parameters will be conducted. A decrease of the transmission parameters will be conducted, if the collision rate is above the threshold. The algorithm favors an adjustment of the transmission rate over an adjustment of the TP, such that TP is only adjusted if the minimum or maximum rate is reached. The selected transmission parameter finally is adjusted using gradual increase or decrease based on the difference between observed CBR and its threshold or observed collision rate and its threshold respectively.

TPC and CW

While TRC adjusts the beacon generation rate directly and thus reducing the load within the region, mitigation of the collision probability is just indirectly achieved. The CW is an effective method to reduce the occurring interference by a dynamic adjustment. However, a higher CW indirectly means higher transmission delay and thus can be interpreted as lower layer rate adjustment. In [101], Rawat et al. propose to use a joint TPC and CW adjustment, where the desired transmission range is calculated based on the vehicle density as calculated in [150] and subsequently used to adjust the TP based on path-loss estimation. The CW is further adjusted using MIMD based on the estimated collision rate, i.e. increase if the collision rate is too high and vice versa. The CW control algorithm of Puthal et al. [141] has already been mentioned. However, the authors combine it with load based transmission parameter adjustment based on TRC and TPC.

Decentralized Congestion Control (DCC)

Although, most of the aforementioned protocols are used for decentralized control of congestion, the term is used by standardization institutes for their congestion control approaches. In Europe, the ETSI has proposed a scheme utilizing multiple transmission parameters in order to control the congestion called DCC [94]. Its cross layer architecture allows to influence several distinct functions of the nodes communication behavior.

The algorithm combines the joint usage of four transmission parameters: TPC, TRC, DRC, and CS threshold adjustment. The intensity of the mechanism is controlled by a top-level CBR dependent state machine with at least three states. Figure 14 illustrates the state machine and the possible transitions for each state. The top-level *ACTIVE* state is surrounded by the two top-level states *RELAXED* (non-regulative) and *RESTRICTIVE* (most rigorous constraints). The *ACTIVE* state can be separated into several sub-states with distinct ascending CBR thresholds. All sub-states are fully meshed with each other and the outer top-level states so that any transition leads to the corresponding state directly.

The state transitions depend on two input signals which are both based on the estimated CBR (ref. table 13):

Table 13: Excerpt of parameters for basic DCC-G5CC config.

Parameter	Value
NDL_timeUp	1 s
NDL_timeDown	5 s
NDL_numActiveState	1

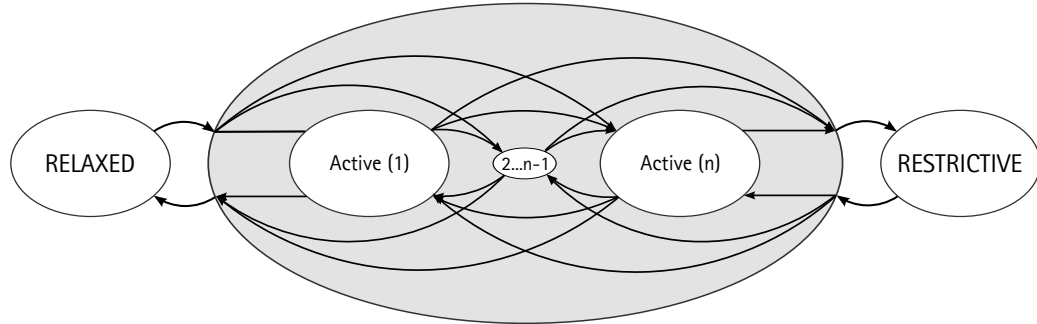


Figure 14: DCC states with up to n active sub-states

- **minCL(NDL_timeUp)** - Minimum CBR for the past time period of length NDL_timeUp .
- **maxCL(NDL_timeDown)** - Maximum CBR for the past time period of length $NDL_timeDown$.

This basically classifies transitions leading to a more restrictive mechanism as *stateUp* and those having less intense constraints as *stateDown*. Furthermore, *stateUp* defines the state which corresponds to the signal $minCL(NDL_timeUp)$, i.e. the Channel Load (CL) threshold of this state is lower and the next higher states threshold exceeds it. While *stateDown* is defined analogically, the next (sub-)state shall be the highest of these states achieving conservative behavior. In other words, high CBRs in the past will lead to high states and thus more restrictive constraints, while lower CBRs in the past will conduce lower states which have less intense regulations.

The default timing values (Table 13) for the transitions are designed for considerate control. The state machine reacts sensitive to peaks or high CL and stays longer in upper, more restrictive states before reacting on low CBR.

Table 14 shows the CL thresholds and values for each mechanism for the default states as specified in [94]. It also reveals the more restrictive behavior with increasing state. In general each *ACTIVE* sub-state might have a different parametrization with respect to the intensity of the specific mechanism, but it is also possible to disable it completely or set a fixed value, e.g. setting TPC to a state independent value of 23 dBm.

As an example, if a vehicle at t is in *ACTIVE* state with $minCBR(1s) = 0.1$ and $maxCBR(5s) = 0.2$, it will be in *ACTIVE* at $t + 1$, because *stateUp* indicates *RELAXED*, but *stateDown* indicates the higher *ACTIVE* state.

However, the basic algorithms parameters are not optimized and evaluations have shown, that the algorithm tends to get instable [173, 210, 211, 212]. The issue of stability and fairness is a concern, that has been focused on since than and adoptions to the DCC are made.

Table 14: Default state configuration for DCC-G5CC

Parameter	Relaxed	Active	Restrictive
TPC	33 dBm	23 dBm	-10 dBm
TRC	0.04 s	0.5 s	1 s
DRC	3 Mbit/s	6 Mbit/s	12 Mbit/s
CS	-95 dBm	-85 dBm	-65 dBm
CBR threshold	-	0.15	0.4

Based on a profound analysis of the weaknesses and problems of the DCC [213, 214], the scheme was enhanced and two different approaches have been considered: the aforementioned state-based reactive DCC with more states and higher CBR thresholds and an adaptive algorithm based on LIMERIC [215]. However, examples are just given for TRC and joint usage of the multiple transmission parameters needs to be evaluated.

AWARENESS CONTROL Sepulcre et al. suggest to use a joint TPC and TRC in [100]. While the major focus is on the control of the TP by the MINT [100] scheme, the authors state that the transmission parameters shall be adjusted by the application in order to reach a vehicle which needs critical information to avoid a collision.

While in [216], TRC is used for the actual control of the awareness based on the estimated headway [196], the authors further propose to utilize TPC in order to utilize the full capacity of the channel. The TRC scheme utilizes a minimum rate unless the headway is below the maximum time headway and thus there are free resources. Awareness will be achieved less frequently, but at higher distances. The power is adjusted based on the perceived vehicle density in order to reach the maximum channel capacity.

AWARENESS AND CONGESTION CONTROL An elegant way to control multiple parameters is to use them distinctly for different objectives. This avoids the problem of correlation for the same feedback parameter, while effectively using control dimensions. Here, one parameter is used to control the objective of awareness, while the other one keeps track of the congestion avoidance function.

Huang et al. propose to use TPC for CC, while TRC is used to maintain awareness in [109]. The TP therefore is linearly scaled to the observed channel utilization, while awareness is based on the suspected tracking error. If this error is below a threshold, beacons are suppressed. Otherwise, the probability of a transmission within an iteration is dependent on the difference between the suspected tracking error and the corresponding threshold.

In [217, 110], Sepulcre et al. propose *INTERN*, a scheme which integrates congestion and awareness control based on *MINT* [100]. The transmission rate of a vehicle is given by

$$T_f = R + \Delta T_f, \quad (3.19)$$

where R is an interval specified by the applications requirements and δT_f specifies a certain margin used to satisfy the application requirements even though packets are lost. The margin is based on the congestion level

$$\Delta T_f = \Delta T_f^T \frac{CBR_{max}}{CBR_{2hops}}, \quad (3.20)$$

where ΔT_f^T is the minimum ΔT_f reported by neighboring vehicles, CBR_{max} is the target load and CBR_{2hops} is the maximum observed load within two hops using the piggyback mechanism introduced by *PULSAR* [14]. The margin ΔT_f is within the interval of 1 and 3 Hz. However, the clear focus of *INTERN* is on awareness, while the congestion control part is very limited to a control dimension of 2 Hz. Based on a self defined metric, the authors show, that their approach can achieve higher application efficiency in critical situations compared to *MINT* and *LIMERIC* with max-min fairness.

Frigau et al. [218] propose to use a *PULSAR* like TRC scheme, where the gravitation pull is based on the observed PDR instead of the reported target rate. Furthermore, they dynamically adjust the TP according to the vehicle density, maximum channel load, SINR, received power of neighbors, and a path-loss model based communication range. The authors show, that compared to *D-FPAV*, their algorithm can reduce packet loss, while maintaining fairness.

In [219], Qian et al. propose a rather simple approach to adjust the transmission parameters based on the vehicle density. The authors assume, that "most of the safety applications enquire a high beaconing rate" and thus suggest to first adjust the TP unless it is reduced to a velocity dependent minimum power. If this is reached and vehicle density still indicates congestion, the beacon rate will be reduced and vice versa.

Aygun et al. introduce *ECPR* [99], a joint TRC and TPC scheme, where the congestion avoidance part is basically conducted by *LIMERIC* using rate control. TPC in *ECPR* aims at achieving a certain awareness range. The authors suggest to calculate the necessary TP in order to reach any neighboring vehicle by estimating the path-loss exponents of a log-distance model utilizing RSSI and the corresponding TP of a packet attached to it. Each vehicle subsequently is assigned a TP, which in average should be sufficient to reach that vehicle. The algorithm than advices to use the TP reaching an application based percentage of the vehicles. However, this TP is only used, if there is no congestion, or in case of congestion, if the previous TP was lower or it is critical in order to provide awareness.

3.3.8 Summary

Several techniques on how to acquire congested channel status and how to control channel congestion have been proposed. Congestion control often also considers the problem of allocating the limited capacity to the individual nodes, which is a resource sharing problem. Thus, fairness is a central issue that needs to be addressed by the protocols on the one hand, while on the other hand awareness among the nodes is the essential criteria that needs to be maximized for VSC. Considering either awareness, fairness or simply targeting at reducing the congestion level to implicitly

achieve both, a couple of transmission parameters can be used. Assuming the fixed size of CAMs and the propagation issues for VANETs, the effect of PSC and DRC in terms of congestion control is limited. The most effective parameters used are the TPC and TRC. However, adjustments of the transmission range due to TPC need to consider the problem of link asymmetry and thus TPC should be combined with CS threshold adjustment. While TPC can effectively reduce the amount of neighbors and range accordingly in order to achieve traffic pattern related awareness, the control of the rate can significantly reduce interference and congestion by the suppression of unnecessary information and limiting the BL. An equal effect can be achieved by controlling the size of the CW on the MAC layer.

In table 15, we provide an overview of the protocols reviewed within this chapter based on the transmission parameter controlled. The highlighted elements are the state-of-the-art protocols, that are used within this thesis for elements of the protocol itself and for the performance comparison.

Table 15: Overview of CC and AC algorithms for VANETs with year of publication and the controlled parameters

	Year	TTC	TFC	CW	CS	DRC	PSC		Year	TTC	TFC	CW	CS	DRC	PSC
Rezaei et al. [194]	2007	x						D-FPAV [156, 157]	2006 2009		x				
DRCV [201]	2009	x						Guan et al. [151]	2007		x				
He et al. [174]	2010	x						DTRA [150]	2007		x				
PULSAR [14]	2011	x						OPRAM [167]	2007		x				
ATB [191]	2011	x						DB-DIPC [152]	2007		x				
Thaina et al. [185]	2011	x						SPAV [158]	2008		x				
Kaul et al. [203]	2011	x						Yang et al. [160]	2008		x				
ARCS [175]	2011	x						Mittag et al. [220]	2009		x				
Huang et al. [193]	2011	x						Jeng et al. [169]	2009		x				
DBFC [176]	2012	x						Cheng et al. [153]	2010		x				
FARE [186]	2012	x						NTPP [221]	2010		x				
LIMERIC [13]	2013	x						ETPC [159]	2010		x				
Bansal et al. [107]	2013	x						Sepulcre et al. [168]	2011		x				
Kennedy et al. [179]	2013	x						Kloiber et al. [154]	2012		x				
Javed et al. [196]	2013	x						Okamoto et al. [155]	2013		x				
BREAVE [180]	2013	x						LMRC [162]	2013		x				
Nguyen et al. [195]	2013	x						GRC [162]	2013		x				
CBA [188]	2013	x						CoopSZ [170]	2013		x				
ABR [198]	2013	x						SBCC [165]	2013		x				
Liu et al. [192]	2013	x						PBCC [161]	2014		x				
EMBARC [181]	2013	x						FCCP [166]	2016		x				
FABRIC [183, 184]	2014 2016	x						SUPRA [163]	2016		x				
Kim et al. [177]	2014	x						MPC [164]	2016		x				
CAM [10]	2014	x						Rawat et al. [133, 101]	2009 2011		x	x			
Zhang et al. [178]	2014	x						Fuemmler et al. [146]	2006		x		x		
Wang et al. [199]	2014	x						Mhatre et al. [80]	2007		(x)		x		
Piao et al. [187]	2015	x						Balon et al. [127]	2006			x			
DynB [189]	2015	x						Zang et al. [139]	2007			x			
Jerk Beaconing [197]	2015	x						Eichler et al. [142]	2007			x			
Joerer et al. [202]	2016	x						C-RACCA [143]	2008			x			
Cheng et al. [182]	2016	x						Stanica et al. [135]	2011			x			
DTRCS [190]	2017	x						Stanica et al. [130]	2011			x			
BRAIN-F [200]	2017	x						Stanica et al. [129]	2011			x			
Sepulcre et al. [98]	2007	x	x					Hsu et al. [131]	2011			x			
CPRC [204]	2010	x	x					Sharafkandi et al. [140]	2012			x			
Huang et al. [109]	2010	x	x					Gomez et al. [132]	2013			x			
Sepulcre et al. [100]	2010	x	x					DACW [136]	2013			x			
Le et al. [205]	2011	x	x					Geo-backoff [137]	2014			x			
Sepulcre et al. [168]	2011	x	x					CEB [134]	2016			x			
Tielert et al. [206]	2013	x	x					Lu et al. [138]	2016			x			
INTERN [217, 110]	2014 2016	x	x					Mertens et al. [128]	2008			x		x	
Javed et al. [216]	2014	x	x					CTA [144, 147]	2010 2011				x		
SuRPA et al. [95]	2014	x	x					Stanica et al. [145]	2011				x		
IBA+TPA [218]	2015	x	x					SR-CSMA [148]	2012				x		
Jose et al. [208]	2015	x	x					UBPFCC. [124]	2005					x	
LIMERIC-RPC [207]	2015	x	x					Yang et al. [120]	2014					x	
ECPR [99]	2016	x	x					DR-DCC [121]	2015					x	
FABRIC-P [209]	2016	x	x					PDR-DCC [122]	2017					x	
Qian et al. [219]	2016	x	x					LORA [123]	2017					x	
DD-FPAV [171, 172]	2013 2014	x	x					Msg. Dispatcher [113, 114]	2006 2007						x
Puthal et al. [141]	2013	x	x	x				NbCO [117]	2010						x
DCC [94, 215]	2011 2015	x	x		x	x		POoC [116]	2011						x
FPAV [108]	2005		x					CbCO [115]	2012						x
Caizzone et al. [149]	2005		x												

x = adjusted parameter

INVESTIGATION OF CONGESTION AND AWARENESS CONTROL

Based on in-depth investigation and evaluation of state-of-the-art schemes, we identify recent problems occurring for VSC. We go through the problems which are found and addressed within this theses as follows (cf. section 4.1): First, we show the problems of a proactive suppression of CAM messages based on the dynamic generation rules introduced by the ETSI in [10]. Secondly, we show the effect of heterogeneous environments in terms of shadowing for a state-of-the-art protocol, which is followed by an evaluation of scalability and stability. We furthermore investigate the problem of channel load assessment and channel smoothing using first-order filtering with fixed weights. ¹

4.1 ADDRESSED PROBLEMS

4.1.1 *Dynamic CAM generation*

The dynamic generation of CAMs is used to prioritize nodes with a higher risk due to the movement status. Fast moving or dynamic vehicles change their status information more frequently and thus the entropy is much higher than for slow or non moving vehicles, where the entropy of the CAM compared with its last message is small or even zero. Since the capacity of the channel is limited, maximal entropy should be provided, while CAMs with no entropy shall be suppressed. The objective here should be to maximize entropy on the one hand, and maintain awareness on the other.

We evaluate the AC approach proposed by the ETSI in [10] using the urban (cf. section A.2.4) and the highway (cf. section A.2.3) scenario with a traffic jam. Figure 15 illustrates the CL observed by vehicles moving through the scenario using dynamically or periodically generated CAMs. The vehicle density in the highway scenario is significantly increased by the simulated traffic jam highlighted in figure 15a. If no AC is used, the nodes continue disseminating the messages at a rate of 10 Hz, which leads to massive channel congestion indicated by the high CL in that area. If dynamic CAM generation is applied, redundant information is suppressed and the message rate of nodes within the traffic jam is decreased to the minimal update rate, significantly reducing the load. An equal effect can be observed for the urban scenario, where a huge amount of vehicles are queued in front of a traffic light. Proactive suppression of redundant information thus can significantly reduce the load.

However, the thresholds introduced by the ETSI are not evaluated in terms of suitability, and thus more or less restrictive values need to be used in order to achieve an optimal trade-off between entropy and awareness. Like congestion control, awareness control will have an effect on the application due to the reduction of the

¹ Parts of this chapter are published in [222, 36, 223] and are under copyright of the IEEE or ACM

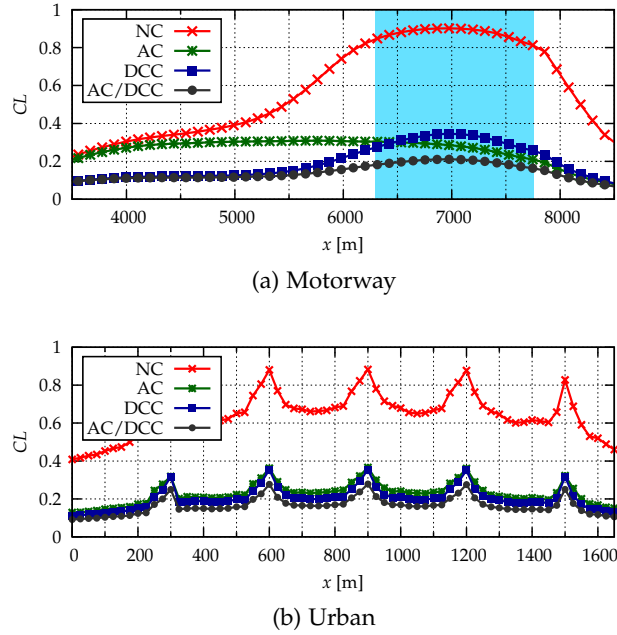


Figure 15: Impact of dynamic CAM generation on the observed CL

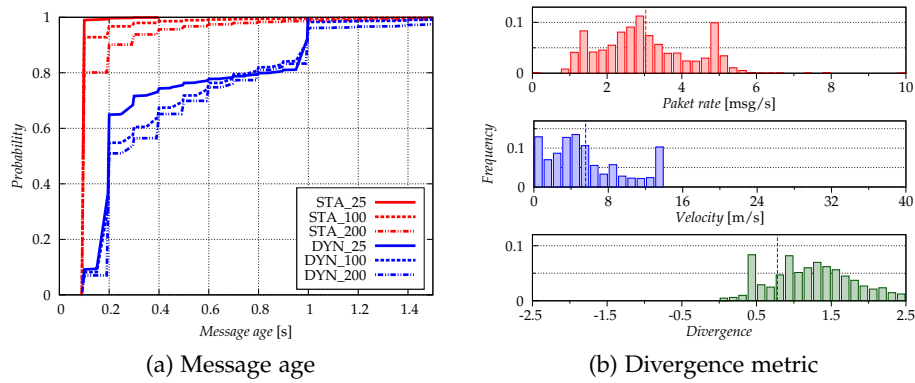


Figure 16: Effect of the AC method on the information freshness in the urban scenario.

message rate. Figure 16a illustrates the Cumulative Density Function (CDF) of the message age for the dynamic method compared with periodic CAMs. Obviously, applying this method will lead to a reduction of the information freshness, because the probability of receiving a new CAM within a certain time interval is lower compared to periodic dissemination. However, this is the expected behavior and it needs to be investigated whether the message age is reduced due to subsequent packet loss. Therefore we analyze the ratio of the average message rate (R) and the velocity of the vehicle (v) divided by the threshold (ΔP_{Thr}) subtracted by one:

$$Div = \frac{R}{v/\Delta P_{Thr}} - 1.$$

A divergence of 0 illustrates an optimal trade-off, values less than zero illustrate that there is a loss of information and values greater than zero represent redundancy. A vehicle driving at 12 m/s should have a rate of 3 Hz considering the default threshold

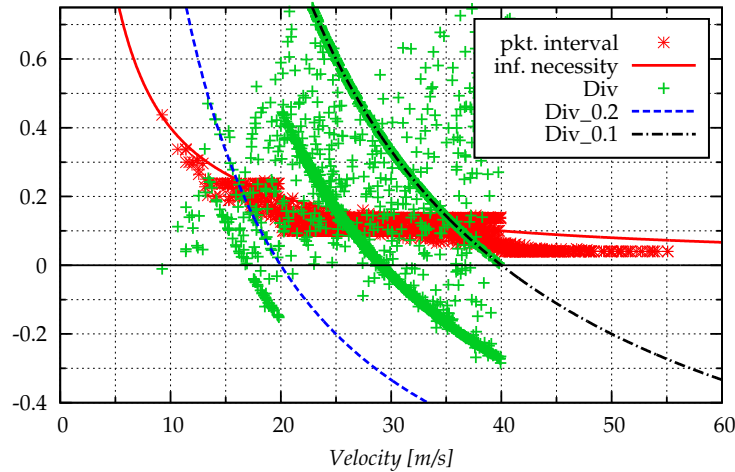


Figure 17: Illustration of the divergence achieved for higher maximal rates in the highway scenario

of $\Delta P_{\text{Thr}} = 4$ m to achieve a divergence of zero. However, we are just investigating one of the thresholds and do not consider subsequent message generation at high rate which is applied, such that slightly higher values for the divergence are expected. The results obviously depict divergence values which significantly exceed the optimal divergence, which means that the default thresholds are not sufficient (cf. figure 16b).

In case of the highway scenario, where there is no traffic jam, a slightly different problem needs to be considered. Vehicles moving on a highway are usually much faster than in urban or rural environments and thus the maximal message rate threshold of 10 Hz will be exceeded for any vehicle moving at 40 m/s. We evaluate the performance for fast moving nodes, where we set the maximal rate to 20 Hz. In Figure 17, we illustrate the results for the divergence based on the velocity of a vehicle. The information necessity curve indicates the packet interval that should be applied, while the curves DIV_0.1 and DIV_0.2 indicate the divergence achieved for a fixed rate of 10 Hz and 5 Hz respectively. The figure reveals, that using high rates, positive divergence and thus awareness can be maintained. However, it also shows that the fixed thresholds and the update interval can lead to negative divergence.

In order to maintain awareness, a proactive AC algorithm needs to have a high maximal rate to support highly risky vehicles, that have a large entropy. The dynamic CAM generation algorithm achieves a sufficient performance in reducing the load, while keeping the information freshness on a suitable level. It needs to be shown, that due to the reduction of the rate, the reliability of an application is not affected. We use a simplified version of the proposed generation algorithm without consecutive CAM generation at high rates for the evaluation of the dynamic part of the thesis. However, due to the modular design of the algorithm any other proactive AC can be applied which targets to limit the maximal rate of a vehicle.

4.1.2 Fairness / Environment Dependency

Fairness is an essential condition for cooperative system. Those systems need to agree on a common architecture to distribute the available resources among each

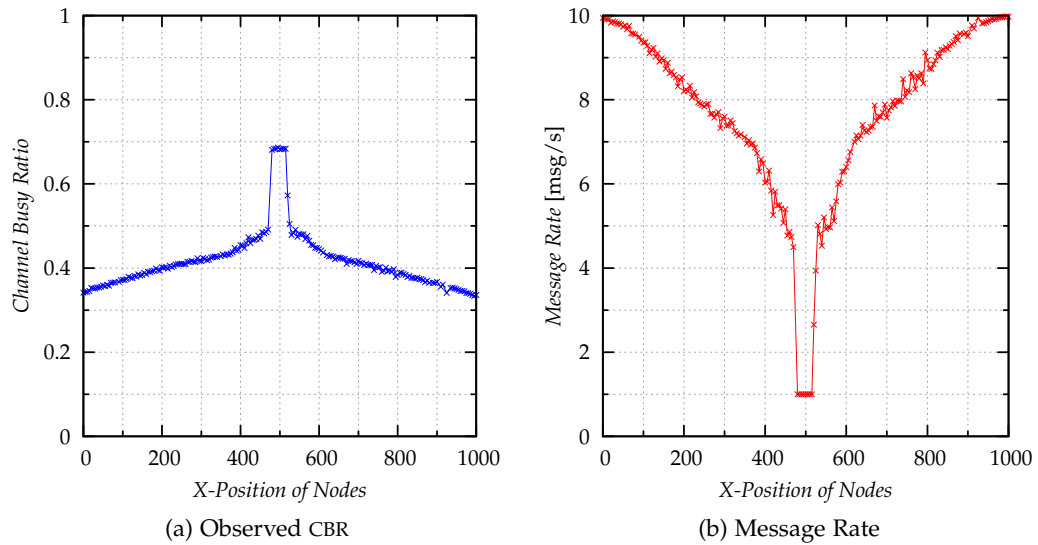


Figure 18: Performance of *LIMERIC* without cooperation at urban intersections. Unfair convergence of message rate for vehicles close and at the intersection. ($K = 200$)

other. If different systems are deployed, algorithms might try to exploit the fairness to achieve the best individual result. However, this is contradictory for cooperative systems, where the individual vehicle is less important than the interest of the group. As illustrated in section 3.2, there might be different definitions of fairness. While local fairness is used to maximize the throughput and global fairness is used to achieve the same with respect to single affected vehicles, weighted fairness gives priority to single vehicles. Although decentralized, the rules for all vehicles are the same and known to them, which means there is a common agreement on this technique. If the rules are followed but they are under environmental influence, it can lead to unfairness.

A major problem in urban environments are buildings so that the communication range of a vehicle is strongly dependent on the street layout [224]. Considering the urban intersection scenario shown in figure 95, there are regions L_i where buildings shadow signals and thus network load is lower than without shadowing. Vehicles which are at or close to the intersection (C) are affected by the *hidden terminal problem* which is indicated by the set of regions being in communication range ($C \rightarrow \{L_1, L_2, L_3, L_4\}$, $L_1 \rightarrow \{C, L_3\}$, $L_2 \rightarrow \{C, L_4\}$, ...). Assuming equal communication parameters, the utilization in C is much higher than in the other regions. Note that there is a minority of vehicles which can communicate through NLOS condition.

The effect is illustrated in figure 18. Here, *LIMERIC* with *gain-saturation* is used with the local fairness principle. The nodes at the intersection are encountered with nearly twice as many incoming messages, than the nodes at the lanes. This results in a much higher network load which significantly exceeds the predefined target resource utilization of $r_g = 0.6$ (cf figure 18a). *LIMERIC* encounters higher loads by reducing the individual message rate. Unfortunately in this situation, the nodes on the intersection are not responsible for the load which is created by the nodes on the lanes. Thus the algorithm keeps reducing the local message rate until the minimal rate is reached (cf. figure 19). Due to the shadowing, the nodes on the lane will keep

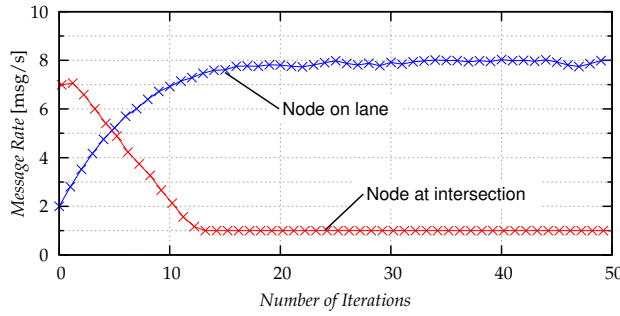


Figure 19: Convergence to unfair message rates for nodes at the intersection and on the lane.

there higher rate leading to an unfair resource allocation due to the environmental influence (cf. figure 18b).

In order to overcome this local unfairness, nodes can cooperate by exchanging and validating their locally observed message rate and react on a common basis. The global fairness principle considers this and can help to reduce unfairness in certain situations like this at the cost of reduced overall throughput. However, environmental influence on this algorithm is immense. Just one exploiting node can lead to a collapse of the system by disseminating a high CL. Verification and cross-validation for the same region needs to be applied in order to prevent this exploitation. Furthermore, environments are hardly predictable and vary a lot from LOS to NLOS, *highways* to *urban* or even from US to Europe. A system however needs to achieve fair allocation of the resources in each of those situation which can only be possible through an adaptive structure.

4.1.3 Stability and Scalability

The scalability describes the capability of a mechanism to adopt to different vehicle densities. A scalable protocol therefore should offer density independent features, such as stability, fairness, and speed. Densities in VANETs have a huge variety from very low (rural area) to very high, i.e. traffic jam on a multi-lane highway. The motivation therefore is to design a protocol, that is robust in terms of scalability. Investigating the effect of scalability on the proposed protocols shows that there is still space for optimization.

For *LIMERIC* the major parameters therefore are the convergence parameters. Especially β as a multiplicand for the utilization difference can have a significant effect on the robustness and needs to be parametrized carefully as already depicted by the authors [13]. The operating range of the vehicle density for *LIMERIC* is specified by the inequality $\alpha + K\beta < 2$, where K indicates the number of vehicles in communication range, such that $K < (2-\alpha)/\beta$. In terms of scalability, β might be chosen small in order to increase the node density.

The supposed solution of *gain-saturation* can help in terms of granting enhanced stability, but this does not solve the initial problem of density dependency.

One major problem of high densities is the influence that minor changes of the message rate have on the network load. Without first-order filtering techniques, this

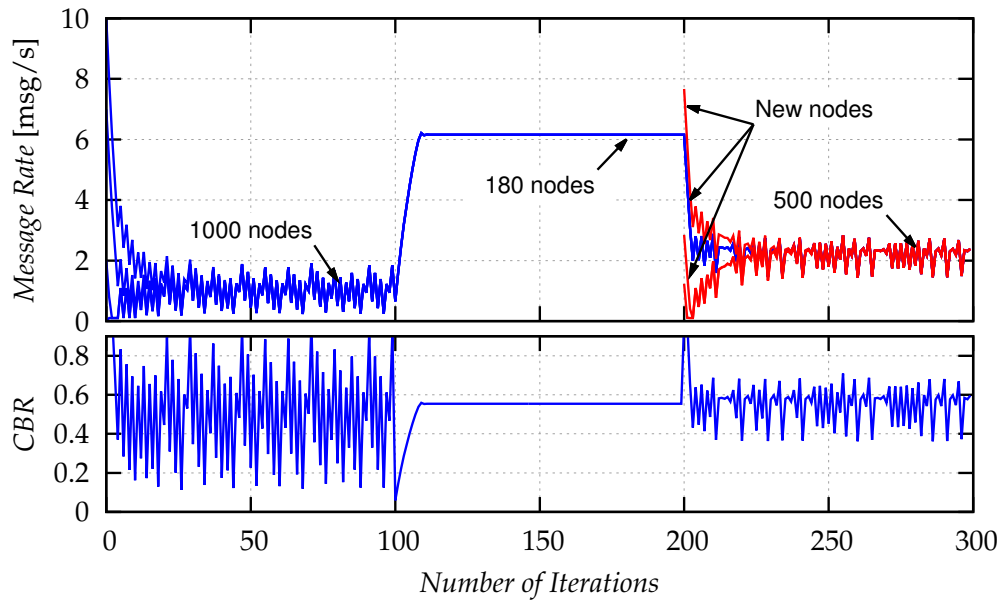


Figure 20: Stability and convergence of *LIMERIC* with *gain saturation* over time for different vehicle densities ($\alpha = 0.1, \beta = 1/150, K = 1000, 180, 500$)

effect has a direct influence on a reactive congestion control technique leading to increased volatility and unstable behavior.

For DCC, scalability is directly influenced by the parameters defined within the states. It is designed to be scalable up to a certain density, which conducts a *RESTRICTIVE* access to the channel. Exceeding this threshold, an increase in the network load is out of the algorithms control.

For control- and feedback control systems, there are different definitions of stability. Basically a system can be described as instable, if it does not converge to a non oscillatory steady-state after a distortion. In terms of congestion control methods, after a certain convergence time, a stable state should be achieved to ensure reliable time independent transmission, i.e. the QoS shall be the same for t and $t - 1$. The stability is closely connected to the scalability. For low densities, congestion control is unnecessary, while for high densities, reactive systems tend to get instable due to the volatile input values, i.e. network load.

Within its operating range and in LOS conditions, *LIMERIC* achieves a stable convergence. Although convergence is given for high vehicle densities using *gain-saturation*, stability can not be provided anymore. This is illustrated in figure 20, where the message rate r_j and resource utilization r_c is plotted over time for differing node densities using *LIMERIC* with *gain-saturation*. We use a simplified MATLAB model where we assume that the utilization is $0 \leq r_c \leq 1$, there is no measurement noise, no packet loss and no path loss, e.g. ideal channel. The parameters are the same as used for *LIMERIC* [13], where $\beta = 1/150, \alpha = 0.1$ and $r_g = 0.6$. The maximum rate is $R_{max} = 10$ Hz and $TXTIME = 0.0005$ s. Any new node is initialized with an initial rate $0 < r_j(0) \leq TXTIME \cdot R_{max}$.

The convergence behavior shows, that *gain-saturation* fails in achieving a stable system behavior for both $K = 500$ and $K = 1000$, due to the high volatility of the CBR (cf. figure 20) and thus high reaction of the β -part of the algorithm.

The state-based system of DCC has a significant drawback in terms of stability. If the network load is around a state-transition, the algorithm will switch between

these two states leading to highly volatile states and in consequence CBR [225, 211]. We investigated this effect in detail by conducting an in-depth simulation study which was published in [173].

For *LIMERIC* a low message rate indicates a high density which benefits volatility in the network load. Since the algorithm adjusts the message rate only on the difference of this load, the same volatile behavior occurs. Assume there are $K = 1185$ nodes, which would lead to an steady-state message rate of $r_j = 0.0005$. Using the convergence parameters of $\alpha = 0.1$ and $\beta = 1/150$, a change of the network load r_c by 0.075 will introduce the adjustment limitation of $X = 0.0005$, which itself is as big as the rate itself. This factor is used whenever a rate adjustment of $\Delta r_j > \pm 6.329e^{-5}$ is done, indeed it is nearly always used. Obviously the system is very sensitive to minor changes and thus stability can not be achieved.

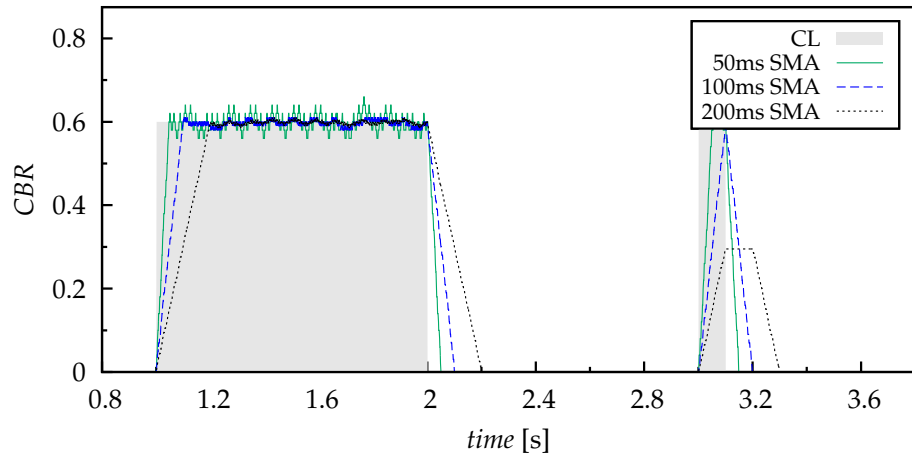
An adaptive protocol should reflect this by applying first-order filter methods to suppress volatility. An unstable congestion control algorithm, does not provide the reliable QoS required by safety applications. Under high densities, volatile CBR can not always be avoided for non ideal systems, but the reaction to it can be adjusted. Nevertheless, an adaptive algorithm needs to grant a scalability independent functionality.

4.1.4 Channel Smoothing

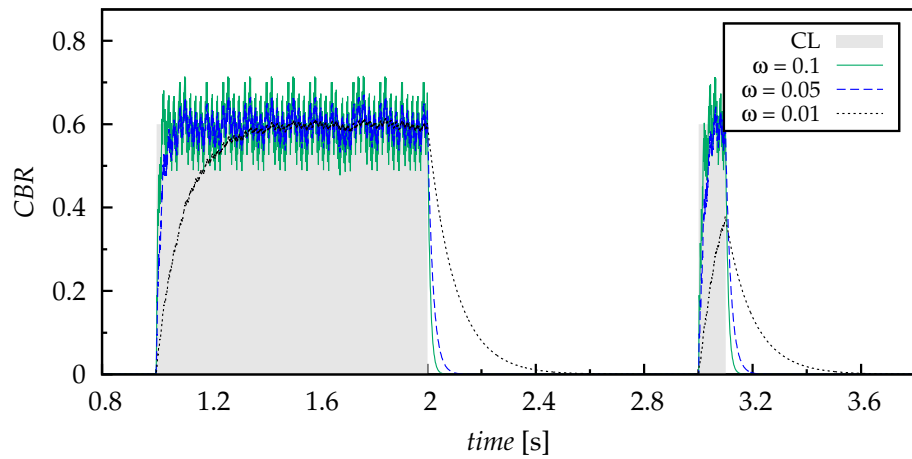
The CBR as input variable (cf. section 3.1.3) indicates the current resource utilization, which is of major interest to the algorithm proposed. Using the measurement setup described in appendix B, it is revealed that one problem of the CBR is the inaccurate measurement itself. Considering a theoretical CBR of 0.6 and a monitoring interval of $t_{\text{CMDI}} = 200\text{ms}$, the average inaccuracy is $\Delta\text{CL} = 0.01$, with higher deviation. In the previous section, it was shown that already minor changes have a significant impact on an algorithm. Besides the inaccuracy of the measurement, the CBR is always an average over a certain time period, such that it can be highly volatile over time. Tielert shows, that this volatility due to the averaging process is significantly influencing the CBR values retrieved during one time period [106].

Low-pass filtering techniques can be used to smooth the inaccuracy of the CBR over time. The CBR calculation itself is a SMA of true and false samples within a sliding window of length t_{CMDI} . In figure 21c we illustrate different filter techniques applied for a certain reference CL pattern, where there is a load of 0.6 between 1.0 s and 2.0 s and another peak load at 3.0 s. This load is generated using the experimental set-up described in section B. The CCA function is evaluated every 1 ms which means there are $N_p = 1000$ probes per second.

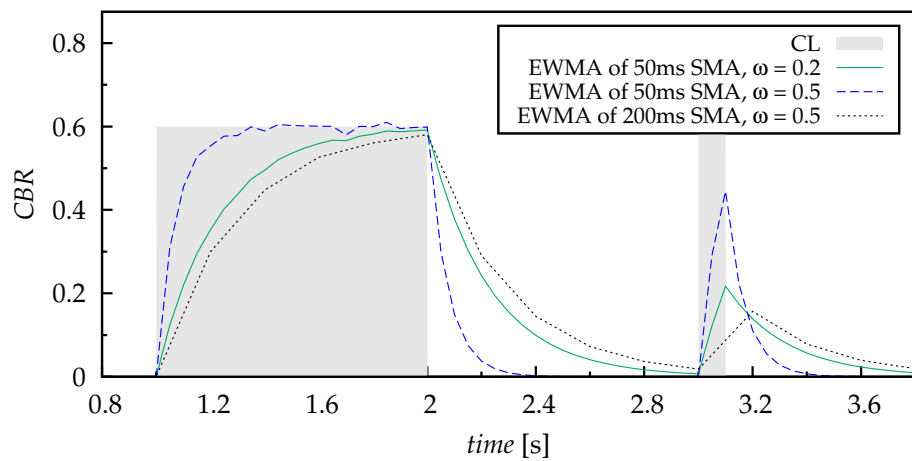
SMA The SMA can be used as a linear filter technique. It calculated the average of an input set during one time window of size t_{CMDI} . The SMA is calculated for every iteration, where the time between to iterations is smaller than the time window itself ($t_I < t_{\text{CMDI}}$). In that way, each value of the input set is used multiple times resulting in a smoothing of the input. A SMA linearly converges to a fixed input set within one time window, which can be beneficial for some applications. Figure 21a gives an example of the functionality of a SMA for different time windows t_{CMDI} and the fixed $t_I = 1\text{ms}$. From the figure it is obvious, that larger time windows increase



(a) SMA based on a probe interval of 1 ms



(b) EWMA based on a probe interval of 1 ms



(c) EWMA of SMA values evaluated at fixed point in time

Figure 21: Impact of filtering techniques on the observed CBR

smoothness at the cost of convergence time, i.e. accuracy. However, it has a finite impulse response.

$$\tilde{x}(t) = \frac{1}{n} \sum_{i=0}^{n-1} x(t-i), \quad (4.1)$$

where n is the number of iterations considered during the time window.

EWMA The EWMA is another low-pass filtering technique which can be described by

$$\tilde{x}(t) = (1 - \omega) \cdot \tilde{x}(t-1) + \omega x(t), \quad (4.2)$$

where ω indicates the averaging parameter, x is the input and \tilde{x} the output value. Unlike the SMA, an EWMA is an infinite filter, i.e. its impulse response is infinite. Furthermore, the filter has an infinite history of previous input such that it is not memoryless, like the SMA. The EWMA assigns a higher weight to newer values, such that it reacts faster to distortions, but needs longer to converge. Thus, compared to SMA it can achieve better smoothness while maintaining fast reaction. Figure 21b illustrates this behavior, where the input values $x(t)$ are the probes itself for different weights. While small weights lead to slow reaction and thus convergence time, larger weights result in highly inaccurate perception of the reference load.

However, in reality the SMA of the probing method is calculated for a certain time-window t_{CMDI} and evaluated at fixed points in time, i.e. the CBR within the last monitoring interval is necessary for the decision process. Based on this retrieved values, an EWMA based filtering is applied to smooth the CL furthermore and suppress volatility. We demonstrated the retrieved CBR based on this channel smoothing method for different weights and time-windows. Studies likely use a fixed weight of 0.5 [14, 226] to smooth out volatility. Obviously for a larger time-window, this leads to long reaction times and inaccurate CBR calculation (cf. figure 21). This Self-Weighting called method was applied for *PULSAR* in [106].

ENVIRONMENTAL INFLUENCE A common drawback is the occurring delay in the time domain between input and output signal. This delay can cause huge inaccuracies, whenever there are distortions. Vehicles are used in different environments, which have different requirements in terms of low-pass filtering of the CBR. A fixed weight for the EWMA of $\omega = 0.5$ is said to be sufficient for channel smoothing [14, 226].

Figure 22 illustrates the impact of different weightings for the channel load smoothing used within a dynamic scenario. When no smoothing is applied, i.e. $\omega = 1.0$, the CBR is highly volatile. While for an urban environment with low vehicle speeds a weight of $\omega = 0.5$ can successfully suppress the volatility, while maintaining high accuracy, volatility is still present for the same weight in the highway scenario (cf. figure 22b). A weight of $\omega = 0.1$ is able to smooth the CBR here, but it has a huge delay, which needs to be considered. However, applying these low weight in urban environment would lead to an unnecessary huge delay.

This illustrates, that using fixed weights for the smoothing of the channel load is not sufficient in order to obtain volatility free, but accurate approximations of the

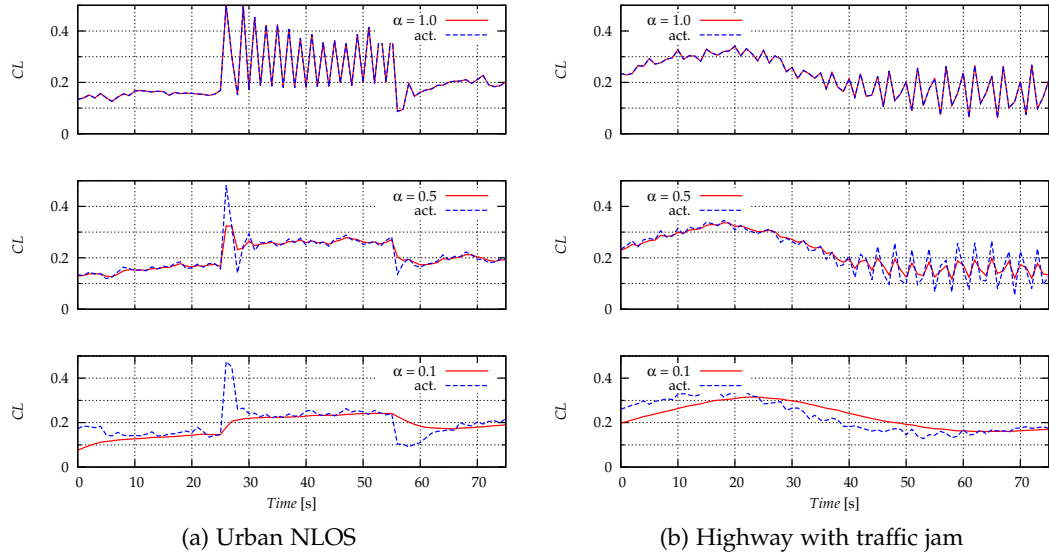


Figure 22: Influence on the environment on the weight chosen for channel load smoothing using EWMA

CBR. A reactive algorithm which reacts sensitive to high delay or volatility of the CBR should reflect this by applying an adaptive weighting strategy, where minor distortions are filtered, but fast reaction to environmental changes is maintained.

4.2 SUMMARY

Within this section, we investigated state-of-the-art schemes for VSC. We show, that the protocols fail in providing a scalable, stable and fair allocation of the resources under congested conditions. It is shown, that cooperation between the nodes is essential in order to maintain a fair sharing of the resources such that each vehicle is able to maintain a certain level of awareness, independently of the environment. Although it is shown, that the proactive reduction of CAMs can result in a leak of awareness, it is a suitable method in order to reduce the load induced by unnecessary CAMs. Finally, it was shown, that the often used input value CBR can be highly inaccurate and volatile over time and simple channel smoothing with fixed weights is not a sufficient method to reduce volatility in VANETs. The findings of this chapter are used to motivate a new protocol addressing these issues in the next chapter.

The focus of this section is to describe the architecture of the adaptive congestion control protocol, namely SWeRC. SWeRC aims at providing a stable, scalable, and fast reaction to different environments and is able to provide local, global, or semi-global fairness due to its cooperative design. Furthermore, dynamic rules for the generation of Cooperative Awareness Messages (CAMs) can be applied to decrease the dissemination of redundant, but, due to minor information content, non-necessary messages. The major benefit of the algorithm is its cooperation in order to grant a fair resource allocation for all nodes within a certain cooperation range.¹

We provide a general overview of the modular protocol architecture in section 5.1 and subsequently introduce and explain the individual modules. A dynamically weighted Channel Busy Ratio (CBR) smoothing module addressing the load volatility problem is introduced in section 5.2. The heart of the algorithm is the transmission rate adaption algorithm which is introduced in section 5.3. This section also includes the description and motivation of the target rate and the used rescheduling mechanisms. The fairness issue is addressed by a piggyback-based exchange of channel status information and its functionality is explained in section 5.4. Finally, we provide an in-depth analysis of the parameters of SWeRC and propose a parameter-optimized target rate adaption scheme in section 5.5.

5.1 PROTOCOL ARCHITECTURE

Figure 23 shows the general structure of the protocol. The protocol consists of two disjunct parts, namely the control and the executive part. The control part includes the feedback control loop which is used for the adaptive transmission rate control, while the objective of the executive part is to apply the rate adaption to the dissemination process.

The heart of the control part is the self-weighted transmission rate adaption (SWeRC) which is based on *LIMERIC* [13] and described in section 5.3. The algorithm is based on feedback retrieved by local CBR measurements and optional information exchange between the nodes. The objective of the mandatory target rate r_t as an input factor and its gathering is explained in detail in section 5.3.1. The resource utilization, indicated by the CBR, is either retrieved by local measurements with optional filtering of the obtained values (cf. section 5.2), or piggyback-based exchange and aggregation of channel status information among the nodes which is used in order to cooperate and adapt the rate on a common basis (cf. section 5.4). Other parts of the algorithm are a limitation of the maximum transmission rate based on vehicle movement patterns as described in [10] and the restriction regarding the minimal rate based on safety requirements.

The control loop is executed synchronously in fixed intervals between all nodes in the network. The interval between two iterations is t_{CMDI} and a trigger causes

¹ Parts of this chapter are published in [93, 223] and are under copyright of the IEEE

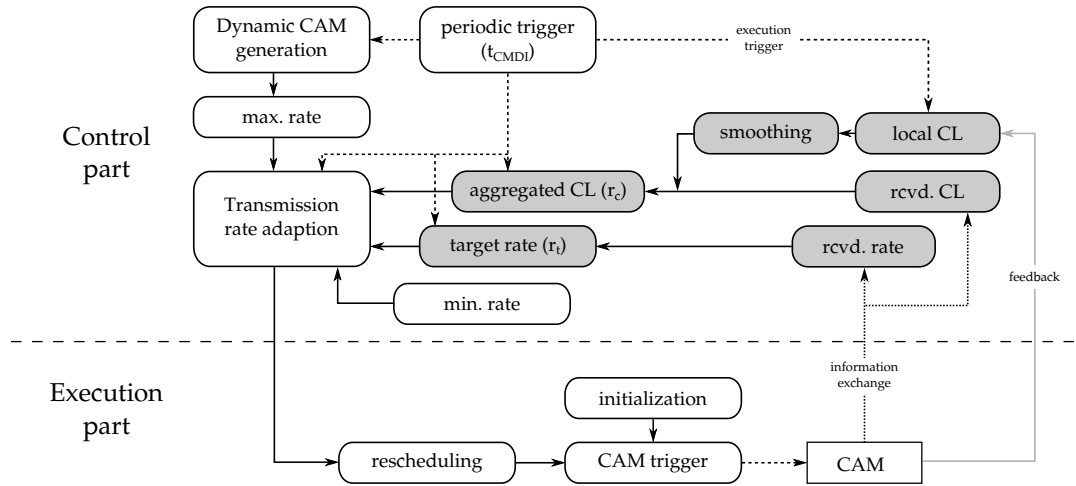


Figure 23: Overview of the elements for the adaptive protocol including control and information flow

the simultaneous execution of different mechanisms within the protocol, including the rate transmission adaption. A new rate is calculated with each iteration and needs to be applied to the CAM dissemination process. The executive part undertakes this task. The major part of the executive part is the rescheduling mechanism (cf. section 5.3.2) which is responsible for an immediate and appropriate mapping of the new rate to the CAM generation process initiated by the trigger. While the control part is time-synchronous, the executive part needs to be asynchronous to avoid message bursts. Thus, the initialization process assigns a random time for the first CAM trigger to each node.

The two parts are interconnected through the rescheduling process and the CAMs, building the overall feedback control system. The number of CAMs generated in a time interval mostly depends on the rate decision which subsequently has a direct influence on the locally assessed resource utilization. The target rate and information exchange also depends on the locally assessed CBR.

5.2 CBR VOLATILITY SUPPRESSION

We show in section 4.1.4 that first-order filtering of the observed channel status information can be beneficial in order to maintain stability of the algorithm due to suppressed volatility. On the other hand, the weights of the filter need to be suitably small to achieve this which leads to inaccuracy for certain distortions of the load, e.g. due to change of the environment. Furthermore, for different environments the weights have to be adopted in order to achieve an optimal result. We conclude that static weights for channel smoothing are not sufficient for the requirements of highly dynamic VANETs. Instead, we propose to use a dynamic filtering technique which still utilizes the EWMA, but the weights are dynamically calculated based on the achieved accuracy and volatility.

The basic idea is that the weight should be high if the accuracy is low and vice versa. To achieve this, the accuracy and volatility are calculated using a SMA for the last n iterations. The accuracy is quantified in terms of the average measurement

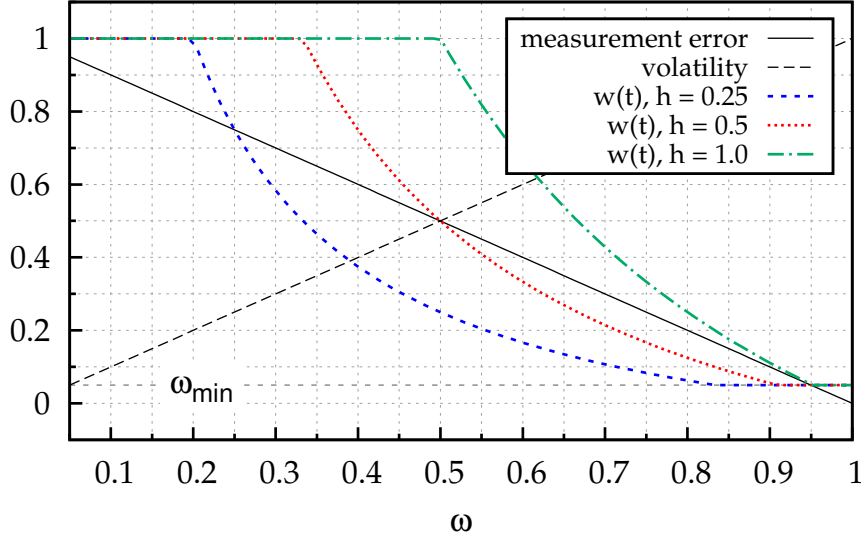


Figure 24: Illustration of the weight ω for different multiplicands h based on the average weight within the last iterations. ($\omega_{\min} = 0.05$)

error which is the difference between the observed r_c and the smoothed utilization \tilde{r}_c :

$$\bar{e}(t) = \frac{1}{n} \sum_{t-n}^t |r_c(t) - \tilde{r}_c(t)| \quad (5.1)$$

The volatility for an iteration is calculated based on the observed loads, where we set the base time to one iteration:

$$\overline{\text{vol}}(t) = \frac{1}{n} \sum_{t-n}^t |r_c(t) - r_c(t-1)| \quad (5.2)$$

This is suitable for algorithms which react in each iteration. For algorithms that do not react in every iteration, the base interval of the calculation should be set to the interval between the reactions of the algorithm. Both volatility and accuracy are subsequently used to adjust the weight $w(t)$ for this iteration

$$\omega(t) = h \cdot \frac{\bar{e}(t)}{\overline{\text{vol}}(t)}, \quad \omega_{\min} \leq \omega(t) \leq 1. \quad (5.3)$$

In figure 24, we exemplarily show the achieved weight for different factors h . We assume that the measurement error is anti-proportional to the weight $\bar{e} = 1 - \omega$ and the volatility is proportional to $\overline{\text{vol}} = \omega$. For $\omega = 1$, the error is 0, while the volatility is 1 and vice versa for $\omega = 0$. On the basis of the figure we see that the factor h influences the convergence of $\omega(t)$ towards the ratio between the inaccuracy and volatility. In other words, a higher factor h will lead to a higher accuracy at the costs of less smoothing.

Finally this weight is used for the EWMA filtering method:

$$\tilde{r}_c(t) = \omega(t) \cdot r_c(t) + (1 - \omega(t)) \cdot \tilde{r}_c(t-1) \quad (5.4)$$

This method does not follow trends. If, for example, a vehicle is moving away from a jam, the utilization will decrease over time which will be indicated as volatility. Linear regression can be used to follow a trend and calculate volatility based on this trend. Furthermore, the proposed method is based on a numerical investigation and thus optimality of the smoothing behavior is not guaranteed.

5.3 TRANSMISSION RATE ADAPTION

Even with the use of gain-saturation, *LIMERIC* fails to provide a stable and scalable rate adjustment due to the fixed convergence parameter β . But densities in VANETs change rapidly and very high densities can occur frequently. The parameter β either needs to be parametrized to guarantee stability under the maximum achievable vehicle densities or has to be dynamic. The author of *LIMERIC* [13] suggests a slowly reacting second loop to control β . Both approaches are non-sufficient solutions and may either lead to slow convergence or oscillations.

Instead, we propose to use a fast reacting self-weighted rate control (SWeRC) based on a local group rate. While the basic enhancement is already usable, we present an optimized version of this algorithm considering the results of the parameter investigation at the end of this section. The weighting of the adjustment should be based on the last rate which is normalized to the maximum achievable rate. This allows stronger reactions for higher rates and weaker reactions for low rates and thus causes less oscillations.

We show that the algorithm converges, but unfortunately, it does not converge to a fair rate allocation (cf. (5.22) with $r_t = r_j$). To guarantee convergence to a fair rate, one has to consider the local group rate r_t instead so that each node converges to this rate with respect to the target utilization r_g . The weight is denoted as follows:

$$\begin{aligned} \omega &= \frac{1}{R_{\max} \cdot \text{TXTIME}} \cdot \frac{r_c(t-1)}{K}, & r_c(t) &= \sum_{j=1}^K r_j(t) \\ &= c \cdot \frac{1}{K} \sum_{j=1}^K r_j(t-1) \\ \omega &= c \cdot r_t(t-1), \end{aligned} \quad (5.5)$$

where c is the maximum local node capacity at the maximum rate R_{\max} considering the transmission delay TXTIME , i.e. $c = 1/(R_{\max} \cdot \text{TXTIME})$. The group rate r_t represents the average message rate of the K nodes. Further details of the group rate r_t are provided in section 5.3.1. The weight ω (5.5) is finally used for the standard *LIMERIC* algorithm:

$$r_j(t) = (1 - \alpha)r_j(t-1) + \omega\beta(r_g - r_c(t-1)). \quad (5.6)$$

Note that r_j does not need to have an upper bound, but it has to be greater than zero ($r_j > 0$), otherwise convergence cannot be guaranteed.

SWeRC (5.6) converges to the following fix point

$$r_j = \frac{1}{K} \left(r_g - \frac{\alpha}{c\beta} \right), \quad j = 1, 2, \dots, K \quad (5.7)$$

For a steady-state fair allocation of the available resources, the proof is as follows:

$$\begin{aligned} r_j(t-1) &= r_j(t), & \text{use (5.6)} \\ r_j(t-1) &= (1-\alpha)r_j(t-1) + \omega\beta(r_g - r_c(t-1)), & \omega = c \frac{r_c(t-1)}{K} \quad (5.5) \\ 0 &= \frac{r_c(t-1)}{K} c\beta(r_g - r_c(t-1)) - \alpha r_j(t-1), & r_j(t-1)^i = \frac{r_c(t-1)}{K} \\ 0 &= r_j(t-1)[c\beta(r_g - Kr_j(t-1)) - \alpha], & r_j(t-1) > 0 \\ 0 &= c\beta(r_g - Kr_j(t-1)) - \alpha \\ r_j(t-1) &= \frac{1}{K} \left(r_g - \frac{\alpha}{c\beta} \right) \end{aligned}$$

This fix point is the same as proved for *LIMERIC* including the weight (5.5) and considering that $r_t = r_j$ in steady-state:

$$r_j = \frac{\omega\beta r_g}{\alpha + K\omega\beta}, \quad j = 1, 2, \dots, K$$

From equation (5.7), one can easily retrieve the steady-state utilization considering $r_c = Kr_j$:

$$r_c = r_g - \frac{\alpha}{c\beta}. \quad (5.8)$$

SWeRC achieves a density-independent steady-state utilization which is only influenced by the convergence parameters and the target utilization r_g itself. This can be used to specify a steady-state utilization r_c directly. We will discuss this in detail in section 5.5.

We verify the enhancements using a simplified MATLAB model where we assume that the utilization is $0 \leq r_c \leq 1$, there are no measurement noises, no packet losses, and no path losses, i.e. an ideal channel. Based on these assumptions, we investigate the stability and convergence for different node densities as shown in figure 25. The parameters are the same as used in *LIMERIC* [13], i.e. $\beta = 1/150$, $\alpha = 0.1$, and $r_g = 0.6$. The maximum rates are $R_{\max} = 10$ Hz and $\text{TXTIME} = 0.0005$ s. Any new node is initialized with an initial rate of $0 < r_j(0) \leq \text{TXTIME} \cdot R_{\max}$.

Figure 25 illustrates the convergence behavior for an initial group of 250 nodes and distortions caused by removing 100 nodes in iteration $N = 100$ and adding 50 new nodes in iteration $N = 200$. Note that this scenario is exactly the same as used in [13]. The convergence time is higher and the steady-state message rate r_j is lower in comparison with *LIMERIC*. The figure also reveals the density-independent channel utilization $r_c = 0.525$ which indeed is lower than for *LIMERIC* ($r_c \approx 0.546$ for

¹ In steady-state, all nodes shall have the same, fair resource share. Hence, the available capacity shall be equally distributed among the K nodes.

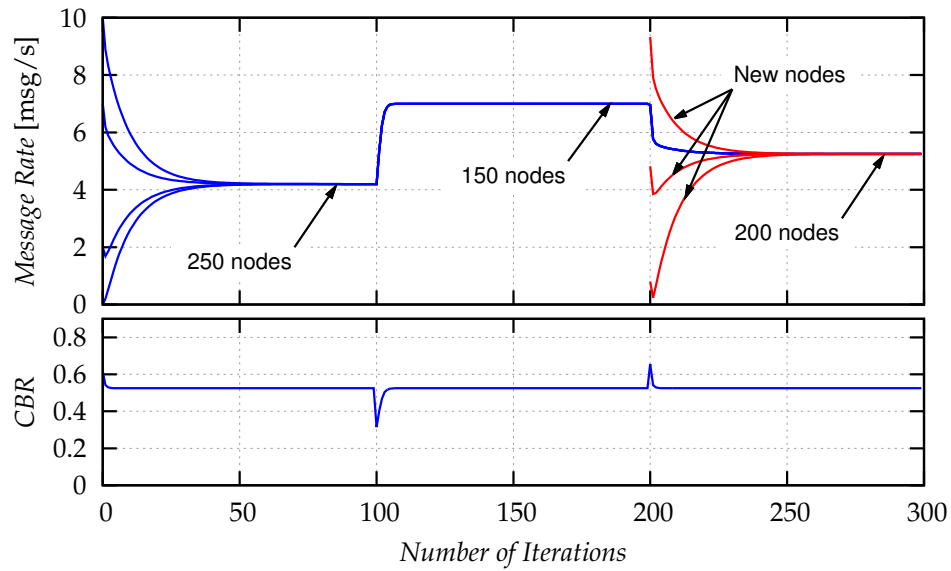


Figure 25: Stability and convergence of the enhanced *LIMERIC* algorithm over time for different vehicle densities ($K = 250, 150, 200$)

$K = 150$). This result is obvious, because the enhancement requires an optimization of the convergence parameters.

5.3.1 Target Rate Mechanism

The target rate mechanism is an essential element for the transmission rate control, because it ensures the convergence of the individual rates to the fair rate. By using the target rate instead of the individual rates, the algorithm becomes semi-cooperative, because a node's decision depends on the perceived group rate. However, it will not need to be highly accurate if the convergence parameters are not chosen too aggressively, because it is just needed for the initial convergence of the individual rates to the fair message rate and is equal in steady-state ($r_t = r_j$) which implies a high accuracy due to redundancy.

The rate adaption algorithm (5.7) will not converge to a fair steady-state rate if no target rate mechanism is used. Assuming that all nodes have an individual rate

$$r_j \neq r_i, \quad \forall i \neq j, \quad (5.9)$$

and the algorithm is in the steady-state, i.e. the utilization is like in (5.8), the individual rates will stay unchanged. Since (5.9) holds, the steady-state rate is not fair. The proof is:

$$\begin{aligned} r_j(t) &= (1 - \alpha)r_j(t-1) + r_j(t-1)c\beta(r_g - r_c) \\ &= r_j(t-1)\left(1 - \alpha + c\beta\left[r_g - r_g + \frac{\alpha}{c\beta}\right]\right) \\ &= r_j(t-1) \end{aligned}$$

The target rate is calculated as the SMA of the individual rates from all nodes within the communication range. All nodes within the communication range contribute to the utilization of the channel such that

$$r_c(t) = \sum_{j=1}^K r_j(t-1). \quad (5.10)$$

Using this, the equation (5.5) holds:

$$r_t(t) = \frac{1}{K} \sum_{j=1}^K r_j(t-1) = \frac{1}{K} r_c(t-1) \quad (5.11)$$

Furthermore, in the steady-state, the rate r_j equals the group rate due to

$$r_j = \frac{r_c}{K} = r_t \quad (5.12)$$

TARGET RATE ACQUISITION The target rate is acquired by using different techniques. If the principle of local fairness is applied, this rate will be obtained by using decentralized methods. In the following, we discuss two different approaches followed by the description of the technique used for this work.

We showed in section 2.1 that C-ITS stations are equipped with a LDM which collects, validates, and aggregates the received environmental information. An essential part is the highly dynamic layer containing information about the neighboring nodes. Based on the number of nodes within the communication range, we calculate the target rate using the measured resource utilization.

Therefore, all valid nodes need to be stored in a list until they expire due to lack of CAM messages. The length of this list approximates the number of nodes K within the communication range from which we can retrieve the group rate by r_c/K . However, the expiration time needs to be parametrized such that it includes low transmission rates (< 1 Hz) without losing accuracy in terms of expired vehicles. Thus, the approximation error will be significant in highly dynamic environments.

Another decentralized method is to approximate the group rate based on the IRT of the received CAMs within one iteration. For the IRT, the group rate is calculated using a SMA by

$$r_t(t) = \text{TXTIME} \cdot \frac{1}{n} \sum_{j=1}^n \frac{1}{\text{IRT}_j}, \quad n \leq K, \quad (5.13)$$

where n is the number of messages received from disjunct nodes during one iteration. For the calculation of the group rate, only the most current IRT of a node is used. While this method benefits from the immediate calculation of the group rate, independent of the number of nodes, the resource utilization affects it in terms of interference still. The interference will increase the IRT of every single node and thus, the approximated group rate will be lower than the theoretical group rate. On the other hand, the interference is also included in the resource utilization leading to an underestimation of the actual utilization. Furthermore, the effect of message

rescheduling is also included. Besides this, at least two CAMs have to be received for the calculation of the IRT.

Semi-cooperative target mechanism

While the afore-mentioned techniques work decentralized, we use a semi-cooperative approach based on piggybacking, as introduced by Tielert et al. in [14]. The benefit of piggybacking (cf. section 5.4) is the accuracy of the offered information and the possibility of supporting the global fairness principle.

Each node appends its current rate r_j to the CAM before disseminating it. A node calculates the group rate r_t based on the received rates within the last iteration using a SMA by

$$r_t(t) = \frac{1}{n} \sum_{j=1}^n r_j(t-1), \quad n \leq K, \quad (5.14)$$

where n is the number of messages received from disjunct nodes during one iteration. Since the direct exchange of the individual rates is used, interferences and rescheduling do not affect the calculation of the group rate. Unlike IRT, this semi-cooperative approach is used from the first message and the group rate is exchanged over multiple hops, i.e. fairness range extension (cf. section 5.4).

Unlike Tielert et al., we use the average of one iteration to calculate the group rate for the next iteration. Moreover, the authors suggest to use an EWMA where each incoming information is treated equally. An EWMA prefers faster transmitting nodes, because their rate is counted multiple times. In addition, it has an infinite history such that precise information of one iteration cannot be achieved. The use of an EWMA is appropriate, though, in case the target rate is highly volatile and smoothing needs to be applied. It will also be useful if the access times are not uniformly distributed, i.e. there are bursts of transmissions. Note that a SMA only considers a subset of vehicles within one iteration ($IRT > t_{CMDI}$).

5.3.2 Message Rescheduling

After each iteration, the new rate needs to be applied to the message dissemination process. Typically, the last disseminated message was sent out less than $TXTIME/r_j(t-1)$ seconds ago. In order to apply the new rate $r_j(t)$ to the dissemination process, there are several methods that can be considered. In the following, t_{prev} determines the time when the previous CAM was generated, t_{rem} indicates the remaining time based on $r_j(t-1)$ and t_{now} specifies the current time.

The following methods are considered for rescheduling for a transition from $r_j(t-1)$ to $r_j(t)$:

- The next transmission takes place for $t = t_{prev} + t_{rest}$, i.e. no rescheduling is done.
- Multiplicative rescheduling which is applied based on the remaining time such that the next transmission takes place for $t = t_{now} + t_{rem} \cdot r_j(t-1)/r_j(t)$ [14].

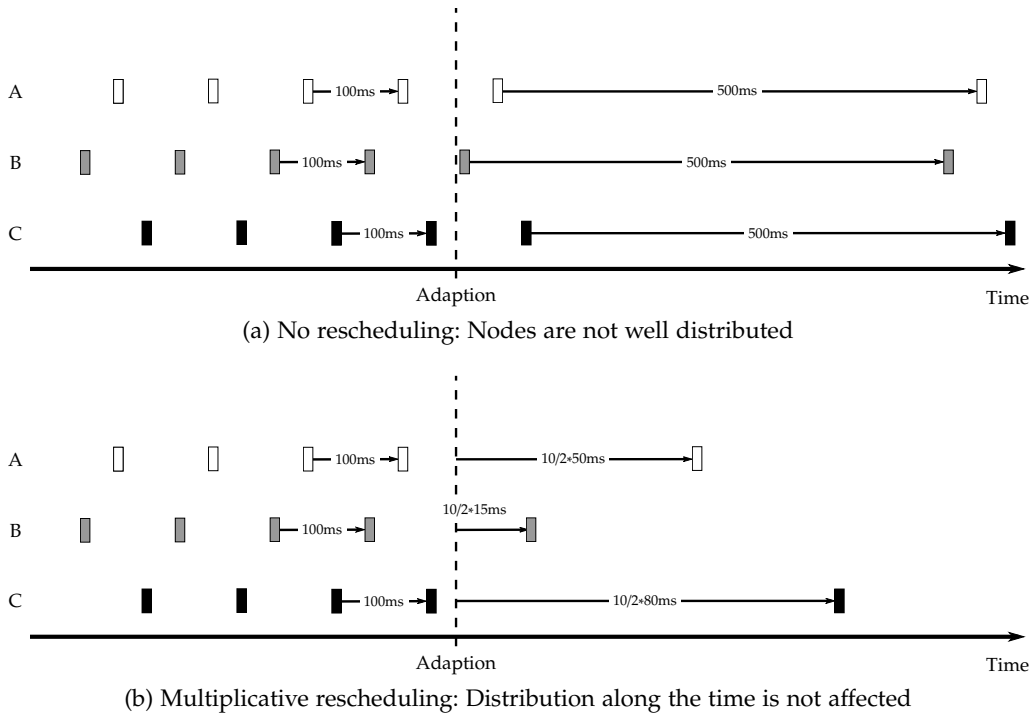


Figure 26: Illustration of rescheduling for exemplary nodes A, B, and C for one iteration, where the rate gets decreased from 10 Hz to 2 Hz.

Rescheduling will only be applied if an adaption takes place, otherwise the time between two subsequent messages is $\text{TXTIME}/r_j(t-1)$.

Figure 26 illustrates the two methods based on a transition from a high rate to a lower rate. If no rescheduling is applied (cf. figure 26a), an adaptation of the new message rate will be applied directly for the next scheduled message after the adaption has taken place. Without rescheduling, the time for the dissemination of the new message is not distributed well along the longer time interval. This will lead to message bursts at a certain time, while in between no messages are generated at all. In the example (cf. figure 26a), an interval of > 400 ms is unused. For higher numbers of contending nodes, the MAC is limited in granting an interference-free access based on the comparably small CW.

The proposed rescheduling technique maps the old generated distribution to the new interval. In the case of a transition from a high to a low rate, the interval will be stretched (cf. figure 26b). For example, the time between the generation of node A and C before the transition is $\Delta t_{t-1} = 30$ ms and afterwards, it is $\Delta t_t = r_j(t-1)/r_j(t) \cdot \Delta t_{t-1} = 150$ ms. This will avoid message bursts. However, since the initial distribution along the time is maintained, rescheduling cannot solve a priori synchronization in message generation.

Figure 27 illustrates a transition from a high to a low rate. If no rescheduling is applied, the adaption will be significantly delayed, because the new rate is not applied until the next message is generated based on the old rate. Considering a message rate of 1 Hz and $t_{\text{CMDI}} = 200$ ms, the adaption to a new rate takes up to 1 s and thus the rate adaption will likely be omitted. Since it generates a significant delay between the control and the execution part, the rate adaption algorithm needs to consider this drawback. Multiplicative rescheduling generates an immediate reaction

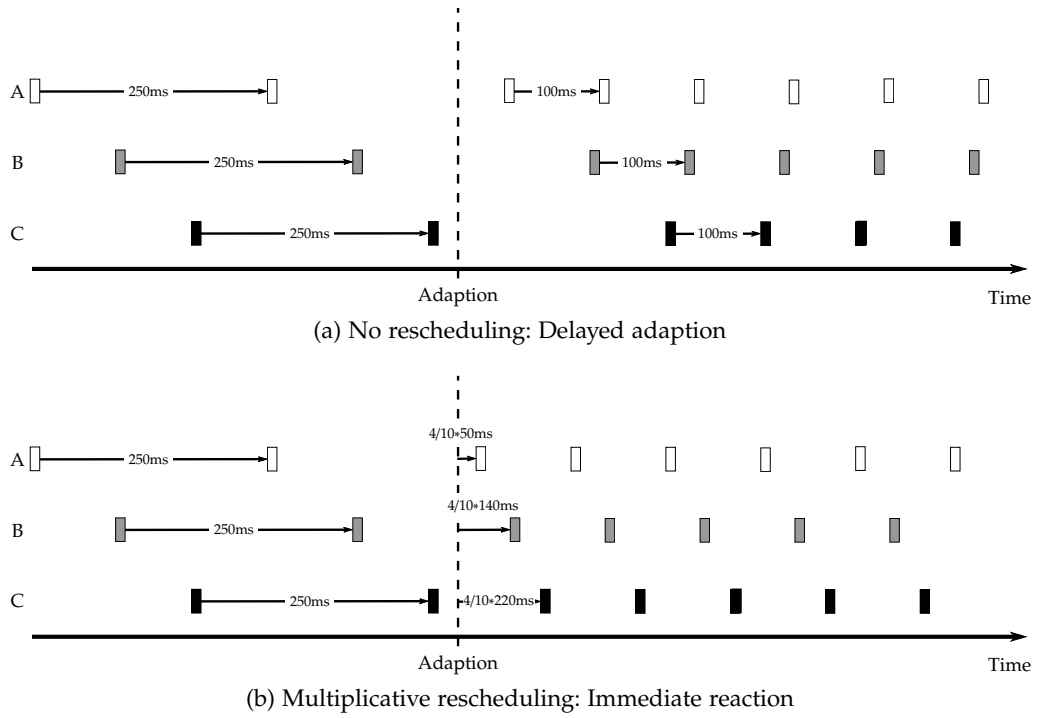


Figure 27: Illustration of rescheduling for exemplary nodes A, B, and C for one iteration, where the rate gets increased from 4 Hz to 10 Hz.

to the adaption process and the maximal reaction time does not exceed the new message interval.

IMPACT OF RESCHEDULING ON THE CBR We illustrate the impact of the rescheduling mechanism on the CBR by a numerical example, where simulation results are obtained within the verification scenario (cf. appendix A.2.1). Figure 28a illustrates the rate of $K = 300$ nodes with and without rescheduling/initialization. While there will be no reaction if the algorithm starts uninitialized (cf. next paragraph), a significant adaption takes place for both of the other two cases. The resource utilization r_c exceeds the target utilization of $r_s = 0.6$ and thus the rate needs to be

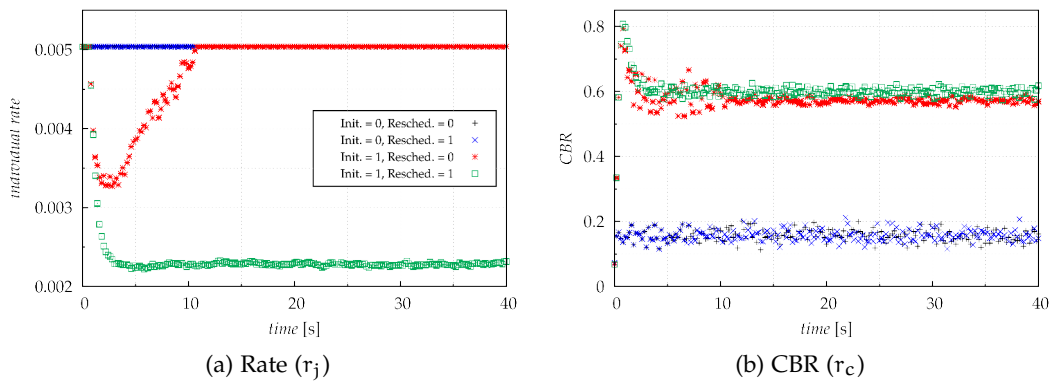


Figure 28: Effect of initialization and rescheduling on the protocol. ($K = 300$, $\alpha = \gamma = 0.4$, $r_s = 0.6$)

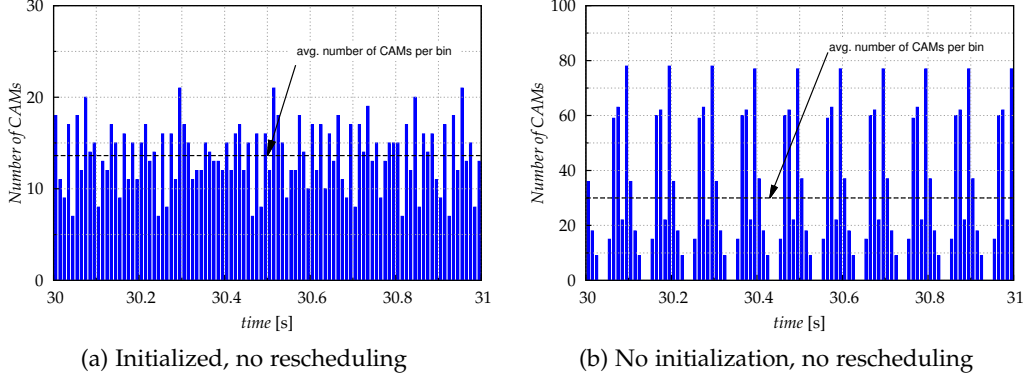


Figure 29: Distribution of the CAM generation times. ($K = 300$, $\alpha = \gamma = 0.4$, $r_s = 0.6$)

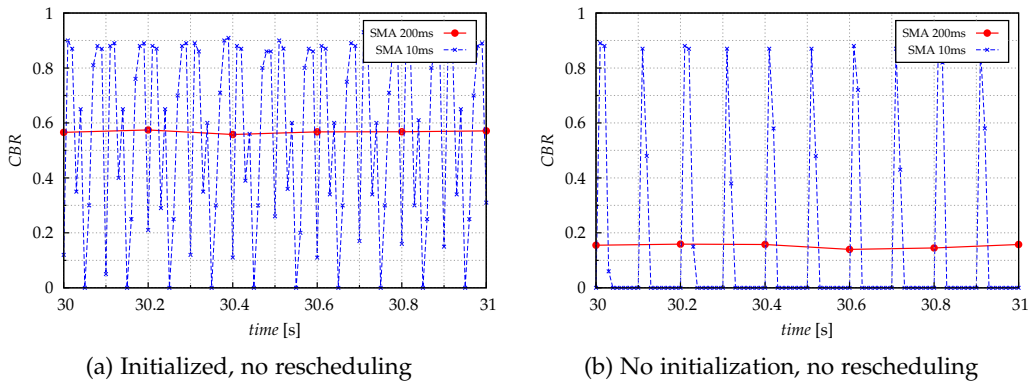


Figure 30: Impact of synchronization on the CBR. ($K = 300$, $\alpha = \gamma = 0.4$, $r_s = 0.6$)

decreased (cf. figure 28b). Figure 27a depicts that without rescheduling, this will lead to message bursts, which are irreversible. These message bursts clearly exceed the average number of CAMs within a time interval (cf. figure 29b) leading to significant loads (cf. figure 30a). However, the load for one iteration is aggregated within this iteration and thus smaller due to the interference.

While rescheduling leads to uniform distribution of the messages over time as illustrated in figure 29a, message bursts occur without it. These message bursts will significantly increase the load within this time interval leading to a higher probability of occurring interferences (cf. figure 30a).

RESOLVING SYNCHRONIZATION While the decision and adaption process takes place synchronously along the whole network, the execution process by generating the actual message is done by an individual separate process. The process is initiated at the start of a node and assigns to it an unique random start time. The only dependency of this process is the rate adaption via the rescheduling method. However, it is important to note that this loop is asynchronous and needs to be initialized with random start times which allow a suitable distribution of generation times along the time-scale.

If this cannot be guaranteed, one method to solve synchronization will be to apply a jitter to the newly calculated rate. The jitter adds an offset to the time when

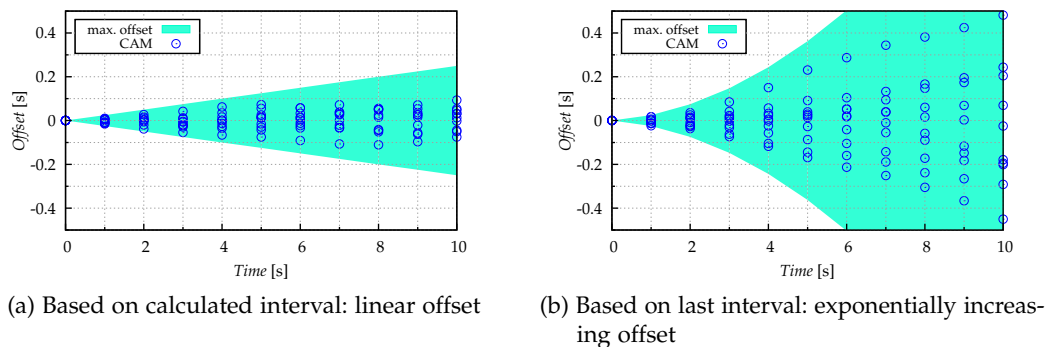


Figure 31: Effect of jitter (2.5%) over time for a set of initially synchronous nodes with a rate of 1 Hz.

the CAM is triggered. Figure 31 illustrates the effect of a jitter. Based on a set of 10 initially synchronous nodes transmitting CAMs at a fixed rate of $R = 1$ Hz, a jitter with a percentage of 0.025 is applied, i.e. the CAM for $t = 1$ is triggered for $\text{unif}(0.975, 1.025)$.

A jitter which is applied to the fixed interval is limited in distributing the CAMs over time. It converges to an offset of 0 such that the n^{th} CAM is triggered at

$$t(n) = \frac{1}{R} \cdot \sum_{i=1}^n x_i \approx \frac{n\mu}{R}$$

where $\mu = 1$ indicates the expectancy value of $X \sim \text{unif}(0.975, 1.025)$ and $x_i \in X$ is an element drawn from this distribution. However, in practice, a jitter will lead to certain offsets at each iteration and thus a better distribution of the generation times as shown in figure 31b. A jitter will only have this behavior if it is applied to the message dissemination loop.

On the other hand, if the jitter is applied based on the last interval, it will result in a better distribution over time. But since the current offset is based on the previous offset, it will grow exponentially and thus has to be limited in time or must be embedded with a rate control. The n^{th} CAM is triggered at

$$t(n) \approx \frac{1}{R} \sum_{k=1}^n \prod_{i=1}^k x_i$$

However, if n is limited, the divergence of the intervals will lead to a suitable distribution of the CAMs over the time interval (cf. figure 31b). A jitter which is applied to the rate adjustment loop will have such a behavior.

In this work, nodes start asynchronously and multiplicative rescheduling is applied. Any new node is initialized first which avoids synchronization in the message dissemination loop. Due to this initialization, a jitter is not necessary and subsequently not applied here.

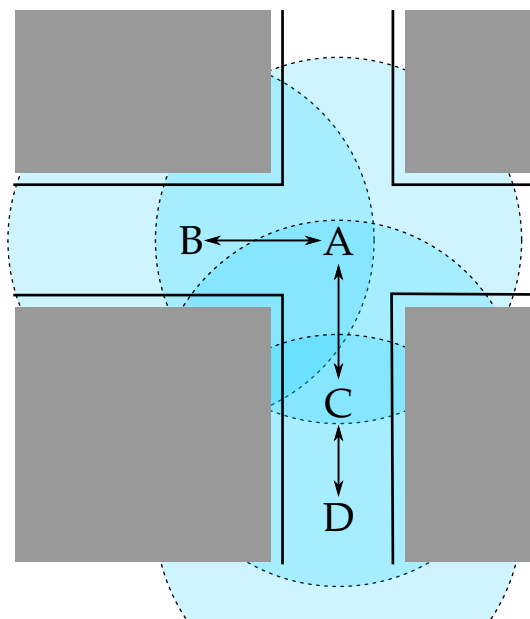


Figure 32: Illustration of the position for the nodes using cooperation.

5.4 AGGREGATION AND EXCHANGE OF INFORMATION

We showed in section 4.1 that local fairness can lead to an unfair resource allocation along the network. It is obvious that a decentralized decision effects other nodes through the commonly used channel. Thus, cooperation is necessary to inform neighboring nodes about congestions to which they contribute, but the nodes do not recognize congestions. In order to do so, the nodes need to exchange the observed channel information with their neighbors.

In section 5.3.1, we proposed to share the adjusted individual rates among the nodes to calculate a common group rate. In order to overcome the problems of local unfairness and achieve a semi-global fair resource allocation, the exchange of the observed CBR needs to be applied as well.

5.4.1 One-Hop Piggybacking

Instead of transmitting any change in the channel or rate status as a separate message which would lead to further congestion, a node appends this information to the periodic CAMs. Each node therefore includes its individual rate $r_j(t)$ and observed load $r_c(t)$. This leads to a small increase of the original CAM size by a few bytes.

Considering the three nodes A, B, and C which are aligned like illustrated in figure 32. An exemplary exchange of the status information from $t - 1$ is shown in figure 33. A node aggregates the information received during one iteration each t_{CMDI} . In the following, $f(\vec{U})$ represents the aggregate information based on the input vector \vec{U} .

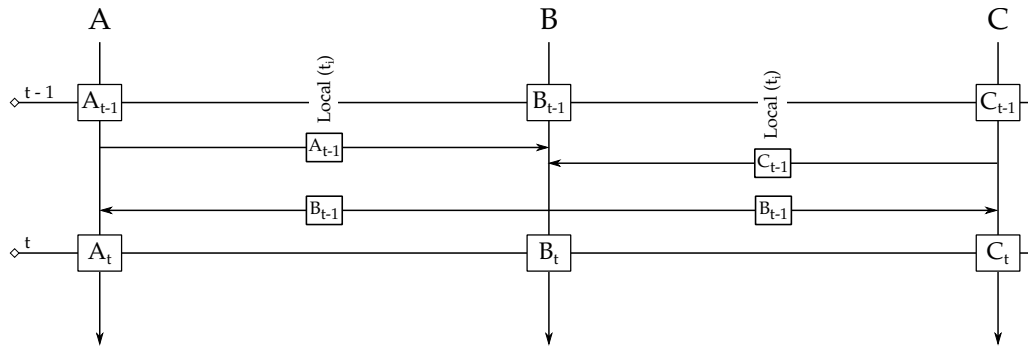


Figure 33: Illustration of the exchange via 1-hop piggybacking.

One possible option is to use the simple average of the received information such that

$$f(u_1, u_2, \dots, u_n) = \frac{1}{n} \sum_{i=1}^n u_i. \quad (5.15)$$

The simple average takes into account all the information received from the neighbors within one iteration and weights them equally. Thus, it would be comparable with the gain of the target rate, which is an average of the rate within the communication range. A simple average can increase stability, because the number of conducted measurements is increased and erroneous values will not have such a strong effect. If we apply this method, we will achieve a semi-fair resource allocation, but it does not resolve the problem of nodes being affected by the hidden-terminal problem.

While the arithmetic mean treats each node equally and thus fair, the maximum-norm takes the maximum CBR received:

$$f(u_1, u_2, \dots, u_n) = \max(u_1, u_2, \dots, u_n) \quad (5.16)$$

By doing this, it acts more conservative, because it will lead to a reduction of the transmission rate if only one neighboring node reports a congested channel. The maximum-norm achieves global fairness by helping to maximize the minimal transmission rate due to the highest observed CBR.

The benefit, but also drawback at the same time, is that it reacts to a minority of the vehicles and affects a majority of the nodes. Considering a minority of 5 nodes at an intersection which report a congestion due to 300 nodes on the lanes leading to the intersection. Those 300 nodes have to drastically reduce their transmission rate in order to reduce congestion at the intersection. However, this is the desired effect and thus used for this work.

Based on the maximum-norm, an exclusive maximum-norm can be defined which excludes a sub-set of vehicles, i.e. 1% of the highest reported CBR values. This exclusive maximum allows to overcome erroneous or maleficent CBR observations reported by neighboring nodes. One may also want to implement a validation for the received information, i.e. sanity checks, by comparing it to values received from the same region or from the stored history. However, malfunctions will not be considered in this work.

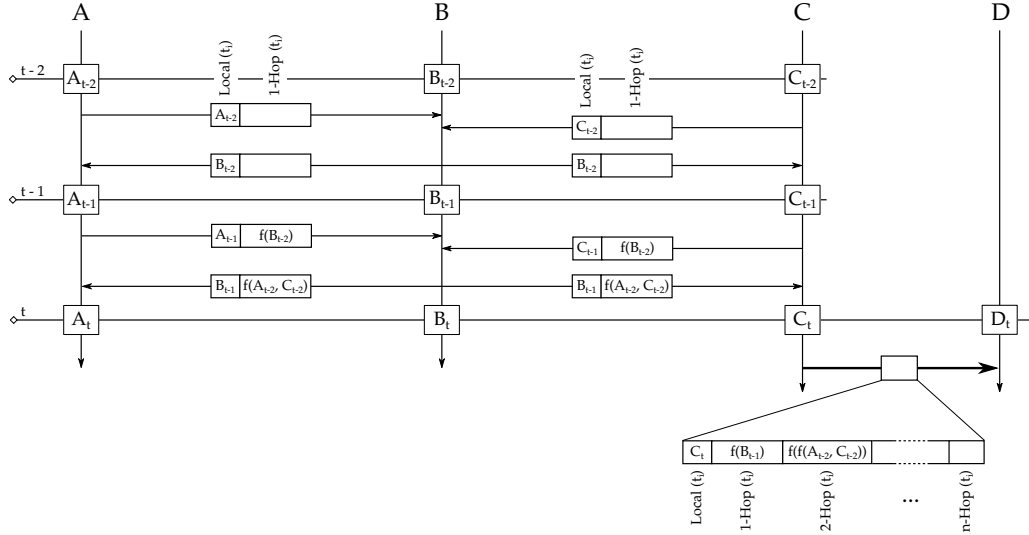


Figure 34: Illustration of information exchange using 2-hop piggybacking. Additionally fairness range extension is illustrated using 3-hop piggybacking.

When using the global-fairness principle, the transmission rate mechanism (cf. section 5.3) reacts on the aggregated information instead of the locally observed CBR. Since each node transmits the observed values of $t - 1$ in between the iterations $t - 1$ and t , the reaction of the network is delayed by one iteration. Furthermore, a node needs to consider its locally observed CBR of the iteration $t - 1$ instead of the more current t to allow a fair convergence. In this way, the utilization $r_c(t)$ for a cooperative 1-hop piggybacking system is calculated as follows:

$$r_c(t) = f(u_L(t - 1), f(\vec{u}_N(t - 1))), \tag{5.17}$$

where $u_L(t - 1)$ determines the locally observed CBR of the last iteration, $\vec{u}_N(t - 1)$ includes the received information from the neighbors and $f(\cdot)$ represents the aggregation method. If the message rate is lower than the Channel Monitoring and Decision Interval (CMDI), just a sub-set of the neighboring vehicles will be considered within an iteration.

5.4.2 Fairness Range Extension

Piggybacking is an efficient method to extend the fairness range and achieve global fairness. While the fairness range for 1-hop piggybacking is limited to the communication range of the nodes, the fairness range can easily be extended by applying multi-hop piggybacking. This can be beneficial, since each node contributes to the interference of far-away nodes. These far-away nodes can most likely not decode, but sense the packet on the channel. Furthermore, if fairness within a certain range is required, for example in an urban area, fairness range extension will be applied. Even if the effective communication range is low due to transmit power control or high interference, multi-hop-piggybacking will increase the probability of receiving the cooperative information.

In order to achieve a fairness-range extension, a node aggregates and piggybacks the received channel status information of the previous iteration. Considering 2-hop-

piggybacking, the received CBR from the neighbors are aggregated and appended to the next CAM together with the locally observed CBR. Figure 34 illustrates this for the nodes A, B, and C. The exchange of information is started at $t - 2$ and no shared information is available before. Thus, between $t - 2$ and $t - 1$ only locally observed utilization is exchanged. At $t - 1$, node C is aware of the channel status from B at $t - 2$ and reacts to it following (5.17):

$$U_C(t - 1) = f(C_{t-2}, f(B_{t-2})),$$

where U_C indicates the utilization at C used for the transmission rate adaption and $f(\cdot)$ follows (5.16). The received CBR is aggregated such that between $t - 2$ and $t - 1$ a CAM from C includes the local measurement B_{t-1} and the aggregated 1-hop information $f(A_{t-2}, C_{t-2})$. At t , C then calculates the cooperative utilization based on the 2-hop-piggybacked information received from B such that

$$U_C(t) = f(C_{t-2}, f(B_{t-2}), f(A_{t-2}, C_{t-2})),$$

Considering an additional node D, which is in communication range of C, it will receive a channel congestion indication from A through the aggregated information used for 3-hop piggybacking (cf. figure 34).

Theoretically, this can be extended to n -hop piggybacking, but with each additional hop, the delay is increased by another iteration in order to guarantee that each node reacts to the same CBR in the same iteration. Otherwise, a node can react multiple times to a congestion indication, while another node just reacts once leading to unfairness.

5.4.3 Cooperative Target Rate

The semi-cooperative target rate (explained in section 5.3.1) is also exchanged along the nodes. Basically, we consider three options.

LOCAL COOPERATION The exchange of the individual rates among the nodes will create a local semi-cooperative approach in which the average neighboring group rate is considered. The exchange will take place as described in section 5.3.1.

WEIGHTED GLOBAL COOPERATION (WGC) Each node calculates the target rate within its neighborhood and appends it to the CAM. A node achieves weighted global fairness by calculating the average target rate within the extended cooperation range, considering the local, and remote information.

FULL GLOBAL COOPERATION (FGC) For full cooperation, a node appends the locally calculated target rate to the next CAM. Within each iteration, each node reacts based on the CBR, and the target rate reported by the node which observed the maximum utilization. For fairness range extension, each node additionally piggybacks the target rate of the node reporting the maximum utilization.

Both weighted global and local fairness use the average of a certain region for the target rate. In this way, the value does not change rapidly, as long as the individual

rates within this region are stable. However, due to the simple average, all nodes are treated equally such that those suffering under bad channel conditions do not have a higher priority. Instead, if full global cooperation is applied, all nodes within the cooperation range will react as if they would be the nodes suffering from the bad channel conditions by applying the same resource utilization and local target rate. Unfortunately, nodes in different regions can report the highest utilization, but will have significantly different target loads. This can lead to instability of the algorithm for nodes which are at the edge of the cooperation range.

We analyse the effect of full global versus local cooperation in section 6.4. If not specified differently, we apply full global cooperation whenever piggybacking is used within this thesis.

5.5 PARAMETER DISCUSSION

In this section, we discuss the parameters of the algorithm from a theoretical perspective. A detailed numerical analysis based on simulation results is conducted in section 6.

5.5.1 Convergence Parameters

The convergence parameter is of major interest for the reliable functionality of *LIMERIC*. It specifies the smoothness and volatility in the steady-state, but also the convergence time. A small value will decrease the volatility at the costs of an increased convergence time and vice versa. While this chapter concentrates on the analysis of the theoretical effect of the parameters, section 6.3 deals with a detailed numerical discussion including suggestions for suitable values.

CONVERGENCE PARAMETER β SWeRC is independent of the scalability effect, thus one may expect that increased volatility is permitted automatically. However, an initial value of β needs to be specified which allows a minimal convergence time with respect to the convergence inequality (3.13).

$$\alpha + \omega\beta K < d, \quad (5.18)$$

where d is the delay constraint which is calculated based on the number of iterations between in- and output of the control loop. Using equations (5.8) and (5.5) in (5.18), we calculate the upper bound for β :

$$\begin{aligned} \alpha + \omega\beta K < d, \quad \omega &= c \frac{r_c}{K} \quad (5.5) \\ \alpha + c \frac{r_c}{K} \beta K < d, \quad r_c &= r_g - \frac{\alpha}{c\beta} \quad (5.8) \\ \alpha + \left[r_g - \frac{\alpha}{c\beta} \right] c\beta &< d \\ \beta &< \frac{d}{c \cdot r_g}. \end{aligned}$$

Hence, β is mainly based on the delay constraint and the predefined target resource allocation r_g .

In order to ease the calibration of the parameter later on, we redefine β to be a function of the parameter γ which leads to

$$\beta = \frac{d\gamma}{c \cdot r_g}, \quad 0 < \gamma < 1, \quad (5.19)$$

where a smaller γ has the same effect like a smaller β .

CONVERGENCE PARAMETER α The convergence parameter α affects the convergence speed from any individual rate to the local fair message rate. The convergence time is independent of the number of nodes and is identified as a discrete exponential $(1 - \alpha)^t$.

Considering SWeRC, we interpret the parameter α as a cooperation factor, because it weighs the individual and the group rate within one iteration. A fully altruistic system achieves optimal convergence by setting $\alpha = 1$. In this way, the algorithm only reacts to the group rate r_t which is included in the weighting factor ω to specify the individual rate:

$$r_j(t) = \omega\beta(r_g - r_c(t-1)). \quad (5.20)$$

Such a system benefits from an immediate reaction time and an optimal convergence. However, it easily becomes instable due to the lack of low-pass filtering.

We have to note at this point that r_j does not have an upper bound, since no *gain-saturation* is used, but it needs to have a lower bound which is greater than zero. Otherwise, ω can reach zero which results in r_j to reach zero and the algorithm to run into a global deadlock.

RESOURCE ALLOCATION r_g One of the key parameters for an efficient resource allocation is the target resource utilization r_g itself. Due to the density-independent steady-state utilization r_c , this value can be specified precisely. Indeed, one can parametrize the resource utilization r_c itself. Therefore, its steady-state value needs to be calculated based on the convergence parameters α and β . By inserting equation (5.19) into (5.8), one receives

$$\begin{aligned} r_c &= r_g - \frac{\alpha}{c\beta}, & \beta &= \frac{d\gamma}{c \cdot r_g} \quad (5.19) \\ r_c &= r_g - \frac{\alpha}{c \frac{d\gamma}{c \cdot r_g}} \\ r_c &= r_g \left(1 - \frac{\alpha}{d\gamma}\right), & \text{substitute } r_c &= r_s \\ r_g &= \frac{1}{1 - \alpha/d\gamma} \cdot r_s. \end{aligned} \quad (5.21)$$

In order to avoid confusion, the steady-state utilization r_c is replaced by r_s , because the parameter r_c is used in a different context within this thesis. r_s specifies both the resource utilization in the steady-state and the desired resource allocation. The

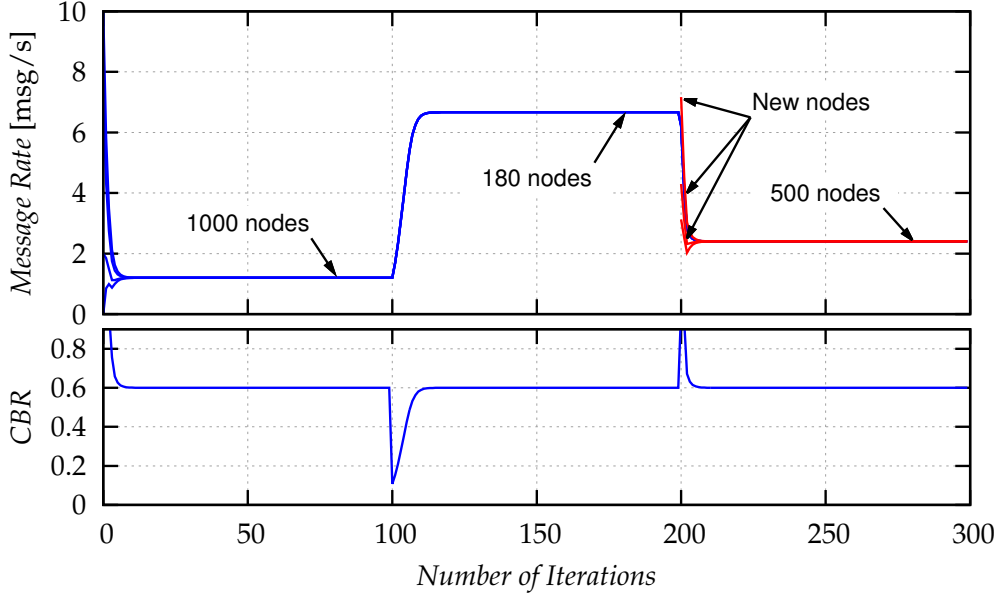


Figure 35: Stability and convergence of SWeRC with parameter optimization over time for different vehicle densities ($\alpha = 0.5, \gamma = 0.5, r_s = 0.6, K = 1000, 180, 500$)

value of r_s is adjusted based on the chosen convergence parameters. However, if r_g is specified using equation (5.21), β has to be specified as in equation (5.19) and α is limited by $0 < \alpha < d\gamma$.

CONVERGENCE SUMMARY Putting the results of the parameter discussion together, one achieves the parameter-optimized algorithm specified by the equations for the target resource utilization (5.21) and the convergence parameter β (5.19) used for the self-weighted rate control (5.6)

$$r_j(t) = r_j(t-1) - \alpha \left(r_j(t-1) - r_t(t-1) \frac{r_c(t-1)}{r_s} \right) + d\gamma \left(r_t(t-1) - r_t(t-1) \frac{r_c(t-1)}{r_s} \right). \quad (5.22)$$

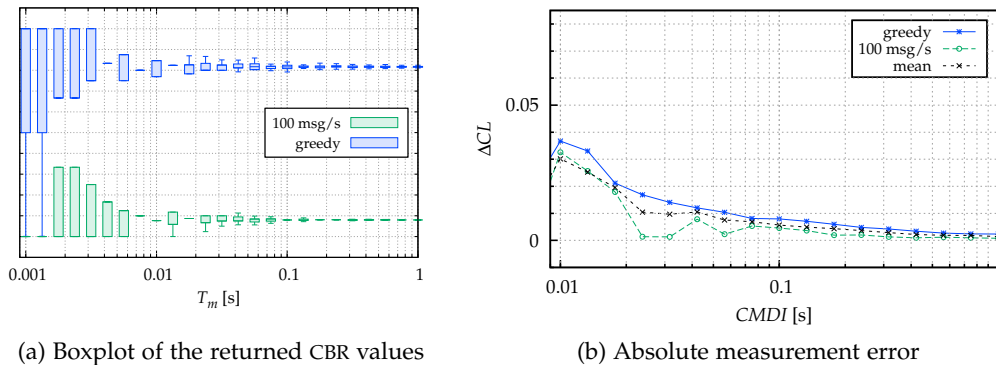
It is not difficult to see that α influences the convergence to the group rate with respect to the target utilization, while γ influences convergence of the group to the target utilization only (cf. figure 58). We illustrate this in two special cases.

In the first case there is no difference between the individual rates of a group, i.e. $r_t(t-1) = r_j(t-1)$, but the target resource utilization is not reached ($r_s \neq r_c(t-1)$). In that case, equation (5.22) simplifies to

$$r_j(t) = r_j(t-1) \left(1 + (d\gamma - \alpha) \left(1 - \frac{r_c(t-1)}{r_s} \right) \right).$$

Hence, the time until the convergence of the group rate to the fair steady-state rate is influenced by $(d\gamma - \alpha)$.

For the second case, we consider that there are individual rates $r_j(t-1) \neq r_t(t-1)$, but resource allocation has been achieved $r_c(t-1) = r_s$. As already outlined in

Figure 36: Impact of measuring interval on CL_{est} ($N_p = 1250$)

the parameter discussion, we see that the convergence speed only depends on the parameter α :

$$r_j(t) = r_j(t-1) - \alpha(r_j(t-1) - r_t(t-1)).$$

We verify the stability and convergence of the parameter-optimized SWeRC for different node densities using the simplified MATLAB model (cf. section 4.1.3). Figure 35 illustrates the convergence behavior for an initial group of 1000 nodes as well as distortions caused by removing nodes at $N = 100$ and adding new nodes at $N = 200$. The convergence speed is faster, the steady-state message rate r_j is higher in comparison with *LIMERIC* (see [13]) and volatility is avoided. The figure also reveals the density-independent channel utilization $r_c = r_s = 0.6$ which fully utilizes the target resources.

5.5.2 Channel Monitoring and Decision Interval (CMDI)

For the implementation of the algorithm, we have to investigate the time needed for an iteration. It needs to be considered with respect to the accuracy of CBR measurements and convergence speed on the other hand. In order to find a suitable value for the CMDI, we conduct an investigation of both aspects.

CHANNEL LOAD ASSESSMENT Two aspects need to be considered in order to evaluate the accuracy of channel load assessment. The first is the measurement error as a result of the probing method and the second is the inaccuracy which is caused by the SMA for time invariant channel loads. A detailed description of the experimental set-up including verification and methods used for the evaluation of the measurement error is given in appendix B.

The number of probes taken within a measuring interval has a significant effect on the accuracy. However, if the CMDI is very small, i.e. just a few multiples of the T_{XTIME} , suitable values will not be conducted as well. Figure 36a illustrates the CBR values retrieved by the lower layers based on a constant message rate as boxplots. If the number of probes is fixed, the accuracy will be increased with an extension in the measuring interval. This induces to have a large CMDI in order to decrease the measuring error.

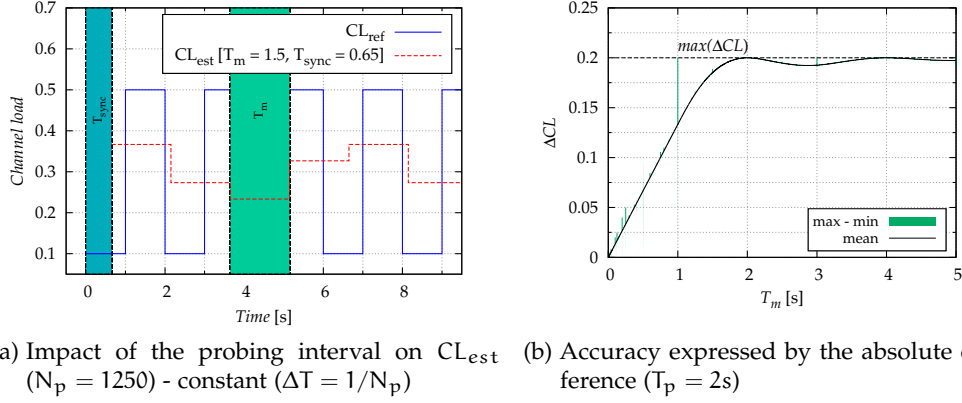


Figure 37: Impact of the measuring interval T_m on the accuracy for a time invariant load pattern. The synchronization effect T_{sync} is implicitly considered by the minimum and maximum values and the average accuracy.

Figure 36b shows the mean absolute error retrieved from the measurement for different measuring interval length. The measurement error is significantly decreased for values $CMDI > 0.01$ s. This error is independent of the message rate and can be approximated by

$$\Delta CL(t) = 10^b \cdot t^m, \quad (5.23)$$

where $m = -0.7227$ and $b = -2.967$ in the interval $[0.01, 1]$ s. Due to its exponential decrease, the mean measuring error is rapidly converging to zero and for $t > 0.1$ s with $\Delta CL(0.1) = 0.0057$ it is already negligibly small.

The above consideration is valid for a constant load which is not time invariant. We showed that due to the architecture of the algorithm and the nature of VANETs, we cannot assume the load to be constant over time. This will be considered in an additional numeric analysis, where the effect of the SMA over the measuring interval for time invariant loads is evaluated.

Figure 37a provides an example which is used for the analysis. A reference load which follows a specific pattern (in this case there is a period of 2 s) is used for the calculation of the retrieved load based on the measuring interval and an offset. Based on these parameters, the estimated load can significantly differ from the reference load (cf. figure 37a). A detailed description of the method and metrics used for this analysis can be found in appendix B.

The average absolute error is calculated for different measuring intervals based on the underlying load pattern used. Figure 37b shows the error for the above presented example. The error obviously increases with an increasing measuring interval length up to a certain maximum inaccuracy. Depending on the used pattern, the slope and the maximum error can differ, but the basic statement is the same. The offset can also have an impact on the accuracy and is implicitly considered, because the error illustrated is the mean of various offsets for one measuring interval. An example: A measuring interval of $t_{CMDI} = 1$ s can lead to an error of 0 in case of no offset or the maximum error of $\Delta CL = 0.2$ for an offset of $T_{sync} = 0.5$ s.

Unfortunately, the two errors are correlated in such a way that a measuring error due to probing can have a positive effect on the average inaccuracy. Figure 38

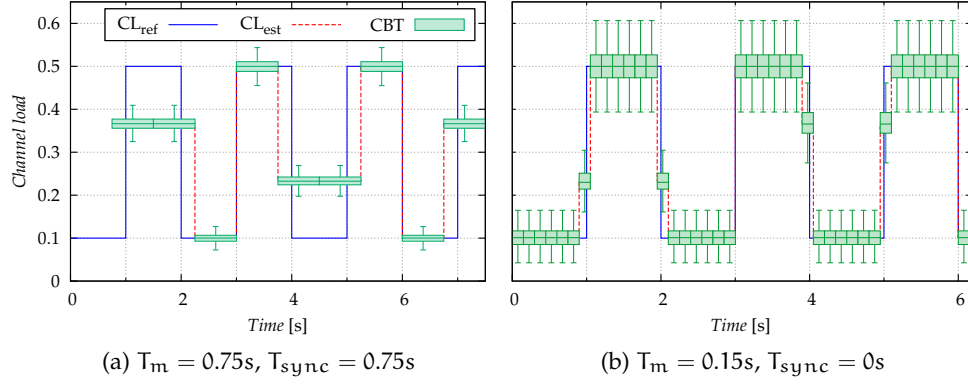


Figure 38: Correlation of the estimated CL for a time invariant pattern ($T_p = 2s$) using the estimation method (CBT)

exemplary illustrates this for the given reference load for a large (cf. figure 38a) and a small measuring interval (cf. figure 38b). During one averaging interval, the actual CBR is retrieved by the probing method including the measuring error.

CONVERGENCE SPEED SWeRC is based on iterations, where the time for one iteration needs to be defined. The feedback control loop is based on these iterations, i.e. a rate adjustment is conducted within every iteration based on the information of the previous iterations. The CMDI is used to map this iteration to the time domain.

The convergence speed obviously benefits from a small decision interval in terms of faster convergence, because there are more iterations per second compared to a larger interval. On the other hand, we have to consider that due to the cooperative aspects, a suitable decision is just possible with a sufficient set of information received within the last interval. Although the CBR can be measured with a certain error during a small CMDI, information exchange within one iteration is limited to the maximum rate itself. In other words: $1/R_{\max} < t_{\text{CMDI}} < 1/R_{\min}$.

The amount of information received during one CMDI is

$$\frac{r_s}{\text{TXTIME}} \cdot t_{\text{CMDI}}. \quad (5.24)$$

The amount is constant, although different sub-sets of vehicles can be observed within one iteration. Due to the random initialization of the nodes, a sub-set includes heterogeneous distributed nodes without correlation. In other words, a certain spatial resolution is achieved as well, because of the specification of the CMDI.

Based on the investigation of the channel load assessment error, the convergence speed, and information necessity, we assign a value of $t_{\text{CMDI}} = 0.2s$. Compared to the lower bound of 0.1 s as depicted by the minimum rate and the assessment error, it offers the ability of considering a bigger sub-set of vehicles or, in case of light congestion, even full information combined with a fast convergence speed. Furthermore, the averaging as well as the measuring error are negligible for this interval. This value for the CMDI is also used in comparable works from Tielert et al. [106] or Bansal et. al [13]

5.6 SUMMARY

In this chapter, we introduced the design of our protocol stack for CC and AC in order to overcome the problems explained in section 4.1. The modular protocol stack is designed as a feedback controller and separated into a control and an executive part, where the major components are described individually.

We explain the rate adjustment algorithm *SWeRC*, which is based on the well-known TRC scheme *LIMERIC*. We describe the changes made in order to achieve the self-weighted algorithm based on the piggybacked group rate, including the analysis of steady-state values and stability.

We show that in order to achieve a scalability-independent convergence, feedback from other nodes is necessary in terms of a local or global group rate. We further illustrate how to acquire these values, either by using cooperation among the nodes or by conducting decentralized observations.

While the control part of the protocol stack is synchronized among the nodes such that control decisions are made based on common information, we show that the executive part needs to be asynchronous in order to mitigate the effect of interference. Consequently, we present the necessity of message rescheduling and random initialization of the nodes. Furthermore, the optional usage of jitters is explained.

Besides the rate adjustment algorithm, the information exchange is explained in detail within this section. We depict how the sharing of the status information, e.g. CBR and target-rate, is achieved and how to extend the fairness range in order to grant participation and global fairness.

In this chapter, we also provide a method how to apply dynamic channel smoothing. Although optional for *SWeRC*, which is self-weighted and does not need channel smoothing, it offers the opportunity to smooth the measurements based on the observed volatility and accuracy coupled with a memory function used to set the weights of a first order filter.

In a final step, we conduct a theoretical parameter discussion and achieve the parameter-optimized rate adjustment expressed by equation (5.22). The parameter optimized algorithm makes use of the scalability-independent convergence of *SWeRC* and optimizes the convergence parameters accordingly such that the best efficiency is combined with fast convergence and maximal stability.

In this section, a numerical analysis of the proposed protocol is conducted. Therefore, we first describe the metrics used for the performance evaluation and comparison in section 6.1. We validate the individual components used within the protocol stack separately granting insights into the functionality within the simulation environment in section 6.2. A major issue for adaptive protocols is the optimization of the parameters used. In order to find suitable values, we conduct an in-depth numerical optimization. The result of this numerical optimization is a threshold for the target utilization (cf. section 6.3.1), as well as best-effort values for the convergence parameters of the transmission rate adjustment algorithm (cf section 6.3.2). The later aims at optimizing the trade-off between stability and convergence time. Using these values, we then conduct the numerical analysis of the protocol for different environments. We analyze the capabilities of the protocols cooperative module to overcome the problem of local unfairness due to building based shadowing of the signal in section 6.4. Furthermore, we use the hybrid simulation set-up described in appendix A in order to evaluate the protocol and especially the target-rate mechanisms proposed with dynamic vehicle movements in different environments in section 6.5. Finally, we compare SWeRC using the defined performance metrics within the dynamic scenarios with state-of-the-art CC algorithms in section 6.6.¹

6.1 DESCRIPTION OF USED METRICS

In this section, we explain the metrics used within this thesis to quantify and compare the performance of the protocols. We therefore use specific metrics granting insight into the algorithm and common metrics used to quantify the performance of the algorithm.

CHANNEL BUSY RATIO (CBR) The CBR is an indicator for the quality of the channel used. It specifies the fraction of time the channel is sensed busy during the measuring interval. A channel is sensed busy, whenever the node itself transmits a frame or it receives a frame from neighboring nodes. Therefore just frames which can be sensed are recognized, such that the signal power of the frame needs to exceed the carrier sense threshold of the node. Thus the CBR measures the utilization of the channel. Since the utilization has a direct influence on the QoS offered, CBR is often used for the quantification of the performance. Furthermore it is often used for the feedback control of reactive CC algorithms and the exact method of gathering the ratio is specified in section 3.1.3.

MESSAGE RATE The message rate is not a metric itself, it rather quantifies the number of messages disseminated by a node within a second. The proposed algorithm SWeRC adopts this message rate periodically and thus it is a significant

¹ Parts of this chapter are published in [223] and are under copyright of the IEEE

indicator of the algorithms performance, and in general for transmission rate adaption algorithms. If measured or averaged over time and space, it quantifies the stability, efficiency and fairness of an algorithm. The message rate is calculated at the transmission rate adaption module and thus does not include rescheduling effects.

FRAME DROP RATE (FDR) The frame drop rate specifies the number of frames which were replaced in the queue of a transmitting node by a newer packet before the transmission divided by the number of generated frames. A frame drop takes place, if a node can not access the channel for a longer period ($1/\text{Message Rate}$), because the CCA indicates the channel as busy. The length of the queue for CAMs is limited to one element, because if a new CAM is generated, the information of former CAMs is outdated and thus transmission does not make sense anymore. Frame drops occur more frequently, if the utilization indicated by the CBR is high and can have an influence on the QoS. In this thesis, we do not directly analyze the number of drops, but rather use the FDR as part of aggregated metrics like the IRT.

COLLISION RATE The collisions rate is specified as the number of frames lost due to collision divided by the number of frames transmitted. A frame collisions will occur, if either two or more nodes within the carrier sense range start the transmission of a frame during the same slot, because they counted their back off down to zero (CSMA collision) or if a node is not aware of an ongoing transmission of another node outside the carrier sense range (hidden-node-collision) (cf. section 2.4.1.1). Nevertheless, each frame contributes to the SINR value necessary for a successful reception of a frame. If a collision occurs, all colliding frames are lost. In case, all nodes are within the carrier sense range, a collision will not contribute to the CBR, which can have critical influence on the algorithm.

PACKET DELIVERY RATIO (PDR) The Packet Delivery Ratio (PDR) quantifies the communication performance as the number of packets successfully received divided by the number of packets transmitted. A frame is successfully received, if the signal power exceeds the receiver sensitivity and there is no interference. In other words, the signal power needs to exceed the receiver sensitivity plus the specific SINR. While the receiver sensitivity and the SINR are fixed values, the signal power depends on the propagation of the signal and is distance dependent (cf. section A.1.2). The calculated PDR is a distance dependent metric, which is specified by the propagation model as upper bound in an interference free case. The PDR indirectly includes the collision rate, but does not include the FDR and the message rate.

PROBABILITY OF PACKET RECEPTION (PPR) The PPR specifies the number of packets successfully received divided by the number of packets generated. It is very similar to the previously specified PDR, but it is rather calculated from application to application layer and includes the FDR. Thus it specifies the reliability of an end-to-end frame transmission. Both, the PDR and the PPR are distance dependent, aggregated metrics which can be used to quantify the performance of a region. In order to achieve suitable results, the region in which this aggregation takes place needs to be carefully selected. This is done by specific regions and further discussed in appendix A.1.

INTER RECEPTION TIME (IRT) The IRT [227] quantifies the time between successfully receiving two subsequent CAMs from a specific node. For VSC, vehicles need to be aware of their environment which is achieved by maintaining a certain information freshness. The metric includes packet losses due to interference or frame drops, but also incorporates the time between two updates due to the specified message rate. Even with a high PDR, subsequent packet losses can occur frequently and thus the information about this vehicle can get outdated. Considering furthermore a low message rate, the time between two successfully received CAMs can exceed several hundreds of milliseconds. Besides the IRT, there are similar metrics for quantifying the information freshness, such as the inter-arrival-time [126], inter-message-delay [228], message lifetime [229] or the update-delay [230]. Since the IRT is dependent on the distance, the IRT is quantified for a certain awareness range within this thesis.

The IRT is closely related to awareness metrics in general. Other awareness metrics, like the *blackout probability* or the *system age* rely on specific thresholds for the IRT (cf. section 7.1). According to the metrics, there are different methods to evaluate the IRT. The CDF of the IRT will result in the probability to receive an information update within a certain time. It is similar to the T-Window reliability introduced by Bai et al. [231] and also used for the *blackout probability*. The average IRT can be used to compare protocols, but it is a poor metric for the evaluation of VSC. The average excludes the effect of volatile and unstable behavior and thus a certain QoS can not be guaranteed. Besides the average, evaluation of certain percentiles of the IRT can be conducted. A value retrieved represents the information freshness for this percentile.

The IRT will be used as CDF and calculated for certain percentiles to evaluate and compare the performance of the different CC protocols. It is a suitable metric to quantify the QoS of VSC.

FAIRNESS In order to quantify the fairness and efficiency of a protocol, we use the metrics explained in section 3.2. The fairness index is calculated based on the individual rates as

$$F(x) = \frac{(\sum_{j=1}^K r_j)^2}{K \cdot \sum_{j=1}^K r_j^2}, \quad (6.1)$$

where K is the number of nodes within a LOS range of 500 m:

EFFICIENCY Following these metrics, the efficiency is expressed as the power divided by the power at the knee. As shown in section 6.3.1, the power in terms of goodput can be expressed as a function of the CBR. Thus the efficiency of a node j based on its locally observed CBR is defined by

$$E(j) = \frac{GP(U_j)}{GP_{\text{knee}}}, \quad (6.2)$$

where U_j specifies the observed load at node j , $GP(U_j)$ is the calculated goodput for this load and GP_{knee} is the goodput at the knee, i.e. the maximum goodput.

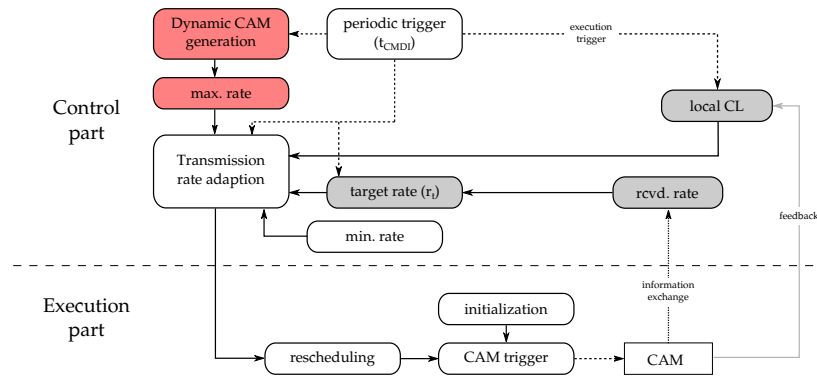


Figure 39: Active protocol elements used for the verification of the dynamic CAM generation element (highlighted)

6.2 VERIFICATION AND VALIDATION

Within this section, we briefly verify the different modules used within the protocol stack individually and give insights to the functionality within the simulation. Therefore simplified protocol stacks are used to focus on the key aspects and specific simulation scenarios are created. We verify the AC, rescheduling and initialization within the executive part, the transmission rate adjustment algorithm itself, and the cooperative information exchange.

6.2.1 Dynamic CAM generation

For the verification of the AC protocol, including the borders for the minimum and maximum message rate, we use a simplified protocol stack. The active modules are shown in figure 39. This protocol stack is embedded in a simplified simulation set-up, where $K = 10$ nodes start at the same position with an offset of $\Delta y = 5$ m each and individual fixed speeds. The minimum rate according to the standard [10] is set to $R_{\min} = 1$ Hz and the maximum rate is capped at $R_{\max} = 10$ Hz. The actual maximum rate, limiting the transmission rate adaption is based on the AC method.

Table 16 gives an overview of the simulated and calculated values for selected speeds. Note, that due to the low amount of $K = 10$ nodes, there will be no congestion and thus SWeRC would allow the maximum rate R_{\max} , if no AC is active. However, the simulated intervals and corresponding rates for the individual speeds do not differ from the calculated ones. Furthermore, for a stationary vehicle, the minimum rate is selected, while for faster vehicles $v > 40$ m/s, the rate is bound by the maximum rate.

VALIDATION IN A DYNAMIC SCENARIO We validate the functionality of the position based dynamic CAM generation in the dynamic highway scenario (cf. appendix A.2.3). In order to give further insights, exemplary results are taken to illustrate the benefits and drawbacks. The proposed AC algorithm can significantly reduce the dissemination of redundant information resulting in a much lower average CBR measured by the individual nodes based on their x-Position (cf. figure 40). It does not only reduce the load at the position of the jam, it furthermore reduces the overall load generated.

Table 16: Simulated and calculated CAM rate for different speeds using AC

		speed (m/s)				
		0	4	13.889	40	60
Simulation	interval (s)	1	1	0.288	0.1	0.1
	rate (Hz)	1	1	3.4722	10	10
Calculation	rate (Hz)	1	1	3.4723	10	10

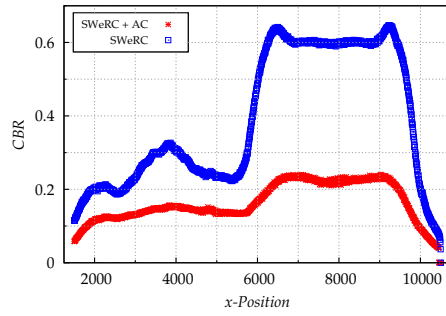


Figure 40: Measured CBR within the highway scenario with traffic-jam using AC

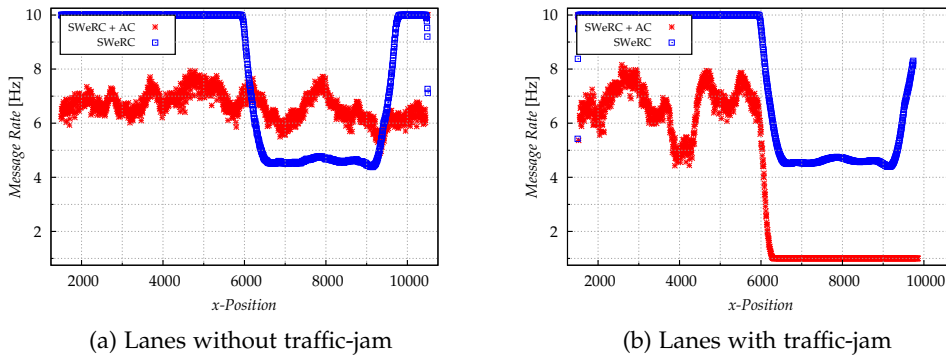


Figure 41: Illustration of the average message rate for the nodes using dynamic CAM generation on the highway scenario.

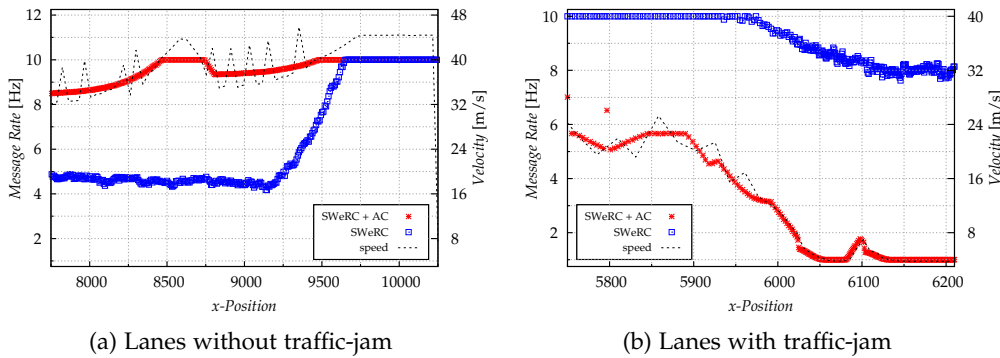


Figure 42: Exemplary message rate of two selected nodes for the highway scenario using AC.

In figure 41, we illustrate the average message rate for the vehicles on the road segment with and without traffic jam respectively. We need to note, that the AC algorithm influences the CAM generation interval in the executive part of the algorithm only and has no impact on the transmission rate adaption. As an example, if the maximum rate is decreased to 4 msg/s due to reduced speed, but the load is below the threshold, r_j would still indicate the maximum specified rate R_{\max} . This is necessary, because the internal rates are exchanged along the nodes and a reduction due to AC should not lead to a reduction of the neighboring rate. For the non congested road, a vehicle is free to choose its speed and thus, the rate should be accordingly. This can be validated by the average rates using AC (cf. figure 41a). In case of a traffic jam or stop-and-go traffic, speeds are significantly reduced and the same applies for the rate (cf. figure 41b). The benefit of AC here is clearly the reduction of the load due to lower overall message rates, which will also have a beneficial effect on the communication of the vehicles which are not on the congested road. If no AC is used, the vehicles will also suffer from a high load and subsequently reduced message rates (cf. figure 41a). However, the major drawback here is, that vehicles which are at the end of a traffic jam will also reduce their transmission rate to the minimum, such that this important position information gets outdated. although, responsible applications can react by disseminating DENMs in order to inform about a congestion, awareness can hardly be maintained.

Figure 42 shows the message rates of two exemplary nodes using AC compared to SWeRC without AC. The speed of the vehicles is approximated based on the change of the position between two CAMs and can be inaccurate in the plot. However, it can be shown, that the AC method maps the speed of the vehicle to the message rate. Furthermore, it is shown, that the upper and lower borders are respected, although the speed is below and above the regarding thresholds.

We disable AC for the later analysis of the adaptive congestion control protocol SWeRC. As stated, AC has a significant impact on the utilization, but on the other hand drawbacks in terms of provided awareness. Furthermore, for the evaluation and comparison of SWeRC, disabled AC is required.

6.2.2 Rescheduling

In order to verify the correct functionality of the executive part within the protocol, the simulation results are crosschecked with expected behavior. Therefore the protocol stack was reduced to a minimal functionality as shown in figure 43. The transmission rate adjustment needs to be active in order to verify the rescheduling module. For the investigation, $K = 300$ nodes with an initial rate of 10 Hz are placed within the verification scenario (cf. section A.2.1). The major parts of the executive part is the initialization and the rescheduling module, which are part of investigation in this section and have been analyzed in section 5.3.2 as well.

The correct functionality of the initialization process will result in a random distribution of the first CAM trigger within a certain initialization interval ($t_{\text{init}} = 1$ s). This distribution of the start time is shown for one exemplary simulation run in figure 44. Each node ID is given a disjunct starting time and the starting times are uniformly distributed. This is the expected behavior.

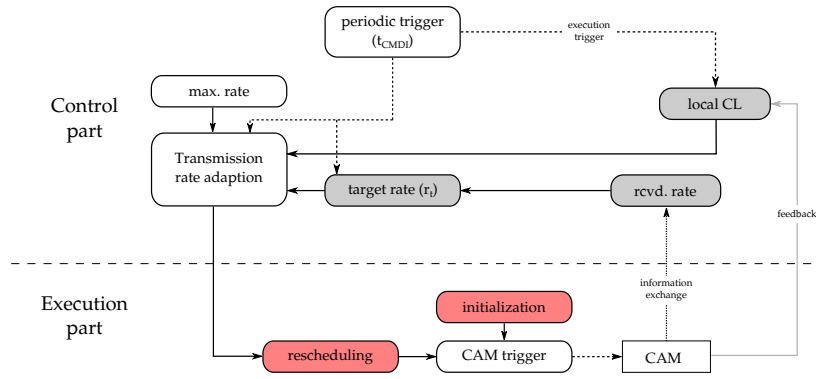


Figure 43: Active protocol elements used for the verification of the rescheduling within the executive part (highlighted).

The rescheduling mechanism works without failure, if the calculated and the simulated trigger time for a CAM is equal. Figure 45 illustrates the individual rates for the nodes as given by the transmission rate adaption module and the CAM generation time based on the rescheduling mechanism for two different nodes. For common perception, the relative time between the generation of a CAM at two different nodes should not be affected by the rescheduling. This is given here, as the second node generates its CAMs at approx. $2/3$ of the first nodes interval.

In table 17 the simulation results for node 1 are listed for the first few CAMs. By comparing the simulated CAM times t_{snd} with the calculated times, the functionality of the rescheduling mechanisms is verified.

6.2.3 Transmission rate adaption

The transmission rate adaption module is the key module of the protocols stack and needs to work with high accuracy. We verify the functionality within the simulation environment using the verification scenario and the set-up including the convergence parameters used for the results shown in figure 35. Therefore a burst of nodes is initialized at iteration $N = 0$ and $N = 200$. Here, we use the simplified protocol stack illustrated in figure 46.

In figure 47, we illustrate the results obtained by the simulation compared with the calculation based on the calculated values from the matlab model used in section 5.3. In order to verify the correct functionality of SWeRC within the simulation environment, it needs to be shown, that the reaction and the convergence of the algorithm in the simulation is equal to the expected values from calculation. From figure 47, it is obvious that this does not always hold on the first view. There are two major discrepancies: the overall message rate is higher and the convergence behavior for a transition from low to high vehicle densities is different. A verification of the rate adaption based on the parameters is part of the verification of the information exchange in section 6.2.4.

NON-LINEARITY The analytical model assumes ideal conditions, i.e. there is no interference and a linear increase of the message rate will consequently lead to the same linear increase of the load. Interference however is considered in the simulation.

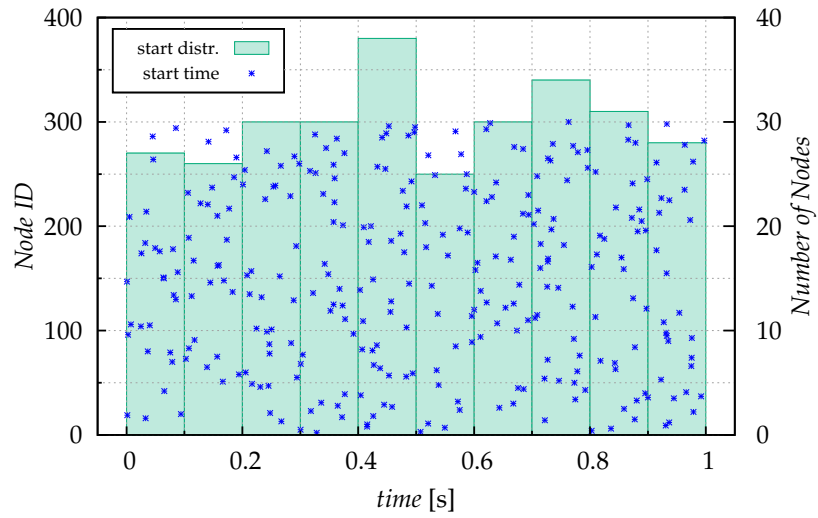


Figure 44: Distribution of the nodes first generation of a CAM based on the random initialization process ($K = 300, \alpha = \gamma = 0.4, r_s = 0.6$)

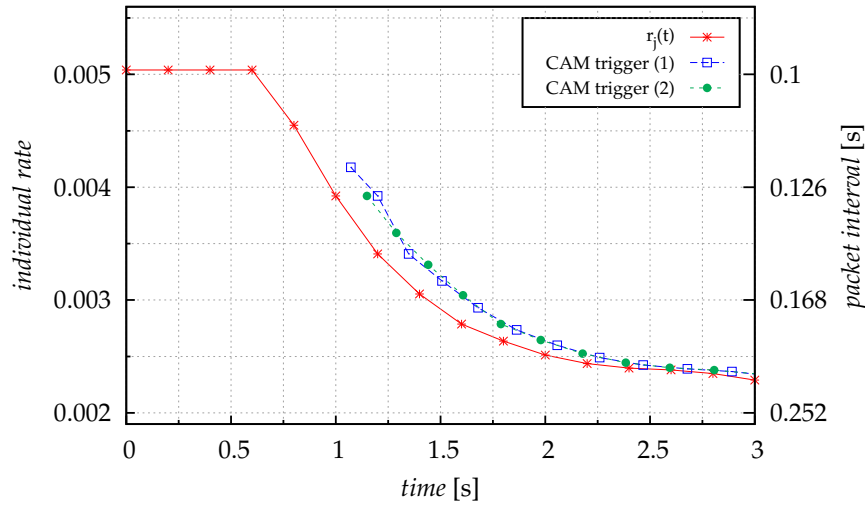


Figure 45: Illustration of the rescheduling process for 2 different nodes. ($K = 300, \alpha = \gamma = 0.4, r_s = 0.6$)

Table 17: Simulated and calculated CAM trigger for Node 1

		t				
		0.8	1.0	1.2	1.4	1.6
Simulation	r_j	0.00455	0.00392	0.00341	0.00305	...
	t_{snd}	0.9511	1.0717	1.2002 1.3481	1.5071	
Calculation	t_{rem}	—	0.0619	0.0002	0.0960	
	$\frac{r_j(t-1)}{r_j(t)}$	—	1.1596	1.1511	1.1161	
	t_{snd}	—	1.0717	1.2002	1.5071	

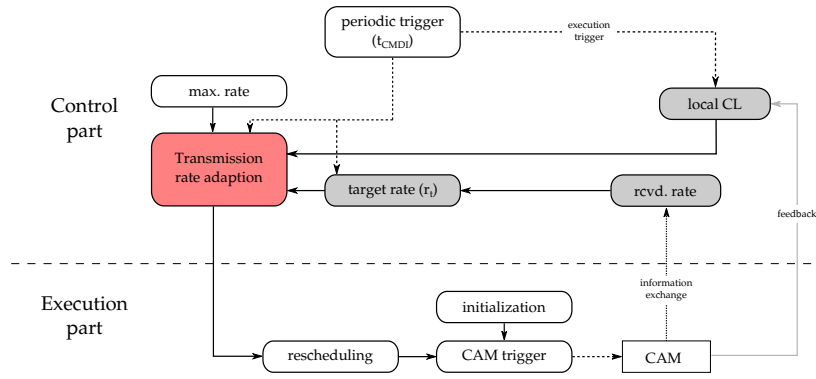


Figure 46: Active protocol elements used for the verification of the target rate adaption element (highlighted)

In section 6.3.1 it is shown, that this interference leads to an increase of non-linearity with increasing loads. While for a load of $r_c = 0.6$, this effect is moderate, it will significantly influence the convergence behavior for higher loads, especially for $r_c > 0.8$. This effect leads to the discrepancies occurring for $N = 200+$ and $N = 0+$, where load is exceeding the predefined threshold significantly. Furthermore, the nodes first need to be initialized and messages need to be rescheduled. This process takes a few iterations. A transition from higher to lower densities ($N = 100+$) does not suffer from non-linearity and the convergence behavior is as expected.

Interference is responsible for the higher rates observed. This effect is discussed in the following paragraph.

UNDERESTIMATION DUE TO INTERFERENCE Interference will occur if multiple CSMA stations transfer a message at the same time, because they either did not recognize the transmission (*hidden station*) or drew the same random backoff (CSMA collision). Since all nodes within the verification scenario (cf. section A.2.1) are in carrier sense range, hidden nodes do not occur. Especially CSMA collisions can have an effect on the algorithm, because they are not recognized by the underlying metric (CBR). As a result, the algorithm underestimates the real resource utilization, leading to a higher message rate. We have to note at this point that the higher the resource utilization $r_c(t)$ the more collisions occur which needs to be considered when defining r_g/r_s .

We illustrate the underestimation in table 18, where the average number of frames sensed (F_{RX}), collided (F_I), and calculated based on the measured CBR (F_{CBR}), and the average message rate \bar{T}_j (F_{SWeRC}) are listed depending on the simulation run number. The number of collided frames (F_I) excludes the first arriving frame and thus is not equal to the number of lost frames. Obviously, the amount of sensed frames equals the number of frames that theoretically should be disseminated following the message rate adjustment ($F_{SWeRC} \approx F_{RX}$). However, the number of frames that should be sent according to equation (5.7) and $r_s = r_c = 0.6$ is $F_{SWeRC} = 238.10$ which shows the underestimation of the real resource utilization. Basically, the real channel load in this case is the sum of F_{CBR} and collided frames which is equal to the amount of sensed frames ($F_{RX} = F_{CBR} + F_I$) (cf. figure 48).

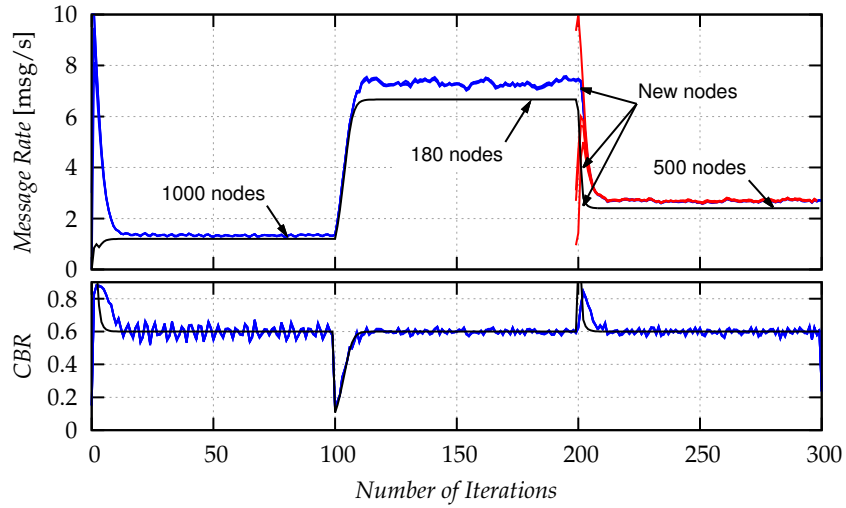


Figure 47: Stability and convergence of SWeRC with parameter optimization over time for different vehicle densities: Simulation compared with calculation ($\alpha = 0.5, \gamma = 0.5, r_s = 0.6, K = 1000, 180, 500$)

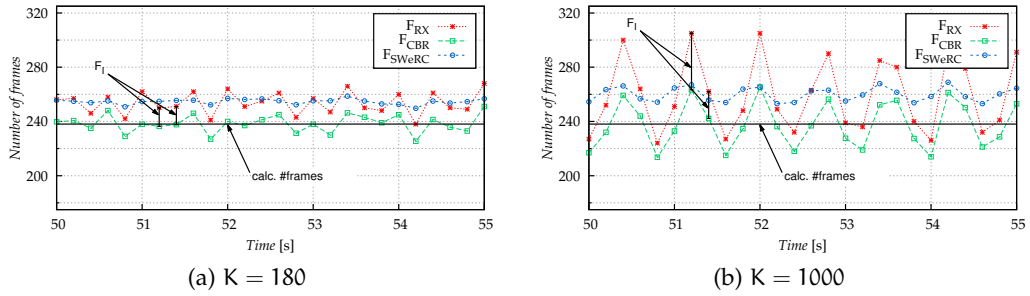


Figure 48: Heterogeneous distribution of frames along the time interval due to message rescheduling and difference between theoretical and real message rate due to interference. ($\alpha = \gamma = 0.4, r_g = 0.6$)

Table 18: Average number of frames ($N > 100, \alpha = 0.4, \gamma = 0.4$)

run No.	K							
	180				1000			
	F_{RX}	F_I	F_{CBR}^1	F_{SWeRC}^2	F_{RX}	F_I	F_{CBR}^1	F_{SWeRC}^2
1	255.51	16.9829	238.06	255.52	260.39	22.2485	237.79	260.49
2	254.59	16.0283	238.08	254.59	257.55	19.2559	237.94	257.56
3	251.45	12.9142	238.10	251.45	262.58	24.3109	237.90	262.60
4	253.49	14.9566	238.08	253.49	258.14	19.8342	237.96	258.15
5	259.76	21.1758	238.05	259.76	260.91	22.7507	237.82	260.91
calc.	238.10	0.00	238.10	238.10	238.10	0.00	238.10	238.10

1) $\bar{r}_c \cdot t_{CMDI} \cdot \frac{1}{T_{XTIME}}$

2) $\bar{r}_j \cdot t_{CMDI} \cdot \frac{K}{T_{XTIME}}$

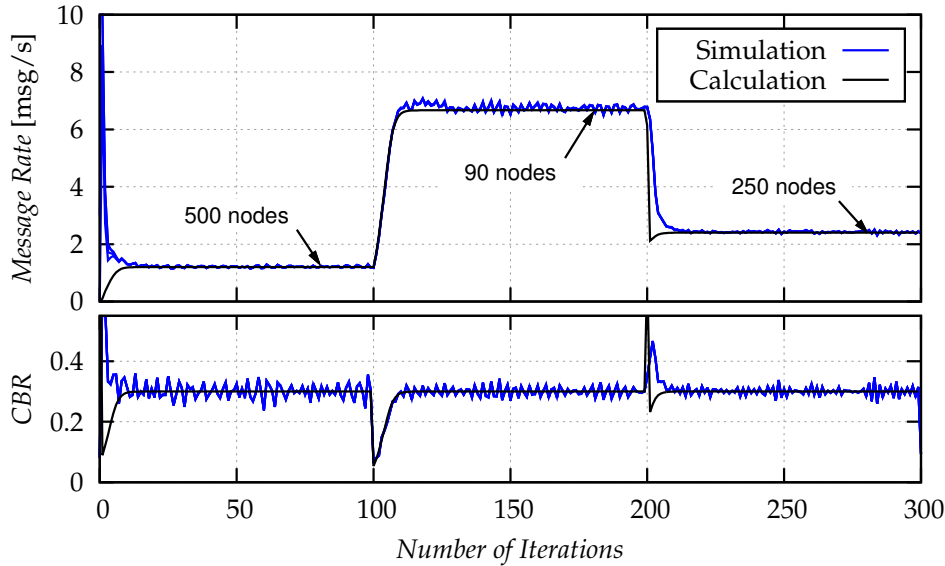


Figure 49: Stability and convergence of SWeRC with parameter optimization over time for different vehicle densities: Simulation compared with calculation ($\alpha = 0.5, \gamma = 0.5, r_s = 0.3, K = 500, 90, 250$)

VERIFICATION USING LOWER TARGET UTILIZATION We eliminate the occurrence of interference by halving the target utilization and the number of nodes respectively (cf. figure 49). For the target utilization of $r_s = 0.3$, linearity of the algorithm can be guaranteed and the occurrence of interference is minimized. The observed steady-state rate is the one, which is calculated using (5.7) and thus the functionality of the algorithm is validated. Unfortunately, rescheduling and node initialization need to take place and thus, the convergence behavior for adding nodes does not strictly follow the calculations (e.g. at $N = 200+$), still.

6.2.4 Information Exchange

For the verification of the exchange and aggregation of the channel status information including the locally measured utilization r_c and the target rate r_t , we use a linear scenario with randomly aligned nodes in three zones. In the center zone with a length of 1 km, there are $K_1 = 700$ nodes. This zone is nestled into two zones of length 1.5 km with $K_2 = 400$ nodes each, which is again surrounded by another zone of 1.5 km with $K_3 = 300$ nodes. Within these zones, the nodes are randomly aligned.

We validate the functionality by investigating the rate adjustment at a certain time for neighboring nodes and compare it with the expected rate for that iteration. For the simulation, the parameter optimized version of SWeRC was used with the default parameters ($\alpha = 0.3, \gamma = 0.4, r_s = 0.6, d = 2$). We use the simplified protocol stack illustrated in figure 50.

For 1-hop piggybacking the expectation is that nearby nodes use the maximum CBR that is observed by neighboring nodes or measured locally at the last iteration. In figure 51a, we illustrate the observed CBR $r_c(t-1)$ and the target rate $r_t(t-1)$ within the last iteration as well as the cooperative CBR and the cooperative target rate of the current iteration for an exemplary iteration ($N = 48$) based on the x-Position

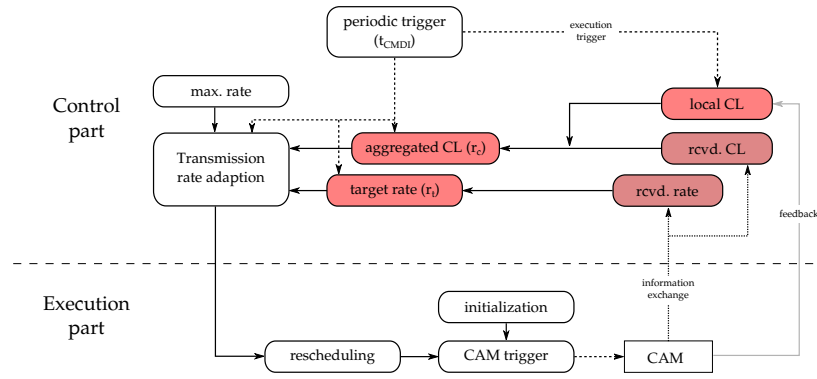


Figure 50: Active protocol elements used for the verification of the information exchange and aggregation (highlighted)

of the nodes. We also highlight the IDs of exemplary nodes, which observe the highest CBR within a region at the iteration $N = 47$, because this load will be used for the target rate decision. The cooperative target rate is the target rate of the node reporting the highest load within the last iteration. As an example, node 325 observes the highest load at $t - 1$ and reports it together with the observed target rate $r_t(t - 1)$. The neighboring node 407 receives this information and will adjust its rate based on the load and target rate reported by 325 (cf. table 19). The horizontal lines in figure 51a represent this cooperation, because the whole region reacts to the same load and target rate. In table 19, we exemplary verify the target rate adjustment based on cooperative information for 1-hop piggybacking for two nodes reporting highest load in the region and corresponding neighboring nodes receiving this.

For 2-hop piggybacking the expectation is that nearby nodes use the maximum CBR that was either observed or aggregated by neighboring nodes or measured locally two iteration ago. The interpretation of the results is according to 1-hop piggybacking. However, for 2-hop piggybacking, the region of nodes reacting to the same load can be higher and thus the cooperative load within a wider area is nearly the same (cf. figure 51b). In table 20, we validate the rate adjustment for the 2-hop channel status information for exemplary nodes.

Another indicator for the validation of the piggybacking used, is the achieved fairness range. The fairness range can be quantified as the range in which vehicles are controlled to the same degree based on their contribution to the channel congestion. The indicator here is the individual rate, which if fair allocation is applied should be equal for all nodes contributing to the congestion within a region. By increasing the number of hops, this range can be extended by several hundreds of meters depending on the reliable communication range. In figure 52, we illustrate this range for local measurements, 1- and 2-hop channel status information exchanged. For 2-hop piggybacking, the fairness range in the middle of the scenario is ≈ 2500 m, while for 1-hop piggybacking it is ≈ 1500 m. Enhanced fairness is achieved at the costs of decreased message rate. Considering a participation range of ≈ 900 m, 1-hop piggybacking can not guarantee that nodes participating in a far congestion will be regulated to the same degree.

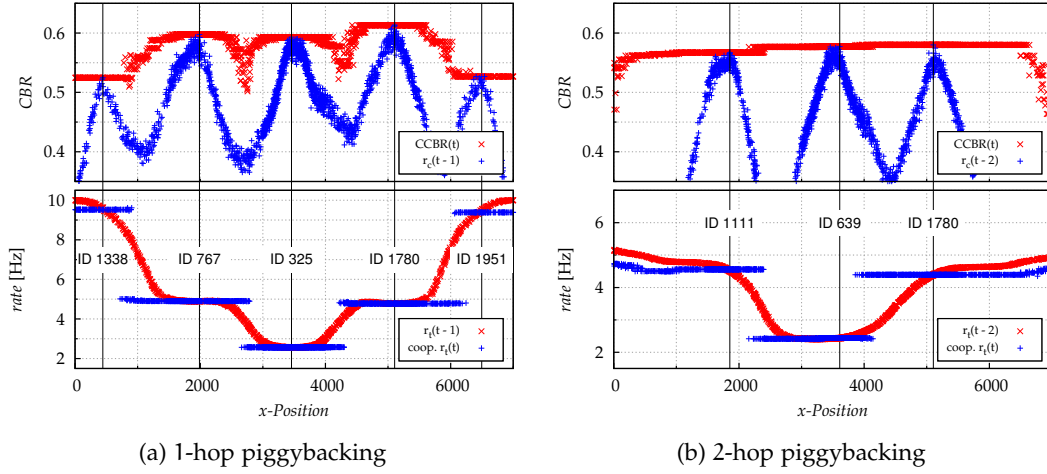


Figure 51: Illustration of the channel status information shared and the according measurements one/two iterations before ($N = 48$).

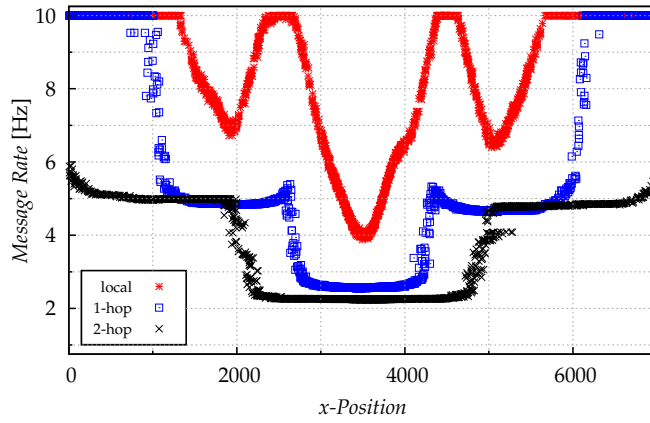


Figure 52: Fairness range achieved by local, 1- and 2-hop piggybacking indicated by the individual message rates for the nodes ($N = 163$).

Table 19: Simulated and calculated rate r_j for selected nodes based on 1-hop channel status information

		ID			
		325	407	1338	1217
	x-Pos.	3458	3325	444	531
Simulation	$r_c(t-1)$	0.59304	0.554628	0.524788	0.484537
	CCBR(t)	0.59304	0.59304	0.524788	0.524788
	$r_t(t-1)$	0.001271	0.001275	0.004767	0.004694
	coop. $r_t(t)$	0.001271	0.001271	0.004767	0.004767
	$r_j(t)$	0.001218	0.001307	0.00504	0.00504
	$r_j(t+1)$	0.001293	0.001304	0.00504	0.00504
Calculation	$r_j(t+1)$	0.001293	0.001304	0.00504	0.00504

Table 20: Simulated and calculated rate r_j for selected nodes based on 2-hop channel status information

		ID			
		639	1511	1111	1297
	x-Pos.	3610	4003	1854	1324
Simulation	$r_c(t-2)$	0.577278	0.396218	0.567097	0.391463
	CCBR(t)	0.577278	0.577278	0.567097	0.567097
	$r_t(t-2)$	0.001231	0.001330	0.002297	0.002407
	coop. $r_t(t)$	0.001231	0.001231	0.002297	0.002297
	$r_j(t)$	0.001198	0.001234	0.002400	0.002400
	$r_j(t+1)$	0.001232	0.001256	0.002432	0.002432
Calculation	$r_j(t+1)$	0.001232	0.001256	0.002432	0.002432

6.3 NUMERIC PARAMETER EVALUATION

6.3.1 Target resource utilization

Besides the convergence parameters, the target resource utilization is a critical parameter of the protocol, which needs further investigation. The protocol shall effectively utilize the available capacity, i.e. the maximum effective resource utilization is needed. For the sake of simplicity, we assume that all nodes are within close distance to each other, i.e. there are no hidden-terminals and no radio-wave propagation effects in this numerical investigation.

The maximum message capacity of a channel is given by the specified data rate of the channel and the length of a message specified by the TXTIME. Assuming a data rate of 6Mbit/s and a TXTIME of 504 μ s, the maximum message capacity is 1984.13 msg/s. Even under ideal conditions, this capacity can not be reached due to the CSMA back off-procedure. The minimum channel access time for a CAM transmitted at the highest priority (AC_VO) needs to be considered as well to obtain the maximum channel utilization under these conditions of $\text{TXTIME}/(\text{TXTIME} + \text{AIFS}[\text{AC_VO}]) \approx 0.897$. Note that hidden-terminal collisions are not considered.

Figure 53a illustrates the observed CBR for different offered loads. For low network loads, the CBR is increasing linearly, because the amount of interference occurring is comparable small. Due to the small CW, the amount of collisions is significantly increased for higher loads, i.e. for loads > 1000 msg/s the linearity is not given anymore. Unlike hidden-terminal-collisions, CSMA collisions do not effect the CBR since the messages are sent within the same slots. The approximation error of the offered load indicated by the CBR is significantly increasing for increasing loads.

However, the criteria for the target resource utilization is to maximize the goodput, i.e. the amount of successfully received messages. In this example, the goodput can be calculated as the amount of messages which are collision free. The goodput for different offered loads is shown in figure 53b. The goodput is linearly increasing with the factor of one for an offered load of up to 800 msg/s, because the amount

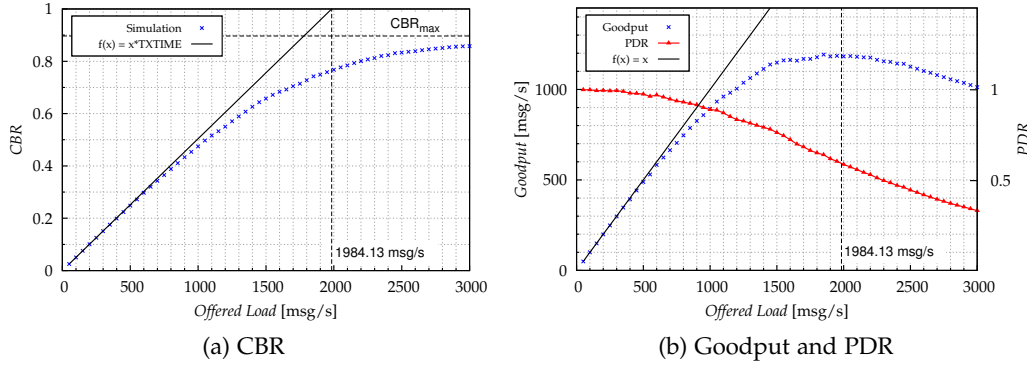


Figure 53: Impact of the offered load generated by K nodes transmitting at a rate of 10 Hz on the CBR, Goodput and PDR compared to theoretic capacity of the channel.

of interference is small. With a further increase in the offered load, the slope of the goodput is decreased up to a maximum of 1200 msg/s for an offered load of 1850 msg/s. The interference for an offered load > 1850 msg/s leads to a further reduction of the communication quality leading to a decrease in the goodput. Note, that even under very high loads > 4000 msg/s, single messages can still be successfully received, because the probability of multiple transmissions at the same time is increased. The results show, that an offered load of 1850 msg/s is maximizing the goodput resulting in a PDR of 0.64. This load is indicated by a CBR of 0.74, if all nodes are within each others communication range.

Obviously, the PDR is significantly decreased due to the amount of collisions. It might be argued, that the PDR should be maximized or kept above a threshold in order to maximize the efficiency of transmissions. In this case, the maximum offered load should be < 1000 msg/s, which under high densities will lead to a reduction of the message rate due to the small target resource utilization. It is more efficient to transmit one message at a high PDR, but the probability of receiving one out of multiple messages send at a lower PDR is higher and thus overall robustness of the system can be increased. In order to investigate this, we illustrate the blackout probability, i.e. the probability that a vehicle does not receive a message from another vehicle for more than one second due to subsequent packet loss is illustrated (cf. figure 54a). The blackout probability (P_B) is calculated based on the PDR (p) and the corresponding message rate (R) for the different loads

$$P_B(X > 1s) = (1 - p)^R \tag{6.3}$$

It is assumed that there are $K = 185$ nodes in the communication range, which transmit messages to create a certain offered load. The message rate itself is the quotient of the targeted offered load and the number of nodes K , i.e. for a load of 1850 msg/s, the rate is 10 Hz and for 925 msg/s, the rate is 5 Hz.

The blackout probability is minimized for offered loads between 800 and 1500 msg/s. If the offered load is too small, the resulting message rate will be low leading to a higher dependency of the PDR. On the other hand, if the offered load is higher, the message rate will be increased, but the PDR will get decreased significantly due to the occurring interference. Although, the probabilities are comparably small on the

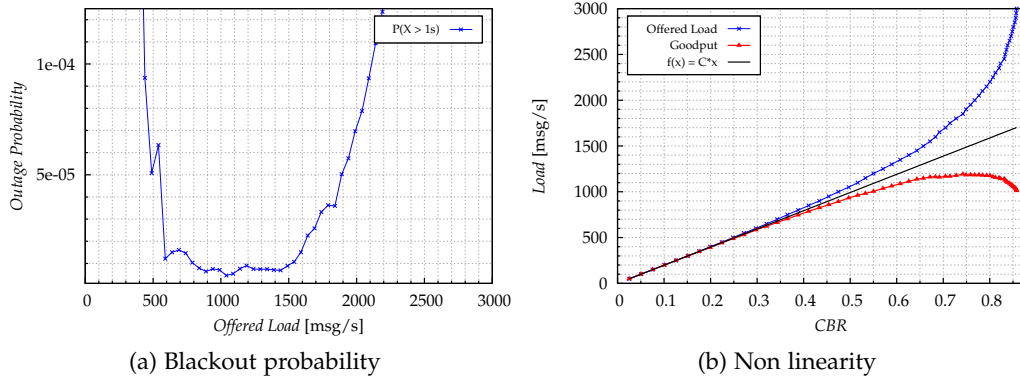


Figure 54: Illustration of the impact of the load on the blackout probability and illustration of the non linearity for high resource utilizations.

first view (cf. figure 54a), with millions of CAMs exchanged, the blackout probability is a significant indicator for the reliability of the system.

Although weighted by the target rate, the rate adjustment algorithm benefits from linearity in terms of convergence speed and predictability. In this context linearity illustrates the linear increase of the individual rate based on the according increase in the utilization. Figure 54b shows the dependency of the simulated goodput and offered load for different CBRs. The function illustrates the theoretic linear increase in the load based on the message capacity $C = 1984$ msg/s. For comparably high CBRs, the linearity between utilization and offered load is not given anymore. Especially for the maximum goodput at $CBR = 0.74$, the deviation between the calculated and the simulated load is significant. The problem here is, that the algorithm targets at a certain load by linearly adjusting the individual rate, i.e. if the load should be 5% higher, the rate is increased by 5%. Now, if the CBR is 0.7 and it should be increased by 10%, the load needs be increased from 1700 msg/s to 2050 msg/s which is an increase of 20%. This will lead to longer convergence time, because more iterations are necessary in order to reach the target utilization.

In order to maximize the resource allocation, while maintaining the linearity and decrease the blackout probability, the target resource utilization used for the algorithm is assigned to be $r_s = 0.6$. The corresponding offered load of 1350 msg/s is minimizing the blackout probability and the goodput of 1100 msg/s is less than 10% behind the maximum, while offering a PDR of 0.8. Nevertheless, the deviation in the linearity is decreased significantly (cf. figure 54b).

6.3.2 Convergence Parameters

While the theoretical analysis of the convergence parameters α and γ revealed the effect of the individual parameters for convergence to fair and steady-state rate, suitable values still need to be found. The rate adjustment algorithm therefore is used as illustrated in figure 55 without cooperation, awareness control and smoothing within the verification scenario.

In order to find the best parameters, two aspects of the algorithm need to be considered: the steady-state stability and the convergence speed. In this section both

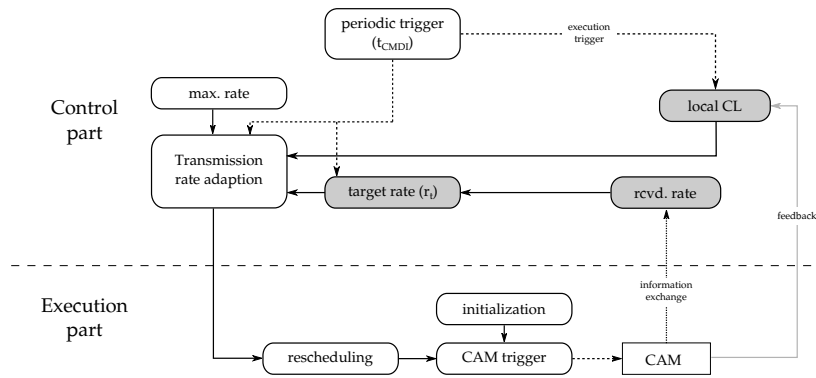


Figure 55: Active protocol elements used for the (parameter) evaluation of SWeRC

aspects are discussed with results giving insights into the impact of the individual parameters. Based on this analysis, the best-effort parameters for a small convergence time and a stable steady-state behavior are depicted.

STABILITY The stability of the target rate algorithm is denoted by the volatility of the steady-state rate. The target of the algorithm is to minimize this volatility in order to guarantee reliable communication at a stable steady-state rate. Figure 56 illustrates the steady-state message rates of K nodes as boxplots for different exemplary values for the convergence parameters in comparison with the result for *LIMERIC* using *gain-saturation* (3.14). When using SWeRC, the gain of the β -part of the algorithm is reduced for low message rates and stays at a high level for high message rates. Thus for the upper bound of β ($\gamma = 1.0$), the volatility is high for any α , especially for low values of K (cf. figure 56a). However, since this is the upper bound, lower values for γ are suitable. For $\gamma = 0.5$, one can already achieve a stable resource allocation which equals *gain-saturation* for $K = 180$ (cf. figure 56a), and deviation is decreased to nearly zero for $K = 1000$, as shown in figure 56d.

The effect of α on the scalability is limited though, because it is rather used to speed up convergence, while stability is influenced by $(d\gamma - \alpha)$ only. Figure 57 illustrates the relative deviation of the steady-state message rate for different convergence values, where the relative deviation is calculated based on a 99% confidence level, i.e. the lower and upper 0.5% of the values are excluded. It quantifies the stability in terms of volatility. The figure shows that if $(2\gamma - \alpha) < 0.8$ holds, volatility can effectively be suppressed independent of α and the node density K . However, if the node density is increased, the effect of convergence parameters outside of the optimal operating range is significantly higher than for low node densities. Table 21 gives an overview of the convergence values which grant maximum and minimum stability for the different node densities. It is shown, that the maximum rel. deviation for $K = 1000$ is more than twice as high as the corresponding value for $K = 180$, while the minimum rel. deviation is nearly the same.

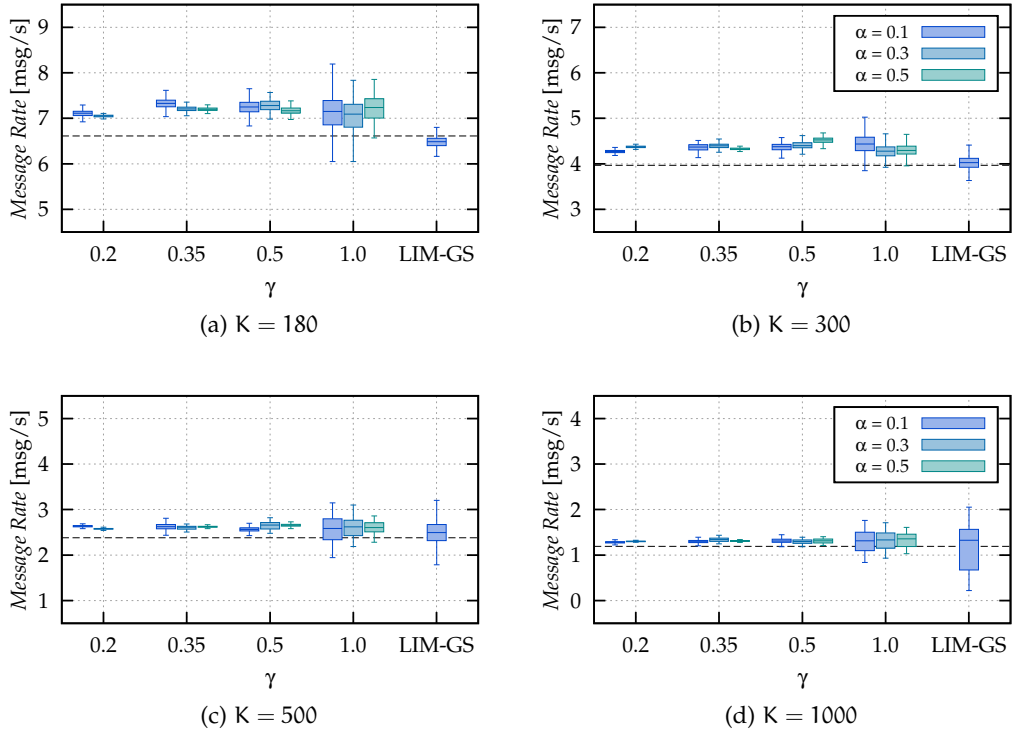


Figure 56: Steady-state message rate distribution for different convergence parameters α and γ in comparison with results for *gain-saturation* for one single simulation run. ($N > 100$)

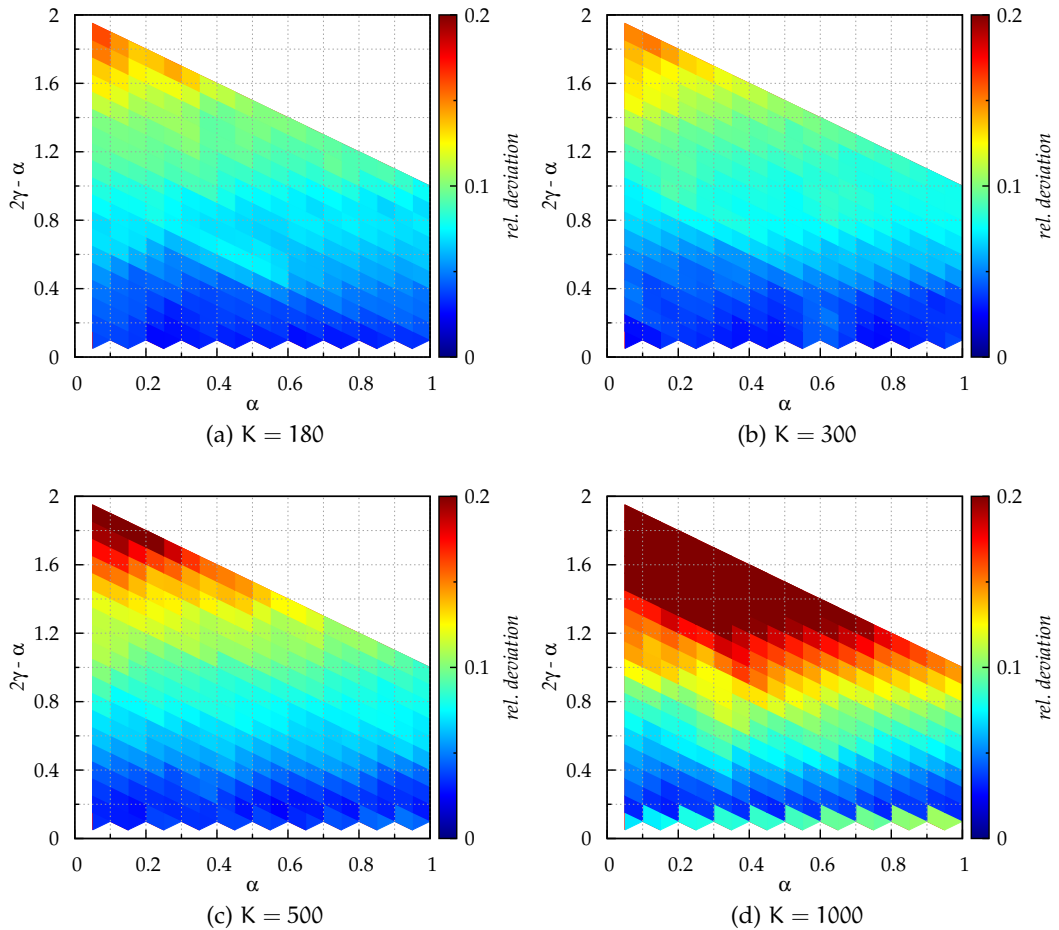


Figure 57: Relative deviation of the steady-state message rate for different values α and γ , denoted by $(2\gamma - \alpha)$ ($N > 100$)

Table 21: Convergence values for minimum and maximum rel. deviation

rel. dev.	K							
	180		300		500		1000	
	min	max	min	max	min	max	min	max
α	0.4	0.1	0.4	0.1	0.65	0.15	0.1	0.05
γ	0.25	1.0	0.25	1.0	0.4	1.0	0.1	0.95

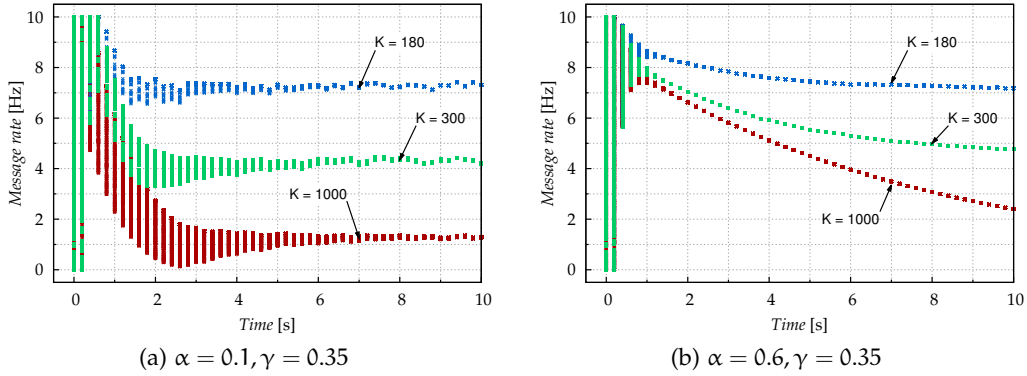


Figure 58: Convergence behavior over time for chosen convergence parameters and node densities K .

CONVERGENCE SPEED The convergence speed acts as the counterpart for stable systems, because it takes a longer time for a slow reacting system to achieve its steady-state after a distortion, while a fast reacting system tends to get unstable. As depicted by (5.22), both α and $(2\gamma - \alpha)$ influence the time needed until a steady-state is reached. Figure 58 shows this convergence behavior for a chosen parametrization. While the convergence towards the fair message rate is fast for $\alpha = 0.1, \gamma = 0.35$, the convergence of the individual rates towards the group rate is slow (cf. figure 58a). For $\alpha = 0.6, \gamma = 0.35$, the opposite is true, because the multiplicand of the gain $(2\gamma - \alpha) = 0.1$ is comparably small and thus the convergence to a fair message rate is slow (cf. figure 58b). This indicates, that in terms of convergence speed, SWeRC profits from a large α and a large multiplicand $(2\gamma - \alpha)$.

The convergence speed is quantified as the point in time at which the difference between the rate $r_j(t)$ and the average steady-state rate \bar{r}_j does not exceed a threshold. The threshold is defined as the maximum difference between \bar{r}_j and $r_j(t)$ in the steady-state ($N > 100$). The results are illustrated in figure 59 for different node densities. Obviously, the convergence speed can be significantly increased when using larger values for the convergence parameters, i.e. $\alpha > 0.2$ and $(2\gamma - \alpha) > 0.4$.

The figures also show a slight dependency of the convergence speed and the vehicle density. Convergence to the fair rate using the same convergence parameters takes longer for higher densities (cf. figure 59a and figure 59d). While the effect of α is limited for low densities, it has a significant impact on the convergence speed for densities $K > 300$ (cf. figure 59b).

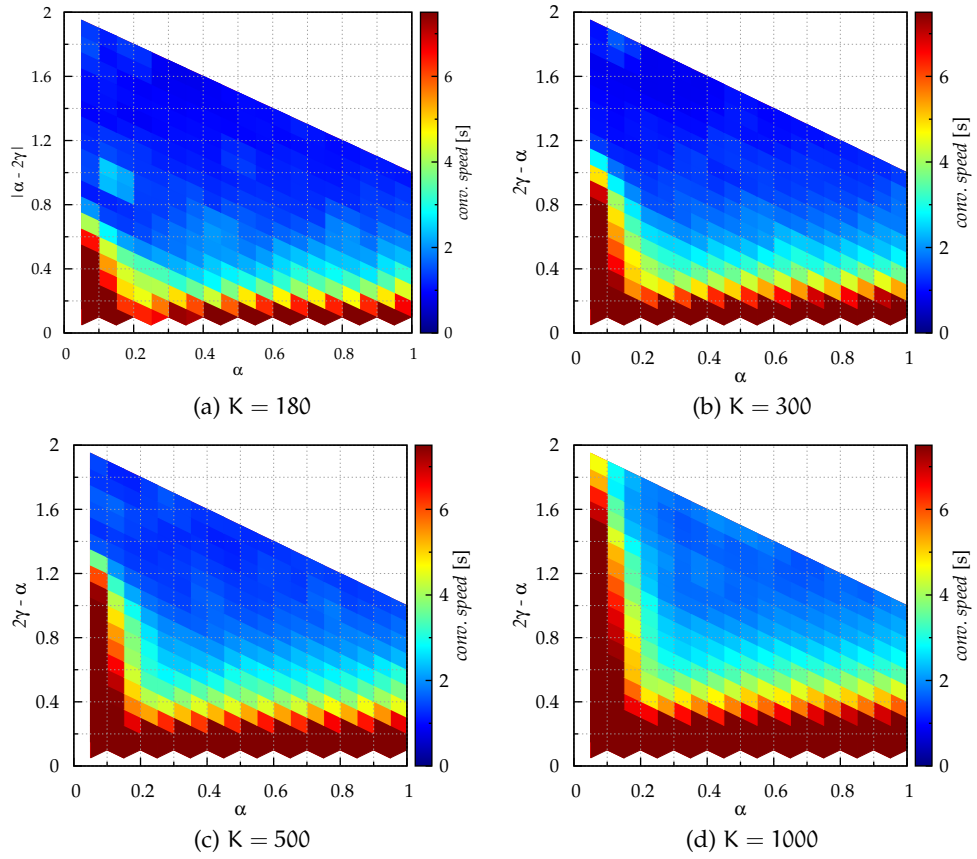


Figure 59: Convergence speed - Overview of the key convergence values of SWeRC for different values α and γ , denoted by $(2\gamma - \alpha)$ ($K = 300$).

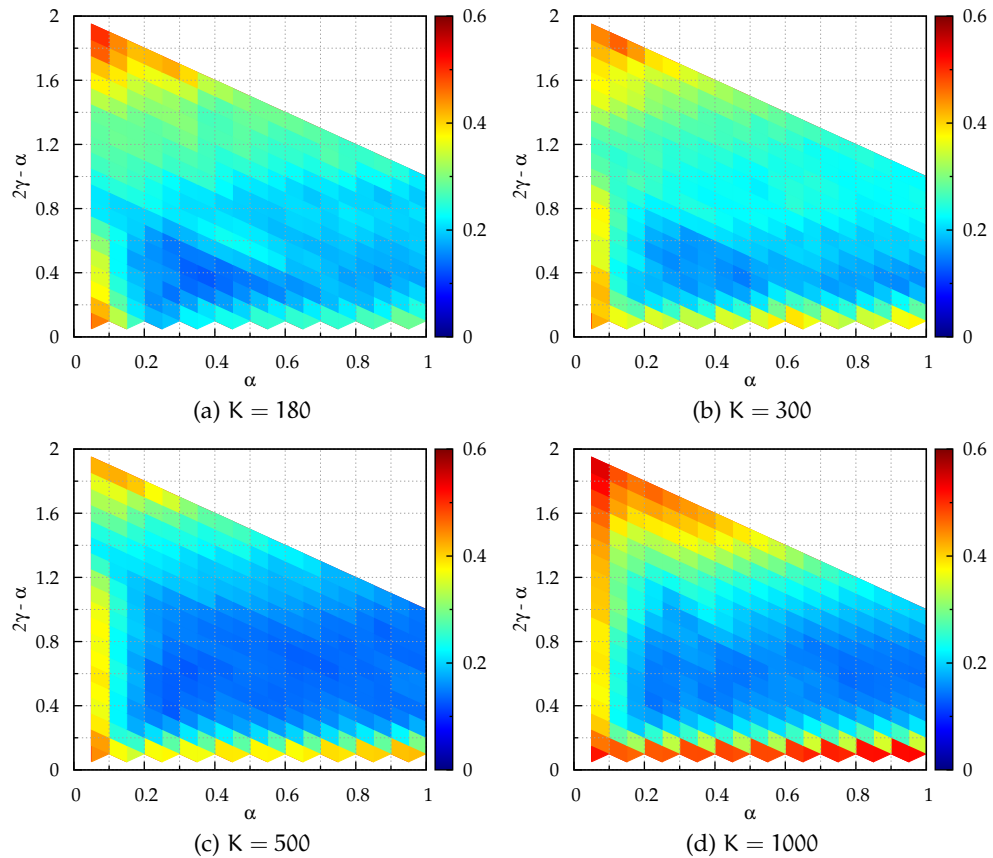


Figure 60: Suitable parameters selection based on numerical results and equal weights regarding stability and convergence speed, where lower values indicate a better overall performance.

Table 22: Convergence values for minimum and maximum convergence speed

	K							
	180		300		500		1000	
	min	max	min	max	min	max	min	max
speed	0.76	20.12	0.64	20.65	1.0	20.24	1.32	20.88
α	0.1	0.05	0.05	0.05	0.2	0.05	0.5	0.05
γ	0.95	0.05	1.0	0.05	1.0	0.05	0.9	0.1

Table 22 gives an overview of the minimum and maximum convergence times and the corresponding convergence values for the different node densities. The minimum and maximum convergence speeds are approximately the same independently of the vehicle density, but with slightly varying convergence parameters. Especially for many nodes having individual rates, a higher α can be beneficial in terms of convergence to the group rate (cf. figure 58a). The self-weighted algorithm reduces the reaction to small message rates in order to guarantee stability. Thus high vehicle densities are effected by this self-weighting by longer convergence speeds. To compensate this here, a larger multiplicand ($2\gamma - \alpha$) needs to be selected.

SUITABLE CONVERGENCE PARAMETERS The best-effort parameters are obtained by a cost function, where both convergence speed (cf. figure 59) and relative deviation (cf. figure 57) are normalized to one as well as equally weighted so that 0 marks the best and 1 indicates the worst parameter combination (cf. figure 60). Considering this, a good parametrization of the convergence parameters is achieved for $0.2 < (2\gamma - \alpha) \leq 1.0$ and for $\alpha > 0.2$ for all vehicle densities.

In table 23, these convergence values and the resulting convergence speed and stability for the different vehicle densities are listed. It is shown, that a convergence value of $0.25 < \alpha < 0.35$ achieves good convergence in terms of minimized overall costs (H) for $0.35 < \gamma < 0.5$. In order to achieve an optimized and scalable parametrization of the convergence values, a common set needs to be found.

In this thesis, the values for the convergence parameters are considered to be $\alpha = 0.3$ and $\gamma = 0.4$, resulting in $(2\gamma - \alpha) = 0.5$. Table 24 gives an overview of the resulting convergence speed and relative deviation of the message rate for exemplary values and different node densities.

Table 23: Best convergence values for different densities based on the cost function (H)

	K			
	180	300	500	1000
speed	2.60	2.12	2.80	3.16
rel. dev.	0.033	0.042	0.048	0.110
H	0.111	0.127	0.101	0.126
α	0.35	0.35	0.25	0.3
γ	0.35	0.45	0.4	0.5
$2\gamma - \alpha$	0.35	0.55	0.55	0.7

Table 24: Exemplary convergence values. Suitable parameters are highlighted

		$\alpha = 0.2$					$\alpha = 0.3$					$\alpha = 0.4$				
		K					K					K				
		180	300	500	1000		180	300	500	1000		180	300	500	1000	
$2\gamma - \alpha = 0.2$	speed	4.68	6.32	8.48	10.56		4.56	6.64	8.40	11.00		5.16	6.48	8.08	11.28	
	rel. dev.	0.038	0.045	0.025	0.028		0.031	0.042	0.036	0.035		0.035	0.042	0.032	0.033	
$2\gamma - \alpha = 0.4$	speed	4.12	4.92	4.76	4.92		2.56	3.04	4.00	4.92		2.32	3.44	4.04	4.96	
	rel. dev.	0.042	0.049	0.043	0.049		0.048	0.044	0.045	0.070		0.041	0.046	0.047	0.056	
$2\gamma - \alpha = 0.5$	speed	2.24	3.76	3.68	4.40		1.76	2.72	3.04	3.88		2.24	2.48	3.12	3.88	
	rel. dev.	0.041	0.046	0.075	0.074		0.043	0.045	0.079	0.087		0.053	0.055	0.079	0.066	
$2\gamma - \alpha = 0.6$	speed	1.40	2.80	3.36	4.04		1.84	2.28	2.48	3.16		1.72	2.24	2.40	3.16	
	rel. dev.	0.068	0.047	0.066	0.089		0.057	0.055	0.057	0.110		0.073	0.064	0.059	0.097	
$2\gamma - \alpha = 0.8$	speed	1.28	1.60	3.32	3.68		1.24	1.40	2.12	2.44		1.44	1.56	1.80	2.48	
	rel. dev.	0.083	0.068	0.087	0.099		0.078	0.090	0.078	0.145		0.064	0.075	0.083	0.107	
$2\gamma - \alpha = 1.0$	speed	1.04	1.28	2.08	3.64		1.12	1.24	1.44	1.76		1.24	1.20	1.88	1.76	
	rel. dev.	0.089	0.100	0.090	0.145		0.083	0.083	0.093	0.122		0.086	0.087	0.090	0.163	

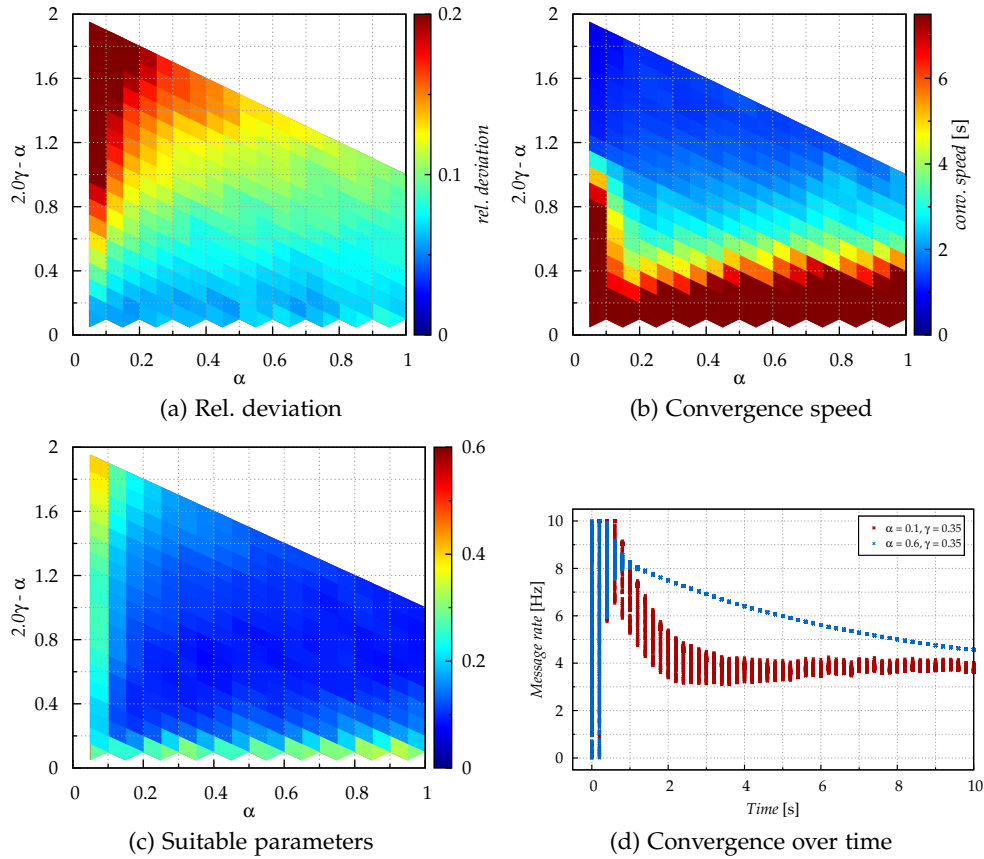


Figure 61: Observed performance of SWeRC with higher target resource utilization parametrized ($K = 500$).

HIGHER TARGET RESOURCE UTILIZATION As stated in section 6.3.1, a higher target resource utilization would benefit the goodput of the channel, but will negatively influence the convergence speed and stability, because the linearity between offered and perceived load is not given anymore. The following results show the performance of SWeRC using the higher resource utilization of $r_s = 0.74$ for $K = 500$. We observe a steady-state message rate of 3.71 Hz, which means there is an offered load of 1855 msg/s on the channel, while for $r_s = 0.6$ the rate is 2.62 Hz and the offered load is 1310 msg/s.

Figure 61 illustrates the performance of SWeRC using the higher resource utilization. In comparison with the same results observed for $K = 500$ nodes and $r_s = 0.6$, the possible parameters in which a high stability is achieved is limited to $2\gamma - \alpha < 0.4$ (cf. figure 61a), while the parameters optimizing the convergence speed should be in the range of $2\gamma - \alpha > 0.7$ (cf. figure 61b). For the parameters optimizing this trade-off (cf. figure 61c), there is no clear indication. Instead a wide range of parameters can achieve a suitable trade-off between convergence speed and stability.

We quantify the minimum and maximum parameters for the convergence speed, relative deviation and the cost function in table 25. Compared to the lower target utilization, there is a higher maximum convergence speed and a higher relative deviation. The non linearity and the interference thus can have a significant influence on the behavior of the algorithm for insufficient parameters. However, if suitable parameters ($\alpha = 0.55, \gamma = 0.65$) are specified, stability and fast convergence is

Table 25: Good convergence values for different densities based on the cost function (H)

	speed		rel.dev.		H	
	min	max	min	max	min	max
speed	0.76	37.32	17.28	0.76	2.72	37.32
rel. dev.	0.409	0.103	0.043	0.433	0.078	0.103
H	0.47	0.578	0.226	0.5	0.072	0.578
α	0.05	0.65	0.5	0.05	0.55	0.65
γ	0.95	0.35	0.3	1.0	0.65	0.35
$2\gamma - \alpha$	1.85	0.05	0.1	1.95	0.75	0.05

obtained. Moreover, the parameters specified for $r_s = 0.6$ do also lead to a good performance for the higher target utilization (rel. dev. = 0.074, speed = 3.72). We conclude, that the algorithm can handle higher target resource utilization, where linearity is not given, if the parameters are sufficiently specified. However, the occurring interference is immense and the PDR and thus blackout probability is significant (cf. section 6.3.1).

6.4 CONVERGENCE IN A STATIC NLOS SCENARIO

In this scenario, the performance of the protocol is evaluated for NLOS conditions. Under these conditions, the cooperation between vehicles is essential in order to achieve a fair and efficient resource allocation. We use the scenario as described in section A.2.2, which offers static nodes and shadowing due to building and allows to review the efficiency of 1- and 2-hop piggybacking. For the evaluation, the optimized convergence parameters from section 6.3.2 are used. Note, that dynamic CAM generation and channel load smoothing are disabled.

LOCAL FAIRNESS In figure 62 the average steady-state key parameters of the protocol are illustrated, if no information exchange between the nodes is applied. Due to symmetry of the scenario, results for nodes at the vertical lanes (L_2 and L_4) are not shown for simplicity of the plots. Here, the local CBR measured by the nodes at and close to the intersection clearly exceeds the target resource utilization of $r_s = 0.6$ (cf. figure 62a). This problem also occurs for *LIMERIC* as described in section 3.2, because the nodes which are at the intersection are affected by the hidden-node problem. In this context, the amount of packets received by nodes at the intersection is twice as high, as for nodes at the lanes (cf. section A.2.2). Thus the nodes at the intersection are not responsible for the traffic generated here and a reduction of the individual rates can not reduce congestion. However, the nodes do not cooperate and thus rates at the intersection are reduced due to high local CBR (cf. figure 62c). This leads to a local unfairness between nodes at the lanes and those which are at the intersection. *SWeRC* profits from the semi-cooperative target-rate here, because the group-rate within the neighborhood is used to adjust the individual rate and thus the reduction of the individual rate will be limited, if unfairness between neighboring nodes gets to harsh. It encounters an exceeding of the target resource utilization. Thus the target rate for a certain node is higher (cf. figure 62d) than the individual rate here.

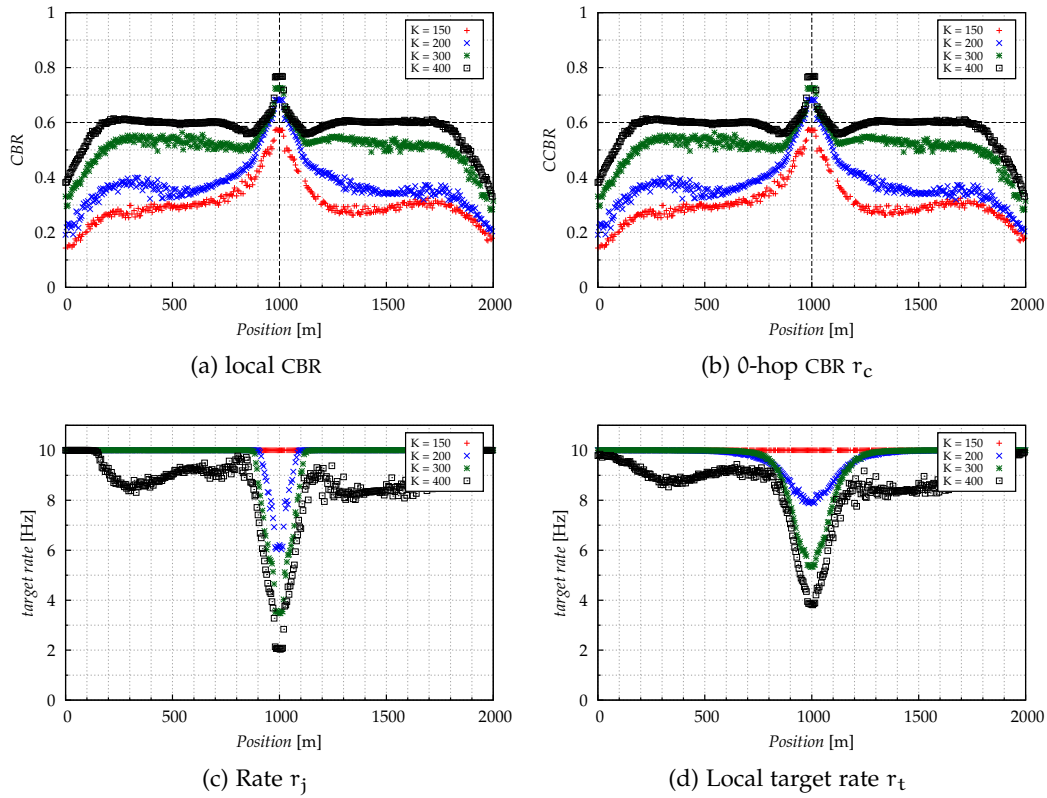


Figure 62: Illustration of average key parameters for different node densities K within the NLOS scenario without cooperation in steady-state ($N > 100$).

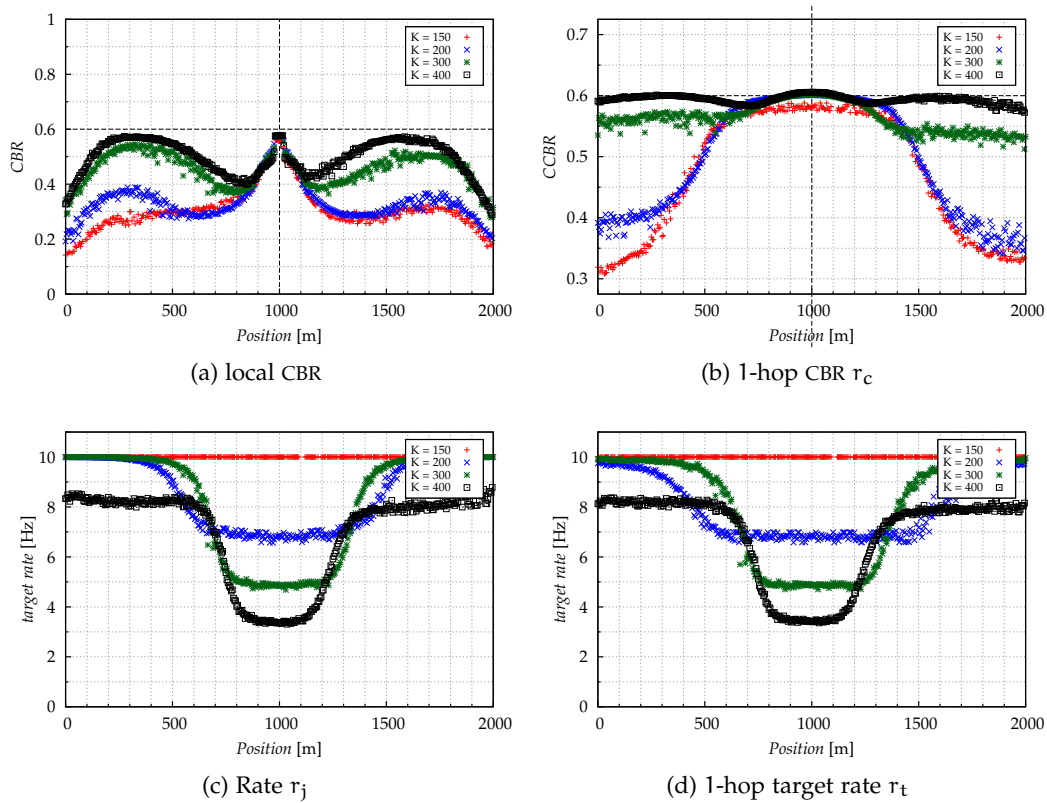


Figure 63: Illustration of average key parameters for different node densities K within the NLOS scenario with 1-hop piggybacking in steady-state ($N > 100$).

1-HOP PIGGYBACKING The respective results for 1-hop piggybacking of cooperative information are illustrated in figure 63. In contrast to none used cooperation, the local CBR does not exceed the target resource utilization at any point within the scenario (cf. figure 63a). This is achieved at the costs of reduced rate for nodes receiving the cooperative information. The nodes react to the maximum CBR measured from the neighboring nodes. This Cooperative Channel Busy Ratio (CCBR) is illustrated in figure 63b. A cooperation range of ≈ 300 m is generated in which nodes react on this cooperative CBR and reduce their rate accordingly (cf. figure 63c). However, there is no clear border, because vehicles at a certain distance receive far away messages with a lower probability and thus can react to a maximum CBR from nodes at the intersection still. This range and probability is dependent on the amount of interference, which is higher for larger node densities and limits the cooperation range.

Another effect which occurs in this scenario for 1-hop piggybacking is the appearance of a local minimum for the local CBR for nodes close to the intersection. This is the case, because those vehicles are not affected by the hidden terminal problem, but the rates of a huge part of the neighbors are reduced due to cooperation (cf. figure 63c). This can be problematic, because those nodes receive a maximum cooperative load as well from nodes at the lane and from nodes at the intersection with different group rates respectively leading to unstable behavior. This problem is further discussed later on, where we discuss the usage of Weighted Global Cooperation (WGC) instead of Full Global Cooperation (FGC).

2-HOP PIGGYBACKING Applying 2-hop piggybacking in this scenario should lead to a common cooperative perspective of maximum loads and channel status information. The results as shown in figure 64 support this hypothesis. The cooperative 2-hop load which is used for SWeRC here (cf. figure 64b) indicates that each node independently of its position within the scenario perceives the same resource utilization. However, due to the limited communication range, some nodes at the edges of the scenario do not receive the maximum CBR in each iteration, such that the averaged CCBR is slightly lower than the target resource utilization of $r_s = 0.6$. This result is also reflected by the individual rates for the different node positions (cf. figure 64c). Depending on the node density, this rate is constant, independently of the nodes position, but with a slight increase of the rate at the edges of the scenario due to the slightly reduced load. Again, SWeRC profits from its semi-cooperative target rate here, which is clearly position independent and thus can limit the reaction of the nodes to fast changes of the cooperative utilization due to packet-loss.

A drawback of 2-hop piggybacking is the comparably slow reaction to distortions of the system. In order to synchronize local, 1- and 2-hop information, a node needs to react to information of the iteration $t - 2$ (0.4 s). On the other hand, it is able to provide *global* fairness and grant rates for nodes at the intersection, which are approximately the same as for 1-hop piggybacking and clearly higher than without cooperation. Furthermore the problem of unstable behavior at bordering zones can be minimized due to the extended cooperation range.

FAIRNESS RANGE BORDER INSTABILITY In figure 65, we illustrated the stability issue induced by the strict border of the cooperation range. This zone is highlighted

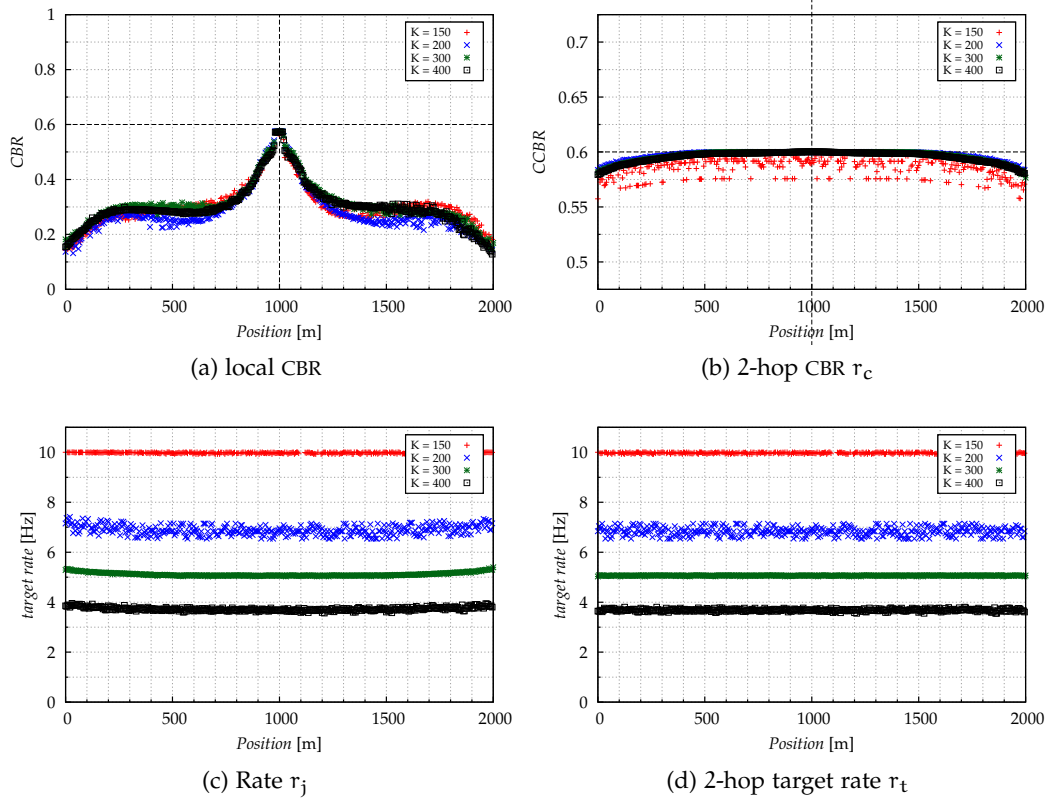


Figure 64: Illustration of average key parameters for different node densities K within the NLOS scenario with 2-hop piggybacking in steady-state ($N > 100$).

in figure 65a, where the individual rates of the different nodes are shown dependent on their positions for a selected time interval in steady-state. In these zones, the rate over time is not stable and nodes tend to instable behavior due to the fast reacting protocol design (cf. figure 65b). While nodes at the intersection or at the border of the scenario converge to a stable steady-state rate, vehicles within this zone receive information from the intersection as well as from the lanes, if the maximum channel status from the intersection is not received correctly or, due to reduced message rate, the load was not considered within this iteration. The major problem is not the received maximum cooperative CBR (cf. figure 65c), but the cooperative target rate. From the figure it is obvious, that during most of the iterations, the node at $x = 700$ receives the maximum CBR from the intersection, but during some iteration, the maximum CBR is lower. At this iteration the nodes also receive the target rate from a node not on the intersection with higher target rate (cf. figure 65d) and react by converging to this target rate with respect to the difference between the cooperative and the target CBR.

In order to overcome this, different methods of calculating the target rate can be applied as discussed in section 5.4.3. In figure 66, some key parameters for the exchange of channel status information with the usage of WGC for target rate acquisition among the extended fairness area is shown. Under these conditions, the individual rates are dependent on the cooperative maximum CBR (cf. figure 66b) with respect to the remote target rate (cf. figure 66c). In other words, the algorithm tries to help nodes which are affected by high loads by reducing their rates, but

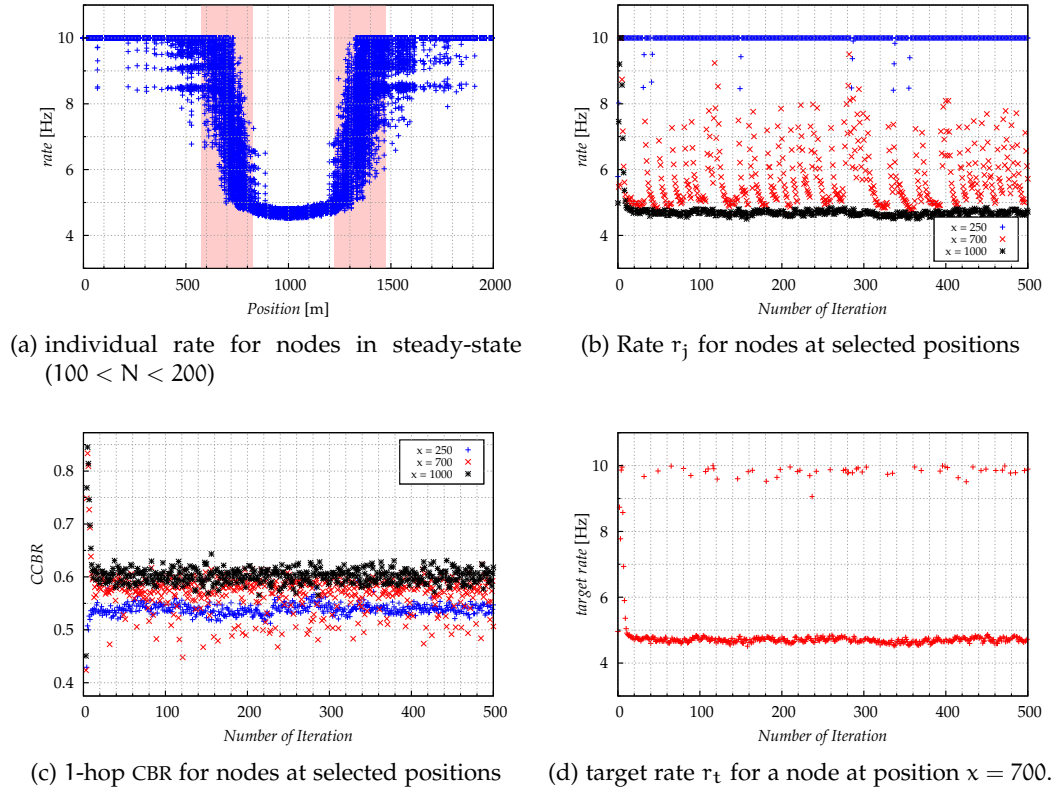


Figure 65: Illustration of the stability problem for nodes at the cooperation range border using 1-hop piggybacking ($K = 300$).

this is done based on fair conditions for the whole region. Obviously, the average 1-hop CBR exceeds the predefined threshold of $r_s = 0.6$ at the intersection region (cf. figure 66b). This effect occurs, because the algorithm tries to converge to the CBR threshold on the one hand to fulfill the aim of congestion control, and tries to satisfy the fairness aspect by converging to the observed group rate on the other hand. The individual rates for 1- and 2-hop piggybacking are reduced close to the intersection (cf. figure 66c), but still higher than without cooperation (cf. figure 62c). increasing the fairness range by utilizing 2-hop piggybacking will result in a global fair allocation of the resources.

However, the stability of the nodes within the bordering region is significantly increased, because there are no harsh transitions. In figure 67, we illustrate this by showing the rate, cooperative 1-hop CBR and target rate for a specific time interval. Because of the different calculation of the target rate (WGC), nodes within the transition border do not tend to volatile behavior (cf. figure 67d) anymore, although the shared CBR values are received from different nodes over time (cf. figure 67b). On the other hand, a globally fair allocation of the resources is not achieved. Furthermore, it is shown that the major effect for the weighted fairness here is the locally assessed target rate (cf. figure 67c). However, if no cooperation is applied, the semi-cooperative exchange of the target rate leads to a certain degree of fairness already, but global fair allocation of the resources can not be guaranteed.

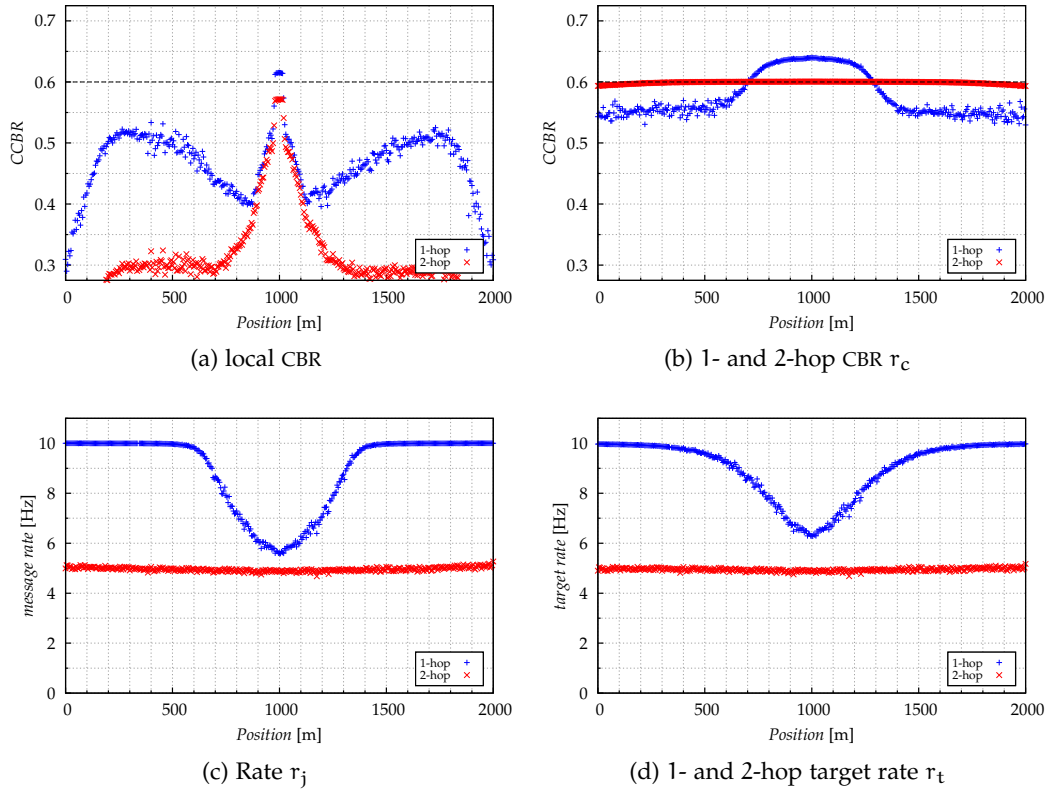


Figure 66: Illustration of average key parameters for usage of WGC within the NLOS scenario in steady-state ($N > 100, K = 300$).

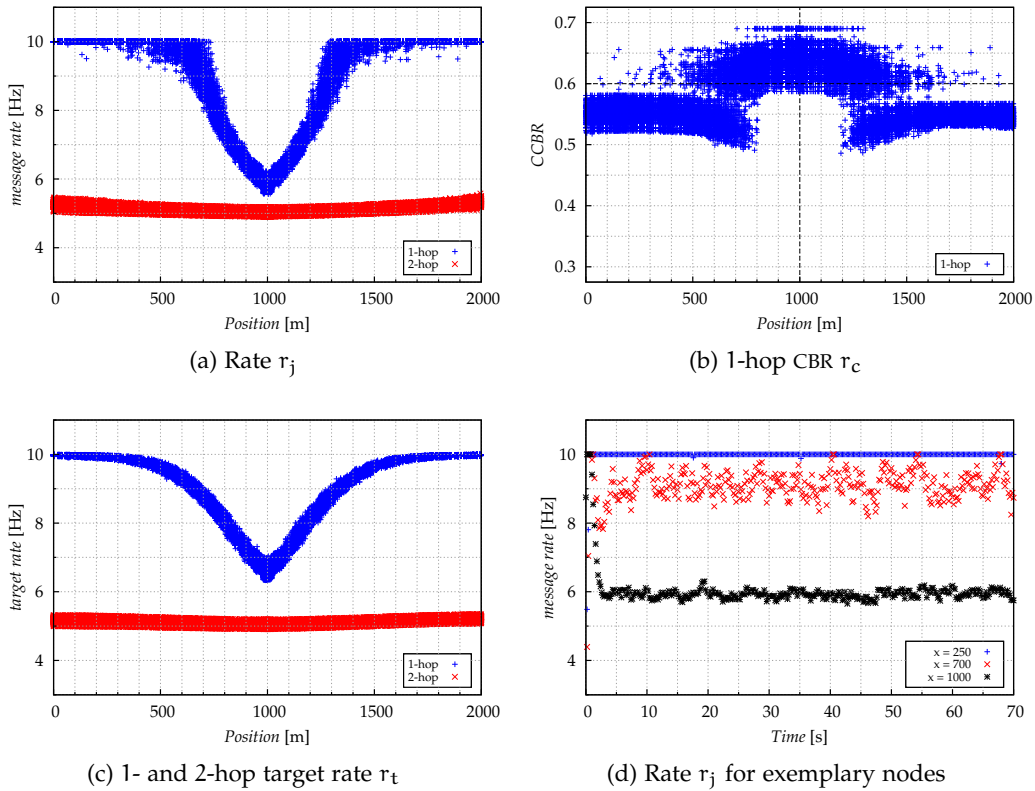


Figure 67: Illustration of average key parameters for usage of WGC within the NLOS scenario for a specific time interval ($100 < N < 200, K = 300$).

SUMMARY The investigation under NLOS conditions revealed, that the semi-cooperative mechanism of the protocol avoids unfairness for nodes which are suffering under high loads. The drawback is, that the observed utilization within this region can not be reduced, because it is generated by nodes which are at the border of the communication range. Applying fairness range extension by piggybacking the channel status and rate information significantly contributed to a fair allocation of the resources. However, fairness is traded in for a lower overall efficiency due to reduced rates and instability at the borders of the fairness range. Using WGC for the target rate acquisition, this border instability is mitigated at the costs of reduced fairness range.

6.5 PERFORMANCE UNDER DYNAMIC CONDITIONS

In this chapter, we provide an in-depth analysis of SWeRC utilizing different scenarios in order to show the functionality under various realistic conditions. In order to provide realistic mobility patterns, we use the hybrid simulation set-up which is explained in detail in appendix A. We focus on two major scenarios, a straight highway scenario with traffic jam and an urban grid scenario.

We investigate the protocols performance without an active awareness control scheme in order to evaluate the stand-alone performance. Furthermore, we deactivate the CBR smoothing module. Unless explicitly outlined, SWeRC is evaluated using the default parameters highlighted in A.1.

6.5.1 Highway

In the following, the performance of SWeRC is evaluated within a dynamic highway scenario. A detailed overview of the scenario and the simulation environment used is given in appendix A. We compare the performance of the non-cooperative approach with 2-hop piggybacking using FGC and WGC. The analysis is based on the key parameters, e.g. message rate and utilization, as well as the performance indicators, e.g. PDR and IRT. A comparison with state-of-the-art protocols is conducted in section 6.6.

VEHICLE DENSITY: The vehicle density has a major influence on the load within the region. We provide an analysis of the position and lane dependent density within the scenario in figure 68. Figure 68a illustrates the vehicle density per lane and km for an exemplary simulation run at time $t = 50$. While for the road segments without traffic-jam the vehicle density is highly volatile within the range of 0 to 20 veh/lane/km, within the traffic jam the vehicle density is in the range of 60 to 75 veh/lane/km. Freight trucks mostly occupy the right lanes leading to a decreased density within the jam (cf. figure 68a). Although not explicitly illustrated, it is obvious, that due to the vehicle movement over time, the vehicle density within the different areas changes rapidly. However, the density, position and length of the jam is nearly independent of the simulation run and time (cf. figure 68b). The cumulative vehicle density per km within the traffic-jam is approx. 400 veh/km, which will clearly exceed the channel capacity, if each vehicle transmits at the default rate of 10 Hz with an average communication range of 500 m. While the start of

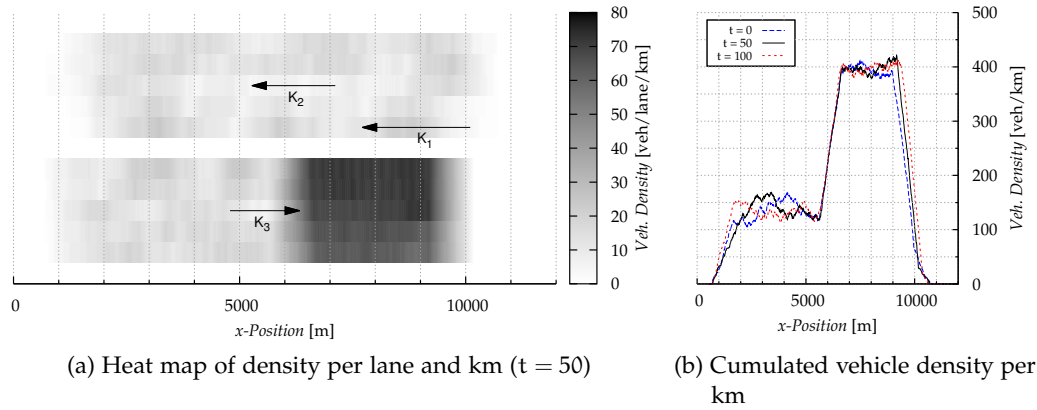


Figure 68: Illustration of the vehicle density within the highway scenario for an exemplary simulation run and a specific point in time.

the traffic-jam is slightly moving, the end is static leading to an increase of the jam length over time (cf. figure 68b).

It is expected, that the channel load is proportional to the vehicle density, if no congestion control is applied. The congestion control applied by SWeRC will lead to a decrease of the message rate for vehicles within and close to the traffic-jam, where this curve is expected to be inversely proportional to the vehicle density and due to multi-hop piggybacking the effect can be ambiguous.

RATE AND UTILIZATION: In figure 69, the results for the key parameters of SWeRC are given. Within the figure, we highlight the traffic-jam region in grey and compare the results for FGC and WGC using 2-hop piggybacking with the non cooperative scheme.

The message rate for both cooperative approaches is significantly lower within the traffic-jam region compared to the non-cooperative approach (cf. figure 69a). While a non cooperative node will react to its own measured load which due to interference and fading can be lower in one and higher in the next iteration, cooperative nodes will react to the maximum load reported by neighboring nodes (cf. figure 69d). In consequence, in each iteration a different node can observe the maximum load, while the locally measured load is below the threshold. This result can be observed by the average locally measured CBR (cf. figure 69c). For the cooperative approaches, the load is significantly lower than the threshold and in consequence the algorithm will converge to a lower rate. The fairness range extension is traded in for a lower overall message rate within the traffic-jam zone and also within the critical zone.

Without cooperation, the target load can get exceeded under certain circumstances (cf. figure 69c). Especially at the edge of the traffic-jam, a higher load is observed. This is due to the load induced from nodes, which do not observe, but participate in the congestion at this point, i.e. nodes which are not stuck in the traffic-jam transmitting at a high rate (e.g. at $x = 5800$ m). Usually, nodes would reduce their rate as long as the load is below the threshold. Through the target-rate mechanism of SWeRC, a certain level of fairness will be maintained under these conditions, because the group perception will cause a contradictory regulation to the locally observed load (cf. figure 69b). Due to the dynamic movements of vehicles within this scenario,

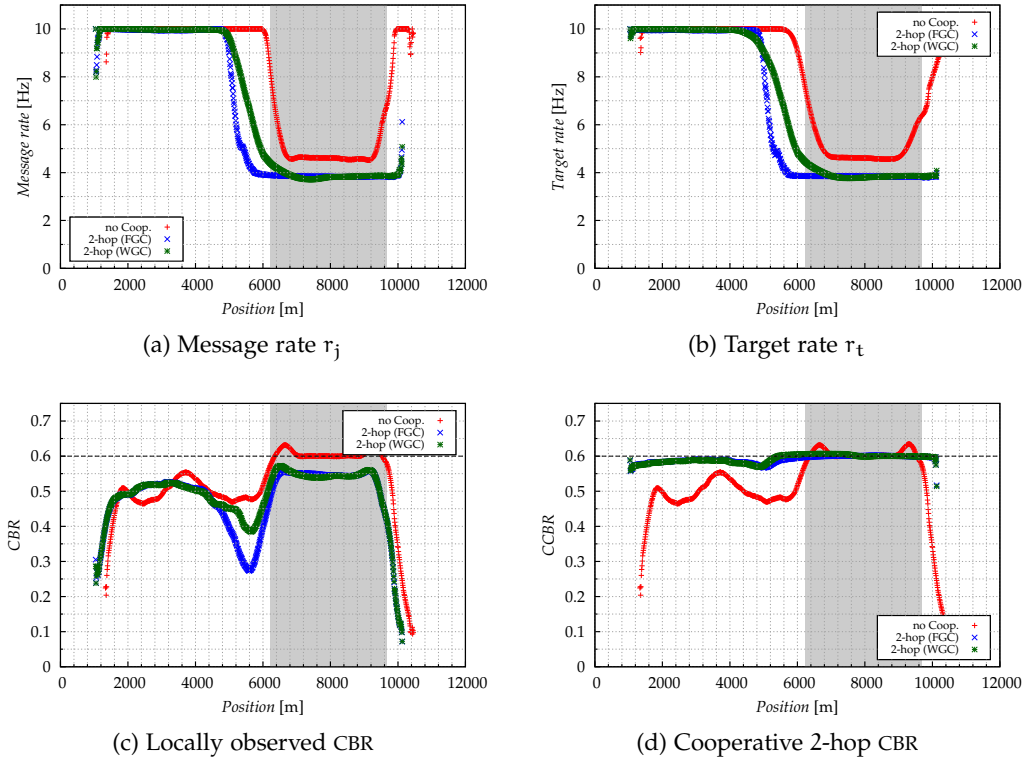


Figure 69: Illustration of the averaged values of the key parameters of SWeRC for the dynamic highway scenario in steady-state ($N > 25$).

nodes will arrive and depart at the edges of the scenario. In consequence, the observed values in this region are non-predictable due to the initialization process and shall be ignored, e.g. $x < 1200$ m.

In figure 69c, it is shown that the locally observed CBR for both WGC and FGC is declining within the critical zone at $5500 \text{ m} < x < 6500 \text{ m}$. The local node density K in this zone is lower than expected for the adjusted rate. As observed before, we thus expect a positive influence on the PDR.

Time-dependent behavior

Unfortunately, average results can be misleading regarding the individual performance and fairness of the protocols. Thus we illustrate the results for the key parameters for exemplary nodes in figure 70. The direction and position of the chosen nodes are illustrated in figure 68a. The nodes are chosen such that the critical zones are covered, i.e. the transition from free-flow to traffic-jam. While the nodes K_1 and K_2 are passing the traffic jam in the opposite direction, K_3 is approaching the traffic-jam. The figures show the time and corresponding distance to the start/end of the traffic-jam on the x -axis and the individual rate and (cooperative) CBR on the y -axis.

The results show, that during the initialization phase, all schemes have a fast convergence to the steady-state rate and utilization. The convergence to the target utilization r_s can be maintained for both cooperative schemes FGC and WGC, while the non cooperative scheme exceeds the predefined threshold within the traffic-jam.

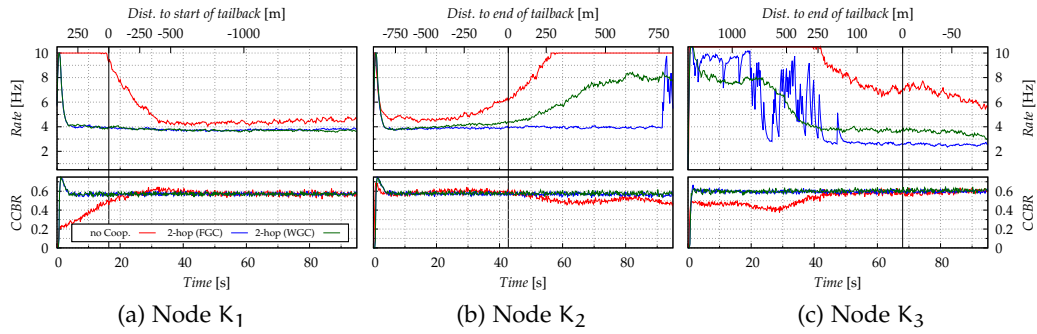


Figure 70: Comparison of the results for the key-parameters of SWeRC for selected nodes over time within the highway scenario.

While both the non cooperative and the WGC scheme provide a stable behavior for the transition phase, SWeRC with FGC suffers from the fairness range border instability as illustrated in section 6.4. Although the maximum CBR reported is the same, the reported and used target rate depends on the reporting nodes. The effect can be seen in at node K_2 for $t > 95$ (cf. figure 70b) and at node K_3 for $t < 50$ (cf. figure 70c).

PERFORMANCE INDICATORS (PDR, IRT): The PDR within the Region of Interest (RoI) is higher for both schemes using 2-hop piggybacking as expected (cf. figure 71a). Within the figure, we also highlighted the maximal interference free PDR measured by the number of sensed, but due to interference lost frames. This sensing probability should and indeed is equal to the calculated ideal PDR of the path-loss model as shown in section A.1.2. The PDR is decreasing rapidly, and reliable communication is not given for high ranges, i.e. for $d > 400$ m, the PDR is less than 30%.

The IRT is illustrated in figure 71b as a CDF, i.e. the probability of having an information freshness smaller than IRT. Considering FGC, the probability of an Information Freshness (IF) < 0.2 is $P[\text{IRT} \leq 0.2] \approx 0.6$. Obviously, up to a certain probability ($P < 0.9$), the non cooperative approach offers the best IRT due to the higher message rate within the critical zone (cf. figure 69a) and WGC outperforms FGC. Although the difference in terms of PDR is minimal, there is a significant difference in terms of IRT.

While the probability for lower IRT values is mostly influenced by the rate adaption, i.e. a higher rate will lead to lower transmission intervals and consequently lower IRT, higher IRT values are caused by (subsequent) packet losses due to interference and path-loss. These subsequent packet-losses are the more critical values that can significantly influence the performance of a safety application. Thus, in chapter 7 this IRT is further used for quantifying the awareness of a vehicle.

An often used method to quantify the performance in terms of IRT is to determine the IRT for a certain probability, i.e. the IF is lower than IRT with a confidence level of X . Using $X = 0.95$, we achieve the following results: $\text{IRT}_{\text{noCoop}}^{0.95} \approx 0.33 < \text{IRT}_{\text{WGC}}^{0.95} \approx 0.415 < \text{IRT}_{\text{FGC}}^{0.95} \approx 0.45$. It is observed, that SWeRC achieves best awareness, if no further cooperation is applied and instead, self-weighted local fairness is used at least for scenarios with LOS conditions.

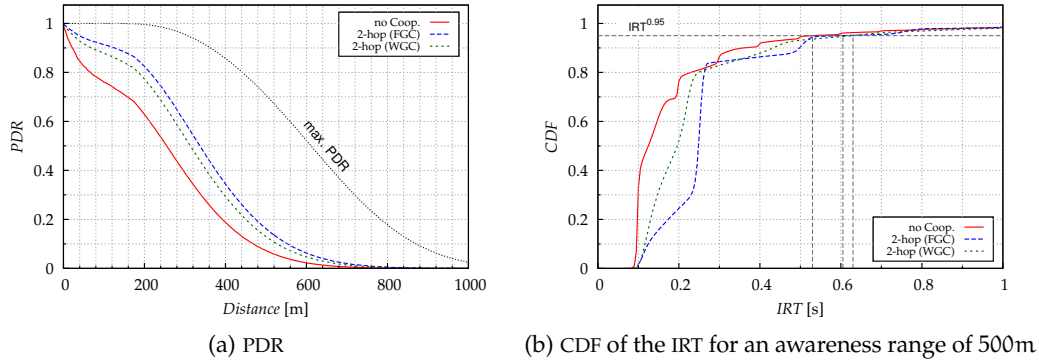


Figure 71: Overview of the performance of SWeRC within the dynamic highway scenario in steady-state ($N > 25$).

6.5.2 Urban

In this section, we analyze the performance of SWeRC using the scenario described in section A.2.4. The major issue in this scenario is the shadowing of signals due to buildings and thus a significant reduction of the communication range. Furthermore due to the shadowing, vehicles located closely will not have common perception and in consequence fairness is a major issue.

VEHICLE DENSITY We estimate the vehicle density as the number of nodes, which are within the communication range at a certain position. We distinguish between LOS and NLOS communication, where conservative communication ranges are used, i.e. the LOS communication range is 300 m and for NLOS it is 150 m. The resulting vehicle density is shown in figure 72.

Due to the shadowing of the buildings, vehicles which are close to the intersections are in LOS with all vehicles on the respective lane and the amount of nodes in range is significantly higher than for the nodes, which are situated between two intersections. Figure 72a shows this effect for the simulated region. Looking closer at a single road, it can be seen, that nodes at the intersection have to handle up to twice as much vehicles ($K \approx 450$) than nodes at the lanes ($K \approx 200$).

During the simulation, we also estimated the number of neighbors based on the disjunct nodes observed during the last second. While calculation and estimation is almost equal for the nodes at the lanes, there is a significant difference at the intersections (e.g. $875 < x < 925$). It can be assumed, that due to the congested conditions at the intersection, interference occurs leading to loss of information. However, the calculated number of nodes are based on a conservative estimation using comparably safe communication ranges.

RATE AND UTILIZATION In figure 73, the key parameters for the dynamic urban scenario are illustrated. The border range instability, which was observed for large scaled scenarios, can not be observed here, because the distance between the intersection is smaller than the fairness range. Thus, the difference between SWeRC using FGC or WGC is minimal here. Both converge to a fair rate of 5 Hz (cf. figure 73a), while maintaining the CBR threshold (cf. figure 73d). However, the algorithm trades

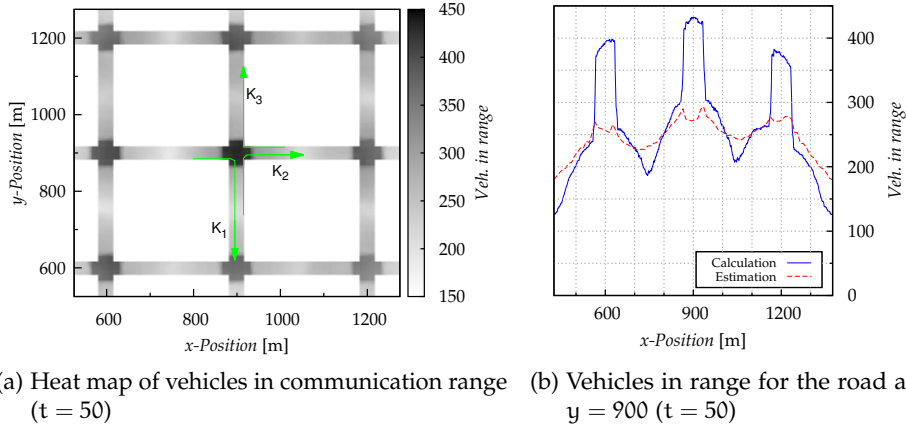


Figure 72: Illustration of the vehicle density within the urban scenario for a specific point in time based on a calculated communication range of 300 m and 150 m for LOS and NLOS comm. respectively.

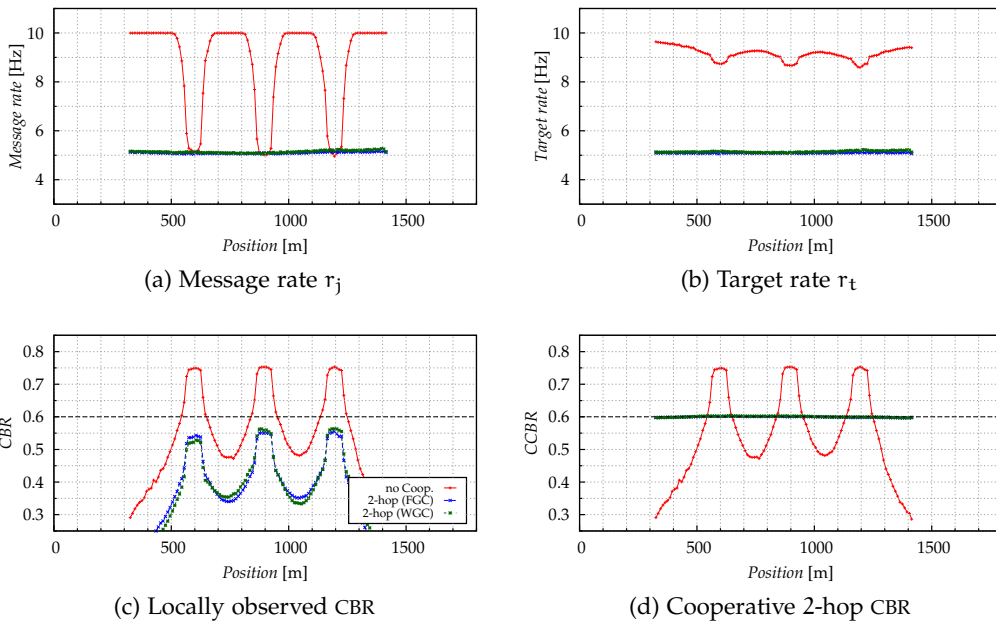


Figure 73: Illustration of the averaged values of the key parameters of SWeRC for the dynamic highway scenario in steady-state ($N > 25$).

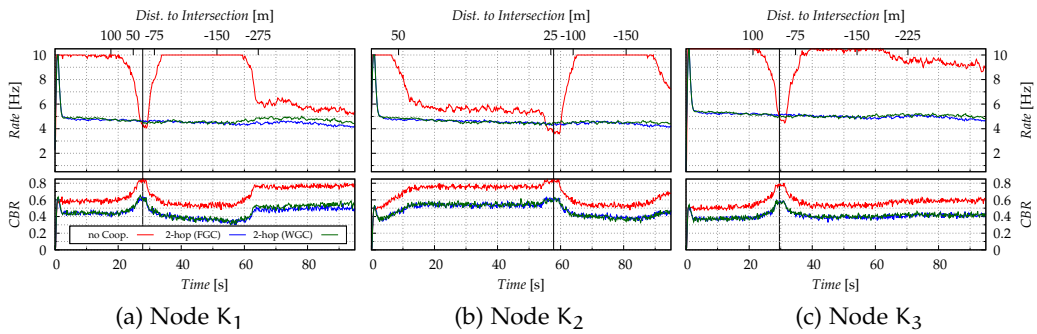


Figure 74: Comparison of the results for the key-parameters of SWeRC with state-of-the-art CC protocols for selected nodes over time within the urban scenario.

in efficiency to maintain a fair resource allocation, i.e. the average locally observed CBR is lower than the threshold even at the intersections (cf. figure 73c).

If no cooperation is applied, the algorithm can theoretically maintain the same effective rate of 5 Hz at the intersection, while reaching the maximum rate for nodes at the lane (cf. figure 69a). While the algorithm tends to decrease its rate on the intersection, because the CBR threshold is exceeded (cf. figure 73c), there is the counterpart of the locally computed target rate, which is close to the maximum rate of 10 Hz (cf. figure 73b).

Time dependent

For the investigation of the key parameters over time, we took three individual nodes which are passing the intersection at (900,900) executing a right-turn. The exact trajectories of the nodes are illustrated in figure 72a. The nodes will be in close proximity at $t \approx 30$ s, where all of them are either passing the intersection or are close to it, e.g. node K_2 has to wait at the traffic-light, but it is in LOS with both K_1 and K_3 .

Without cooperation, the conditions at the intersection change rapidly from very good to very bad, i.e. the message rate and CBR will have significant fluctuations. On one hand, this indicates fast reaction of the protocol to changes in the environment, but on the other, it indicates the unfairness at the intersection. Close to the intersection, all nodes perceive high loads and in consequence, the rate is reduced. However, they all perceive the same conditions, thus the change over time is not a time dependent, but a space dependent effect (cf. figure 74).

If cooperation is applied by either WGC or FGC, the message rate is stable over time and space, i.e. the rate is independent of the position and time of a node at least if the nodes are within the fairness range (cf. figure 74b). A minor change over time from 5 Hz to 4 Hz is observed for the three nodes, because the distribution of the vehicles can change leading to utilization peaks and consequently lower rates. While the cooperative utilization over 2-hops can be maintained, it is observed, that the local CBR (cf. figure 74a) is still at the maximum close to the intersection. The algorithm is capable of adjusting the rate in order to achieve a max-min fair allocation by maximizing the minimum rate, i.e. the rate at the intersection, but it can not avoid the hidden-terminal effect which is occurring due to the shadowing of the buildings.

PERFORMANCE INDICATORS In figure 75, the performance indicators measured within the steady-state and the RoI (cf. section A.2.4) are shown. We separate the LOS and NLOS packets and evaluate the PDR separately.

Since the adjusted rates for both WGC and FGC are approximately the same within this scenario, we can observe an equal PDR here. The PDR in LOS is dropping fast, such that at a distance of 160 m already 50% of the packets are lost, if cooperation is applied (cf. figure 75a). If no cooperation is applied, the range is further decreased to ≈ 90 m. For NLOS the results predict a short communication range as well, with a PDR of 0.5 at a distance of 80 m and 95 m for non cooperative and cooperative VSC respectively (cf. figure 75b). However, these are averaged values and the actual PDR is more likely dependent on the load and can be influenced by the hidden-terminal effect as well, such that it can be significantly lower at the intersection.

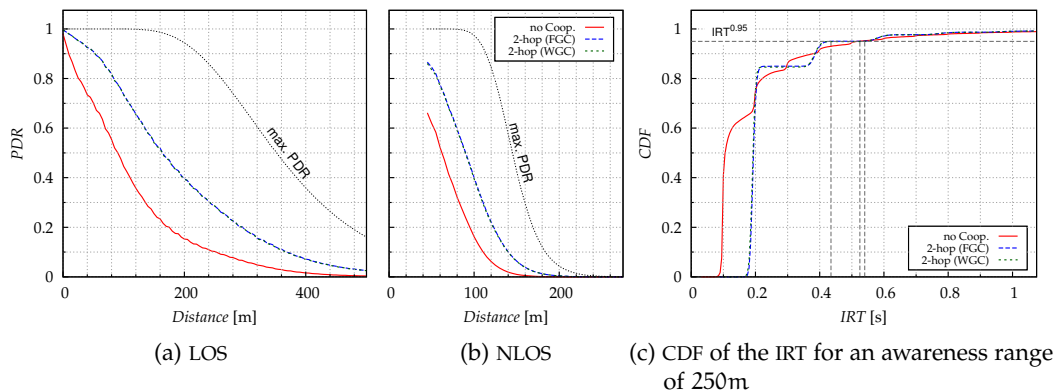


Figure 75: Overview of the performance of SWeRC within the dynamic urban scenario in steady-state ($N > 25$).

A low PDR indicates, that there is a low efficiency in the transmission, but it does not necessarily indicate low information freshness. Again, this is shown by the $IRT_{0.95}$, which indicates values between 0.4 s and 0.55 s for the approaches, significantly below the blackout probability of 1 s (cf. figure 75c). While more packets are delivered at a high rate for the non cooperative approach indicated by the higher probability of having an $IRT < 0.2$ s, the amount of interference leads to a significant probability that several consecutive packets are lost.

6.6 DISCUSSION AND COMPARISON WITH RELATED-WORK

In the following, we compare SWeRC with two state-of-the-art protocols, namely *LIMERIC* with *gain-saturation* and *PULSAR*. SWeRC will be compared as 2-hop piggy-backing using WGC. The modules for dynamic CAM generation, and channel load smoothing are disabled.

We analyze the performance as well for common perception and the dynamic highway, and urban scenario. Stability, fairness, efficiency as well as the key-parameters and performance metrics are used for the in-depth evaluation.

CONVERGENCE BEHAVIOR In the following, we review the convergence behavior for SWeRC for common perception and compare it with *LIMERIC* and *PULSAR*. We exemplarily illustrate the convergence to steady-state for $K = 1000$ nodes in figure 76. As expected, *LIMERIC* acts unstable and overreacts in each iteration leading to highly volatile CBR over-time (cf. figure 76c). *PULSAR* on the other hand converges to a stable steady-state rate, but the convergence time is comparably long due to the underlying AIMD mechanism (cf. figure 76b). SWeRC combines both fast and stable convergence due to the dynamic weighting of the rate adjustment (cf. figure 76a). Although, the volatility of the CBR is comparable to *PULSAR*, it achieves a much better stability.

In table 26, we list the time needed until the algorithm converges against its steady-state rate and also list the relative deviation for the different algorithms for various node densities for common perception. We highlighted the best performance in green and the worst in red. SWeRC clearly outperforms the other approaches independently

Table 26: Comparison of the convergence values for the evaluated protocols for common perception. The best/worst values are highlighted.

		K			
		180	300	500	1000
SWeRC ($\alpha = 0.3, \gamma = 0.4$)	speed	1.76	2.72	3.04	3.88
	rel. dev.	0.043	0.045	0.079	0.087
LIM-GS ($\alpha = 0.1, \beta = 1/150$)	speed	6.04	7.32	7.00	5.32
	rel. dev.	0.093	0.177	0.348	0.814
PULSAR ($\alpha = 0.1, \beta = 0.03$)	speed	9.88	8.40	8.16	10.68
	rel. dev.	0.103	0.119	0.133	0.186

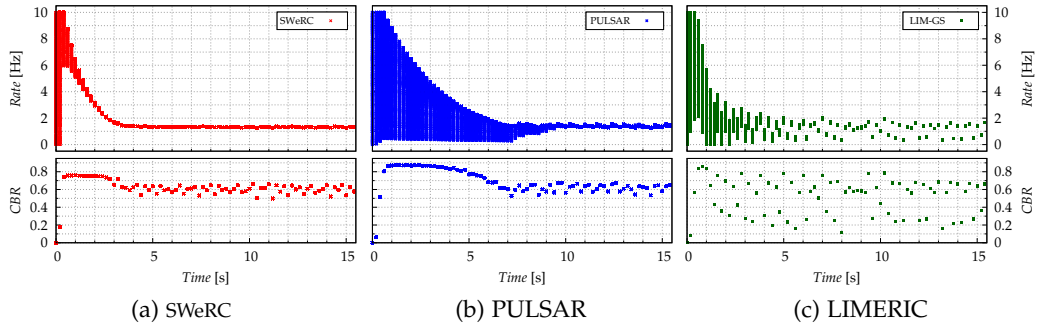


Figure 76: Comparison of the key-parameters of SWeRC with state-of-the-art CC protocols for the verification scenario over time ($K = 1000$).

of the vehicle density. As expected, PULSAR suffers from high convergence times, while LIMERIC suffers from scalability dependent volatility.

However, we use the optimized parameters for SWeRC and do not prove optimality for the parameters of the other approaches. Instead we use the default values as suggested by the respective authors themselves. Furthermore, the results are conducted for common perception and static nodes, such that the effect of shadowing, hidden-terminals and mobility are not considered. SWeRC proved that it achieves a scalable and fast convergence to a stable and fair steady-state rate, which significantly improves the performance of state-of-the-art protocols.

HIGHWAY On the Highway, LIMERIC is expected to achieve a good performance due to the absence of shadowing. In the critical zone beyond the traffic-jam, it is expected to grant highest rates, while the cooperative approaches have an extended fairness range here.

Key parameters

The average key-parameters for the different protocols are illustrated in figure 77 dependent on the x-position. Note, that the vehicles at the edge of the scenario

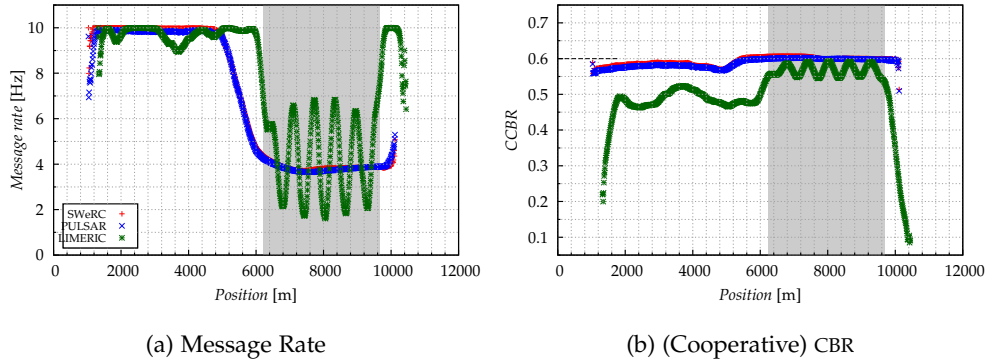


Figure 77: Comparison of the averaged performance of SWeRC with related protocols within the dynamic highway scenario in steady-state ($N > 25$).

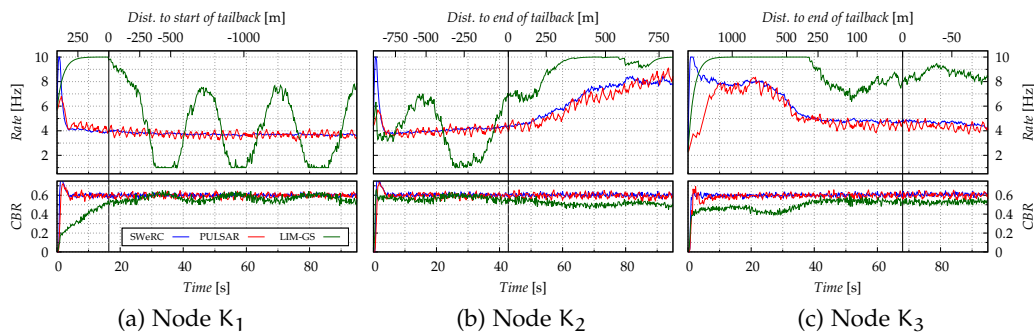


Figure 78: Comparison of the results for the key-parameters of SWeRC with state-of-the-art CC protocols for selected nodes over time within the highway scenario.

($x \approx 1200$ and $x \approx 10200$) are dynamically initialized during the simulation time and thus nodes close to this positions are not in steady-state.

While the average message-rate for PULSAR and SWeRC is almost equal due to the used cooperative exchange of remote information, the average performance of LIMERIC shows an unstable behavior (cf. figure 77a). Although, the rate is stable outside the traffic-jam region, because the utilization is below the predefined threshold and no reaction is necessary, within the jam both, the message-rate and the locally observed CBR are highly volatile (cf. figure 77b). We can assume, that the vehicle density within the traffic-jam is homogeneous and thus position dependent volatility of the load is not dependent on the local node density, but rather on the algorithm itself.

This assumption can be validated by evaluating the different protocols for exemplary nodes over time. We therefore select three exemplary nodes from the scenario. The positions and directions of the nodes are shown in figure 68a. While K_1 and K_2 are on the opposite lane driving into and out of the traffic-jam zone respectively, K_3 is approaching the congestion on the same road. The time and distance to the start (K_1) and end (K_2, K_3) of the traffic-jam is on the x-axis, while on the y-axis are the adjusted rate and the corresponding utilization, either locally (LIMERIC) or 2-hop (SWeRC, PULSAR).

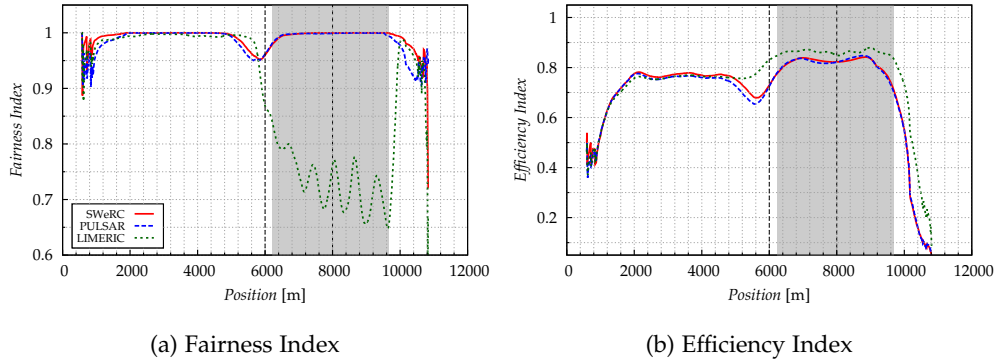


Figure 79: Comparison of the average fairness and efficiency index of SWeRC with related protocols within the dynamic highway scenario for a range of 500 m at $t = 50$.

K_1 is initialized in an uncontested area driving into the traffic-jam. The observed load is rapidly increasing for LIMERIC, while for the cooperative approaches, the reported maximum load already exceeds the predefined threshold (cf. figure 78a). Due to the initial rate of ≈ 5 Hz, PULSAR can achieve a fast convergence to a steady-state rate of ≈ 4 Hz. SWeRC converges equally, but the adjusted rate is less volatile. As depicted before, LIMERIC does not converge to a stable rate. As soon as the channel congestion is indicated, the rate is decreased to the minimum leading to a decrease in load and subsequent increase of the rate to ≈ 7.5 Hz.

A similar behavior can be observed for the vehicle K_2 leaving the congested area. Due to the local observation of CBR, LIMERIC however converges to the maximum rate as soon as the vehicle left the congested area (cf figure 78b). Due to the strict fairness requirements, the cooperative approaches need to provide a larger fairness area and convergence to the maximum rate is much slower. Surprisingly, both SWeRC with WGC and PULSAR have the same slope for the rate adjustment although the underlying approach is different (group/target rate vs. gravitation-pull). SWeRC however, outperforms PULSAR, if the difference between current and target steady-state rate is high in terms of convergence speed. This is observed for node K_3 in figure 78c. During the initialization, both nodes start with the same rate of ≈ 2.5 Hz and converge to a rate of 8 Hz within 4 s and 9 s respectively.

Stability, Efficiency, and Fairness

The fairness index and the efficiency index are shown in figure 79 based on the x -position. For this illustration, we evaluated a single iteration and averaged the results for multiple repetitions and nodes within intervals of 10 m.

The cooperative approaches can achieve and maintain fairness for nodes observing the same conditions, e.g. in the traffic-jam (cf. figure 79a). However, within the region, where the transition from low to high rate takes place (cf. figure 77a) ($4800 < x < 6200$), closely situated nodes will observe different rates and thus the fairness index drops to a minimum of 0.95 indicating minor unfairness. For LIMERIC, where no cooperation is used, fairness can not be guaranteed at all. While nodes outside the jam are not controlled by the algorithm due to insufficient resource utilization, within the jam, the volatile rate causes an unfair allocation of the rate to closely situated vehicles. LIMERICs lowest fairness index is 0.65, where 0.5 indicates the

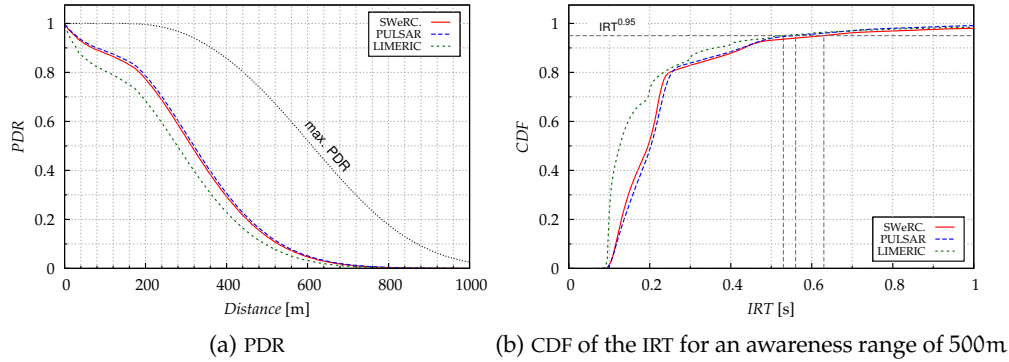


Figure 80: Comparison of the averaged performance of SWeRC with related protocols within the dynamic highway scenario in steady-state ($N > 25$).

minimum value achievable at all. Thus major unfairness is indicated for nodes controlled by this algorithm.

On the other hand, LIMERIC outperforms the cooperative protocols in terms of efficiency. The algorithm achieves an efficiency index of 0.9 due to the selected target resource utilization of $r_s = 0.6$. Obviously, the other protocols fall short in reaching this efficiency value, while LIMERIC nearly reaches it within the traffic-jam, although it encounters volatile CBR. SWeRC and PULSAR obviously have a decreased efficiency index in the critical zone, where the CBR is decreased due to reported maximum load and subsequent reduction of the rate (cf. figure 79b).

Performance indicators

Within the critical zone, the performance indicators are collected and aggregated. The PDR is significantly lower, than in an interference free environment. LIMERIC offers the worst PDR, while PULSAR and SWeRC offer almost the same PDR (cf. figure 80a). Due to the higher rate in the critical zone, LIMERIC can achieve a better IRT than the cooperative approaches. The probability for low IRTs is especially higher for LIMERIC. However, focusing on the $IRT_{0.95}$, the timings do not vary significantly. All protocols suffer from the occurring interference. However, within the awareness range of 500 m, the $IRT_{0.95}$ is below 0.5 s in any case.

URBAN In urban environments, SWeRC is expected to perform well compared to state-of-the-art protocols. It combines fast adaption to changing topologies with stable convergence. In terms of fairness, LIMERIC is expected to fail in providing a fair allocation of the resources.

Key parameters

The averaged key-parameters for the lane at $y = 900$ m are illustrated in figure 81 for the steady-state.

While the utilization used as input parameter for SWeRC and PULSAR are both at $r_c = 0.6$, fully utilizing the predefined threshold (cf. figure 81b), there is a surprising gap between the adjusted rates. SWeRC converges to a steady-state rate of 5 Hz, while the average rate of PULSAR is reported to be 4 Hz only. This can be explained by the

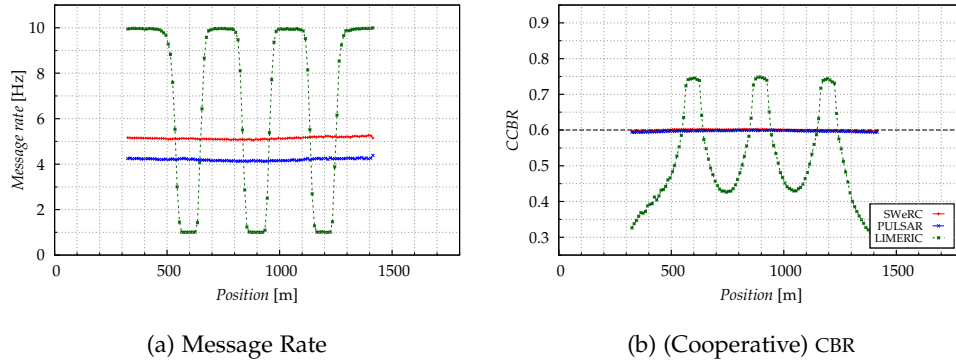


Figure 81: Comparison of the averaged performance of SWeRC with related protocols within the dynamic urban scenario in steady-state ($N > 25$).

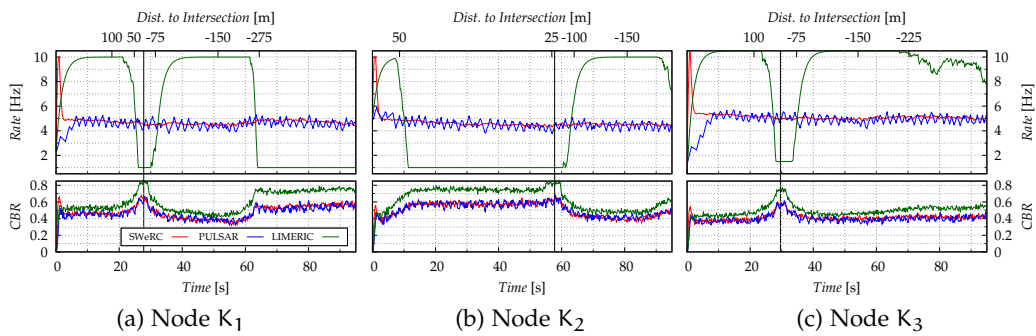


Figure 82: Comparison of the results for the key-parameters of SWeRC with state-of-the-art CC protocols for selected nodes over time within the highway scenario.

underlying adjustment protocol. AIMD has a slow convergence from lower to higher rates, e.g. the maximum step is 0.2 Hz with the gravitation pull used, while decrease for 5 Hz is approximately 0.3 Hz in one iteration. Thus, the algorithm achieves low rates more likely leading to a lower average utilization.

LIMERIC utilizes the local fairness principle and thus the rate and load is dependent on the position of the node. Nodes, which are at the intersection (e.g. $x = 900$ m), will observe higher load inducted by the nodes on the lane, which itself do not recognize the congestion (cf. figure 81b). Thus, at the intersection the utilization is exceeded and in consequence the nodes try to counteract by decreasing their node to the minimum (cf. figure 81a).

In figure 82, the time dependent key-parameters for this scenario for chosen nodes (cf. figure 72a) are illustrated. The mentioned effect of AIMD can be observed here, where the rate of all three nodes is oscillating between a rate of 4 Hz and 5 Hz, because of the threshold based adoption of the rate. SWeRC utilizes a linear function with implicit weighting which leads to a much smoother convergence of the rate and also the load.

While in the highway scenario, we have observed an unstable behavior of LIMERIC, in the urban scenario, LIMERIC achieves a stable convergence. However, the rates are dependent on the position of the nodes, such that a node, which is at the intersection has the minimum rate, whereas a node on the lane has the maximum

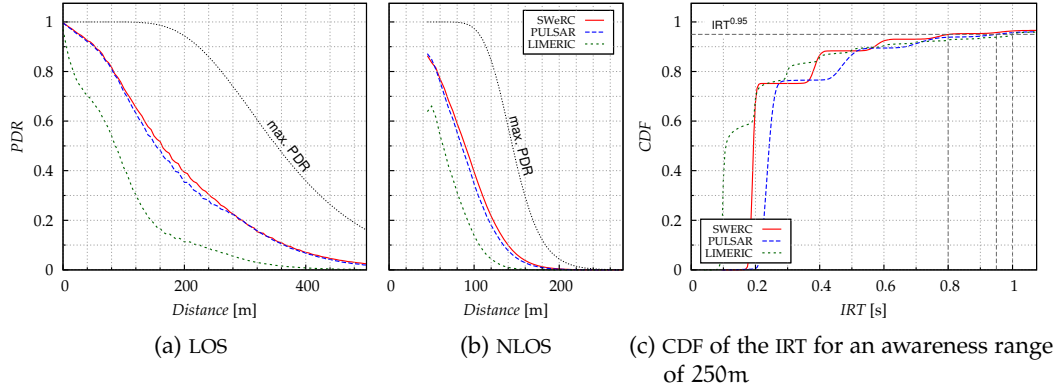


Figure 83: Overview of the performance of SWeRC compared with other algorithms within the dynamic urban scenario in steady-state ($N > 25$).

rate. Consequently, the algorithm is not active here, and just regulates the transitions from maximum to minimum rates. A major drawback of the local fairness principle is observed by node K_2 (cf. figure 82b). While it is approaching, waiting at, and leaving the intersection it has its rate reduced to the minimum rate all the time. Thus, if just some consecutive messages get lost, neighboring nodes are not aware of this vehicle.

Performance Indicators

Figure 83 shows the performance indicators for the related protocols within the urban scenario. The IRT is calculated based on an awareness range of 250 m, i.e. nodes which are in a communication range of up to 250 m are considered.

SWeRC and PULSAR achieve an almost equal performance in terms of PDR. Thus, while granting better convergence speed and stability, SWeRC performs well in terms of average PDR (cf. figure 83a). However, LIMERIC has a very limited communication range due to the high amount of interference occurring. A communication range of ≈ 85 m in LOS and ≈ 65 m in NLOS with a PDR of 0.5 is achieved (cf. figure 83b). Imagine a vehicle driving at 14 m/s, the range is sufficient for a TTC of 6 s in LOS, which is unacceptable for VSC.

The observed lower average rate of PULSAR has a major influence on the IRT. SWeRC outperforms both approaches here, especially for the $IRT_{0.95}$. Here, the following relation can be observed (cf. figure 83c): $IRT_{0.95}^{SWeRC} < IRT_{0.95}^{PULS} < IRT_{0.95}^{LIM}$

SUMMARY SWeRC utilizing 2-hop piggybacking and Weighted Global Cooperation (WGC) can easily outperform the current state-of-the art algorithms for Transmit Rate Control (TRC) in terms of convergence speed, stability and scalability. SWeRC is based on LIMERIC, with major enhancements, such that it achieves an environment independent fair and efficient allocation of the resources. PULSAR often reaches an equivalent performance in terms of fairness, efficiency, Packet Delivery Ratio (PDR) and Packet Inter-Reception Time (IRT), but fails to provide a scalable stability and fast convergence.

6.7 SUMMARY

In this section, we investigated the proposed Congestion Control (CC) algorithm called SWeRC. First we verified the major components of the protocol, including the rate adjustment-algorithm itself, the exchange of channel status information and the rescheduling mechanism. Furthermore, we validated the modules and granted insights into the properties of them.

Based on the theoretical investigation of the parameters, we conducted an in-depth numerical analysis to find suitable values for the convergence parameters of the algorithm. We show, that a good target utilization is $r_s = 0.6$, because it maximizes the goodput, while minimizing the blackout probability. We show, that there are density independent convergence parameters, which optimize the trade-off between the convergence time and relative deviation of the rate in steady-state respectively. Those values are $\alpha = 0.3$ and $\gamma = 0.4$.

Subsequently, we used this convergence values to evaluate the performance of the algorithm in dynamic environments. Even without cooperation, SWeRC can achieve very good adaption of the rate, because of the target-rate mechanisms used. Through it, group fairness within the neighborhood even under heterogeneous conditions (NLOS) is achieved. SWeRC can maintain the same minimum rates, than the algorithm utilizing cooperative information. However, the utilization exceeds the threshold under congested conditions, such that the PDR is decreased and interference occurs more frequently. Using Weighted Global Cooperation (WGC) for the cooperative target-rate mechanism has been shown to be the best option for a fair and stable rate adjustment in time and space.

Comparing SWeRC using 2-hop piggybacking and WGC to related Transmit Rate Control (TRC) protocols, revealed the outstanding convergence behavior, while the communication performance in terms of PDR and IRT is maintained.

In this section, we analyze the reliability of VSC achieved by the CA service. Therefore, we first review different metrics for quantifying the awareness in VSC in section 7.1 and subsequently compare the results of the different CC protocols regarding selected awareness indicators in section 7.1.1. We identify the awareness probability describing the probability that the information demand of a node within a time window is satisfied as most promising for the quantification of the reliability. For exemplary use-cases, we evaluate the awareness range and probability in section 7.2. Based on desired TTC values, we analyze the capabilities of the CC protocols to achieve awareness and quantify the reliability.

7.1 AWARENESS METRICS

The reliability for an application is strongly correlated to the amount and quality of information available at the ITS station. Especially cooperative information shared between the vehicles via CAMs is essential for an application, because through them enhanced (*cooperative*) awareness is achieved. In this context different metrics have been developed to quantify the awareness based on the IRT. The IRT specifies the time between the successful reception of two subsequent messages disseminated by one station [235, 227]. It is evaluated at the application layer and includes propagation and transmission delay as well as consecutive packet losses. For a pair of stations, it identifies the freshness of the information at the receiving station. Obviously it is also influenced by the CAM dissemination rate.

Packet losses and drops are summarized as communication reliability or performance and can be expressed by the PDR, i.e. the probability of receiving an individual message from a node. The *T-window-reliability* introduced by Bai et al. in [231] studies the relation between the PDR and application reliability. The application level metric is defined as the successful reception of at least one packet from neighbor vehicles within the time horizon T . In a constant environment in can be calculated as

$$P_{TW}(d) = 1 - (1 - p(d))^{r \cdot T} \quad (7.1)$$

where P_{TW} indicates the *T-window-reliability*, $p(d)$ is the distance dependent PDR, T is the time window size and r is the dissemination rate of the transmitting vehicle. The metric can be interpreted as the probability of having an IRT less than the time-window T .

Based on the IRT and T-window reliability, there have been a lot of works and extensions by other studies. Table 27 summarizes the awareness metrics developed and gives a short description. In [220] neighborhood awareness is introduced as "the probability of having received at least one beacon message within the past second" which is based on the *T-window-reliability* with $T = 1$. As depicted in figure 11, an application needs to be aware of a potential risk in advance. Sepulcre et al. [100]

Table 27: Awareness metrics based on IRT and T-Window reliability as listed in [106].

Metric	Description
T-Window reliability [231]	"[...] probability of successfully receiving at least one packet during tolerance time window T , at distance d ."
Neighborhood awareness [220]	"[...] probability of having received at least one beacon message within the past second."
Application reliability [100]	"[...] probability of receiving at least one CAM before D_w in a given time window T ."
Awareness probability [232]	"[...] probability of successfully receiving at least n packets in the tolerance time window T ."
Awareness range [232]	"[...] the maximum distance at which the awareness probability P_A is greater than or equal to a certain threshold."
Awareness [35]	"[...] relation between knowledge of vehicles that are stored in a vehicle's neighbor table and the knowledge of vehicles that should be stored.", where last CAM was received within a distant-dependent lifetime
Invisible neighbor [233]	"[...] a vehicle v_j is an invisible neighbor of v_i if $v_j \in \text{Neighbor}_i^t$ and v_i has not received any broadcast packet from v_j for a certain time interval T ."
Blackout probability [234]	"[...] probability that the IRT time exceeds 1 [...]"
Update delay [230]	"[...] elapsed time, while expected CAMs from vehicle j are not received by vehicle i ."
System age [203]	Average IRT of a vehicle's neighbors, averaged over all vehicles

Table 28: Blackout probability for different protocols

	Highway	Urban
SWeRC w. WGC	0.0021	0.0368
SWeRC wo. coop	0.0012	0.0387
PULSAR	0.0032	0.0438
LIMERIC	0.0013	0.0536
10 Hz	0.0053	0.0406

takes this into account by calculating the *T-window-reliability* at a critical distance. Applications have different requirements regarding the amount of information required in order to work reliable. A more generalized specification of the T-Window metric is introduced by An et al. in [232]. The awareness probability is specified as the probability to receive at least n packets within the time-window T .

$$P_A(d) = \sum_n^{r \cdot T} \binom{r \cdot T}{n} p(d)^n (1 - p(d))^{r \cdot T - n} \quad (7.2)$$

The authors also introduced the awareness range specified as the maximum distance for which the awareness probability exceeds a predefined threshold ($P_A = 0.99$) or in other words, the maximum range in which the application works reliable considering the amount of information needed within the time window T .

Schmidt et al. introduced *awareness* in [35] as the ratio of known vehicles by all vehicles within communication range. To consider the fact, that close vehicles are more critical than far vehicles, a vehicle is known as long as the *distance-dependent-lifetime* of a CAM is not exceeded, i.e. the IRT is below a distant-dependent threshold. Some works focused on the inverse of the two metrics, i.e. no packet was received within the time window T [233] or the IRT exceeds a predefined threshold [234, 230]. An aggregation of the average perceived IRT for a cluster of vehicle is used in [203] for the *system age*, granting a top level overview of the average IRT within a VANET.

7.1.1 Awareness evaluation

In this section, we briefly quantify the awareness within the two scenarios based on general indicators.

BLACKOUT PROBABILITY The blackout probability of the different protocols is summarized in table 28. The probability of not receiving a CAM within one second on the highway is comparable small, while for the urban environment there is a significant probability of 3% – 5%. This is significant due to the amount of CAMs being exchanged and the requirements of VSC regarding the reliability of the CA service. LIMERIC has the highest blackout probability and SWeRC has the lowest in urban environments, which shows the benefits of the protocol.

Table 29: System age [s]

	Highway	Urban
SWeRC w. WGC	0.2599	0.3258
SWeRC wo. coop	0.2069	0.2718
PULSAR	0.2665	0.3801
LIMERIC	0.2071	0.2959
10 Hz	0.2449	0.2741

SYSTEM AGE According to [203], the system age is defined as

$$\Delta = \frac{1}{N} \sum_{u \in K} \sum_{v \neq u} \Delta_{uv}, \quad (7.3)$$

where K indicates the number of neighbors, $N = K(K - 1)$ the number of samples and Δ_{uv} is the average age of vehicle u 's information at vehicle v , i.e. the information freshness. The system age is taken within a period of T .

In our results, we already aggregated the average information freshness based on the probability of occurrence within the simulation time. Thus, we calculate the system age as follow:

$$\Delta = \sum_{IRT \leq T} IRT \cdot p(IRT),$$

where $p(IRT)$ is the probability that a node has an information freshness of IRT .

Table 29 summarizes the system age for different protocols and the two dynamic scenarios used within the RoI and a maximal IRT of $T = 10$ s. As illustrated in the previous chapters, the uncooperative protocols (LIMERIC, SWeRC wo. coop) achieve a higher average information freshness, because they utilize a higher rate. Obviously, periodic dissemination does not lead to a better system age under congested conditions due to interference. In general, the system age is an indicator for the information freshness, but does not reflect worst case situations. According to the results, the maximal system age within the interval T is $\Delta = 0.3801$ s for PULSAR in the urban scenario. According to table 28, PULSAR however has a blackout probability of 4.38% in the same scenario. LIMERIC on the other hand has a far better system age, but the blackout probability is higher. Thus a simple average is not a sufficient indicator for the reliability of an ADAS.

AWARENESS PROBABILITY The awareness probability P_A as calculated in (7.2) is illustrated in figure 84. The PDR is the ideal, interference free PDR observed within the highway scenario dependent on the distance. The P_A is evaluated for each distance bin ($s_B = 5$ m) for a fixed rate of 10 Hz for different time windows T and an information demand of n packets that need to be received within T .

From the equation (7.2), we can see, that in terms of P_A there is no difference between increasing the time window or the rate by the same factor, because it will just increase the number of packets that could have been received. Thus a bigger

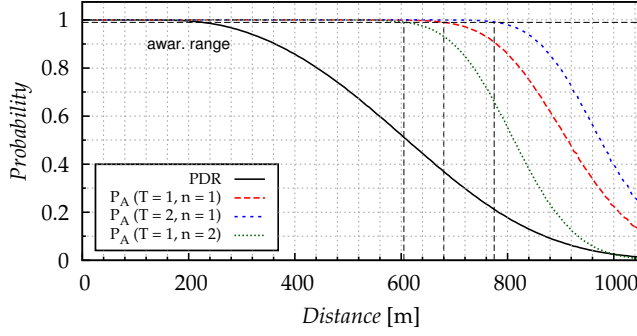


Figure 84: Illustration of the awareness probability metric for different time-windows T and information demand n based on the ideal PDR for the highway scenario

time window or higher rate will increase the awareness probability, while a higher information demand (n) will decrease P_A (cf. figure 84).

Considering, that each received CAM can be used, a node will be aware of the position and heading of a neighboring node, if at least one CAM has been successfully received within the time interval T . Thus, instead of calculating the probability, that a node receives n CAMs, we can calculate the probability of not receiving any CAM within the time interval and take the complementary value, which results in the T-Window reliability:

$$P_A(d) = 1 - P(n = 0) = 1 - (1 - p(d))^{rT}, \quad (7.4)$$

where r is the message rate, T is the time window and $p(d)$ is the distance dependent PDR.

In figure 85, we illustrated the awareness probability based on the average distance dependent PDR values for SWeRC using WGC within the highway and urban scenario (cf. figure 71a and figure 75). Within this scenarios and the corresponding RoI, SWeRC has an average message rate of 5 Hz and the time window is chosen to be $T = 1$ s. Obviously, the P_A is decreasing much faster, if non-ideal values are used and thus it can be assumed that awareness especially in urban environments with buildings or for vehicles with high velocities at the highway can not be guaranteed.

Using single distance bins is however misleading, because a speed of 5 m/s is assumed for a vehicle. Fast vehicles would pass different bins within the time window, such that the actual conditions in terms of PDR and rate can change significantly. In the next section, we will provide a speed dependent analysis for different use-cases for both scenarios.

AWARENESS RANGE The awareness range as introduced in [232] can be used to determine the maximal range in which a vehicle is safely aware of its neighbors. Therefore, it is assumed, that a $P_A > 0.99$ is a sufficient indicator for a reliable awareness. In figure 85, we illustrated the awareness ranges d_A for the different conditions based on this assumption. For NLOS, the awareness range is $d_A = 80$ m, while for LOS in the urban scenario, it is $d_A = 135$ m and $d_A = 275$ m at the highway. Those values show, that the achievable awareness created by VSC can be significantly degraded by congestion which needs to be considered for the design of ADASs.

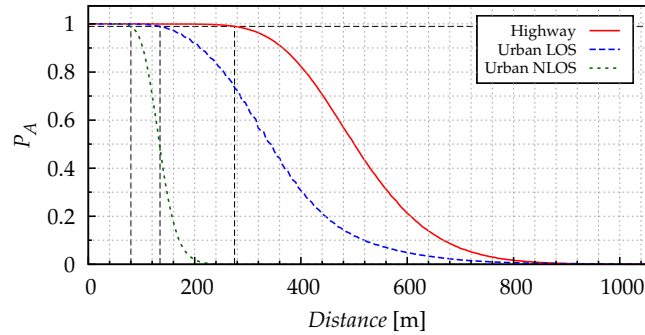


Figure 85: Ideal awareness probability of SWeRC for the different scenarios ($T = 1, n = 1$).

The awareness range furthermore indicates the range in which nodes are aware of each other only. In case an emergency is detected, e.g. an Intersection Collision Warning (ICW) application triggers, further DENMs need to be exchanged which is time consuming and in consequence, the real minimal range in which a reliable service is provided is further decreased.

7.2 EVALUATION FOR DIFFERENT APPLICATIONS AND SCENARIOS

We analyze the reliability of the CA service within this section based on the use-case of FCW and ICW. Prior to the analyzes, we specify the calculation of the reliability and the dependency to the traffic-safety.

7.2.1 Calculation of the Awareness Probability

The aim of the following metric is to determine the probability, that a vehicle is aware of another vehicle. Therefore, we assume that a stored information about a vehicle expires after a certain amount of time and a vehicle is in need of only one valid CAM to ensure awareness for an expiration period. In terms of awareness probability, this would indicate a time-window of $T = 4$ s and information demand of $n = 1$.

The awareness probability for $n = 1$ (7.4) needs to be extended in order to reflect the distant dependent PDR and rate. In the previous section, the rate was assumed to be constant and the P_A was calculated for each distance bin utilizing the corresponding PDR at this bin. However, for large time windows T , the PDR can have a significant difference.

There are different methods of calculating the according awareness probability:

Upper Bound: Assuming, the PDR and rate are monotonically decreasing or constant, an upper bound is calculated by taking the values of the current distance bin as shown in the previous section.

Simple Average: The P_A can be calculated using the simple average of the PDR and rate within the time window T , where the average is calculated by:

$$\overline{\text{PDR}}(d, T) = \frac{1}{v_0 T} \int_d^{d+v_0 T} \text{PDR}(d) = \frac{1}{\|\frac{v_0 T}{s_B}\|} \sum_{i=0}^{\|\frac{v_0 T}{s_B}\| - 1} \text{PDR}(d + i \cdot s_B), \quad (7.5)$$

where $\|\frac{v_0 T}{s_B}\| \geq 1$ is the number of distance bins with size s_B for the vehicles speed v_0 within the time window T . The corresponding rate is averaged accordingly

$$\overline{R}(d, T) = \frac{1}{\|\frac{v_0 T}{s_B}\|} \sum_{i=0}^{\|\frac{v_0 T}{s_B}\| - 1} R(d + i \cdot s_B), \quad (7.6)$$

Averaging of the values usually does not lead to appropriate results. Considering a change of the PDR from 0 to 1 within one distance bin, while the rate is maintained. Obviously, the P_A should be 1 for a sufficient rate R , because a packet can safely be transmitted in the second distance bin. Averaging would lead to a PDR of 0.5 and thus a significantly lower P_A . However, for a sufficient small time window T , the change within the distance bin for this thesis is more fluid.

Stochastic independence: Assuming, that the PDR within two disjunct distance bins is independent, we can calculate the probability of not receiving any message within a distance bin separately and take the complement of the product of it as the awareness probability:

$$P_A(d) = 1 - \prod_{i=0}^{\|\frac{v_0 T}{s_B}\| - 1} (1 - \text{PDR}(d + i \cdot s_B))^{R(d + i \cdot s_B) \cdot \frac{1}{\|\frac{v_0 T}{s_B}\|}} \quad (7.7)$$

Assuming a constant PDR and rate, the equation can be simplified and is equal to the T-Window reliability (7.1). The probability of not receiving a packet is calculated for each distance bin with individual PDR and the number of CAMs disseminated within this bin. The rate therefore needs to be divided by the number of bins passed in one second.

The later calculation is used in order to quantify the distance dependent reliability of the CA service.

TIME-TO-COLLISION The distance between two vehicles which are on an collision course can also be expressed as a time depending on the vehicles speeds as

TIME-TO-COLLISION (TTC): The TTC quantifies the time, until the event, if the current speed is maintained, i.e. $TTC = \frac{d_{AB}}{|v_A - v_B|}$, where d_{AB} specifies the distance between A and B and v_A, v_B specify the speed of A and B respectively. In case of ICW, the distance to the intersection is calculated, where $v_B = 0$.

TIME-TO-AVOIDANCE (TTA): Unlike the TTC, the Time to Avoidance (TTA) describes the time until an event is unavoidable. For a collision event, the actual stopping distance needs to be considered. Having a non-moving obstacle, the TTA can be simplified to $TTA = \frac{d_O}{v_0} - (v_0/a + t_r)$, where d_O is the distance to

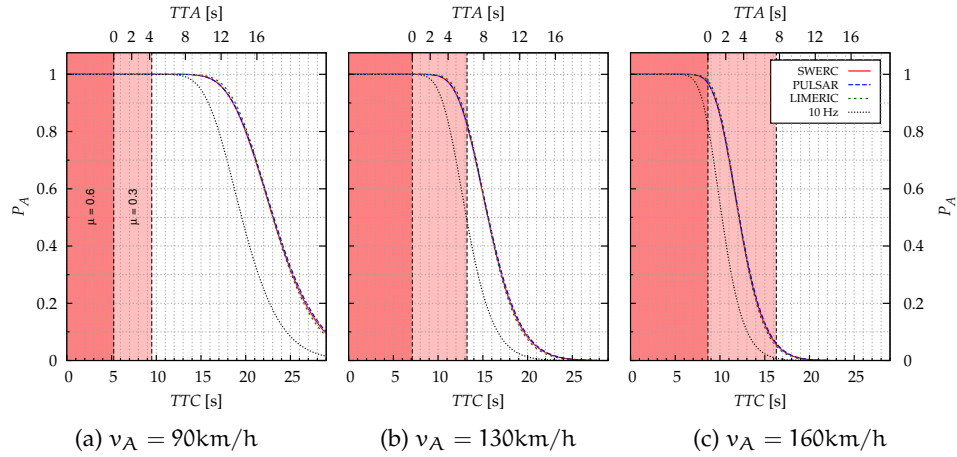


Figure 86: Comparison of the awareness probability within the highway scenario considering a FCW use-case for different protocols and vehicle speeds.

the obstacle, v_0 is the initial speed of the vehicle, a is the deceleration and t_r specifies the reaction time of the driver.

We consequently calculate the TTC and TTA for the use-cases specified. Studies have shown, that the reaction time follows a gamma distribution [236, 237]. Out of this distribution, we use a value of $t_r = 1$ s. The deceleration a of a vehicle depends on its braking coefficient μ , where $a = 9.81\mu$. This coefficient depends on the quality of the braking system, the level of braking and the road conditions. Considering a dry, maintained road and a normal vehicle type, this coefficient can be assume to be $\mu = 0.6$ for an emergency brake and $\mu = 0.3$ for a strong, but not full brake.

7.2.2 Reliability of VSC

According to [238, 239], a driver desires an information regarding a critical event at a $TTC > 20$ s, where the optimal TTC is found to be 26 s. A warning is required to be given for a $TTC > 8$ s with an optimal value of 12 s. In the following, part of the investigation is, whether the strict timings can be achieved by the CA service. Awareness is the precondition in order to give an information or a warning to the driver. Notifications based on DENM require awareness of the situation as well.

FORWARD COLLISION WARNING (FCW) For the use-case of a FCW, we consider the highway scenario, where there is a traffic-jam. At the end of the jam, a vehicle B has stopped disseminating CAMs at the adjusted rate. We assume, there is a vehicle A, which is approaching the traffic-jam.

For this scenario, we use the distance dependent average PDR observed from the different protocols within the RoI (cf. figure 80a). The vehicle B, located at the end of the traffic-jam at $x = 6225$ m has a fixed rate, which is adjusted accordingly by the CC protocol (cf. figure 77a). The awareness probability of vehicle B at A thus is dependent on the dissemination rate of B.

We show the results in figure 87 for three different velocities. In the figures, we highlight the stopping distance for an emergency brake and hard brake, and

Table 30: Awareness Range and corresponding timings for SWeRC using WGC for different velocities within the highway scenario and FCW use-case.

		velocity [km/h]		
		90	130	160
awar. range [m]		390	370	355
TTC [s]		15.6	10.28	7.89
TTA [s]	emerg.	10.35	3.16	-0.76
	hard	6.11	-2.96	-8.40
$P_A(TTC_{opt})$		1.00	0.94	0.52

indicate the TTA based on this emergency brake. Obviously, compared to periodic dissemination of CAMs, the awareness probability and range is higher using any CC approach. Thus, we can conclude that a higher rate does not always bring benefits in terms of awareness. Furthermore, within the highway scenario, the PDR of the CC approaches are approximately the same (cf. figure 80a), which explains the equal performance in terms of awareness. The lower PDR of LIMERIC is counteracted by a much higher rate.

In table 30, we give the awareness quantification for the different velocities for the FCW use-case using SWeRC with WGC. Based on the awareness range, i.e. the range where $P_A = 0.99$, we calculate the TTC and TTA. While for comparably slow velocities ($v = 90$ km/h), the awareness range is sufficient to allow second stage warnings before the optimal TTC ($TTC_{opt} = 12$ s), this is not the case for higher speeds anymore. Especially for $v = 160$ km/h, the TTC of 7.89 s is outside of the desired warning time.

Although often used for evaluation, the TTC is not always a good quantification of the time needed for taking an action. Assuming a high velocity and low braking capabilities, the TTC might indicate there is still time to react, although the TTA is already negative, which in consequence means that even through an immediate reaction the collision is unavoidable. For the FCW use-case evaluated here, this is the case for $v = 160$ km/h, where the TTA is -8.40 considering the awareness range. Thus, at the time the vehicle is aware of the upcoming collision, it can not evade it anymore.

It is obvious, that the desired awareness range and thus TTC for the first stage information regarding the critical event can not be provided by the basic CA service (cf. figure 86). However, for slow velocities, the application works reliable for the desired optimal TTC of second stage warning (cf. table 30). For fast vehicles the reliability is drastically decreased, i.e. $P_A = 0.94$ for a speed of $v = 130$ km/h and for even higher speeds of $v = 160$ km/h, awareness range is insufficient to ensure collision mitigation.

INTERSECTION COLLISION WARNING (ICW) While for LOS conditions as evaluated in the previous paragraph, sensors can be used to improve awareness, there are no sensors available for NLOS conditions. Furthermore in the previous use-case the

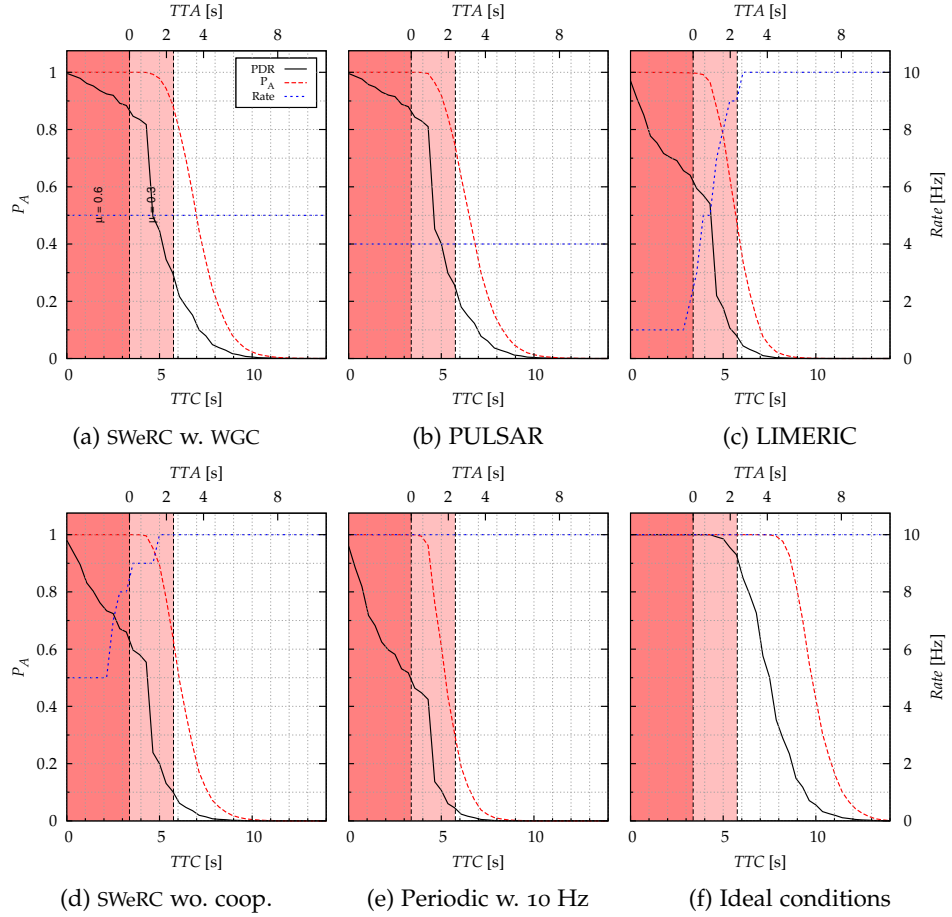


Figure 87: Comparison of the awareness probability within the urban scenario considering an ICW use-case for different protocols ($v_A = v_B = 50$ km/h).

vehicle can transmit multi-hop DENMs informing far-away vehicles of the traffic-jam. In the use-case of ICW, the vehicles first need to be aware of a critical situation, which is the fact if they are aware of each other. Thus, awareness is a critical factor for ICW. Deployed RSUs forwarding CAMs in the middle of the intersection or cluster based forwarding as explained in section 2.4.2 can help, but this is not part of the investigation. In this experiment, two vehicles A and B are approaching a common intersection with individual speeds v_A and v_B . The initial distance to the intersection is chosen such that a collision will occur on the intersection.

For the evaluation, we use the averaged PDR values calculated for the RoI (cf. figure 83). The PDR is used based on the distance between the two vehicles and separated into a LOS and NLOS part by

$$d_{\text{NLOS}} = d_B \left(1 + \frac{v_A}{v_B} \right) \sqrt{1 + \left(\frac{v_B}{v_A} \right)^2}, \quad (7.8)$$

where d_B indicates the offset of the building from the intersection in either x or y direction and v_A and v_B are the velocities of the involved vehicles A and B respectively. The distance d_{NLOS} indicates the breakpoint at which the two vehicles are in LOS with each other, i.e. if $d_{AB} < d_{\text{NLOS}}$ the PDR observed under

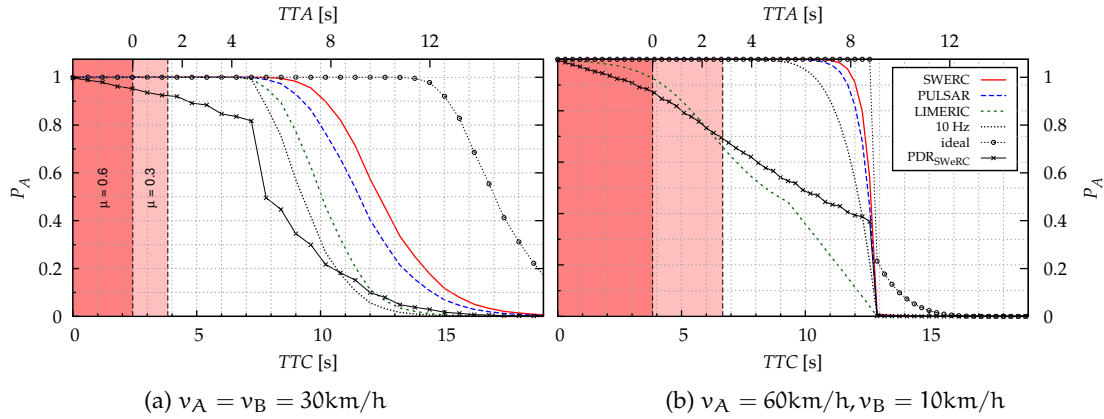


Figure 88: Comparison of the awareness probability within the urban scenario considering an ICW use-case for different protocols and speeds.

LOS conditions is used, while before the NLOS PDR is used. Furthermore, we will investigate the reliability of the use-case at vehicle A, which will receive the CAMs of vehicle B. We use the average distance dependent rate for vehicle B, where we identify the distance as the distance between the vehicle and the intersection. Finally, a mapping function for translating the PDR between A and B at a distance d_{AB} to the distance between A and the intersection d_{AI} is used:

$$PDR_{AI}(d_{AI}) = PDR(d_{AI} \cdot \sqrt{1 + \left(\frac{v_B}{v_A}\right)^2}) \quad (7.9)$$

The results for the different protocols are shown in figure 87. The figure illustrates the TTC dependent rate and PDR of each protocol and the resulting awareness probability. Both vehicles are driving at a speed of 50 km/h resulting in the highlighted stopping distances and TTA. According to (7.8), the breakpoint for NLOS is at a distance of $d_{AB} \approx 85$ m, corresponding to a distance to the intersection of $d_{AI} = 60$ m. Thus the breakpoint is located at a TTC of ≈ 4.3 s (cf. figure 87), leading to a significant drop of the PDR with an increase in the distance due to NLOS conditions.

Obviously none of the protocols is able to provide a suitable level of awareness for the desired TTC (cf. figure 87). Although, SWeRC provides the highest awareness range, which is at least able to provide the necessary awareness for an emergency braking, the reliability at the desired TTC of 12 s is approximately 0. While under LOS conditions, the PDR is suitable high to provide awareness, unless the rate is too low (cf. LIMERIC), fading due to NLOS conditions breaks the communication between two vehicles. Even under ideal conditions, where there is no interference and the rate is $R_{max} = 10$ Hz, the desired awareness range can not be achieved (cf. figure 87f). We further need to note, that in this scenario, the offset between the middle of the street and the buildings is large ($d_B = 30$ m), such that for smaller offsets, the awareness range can be significantly lower.

However, vehicles do not always drive at 50 km/h, but might be faster or slower. We evaluate two more use-cases, in which either both vehicles are slow (cf. figure 88a), or one vehicle is approaching the intersection slowly, while the other is slightly

exceeding the speed limit (cf. figure 88b). In figure 88, we illustrate the awareness probability of the different protocols for the two use-cases.

When the vehicles are slower, the awareness range can be smaller leading to higher reliable TTC values. Still, the periodic dissemination of messages under congested conditions has a negative effect on the awareness probability. However, there are differences in the performance of the individual protocols, that need to be highlighted (cf. figure 88a). The proposed SWeRC achieves the highest awareness range, although it can still not satisfy the desired TTC. Unlike the previous example, under ideal conditions, it is possible to reach this TTC. However, channel congestion leads to interference, packet losses and decreased performance such that a degradation of the awareness range is logically. While PULSAR suffers from the lower steady-state rate, LIMERICs awareness probability is affected by both, the low rate and the low PDR. However, vehicles driving at this speed are aware of an upcoming collision, and mitigation system can react by initiating soft braking, if the driver of the vehicle is not able to react within this time.

Figure 88b illustrates the probability of vehicle A to be aware of the vehicle B, which is slowly approaching the intersection. Under ideal conditions, a TTC of ≈ 14.5 s can be achieved, satisfying the requirements of the drivers. The NLOS breakpoint for this use-cases is located at $d_{\text{NLOS}} = 212.9$ m, at this point $d_{\text{AI}} = 210$ m. The maximal communication range under NLOS conditions is < 300 m with a very low PDR (cf. figure 94). Unless ideal conditions, it can be assumed, that awareness at this distance can not be maintained under NLOS (cf. figure 88b). For this use-case SWeRC still achieves the highest awareness range, followed by PULSAR and the periodic messaging. LIMERIC does not achieve a sufficient awareness, because the rate of the vehicle B is reduced to the minimum close to the intersection on the one hand and the PDR is low on the other. We need to note, that the used PDR is the average PDR within the region and does not reflect the real conditions for vehicle A and B. However, it can be assumed, that a vehicle on the intersection is affected by bad channel conditions and transmissions might be dropped.

7.3 SUMMARY

In this section, we have investigated the capabilities of the different protocols to achieve and maintain awareness. Therefore, we first analyzed the general indicators for the performance, like the blackout probability and the awareness probability. We used this awareness probability to specify a range in which nodes are aware of each other, by calculating the probability of not receiving any CAM, before the stored information expires.

We identified two use-cases, namely FCW and ICW, which are of major interest in terms of traffic safety and analyzed the capability of the different CC algorithms to achieving awareness considering this use-cases.

A driver wants to be warned within a specific interval before a critical event occurs. This interval is measured in terms of TTC, and the optimal value is shown to be $\text{TTC}_{\text{opt}} = 12$ s. Following this assumptions, it can be shown, that a FCW can achieve a reliable awareness for speeds up to 90 km/h, but fails for higher speeds. Furthermore, it is shown, that for very high speeds ($v > 160$ km/h), the awareness

range is insufficient to prevent the collision, although an immediate emergency brake is conducted.

The performance of ICW is evaluated for urban conditions with shadowing due to buildings. It is shown, that for vehicles with a speed of $v = 50$ km/h, even under ideal conditions, the communication range is too small to provide awareness among the affected vehicles. However, if the vehicles are slower, or one of them is slowly and thus they are in LOS for a longer time before the critical event, a sufficient, but not optimal, $TTC > 8$ s can be achieved in terms of awareness for SWeRC, which achieves the overall highest awareness ranges here.

It is shown, that periodic dissemination at high rates will lead to a decreased awareness range and thus degradation of application performance compared to the usage of the analyzed CC protocols. Furthermore, we show, that cooperative approaches outperform LIMERIC, which suffers from locally unfair conditions especially at urban intersections.

CONCLUSION AND OUTLOOK

Next generation ADAS have the potential to significantly improve traffic safety by employing communication based cooperation. In this thesis, we address the scalability issues occurring when more and more vehicles are connected among each other. To enhance the awareness of the environment, vehicles disseminate their current status periodically. Without regulation, the dissemination of these CAM named packets will lead to channel congestion under high densities and loss of awareness in consequence. Without awareness, reliability of future ADAS will become significantly degraded.

In this thesis, we address the scalability problem by developing a load adaptive, density independent rate control algorithm. Therefore, we investigate the available degrees of freedom for the decentralized regulation of the periodic messages and find rate control, i.e. the amount of CAMs generated per second, as most promising. Subsequently, we focus on the problems of state-of-the-art algorithms, which are insufficient in terms of information freshness, unfairness, volatility, as well as stability. We enhance the well-known state-of-the-art CC algorithm LIMERIC in order to address these issues. By applying cooperation among the nodes to overcome locally unfair conditions, we achieve an environment-independent fair allocation of the available resources. Scalability-independence is achieved by applying a dynamic, fast reacting weighting of the rate control based on a group rate. With further optimization of the SWeRC called algorithm, we maximize the efficiency and combine a fast reaction with a stable steady-state convergence.

We use a verified simulation environment to verify, validate, and evaluate the proposed CC algorithm. We investigate the individual components of SWeRC separately to illustrate and validate the functionality. Moreover, we conduct a numerical evaluation to find suitable values for the convergence parameters, optimizing the efficiency, stability, and convergence speed. The protocol performs well under NLOS conditions, where fairness is a major issue. Compared to LIMERIC, it can achieve better allocations for affected nodes even without cooperation. Finally, we test the protocol under realistic traffic conditions using a traffic simulator for the vehicles movement and measurement-based, validated path-loss models for both urban and highway propagation. Even under these challenging conditions with high density and volatile topologies, the algorithm provides a fast and very stable convergence, where other algorithms fail to provide stability at all.

While stability, fairness, efficiency, and convergence speed are issues for CC algorithms, a well performing scheme still needs to optimize the awareness granted. We show that regulating the dissemination using CC can significantly improve the awareness among the vehicles. In certain conditions, the proposed protocol can achieve nearly ideal awareness ranges (where others fail to provide awareness at all) and in general, it achieves the best overall awareness for the investigated use-cases. However, the evaluation also shows that VSC cannot provide the necessary awareness range to inform the driver about a critical event, when she or he desires it. On the

other hand, the range will be sufficient to warn the driver within sufficient timings, if she or he drives within certain speed limits.

In conclusion, we develop an adaptive protocol that is scalability-independent and achieves the comparably best reliability in terms of awareness. It guarantees an environment-independent fair resource allocation among the nodes maximizing the minimal throughput. A major advantage of the protocol is its trade-off optimization to achieve a fast convergence and a very stable steady-state rate.

During our investigation, we found the following points interesting for future research:

- Due to the strict specifications of the IEEE 802.11p protocol, CAMs are transmitted at the highest possible EDCA access category. For high vehicle densities, the minimal size of the CW leads to massive interferences for the mid-range communication degrading the communication performance on the one hand, and causing miscalculation of the rate adjustment on the other hand. We suggest to address this issue by applying a **dynamic Contention Window (CW) control** based on the communication performance. An idea is to adjust the CW based on the deviation between the decentralized observed Packet Inter-Reception Time (IRT) and the reported rate.
- Feedback based reactive CC protocols rely on accurate observations of the input parameter. As stated in the previous suggestion, these inputs can be erroneous resulting in non-optimal, volatile rates. Although we propose a volatility suppression method for the input parameters, recurring events like a certain interference ratio will cause offsets between the theoretical and real system output. However, the number of nodes within the carrier sense range and the Channel Busy Ratio (CBR) are two indicators that quantify the load. Applying appropriate methods to estimate the vehicle density, we suggest to **combine density with CBR observations** in order to cross-validate the feedback and mitigate errors.
- Although vehicles need to be treated fairly in terms of resource sharing, it can be beneficial to prioritize the dissemination of CAMs by vehicles which state a higher risk, or need to maintain a higher awareness probability. This priority setting can be achieved by giving a higher rate to these vehicles. In comparable works, the authors accomplish this by applying different convergence parameters to the vehicles. However, SWeRC reacts to a cooperative group rate and thus different convergence parameters would affect the stability rather than the priority. Under common perceptions, we conduct tests in which we **assigned different CBR thresholds** r_s to the nodes and they converge to a stable steady-state rate proportional to the threshold r_s . However, the relation needs to be analyzed and the convergence needs to be proven under dynamic conditions. Furthermore, it has to be demonstrated whether dynamic adjustment during the runtime also leads to convergence.

- Using numerical evaluation, we obtained good values for the convergence of the algorithm. Future work should **investigate the optimality based on an analytical approach.**

SIMULATION ENVIRONMENT AND CONFIGURATION

For the numerical evaluation, we use the discrete event-driven network simulation tool *OMNeT++* in the version 4.5. Simulations in *OMNeT++* are based on modules, where each node and layer within the node is represented by a module which itself can consist out of submodules or implements the behavior defined by program code. Interactions between the modules is based on messages exchanged via interfaces. In this way, single modules can be easily replaced by others in order to evaluate different module behaviors. However, *OMNeT++* offers the simulation environment, but does not come along with predefined modules. Thus frameworks have been developed which offers a wide set of modules usable for network simulation. For this work, we use an early version of the *iNetManet*¹ framework. Bases on this framework a couple of modules were developed for VSC including a basic ITS-G5 protocol stack with a fully functional IEEE 802.11p access layer within our project group.²

While *OMNeT++* offers good accuracy for network simulation, its capabilities for traffic simulation are limit. For simple scenarios, where nodes are not moving, or just moving linear, modules can be developed, but real traffic simulation is a complex task. The Traffic Control Interface (TraCI) is part of the framework and allows a TCP based control and exchange of information between the network simulation tool and any client. In this thesis, we coupled *OMNeT++* with the open-source traffic simulation tool *SUMO* in the version 0.19 via the TraCI. Figure 89 illustrates this hybrid simulation set-up. In this configuration, *SUMO* works as a module within *OMNeT++* responsible for the mobility of the nodes. If necessary, *OMNeT++* can also influence this mobility by sending control messages used to control the traffic simulation, simulation environment or individual nodes, e.g. position or speed of a node. This hybrid simulation set-up is used for the dynamic scenarios, while the static scenarios utilize *OMNeT++* only.

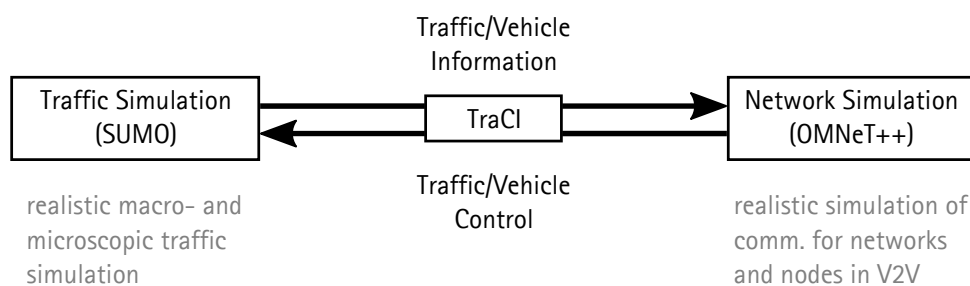


Figure 89: Interconnection of traffic and network simulation tools *OMNeT++* and *SUMO*

¹ <https://github.com/aarizaq/inetmanet-3.x>, Accessed: 06/07/2017

² Parts of this chapter are published in [173] and are under copyright of the IEEE

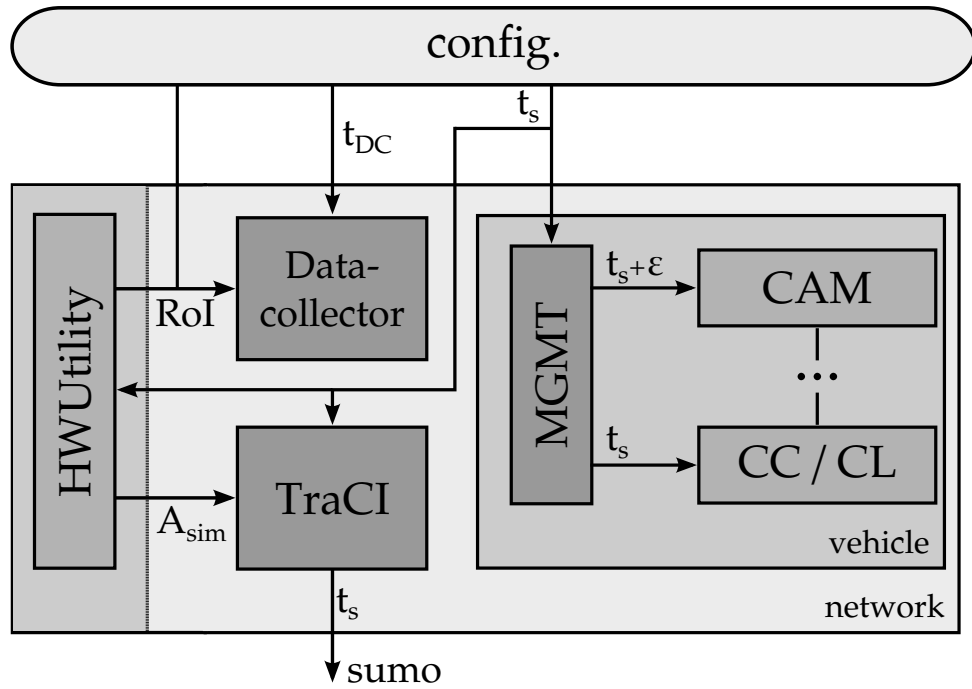


Figure 90: Specification of initialization times and regions for certain modules

A.1 SIMULATION ENVIRONMENT

Simulation results may differ a lot using the same parametrization for a proposed method due to non-carefully selected parameters for the simulation environment itself. However, an all-round simulation can not be designed, but paying attention to some constraints conduce higher quality results. One of these fields is the initialization of the simulation environment and the modules included. We present an extract of our simulation stack in Figure 90. Here we focus on two important aspects: the initialization time and the area of interest for certain modules.

The start time t_s indicates the start of the network simulation. This time is especially important for the warm-up phase of the traffic simulation in order to have a steady-state traffic behavior. Usually traffic flows are randomized which is used for vehicles arriving during the simulation anyway, but it is not valid for steady-state initialization. The executive and the control part are controlled by two disjunct loops, which needs to be initialized correctly. Thus the CAM generation process for a vehicle starts at $t = t_s + \epsilon$, where $\epsilon = \text{unif}(0, 1/R_{\min})$. This holds for vehicles arriving during the simulation ($t > t_s$) as well, i.e. these nodes are initialized immediately considering the random offset ϵ .

On the contrary, the control loop shall be synchronized among the vehicles. To guarantee this, it is started immediately at $t = t_s$. At this point, there is no load generated and control within the first $1/R_{\min}$ s should not be considered for the results. Nodes which arrive during the simulation need to be started such that they're synchronized with the others. However, we set the update interval for TraCI to the CMDI, such that a node is started immediately whenever it arrives. The respective time of the data collection start should be set to a time where the warm-up phase for the network stack is over so that $t_{DC} \geq t_s + t_w$, where t_w specifies the warm-

up time necessary to reach a stable steady-state behavior. Basically, more time for initialization allows for more accurate results at the cost of computing time.

As indicated before, the second essential parameter is the region of the simulation. While simulating huge areas costs a lot of computing time, the offered result quality is most likely higher than simulating small areas not paying attention to boundary effects. Thereby the RoI can be quite small compared to the whole scenario. To notice at least a minor effect of the *hidden-terminal-problem*, the dimension of the network simulation area A_{sim} should be at least twice as big as the (effective) communication range. However, it might be smaller for the urban environment due to NLOS communication. The scenario itself can have a larger dimension to allow for further area based warm-up procedure, e.g. to concede speed-up and lane changes before entering the simulation area contributing to steady-state traffic behavior.

We furthermore dynamically set those regions in case of traffic-jams for the motorway scenario, since the most important area is right beyond the tailback where vehicles are swiftly approaching the tailback. If there would be no adjustment, results would deliver a mix of in traffic-jam and semi-free-flow communication.

In conclusion, the data collector, starting at t_{DC} is used to collect and aggregate relevant simulation events within the configure RoI. The aggregated output of the data collector are the metrics introduced in section 6.1. Therefore the parameters described above are of major interest to ensure high quality results.

A.1.1 Simulation Parameters

This parameters used for the simulations within this thesis are summarized in table 31. The simulation environment was parametrized such that it follows the standards and settings used in state-of-the-art studies. This holds especially for the parameters for the access layer, which is based on the IEEE 802.11p architecture, but also holds for the congestion control protocols evaluated. Most values have been either described or investigated in order to obtain an optimized parameter set. Further information for those parameters can be found in the tables specified. Each node draws a random message rate $r_j(0)$ and the resource utilization $r_c(0)$ is set to zero at the start of the simulation. The target resource utilization is set to $r_g = r_s = 0.6$ for *LIMERIC*, *PULSAR* and *SWeRC*. For both *LIMERIC* and *PULSAR*, we use the predefined parameters which were found to achieve a suitable performance by the authors respectively [13, 14].

A.1.2 Propagation Model

Propagation models are used in order to provide a realistic approximation of the attenuation, shadowing and fading occurring to signals. For the simulation study of this thesis, three scenario based propagation models are used. We use the measurement based NLOS and LOS propagation model from [224] for urban environments, and the measurement based propagation model from [229] for the highway and rural environments.

URBAN In urban environments, we differentiate between LOS and NLOS conditions between two communicating nodes. Both models are based on a measurement cam-

Table 31: Simulation parameters

	Parameter	Value	Table		
Access	PHY	Carrier freq. / BW	5.9 Ghz / 10 Mhz	6	
		Data rate (R_b) / SNIR _{Thr}	6 Mbps / 8 dBm		
		Noise / Sensitivity (S)	-100 / -92 dBm		
		Carrier sense threshold	-95 dBm		
		TX-Power (P)	23 dBm		
		CMDI (T_m)	200 ms		
	MAC		TXTIME	504 μ s [11]	5
			aSlotTime	13 μ s	7
			aSIFSTime	32 μ s	7
			AC / AIFSN	AC_VO / 2	8
		CW _{min}	3	8	
CAM		packet size (L)	302 Byte		
		Awareness Control (R_{max})	as in [10]		
		Message rate (def.)	10 Hz		
		R_{min} / R_{max}	1 Hz / 10 Hz		
Congestion Control		$r_c(0)$	0		
		$r_j(0)$	unif(0, R_{max})		
	SWeRC		α	0.3	
			γ	0.4	
			r_s	0.6	
	PULSAR		α_I	0.1 Hz	
			α_t	0.1	
			β_D	0.03	
			a_c	2	
			U_t	0.6	
	LIMERIC		α_L	0.1	
			β_L	1/150	
			r_g	0.6	
	Repetitions	5 – 25			
	Simulation Time	100 s (N = 500)			

paign and where retrieved by using ray-tracing techniques. For LOS communication conditions, a simple log-distance path loss model is used

$$PL_{LOS}(d) = PL_0 + 10n \log_{10}\left(\frac{d}{d_0}\right) + X_g(0, \sigma), \quad (A.1)$$

where PL_0 is the path loss at the reference distance d_0 , n is the path loss exponent and d is the distance between receiver and transmitter. $X_g(0, \sigma)$ is a gaussian variable which is used to model shadow fading. For this thesis, values of $PL_0 = 50$ dBm, $n = 2.55$, $d_0 = 1$ m and $\sigma = 3.9$ are used according to [224]. Figure 91 illustrates the corresponding path loss depending on the distance between the communicating nodes. Since the sensitivity of a node is $S = -92$ dBm and the transmit power is $P_{TX} = 23$ dBm, a signal with a path loss of up to 115 dBm can be decoded at the receiver. Thus, the reliable communication range (99% PDR) can be calculated to be 156 m, whereas the maximum communication range is approx. 804 m.

The propagation model for NLOS is based on a look-up table which offers the path loss for the distance of sender and receiver to a common intersection. A surface

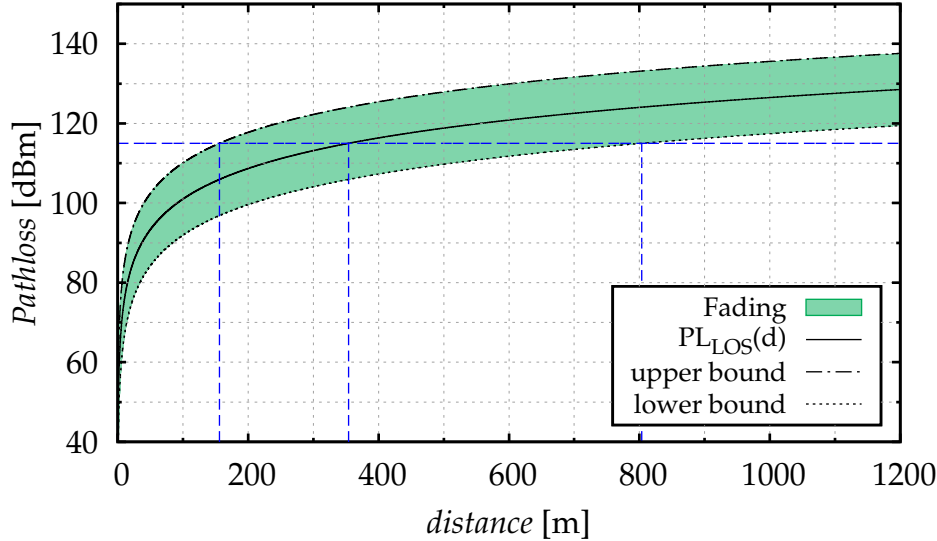


Figure 91: Illustration of the LOS path loss for different distances and calculation of the reliable and maximum communication range based on the 99% confidence level of shadow fading.

fitting tool is used to search for an error minimizing fitting of the data to an equation, which is

$$PL_{NLOS}(x, y) = \frac{a + bx + cy + dxy}{1 + ex + fy + gxy} + X_g(0, \sigma), \quad (\text{A.2})$$

where x and y are the distances of the nodes to the common intersection respectively, a - g are the coefficients and X_g is the shadow fading component. Figure 92a illustrates the deterministic component of the NLOS propagation model based on the distances of the nodes to the intersection. In order to illustrate the reliable communication range, we also fitted this model to a distance based 2D model (cf. figure 92b). Based on the measurement data, the values mentioned above, and the 99% confidence level, the reliable communication range for NLOS communication is 106 m, whereas the maximum communication range is 287 m.

$$PL(x, y) = \begin{cases} PL_{NLOS}(x, y), & \text{if } NLOS, \\ PL_{LOS}(d), & \text{if } LOS, d = \text{distance}(x, y), \end{cases} \quad (\text{A.3})$$

Considering the propagation models, we can calculate the PDR for different distances between the vehicles, i.e. the probability that the receiving power $P_r = P_{TX} - PL(x, y)$ exceeds the sensitivity S ($P[P_r > S]$). Figure 94 illustrates this PDR for both models used for urban environments. Note that the probability is calculated for ideal probabilities, i.e. no interference.

HIGHWAY For highway scenarios, the propagation model proposed by Schuhmacher in [229] is used. Like the urban model, it is based on accurate measurements

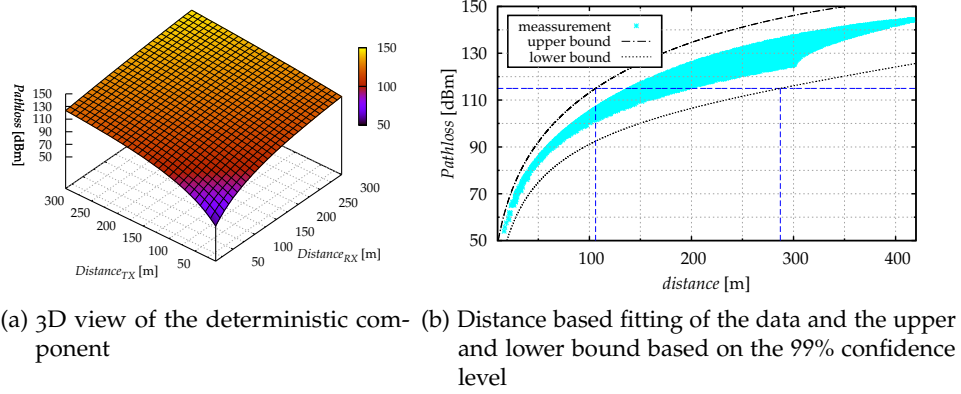


Figure 92: NLOS path loss model used for simulating shadowing caused by obstacles in urban environments.

conducted on a much-used highway. Thus the model implicitly considers the effect of multi-path propagation due to reflection at vehicles.

The propagation model consists of a dual-slope path-loss model with nakagami-fading. While the former is used to model slow fading, while the latter models the fast fading through a suitable distribution. The dual-slope path-loss model is described by the following equation

$$PL(d) = PL(d_0) + \begin{cases} \alpha_1 10 \log_{10} \left(\frac{d}{d_0} \right), & d \leq d_{bp}, \\ \alpha_1 10 \log_{10} \left(\frac{d_{bp}}{d_0} \right) + \alpha_2 10 \log_{10} \left(\frac{d}{d_{bp}} \right), & d > d_{bp}, \end{cases}$$

where $PL(d_0) = 47.86$ dBm is the path-loss at the distance $d_0 = 1$ m, $d_{bp} = 177$ m is the breakpoint distance and $\alpha_1 = 2.1$, $\alpha_2 = 3.4$ are the environment dependent path-loss coefficients. The values are the same as used by the author himself in [229]. Note that this equation gives the path-loss in dBm and conversion to mW might be necessary.

Based on this deterministic distance based path-loss a nakagami fading model is proposed, which is used to model the reflections and propagation details of highway environments. Nakagami-fading usually uses the gamma distribution with a shade parameter m and a scale parameter Ω_p/m resulting in the density function

$$p(P_r) = \begin{cases} \frac{m}{\Omega_p \Gamma(m)} \left(\frac{m P_r}{\Omega_p} \right)^{m-1} e^{-m P_r / \Omega_p} & P_r \geq 0, \\ 0 & P_r < 0, \end{cases} \quad (A.4)$$

where $\Gamma(\cdot)$ is the gamma function, Ω_p is the average path-loss in mW retrieved by the dual-slope path-loss model and m is the fading parameter adjusting the fading intensity. The distribution calculated the probability that a signal has a received power of P_r for a certain fixed distance. Figure 93 illustrates the received power dependent on the distance between two communicating nodes based on a transmitting power of $P_{TX} = 23$ dBm. The effect of fading based on the distance dependent fading parameter m and the average path loss due to the dual-slope path-loss model is

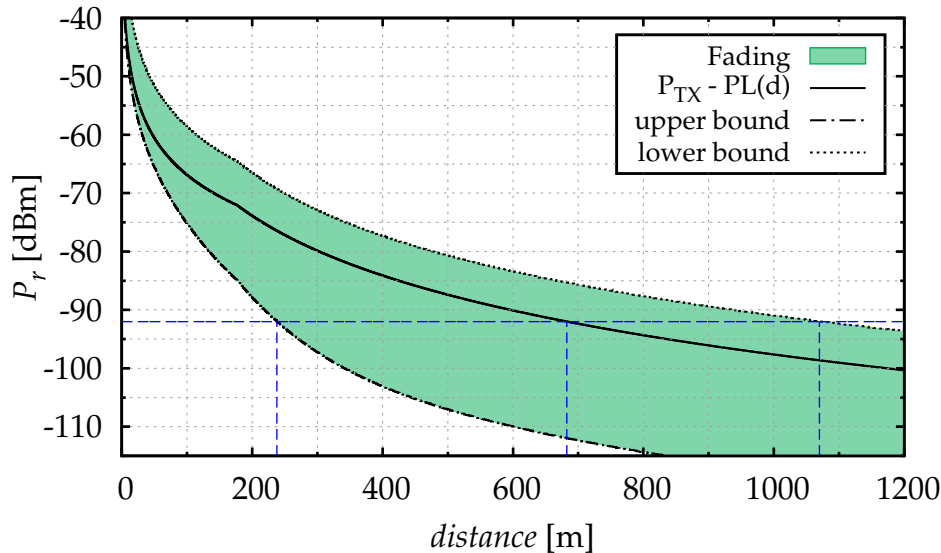


Figure 93: Illustration of the received Power P_r for different distances and calculation of the reliable and maximum communication range based on the 99% confidence level of nakagami fading.

highlighted for the 99% confidence level leading to an upper and lower bound of the signal strength.

The reliable communication distance, where 99% of the signals are above the sensitivity is 238 m and the maximum communication range, where less than 1% exceed the sensitivity is 1080 m. Figure 94 shows the probability that the received power is above sensitivity for the propagation models used within this simulation depending on the distance between the communicating nodes. The communication range in urban areas can be significantly reduced due to shadowing by buildings and also the communication range is slightly lower than for highway environments, where negative interference is reduced.

A.2 DETAILED SCENARIO DESCRIPTION

A scenario is used to evaluate the impact of specific environments and use-cases on the performance of the protocol. Vehicles are usually used in different environments, such that used communication protocols need to work in various scenarios. In order to evaluate SWeRC, various scenarios are used to analyze different aspects of the protocol. In general, two classes of scenarios are used here: static and dynamic. The static scenarios (cf. A.2.1 and A.2.2) are used to verify and illustrate the functionality of the different protocol features. Whereas the dynamic scenarios (cf. A.2.3 and A.2.4) demonstrate the performance of the protocol under realistic conditions. Besides the layout, the major difference is that in static scenarios, vehicle movement is permitted, such that each vehicle has a fixed position.

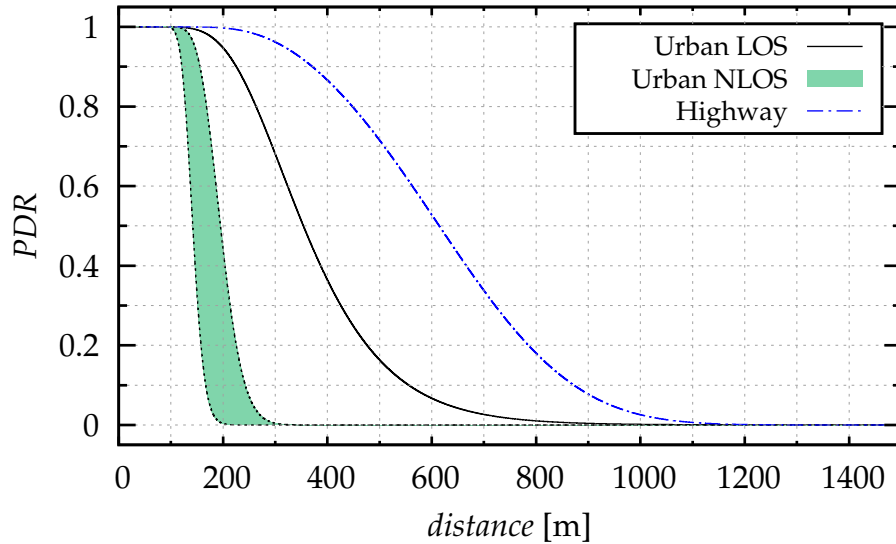


Figure 94: Probability of receiving a signal for the propagation models based on the distance between the communicating nodes.

A.2.1 Verification (LOS)

This is a simple scenario which is used to demonstrate the basic functionality of the protocol under common perception of all nodes. Therefore all static nodes (K) are distributed within a close area with a dimension of $100\text{ m} \times 100\text{ m}$. Since maximum distance between two nodes is $< 142\text{ m}$, which is below the reliable communication distance (cf. A.1.2), all nodes perceive the same channel status information.

A.2.2 Intersection (NLOS)

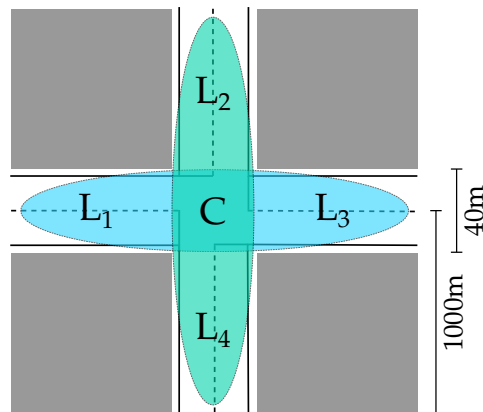


Figure 95: Illustration of the static NLOS intersection scenario used for evaluation of SWeRC's cooperative aspects.

In order to evaluate the performance of the cooperative aspect of the protocol under controlled conditions, an intersection which is surrounded by buildings is used. It has a total dimension of $2000\text{ m} \times 2000\text{ m}$ and the distance between the

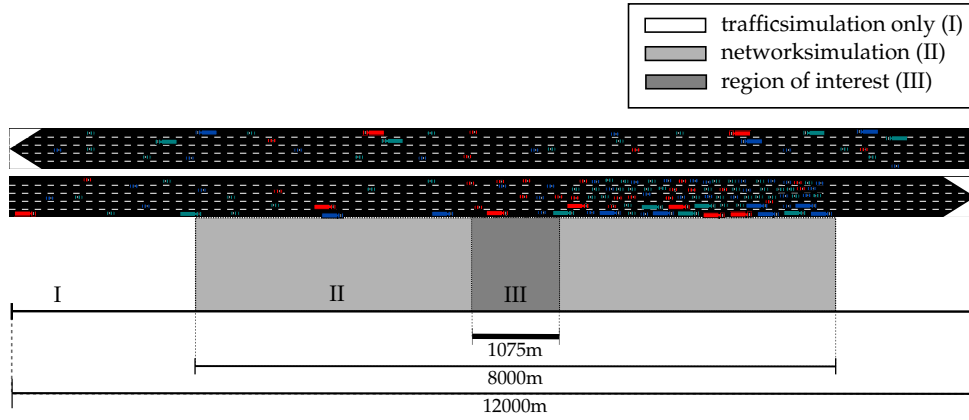


Figure 96: Illustration of the dynamic highway scenario

buildings is 40 m (cf. figure 95). The scenario consists of different zones (L_i and C) in which the amount of vehicles can be parametrized. Due to the shadowing of the buildings, common perception is not given, instead LOS conditions and thus communication is possible for the following zones:

$$\begin{aligned}
 C &\rightarrow \{L_1, L_2, L_3, L_4\}, \\
 L_1 &\rightarrow \{C, L_3\}, L_2 \rightarrow \{C, L_4\}, \\
 L_3 &\rightarrow \{C, L_1\}, L_4 \rightarrow \{C, L_2\}.
 \end{aligned}$$

This implies that ability of communication between zones affected by the buildings, i.e. $L_1 \rightarrow L_2$, is significantly reduced due to shadowing caused by the NLOS conditions.

The vehicles are represented by static nodes which are aligned randomly with a dedicated amount for each zone at the start. The total amount of vehicles (K) is specified as the sum of vehicles on the lanes L_i ($K = \sum_{n=1}^4 K(L_i)$). The vehicles at the intersection are parametrized by an additional fixed percentage (default 5%) of the total nodes (K). For example if $K(L_i) = 25$, there will be $K = 100$ nodes at the lanes plus $K_C = 5$ nodes at the intersection.

A.2.3 Highway

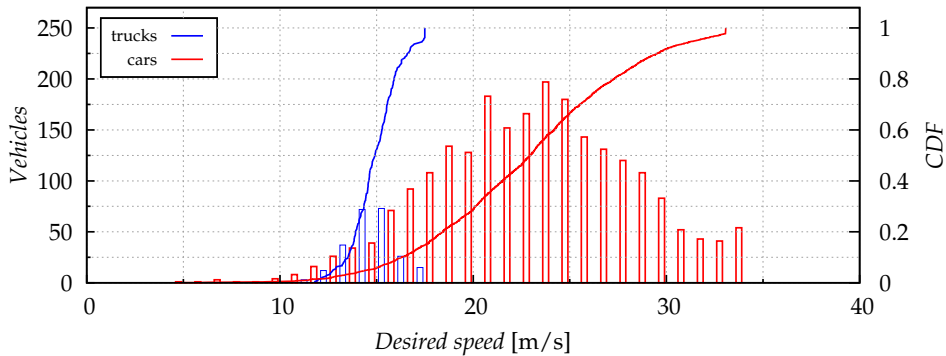


Figure 97: Distribution of vehicle speeds for free flow highway (including freight trucks)

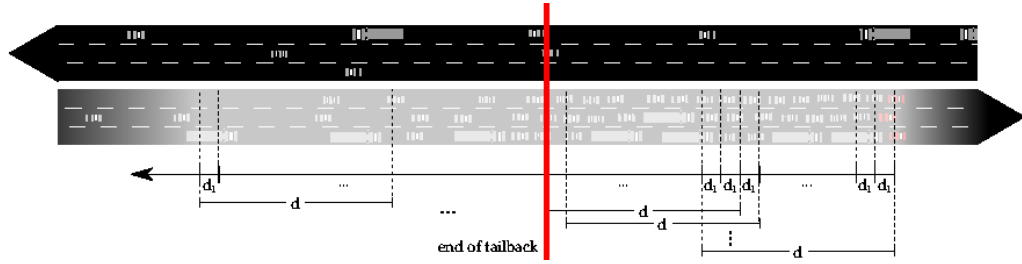


Figure 98: End of tailback prediction method

Figure 96 shows the motorway scenario used for the evaluation. It has five lanes for each direction and a total length of 12 km. There are sub-regions within the scenario indicating the RoI (III) for data collection, network simulation area (II), and an area which is only simulated within the traffic simulation tool (I) to allow sufficient warm-up. The RoI starts at the end of the tailback. Since this scenario is used to simulate a traffic-jam, we needed to dynamically adjust those important regions. The mechanism and importance for this is described later on.

The desired velocities of the vehicles are specified to follow a normal distribution for both freight trucks (quota 10%, length 15 m) and cars (length 5 m) with an average speed of $\mu = 15$ m/s and $\mu = 23$ m/s respectively (cf. figure 97). Vehicles stuck in a congestion do not fully stop, but rather have a speed of ~ 3 m/s. The number of vehicles in the different regions might vary a lot over time leading to the distribution shown in figure 68. The average gap between vehicles is velocity dependent with a minimum of 2.5 m in case the vehicle has stopped.

In order to set the regions for the motorway scenario with congestion, the end of the tailback needs to be obtained, as the RoI is the area right beyond the tailback. Since all traffic related control is done by SUMO, we use the retrieved information in OMNeT++ to calculate the position of the tailbacks end, because SUMO does not offer this functionality. An illustration of the algorithm achieving this is presented in Figure 98.

The algorithm combines the calculation of vehicle density and average speed using a moving average in order to receive accurate volatility suppressed prediction. The actual measured position for the end of the tailback E_t is indicated by

$$E_t = \beta x_k + (1 - \beta) x_v$$

where x_k indicates the measured end of the tailback based on the vehicle density and x_v for the vehicles average speed. Therefore the vehicle density k is calculated for every distance d_l in the area with length d starting at the front of the queue. The average velocity for all vehicles in this area is calculated accordingly.

The position x_k marks the position furthest away from the queue start where the vehicle-density falls below the adjusted jam-density $k \leq a k_j$ with $k_j = N_l \cdot d / (g + l)$, where a is the adjustment factor, N_l is the number of lanes, g is the average gap size and l is the average length of a vehicle. The position x_v is calculated analogously if it exceeds the jam-velocity v_j .

The volatility suppressed calculated end of the tailback \tilde{E}_t at time t is then expressed by

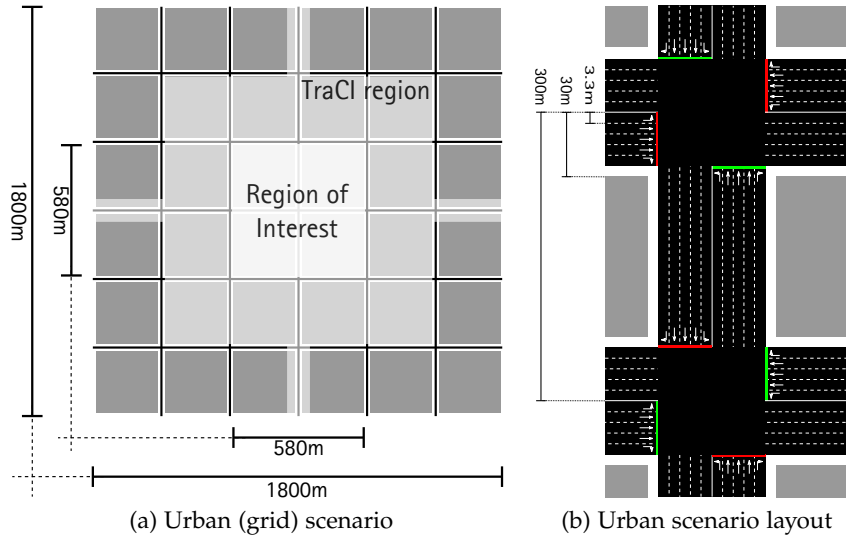


Figure 99: Illustration of the generic urban scenario

$$\tilde{E}_t = \alpha E_t + (1 - \alpha) \tilde{E}_{t-1}$$

where α indicates the weighting factor for the measured and last calculated value.

This method offers an accurate prediction of the end of a traffic-jam and avoids high variation allowing a suitable dynamic adjustment of the regions used for simulation.

We schedule the start of the simulation at $t_s = 2500$ s. At this time the length of the traffic jam is ≈ 3000 m and the end of the traffic-jam is close to the middle of the scenario. The data collection time is scheduled at $t_{DC} = 2505$ s.

A.2.4 Urban

The urban scenario shown in Figure 99 is a grid with a dimension of 1.8×1.8 km² and 25 traffic-light-controlled intersections with buildings representing urban environments. The RoI in this scenario is one single intersection including incoming and outgoing lanes with a dimension of 580×580 m to cope with boundary effects. While traffic simulation takes place in the whole scenario, we define another region (*TraCI region*), where network simulation is conducted. This region excludes the outer streets and intersections, with an exception for the streets and intersection within LOS to the RoI.

A script based on the SUMO tools is used in order to create the network-, polygon-, and routing-files for the traffic simulation for each simulation run. This allows a randomization of the vehicle flows used for traffic simulation. These flows arrive and depart at the boundaries of the scenario using turning probabilities (left 0.1 / right 0.2 / straight 0.7) for the route choice. The network file is edited a priori, since the SUMO tool does not offer a fully symmetric result.

We adjust the turning rules for the lanes and the traffic light settings to achieve the layout presented in Figure 99b. The figure also presents the dimensions of the roads, the road-building-distance, and the length of the road between two intersections.

Furthermore, the arrows and lane alignments are illustrated. We use 5 lanes for each direction in order to simulate worst-case scenarios, e.g. rush hours in mega-cities like *New York*. One phase of a traffic light is 35 s, where all vehicles of one road have green light, followed by 10 s for left turns and afterwards the other road has the same phases. Each traffic-light has a random offset, such that there is no phased traffic-lights.

Vehicles try to drive at the maximum speed which follows a Gaussian distribution with the mean at $v = 14$ m/s. The vehicle density within the traffic simulation is chosen such that at the start of the simulation there are between 6000 – 7000 vehicles within the scenario. The number of vehicles within the TraCI zone however is fixed to 2000 vehicles.

We schedule the start of the simulation at $t_s = 300$ s. At this time a sufficient amount of vehicles have entered the scenario and the RoI. The data collection time is scheduled at $t_{DC} = 305$ s.

CHANNEL BUSY RATIO MEASUREMENT SETUP

Motivated by the understanding of the accuracy of channel load, we perform a profound measurement campaign in a controlled laboratory environment. Moreover, to ensure the applicability of measurement results for prospective congestion control algorithms in **vanet!s** (**vanet!s**), the utilized hardware components including the wireless module and antenna were IEEE 802.11p or ITS-G5 compliant. This allows a V2V communication on a 10 MHz channel centered at 5.9 GHz. Detailed information about the characteristics of the wireless radio module can be found in [240].¹

B.1 EXPERIMENT SETUP

The experimental setup as illustrated in Figure 100 includes a wireless radio module, a spectrum analyzer and a PC. Both the radio and spectrum analyzer are located at close distance of about 30 cm to each other and remain stationary during the whole measurement. While the wireless radio is configured as transmitter source, the spectrum analyzer collects wide-band measurements and dumps the result data on the connected PC.

The transmitter is assumed to broadcast periodic CAMs with a constant generation rate and a net message size of 500 Bytes. Including UDP, IP, Logical Link Control (LLC) and MAC header (8/20/8/28 bytes), this results in a MAC frame size of 564 bytes. During the experiments, CAMs are sent with a transmission power of 23.2 dBm (EIRP) and a data rate of 6 Mbps. On the receiving side, the real-time spectrum analyzer Tektronix RTSA can perform power measurements both in the frequency and time domain. It is able to capture the samples into streams of in-phase (I) and quadrature (Q) baseband signals at a very high sampling rate. To obtain a time domain signal, we integrate the measured power in the I and Q baseband signals within a specified time interval. For each time domain sample point, the received signal power S is calculated as follows:

$$S[\text{dBm}] = 10 \times \log_{10} \left[\frac{I^2 + Q^2}{1 \text{ mW}} \right] \quad (\text{B.1})$$

To configure and automatically trigger measurement experiments, we implement a MATLAB script running at the PC. The bandwidth (20 Mhz) used for the spectrum analyzer for the verification is high enough to allow for a particular precise measurement at the cost of computing power. For the accuracy analysis which is presented in section, a lower bandwidth (1 Mhz) is used to handle the amount of data while keeping the precision at a suitable level. We show in section B.3 that this is a feasible approach. After each measurement run, the time domain gathered I/Q data is post-processed and visualized using a second script according to Equation B.1. By looking at the characteristics of the received signal waveform in the time domain,

¹ Parts of this chapter are published in [93] and are under copyright of the IEEE

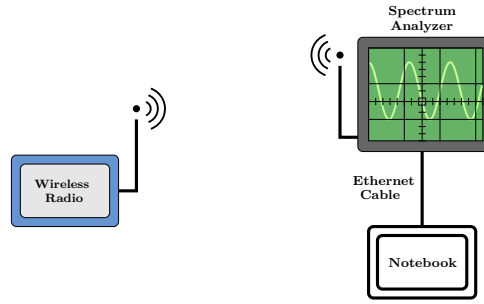


Figure 100: Illustration of the controlled lab composed of a wireless module, a spectrum analyzer and a PC for the control and configuration of experiments.

all-important properties of the signal such as signal width, duty cycle, peak, and average power, can be measured with high accuracy. In this way, we particularly analyze the duty cycle of the captured waveform to estimate the corresponding channel load.

B.2 THEORETICAL ANALYSIS OF CHANNEL LOAD

Prior to the verification of the measurement set-up, we provide a theoretical analysis of the channel load under interference-free conditions. Using timing parameters of the physical and MAC layers of the IEEE 802.11p protocol, it is then possible to derive signal characteristics such as busy and idle periods of a transmitted packet. It should be noted that the 802.11p is essentially deduced from 802.11a, but operates in a 10 MHz bandwidth instead of the usual 20 MHz. This change in channel implies a doubling of all relevant timing parameters associated with the physical layer convergence procedure PLCP.

To reduce the degree of complexity and therefore being able to concentrate on the accuracy of the measured CL, we consider a simple scenario composed of a single node in my analysis. Figure 101 schematically illustrates the signal power observed at the spectrum analyzer in the time domain as an example. In this figure one observes two different signal periods B and I that represent busy or idle duration, respectively. Considering the overhead introduced by the PLCP preamble, the busy period B is deduced as the time the medium is sensed as busy during a packet transmission. This duration corresponds to the effective transmission time T_{XTIME} proposed by the standard [11] and derived as

$$T_{XTIME} = T_{pre} + T_{signal} + \left\lceil \frac{16 + 8 \times L + 6}{R} \right\rceil + \frac{T_{sym}}{2} \quad (B.2)$$

where L denotes the packet size, T_{pre} is the preamble duration, T_{signal} marks the signal symbol time, and T_{sym} is the duration of an OFDM symbol.

Regarding the estimation of the duration of I, it may depend on the overhead introduced by the EDCA based on the Hybrid Coordination Function (HCF) protocol (cf. section 2.4.1.1). Additionally, a node then waits for a random backoff time choose from the interval $[0, CW_{min}[AC]]$, where $CW_{min}[AC]$ denotes the contention window size for a specific AC which will be decremented if the medium is idle. This simplification can be done, because there is no exponential backoff due to the one node scenario. Based on the medium access strategy and considering a single

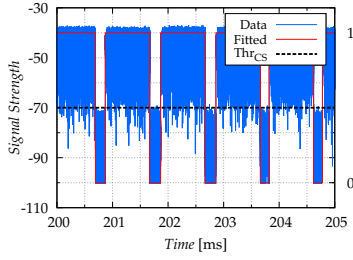


Figure 101: A sample of a measured received signal power S .

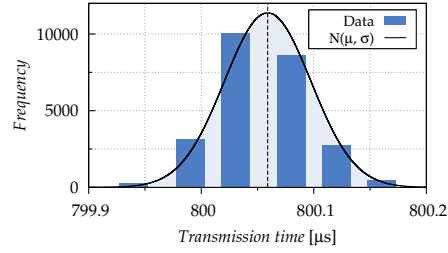


Figure 102: Measured distribution of the transmission time B

greedy node scenario, the interpacket gap IPG corresponding to the idle time I can be derived as

$$\text{IPG} = \text{AIFS}[AC] + \frac{\text{CW}_{\min}[AC]}{2} \times a\text{SlotTime} \quad (\text{B.3})$$

B.3 TESTBED VERIFICATION

To gather signal characteristics and therefore measured CL, we analyze the signal strength S based on the setup presented in section B.1. The transmitter is calibrated to send at a very high packet rate in order to receive the maximum achievable throughput (greedy mode) by avoiding the delay due to consecutive packet intervals. S is then converted to a square-wave form by using an adequate method based on information known beforehand on signal characteristics such as signal width and average power. This is necessary, because the SNR is lower than usually in consequence of a higher noise level of the used spectrum analyzer. The filtered signal is then consequently used to calculate the length of idle and busy phases. A sample of a measured signal strength S and its corresponding square-wave form is depicted in figure 101.

To identify the periods B and I , the signal power level is evaluated according to the CCA mechanism which specifies how a radio module should identify the status of the medium. For the sake of simplicity, a medium is considered to be busy if the received signal power S is higher than a certain threshold Thr_{CS} . Figure 102 presents the distribution of the measured busy period B for $\text{Thr}_{CS} = -70$ dBm, where

$$E[B] \approx 800.06 \mu\text{s}$$

Taking $T_{\text{pre}} = 32 \mu\text{s}$, $T_{\text{signal}} = 8 \mu\text{s}$, $T_{\text{sym}} = 8 \mu\text{s}$ for the 802.11p and considering $L = 564$ bytes [240], one gets theoretical busy duration $\text{TXTIME} = 800 \mu\text{s}$.

The interpacket gap I depends on the transmit rate of the transmitter and for a greedy transmitter it can be calculated using (B.2). An average interpacket gap of

$$E[I] \approx 186 \mu\text{s}$$

is retrieved from the measurements. Taking $\text{AIFSN}[AC] = 6$, $\text{CW}_{\min}[AC] = 7$ [241], $a\text{SIFSTime} = 16 \mu\text{s}$ (cf. 802.11a [11]) and $a\text{SlotTime} = 18 \mu\text{s}$ (doubled value because of $a\text{CCATime}$), one gets the theoretical average interpacket gap $\text{IPG} = 187 \mu\text{s}$.

The average CL is retrieved as the fraction of time the channel is busy. Thus the

average CL is calculated using the values for idle and busy duration as it is a renewal process [242] by

$$CL_{\text{avg}} = E\left[\frac{B}{B+I}\right] = \frac{E[B]}{E[B] + E[I]} \approx 0.811$$

For the lower bandwidth used for the evaluation, the TXTIME is measured as $E[B] \approx 813 \mu\text{s}$ and interpacket gap $E[I] = 173 \mu\text{s}$. Instead of using the theoretical values used for verification, the measured signal strength is used to calculate the average CL for each measurement. Thus, it can be ensured that the accuracy of the channel busy time estimation is independent of the bandwidth selected for the spectrum analyzer.

B.4 EVALUATION METHOD

B.4.1 Accuracy of CBR estimation

In terms of evaluation, we implement this estimation method as follows: The retrieved signal from the measurement itself consist of a huge set of samples N_S so that the number of probes taken by the estimation method is a subset and can be mapped to the samples

$$N_p \subseteq N_S$$

For $N_p = N_S$ the exact CBR is retrieved by the measurement, because each sample is taken into account (continuous probing). The default threshold values Thr_{DCC} and Thr_{CS} are equal so that the channel is assumed to be busy if the probed sample P_n is above Thr_{CS} .

PROBE DISTRIBUTION The estimation method assumes that the probes are uniformly distributed among the measuring interval. Thus the time between two probes shall be determined by $\Delta T = 1/N_p$ and the time of the n^{th} probe P_n is then retrieved by

$$T(P_n) = \frac{n}{N_p}$$

The time $T(P_n)$ is mapped to the closest sample $\in N_S$ at that time. In other words, the measured discrete signal is used as a lookup table. However, there is no guarantee that the probes are disjoint, e.g. P_n and P_{n-1} can be mapped to the same measured sample $\in N_S$. Furthermore, for $N_p = N_S$ we get the exact CBR retrieved by the measurement, because each sample is taken into account, i.e. continuous probing. However, this is not suitable for distributed inter probe times as for reasons mentioned above.

ACCURACY METRIC Although the accuracy is implicitly expressed by the distribution itself and can be retrieved from the figures within the evaluating paragraphs, we provide it as a quantitative value for comparison and compression reason. It is

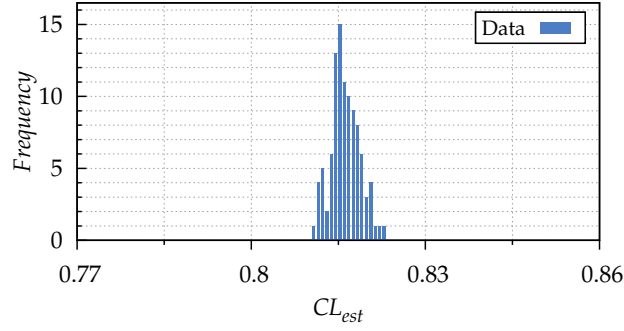


Figure 103: Distribution of estimated CL for uniformly distributed probes (greedy TX, $T_m = 1$ s, $N_p = 1250$)

expressed by the average absolute difference of the average measured and estimated CL as

$$\Delta CL(T_m, N_p) = \frac{1}{N_r \cdot N_m} \sum_{i=1}^{N_m} \sum_{j=1}^{N_r} |CL_{est}(i, j) - CL_{avg}(i)| \quad (\text{B.4})$$

where

$$CL_{est}(i, j) = \text{CBT}$$

denotes the estimated CL with respect to the measurement number and probe distribution, N_m denotes the amount of measurements, N_r is the number of disjunct repetitions for the probe distribution, and CL_{avg} is the average CL of the indicated measurement. This metric actually returns the absolute inaccuracy such that smaller values reveal higher accuracy. Since CL_{avg} slightly varies for each measurement from the experimental set-up, it is calculated explicitly for each $i \in N_m$ using the CBR method with $N_p = N_s$ (continuous probing). The distribution of the estimated CL (cf. figure 103) is implicitly considered in this accuracy by the probability itself, i.e. values with low accuracy occur less often.

ANALYSIS SPECIFICATION The analysis is done using a total of $N_m = 100$ measurements with 1 s each for every packet interval to eliminate effects emerging at a specific channel layout, i.e. there is a wider spectrum of packet distributions. Upon these measurements the CBR is evaluated according to the specified parameters. As constant probing times have deterministic results, there is no need for repetitions ($N_r = 1$) so that there are $N_m = 100$ estimated CLs (figure 103).

B.4.2 Accuracy for time (in-)variant deterministic CL

In order to evaluate the accuracy of the time (in-)variant channel behavior, we focus on a numerical analysis instead of a measurement campaign to show the effects of the synchronization effect and the measuring interval. Therefore we assume there is a precisely acquired reference CL following specific patterns. For the sake of simplicity,

we use a periodic pattern in this thesis with a period time of T_p . Investigations for time variant CL can be found in [93].

In figure 37a we illustrate the evaluated pattern and also mark the important parameters which have an impact on the accuracy. The synchronization effect for highly dynamic **vanet**s, where static networks with fixed time allocations do not exist, is considered by the T_{sync} variable causing a shift in the estimation. The measuring interval, indicated by T_m , influences the accuracy by a deviating estimated CL (CL_{est}). The reference CL (CL_{ref}) indicates the measured CL which is the real channel utilization.

ACCURACY METRIC Both estimated and reference CL are changing over time. While CL_{ref} is given by time (in-)variant behavior, CL_{est} is calculated based on the shift of T_{sync} and the probing interval T_m as the average CL within this measuring interval by

$$CL_{est}(t) = \frac{1}{T_m} \int_{t-T_m}^t CL_{ref} dt$$

The accuracy is expressed by the average difference per second between estimated and reference CL:

$$\Delta CL(T_m, T_{sync}) = \frac{1}{T} \int_{T_{sync}}^{T+T_{sync}} |CL_{ref} - CL_{est}| dt \quad (B.5)$$

where T denotes the specific maximal period time for each T_m with respect to the period T_p of the time invariant reference CL as illustrated in Figure 37a and is calculated by

$$T = \text{lcm}(T_p, \text{lcm}(T_m, 1)), \quad T_m \in \mathbb{Q}^+, T_p \in \mathbb{N}$$

where $\text{lcm}(T_m, 1)$ returns the least common natural number of a rational number which might be asynchronous with the period T_p of the reference CL. In any case the least common multiple of this result and T_p yield the synchronous complete period T of the estimated CL.

A sufficient large chosen T can also result in a good approximations for the accuracy evaluation and can be used if the period T_p is not known, i.e. for time variant CL.

BIBLIOGRAPHY

- [1] Xavier Mosquet, Michelle Andersen, and Aakash Arora. A roadmap to safer driving through ADAS. *The Motor & Equipment Manufacturers Association*, 2015.
- [2] KPMG. Connected and Autonomous Vehicles - The UK Economic Opportunity. Technical report, 2015.
- [3] Hermann Winner, Stephan Hakuli, and Gabriele Wolf. *Handbuch Fahrerassistenzsysteme*. Vieweg+Teubner Verlag, 2 edition, 2012.
- [4] Remi Tachet, Paolo Santi, Stanislav Sobolevsky, Luis Ignacio Reyes-Castro, Emilio Frazzoli, Dirk Helbing, and Carlo Ratti. Revisiting Street Intersections Using Slot-Based Systems. In *Plos One*, volume 11, page e0149607, 2016.
- [5] 5G Automotive Association - The Case for Cellular V2X for Safety and Cooperative Driving. Technical report.
- [6] Intelligent Transport Systems (ITS); Communications Architecture. Standard ETSI EN 302 665 v1.1.1, 2010.
- [7] John B. Kenney. Dedicated short-range communications (DSRC) standards in the United States. *Proceedings of the IEEE*, 99(7):1162–1182, 2011.
- [8] Final report on the METIS 5G system concept and technology roadmap. Technical report, 2015.
- [9] A European strategy on Cooperative Intelligent Transport Systems, a milestone towards cooperative, connected and automated mobility. Technical Report EC COM(2016) 766 final, 2016.
- [10] Intelligent Transport Systems (ITS); Vehicular Communications; Basic Set of Applications; Part 2: Specification of Cooperative Awareness Basic Service. Standard ETSI EN 302 637-2 v1.3.1, 2014.
- [11] Wireless LAN Medium Access Control (MAC) and Physical Layer (PHY) Specifications. Standard IEEE 802.11, 2012.
- [12] Van Jacobson. Congestion avoidance and control. In *ACM SIGCOMM computer communication review*, volume 18, pages 314–329. ACM, 1988.
- [13] Gaurav Bansal, John B Kenney, and Charles E Rohrs. LIMERIC: A linear adaptive message rate algorithm for DSRC congestion control. *IEEE Transactions on Vehicular Technology*, 62(9):4182–4197, nov 2013.
- [14] Tessa Tielert, Daniel Jiang, Qi Chen, L Delgrossi, and H Hartenstein. Design methodology and evaluation of rate adaptation based congestion control for Vehicle Safety Communications. In *IEEE Vehicular Networking Conference (VNC)*, pages 116–123, nov 2011.

- [15] Luisa Andreone, Roberto Brignolo, Sergio Damiani, Fulvio Sommariva, Giulio Vivo, and Stefano Marco. D8.1.1 - SAFESPOT Final Report. Technical Report July, 2010.
- [16] Intelligent Transport Systems (ITS); Vehicular Communications; Basic Set of Applications; Local Dynamic Map (LDM); Rationale for and guidance on standardization. Technical Report ETSI TR 102 863 V1.1.1, 2011.
- [17] Intelligent Transport Systems (ITS); Vehicular Communications; Basic Set of Applications; Local Dynamic Map (LDM). Standard ETSI EN 302 895 v1.0.0, 2014.
- [18] Intelligent transport systems – Co-operative ITS – Local dynamic map. Standard ISO/DIS 18750:2017(E), 2017.
- [19] Azzedine Boukerche, Horacio A. B. F. Oliveira, Eduardo F. Nakamura, and Antonio A. F. Loureiro. Vehicular Ad Hoc Networks: A New Challenge for Localization-Based Systems. *Comput. Commun.*, 31(12):2838–2849, 2008.
- [20] Kashif Nasee Qureshi and Abdul Hanan Abdullah. Localization-Based System Challenges in Vehicular Ad Hoc Networks: Survey. *The Smart Computing Review*, 4(6):515–528, 2014.
- [21] Elliott D. Kaplan and Christopher J. Hegarty. *Understanding GPS - Principles and Applications*. Artech House, 2. edition, 2006.
- [22] Global Positioning System (GPS) Standard Positioning Service (SPS) Performance Analysis Report, 2017.
- [23] M. Lu, K. Wevers, and R. Van Der Heijden. Technical Feasibility of Advanced Driver Assistance Systems (ADAS) for Road Traffic Safety. *Transportation Planning and Technology*, 28(3):167–187, 2005.
- [24] S. Olariu and M. C. Weigle. *Vehicular Networks: From Theory to Practice*. CRC Press, 2009.
- [25] Adam Ziebinski, Rafal Cupek, Hueseyin Erdogan, and Sonja Waechter. A Survey of ADAS Technologies for the Future Perspective of Sensor Fusion. In Ngoc Thanh Nguyen, Lazaros Iliadis, Yannis Manolopoulos, and Bogdan Trawiński, editors, *Computational Collective Intelligence: 8th International Conference, ICCCI 2016, Halkidiki, Greece, September 28-30, 2016. Proceedings, Part II*, pages 135–146. Springer International Publishing, Cham, 2016.
- [26] Paul Widdowson. Sensing for ADAS & Automated Driving - a vision of present and future needs. In *Intelligent Sensing Programme*, 2014.
- [27] Wireless LAN Medium Access Control (MAC) and Physical Layer (PHY) Specifications. Standard IEEE 802.11, 2010.
- [28] Intelligent Transport Systems (ITS); Radiocommunications equipment operating in the 5,855 MHz to 5,925 MHz frequency band; Harmonised Standard covering the essential requirements of article 3.2 of Directive 2014/53/EU. Standard ETSI EN 302 571 v2.0.0, 2016.

- [29] Intelligent Transport Systems (ITS); Access layer specification for Intelligent Transport Systems operating in the 5 GHz frequency band. Standard ETSI EN 302 663 v1.2.0, 2012.
- [30] The harmonised use of the 5875-5925 MHz frequency band for Intelligent Transport Systems (ITS). Technical Report CEPT ECC Decision (08)01, 2015.
- [31] Use of the band 5855-5875 MHz for Intelligent Transport Systems (ITS). Technical Report CEPT ECC Recommendation (08)01, 2015.
- [32] Intelligent Transport Systems (ITS); Harmonized Channel Specifications for Intelligent Transport Systems operating in the 5 GHz frequency band. Technical Specification ETSI TS 102 724 v1.1.1, 2012.
- [33] Daniel Jiang, Qi Chen, and Luca Delgrossi. Optimal Data Rate Selection for Vehicle Safety Communications. In *Proceedings of the 5th ACM International Workshop on Vehicular Inter-NETworking (VANET)*, pages 30–38, 2008.
- [34] Razvan Stanica, Emmanuel Chaput, and André-Luc Beylot. Properties of the MAC layer in safety vehicular Ad Hoc networks. *IEEE Communications Magazine*, 50(5):192–200, 2012.
- [35] Robert Schmidt and Tim Leinmüller. A Spatio-Temporal Metric for the Evaluation of Cooperative Awareness. In *Proceedings of the 18th World Congress on Intelligent Transport Systems*, pages 1–7, 2011.
- [36] Torsten Lorenzen and Mehdi Tavakoli Garrosi. Achieving Global Fairness at Urban Intersections Using Cooperative DSRC Congestion Control. In *Proceedings of the First ACM International Workshop on Smart, Autonomous, and Connected Vehicular Systems and Services at ACM MobiCom'16, CarSys '16*, pages 52–59, New York, NY, USA, 2016. ACM.
- [37] Intelligent Transport Systems (ITS); Vehicular Communications; GeoNetworking; Part 1: Requirements. Technical Specification ETSI TS 102 636-1 v1.1.1, 2010.
- [38] Intelligent Transport Systems (ITS); Vehicular communications; GeoNetworking; Part 4: Geographical addressing and forwarding for point-to-point and point-to-multipoint communications; Sub-part 1: Media-Independent Functionality. Technical Specification ETSI TS 102 636-4-1 v1.1.1, 2011.
- [39] Intelligent Transport Systems (ITS); Vehicular Communications; GeoNetworking; Part 5: Transport Protocols; Sub-part 1: Basic Transport Protocol. Standard ETSI EN 302 636-5-1 v1.2.0, 2013.
- [40] Intelligent Transport Systems (ITS); Vehicular Communications; GeoNetworking; Part 6: Internet Integration; Sub-part 1: Transmission of IPv6 Packets over GeoNetworking Protocols. Technical Specification ETSI TS 102 636-6-1 v1.1.1, 2011.
- [41] Brad Karp and H. T. Kung. GPSR: Greedy Perimeter Stateless Routing for Wireless Networks. In *Proceedings of the 6th annual international conference on Mobile computing and networking (ACM MobiCom)*, pages 243–254, 2000.

- [42] Intelligent Transport Systems (ITS); Users and applications requirements; Part 1: Facility layer structure, functional requirements and specifications. Technical Specification ETSI TS 102 894-1 v1.1.1, 2013.
- [43] Intelligent Transport Systems (ITS); Vehicular Communications; Basic Set of Applications; Part 3: Specifications of Decentralized Environmental Notification Basic Service. Standard ETSI EN 302 637-3 v1.2.1, 2014.
- [44] Intelligent Transport Systems (ITS); V2X Applications; Part 1: Road Hazard Signalling (RHS) application requirements specification. Technical Specification ETSI TS 101 539-1 v1.1.1, aug 2013.
- [45] Intelligent Transport Systems (ITS); V2X Applications; Part 3: Longitudinal Collision Risk Warning (LCRW) application requirements specification. Technical Specification ETSI TS 101 539-3 v1.1.1, 2013.
- [46] Intelligent Transport Systems (ITS); Vehicular Communications; Basic Set of Applications; Definitions. Technical Report ETSI TR 102 638 V1.1.1, 2009.
- [47] Claudia Campolo, Antonella Molinaro, and Riccardo Scopigno. *Vehicular ad hoc networks standards, solutions, and research*. 2015.
- [48] Intelligent Transport Systems (ITS); Framework for Public Mobile Networks in Cooperative ITS (C-ITS). Technical Report ETSI TR 102 962 v1.1.1, 2012.
- [49] Alexey Vinel. 3GPP LTE versus IEEE 802.11p/WAVE: Which technology is able to support cooperative vehicular safety applications? *IEEE Wireless Communications Letters*, 1(2):125–128, 2012.
- [50] Thomas Mangel, Timo Kosch, and Hannes Hartenstein. A comparison of UMTS and LTE for vehicular safety communication at intersections. In *2010 IEEE Vehicular Networking Conference (IEEE VNC)*, pages 293–300, 2010.
- [51] Lung-Chih Tung, Jorge Mena, Mario Gerla, and Christoph Sommer. A Cluster Based Architecture for Intersection Collision Avoidance Using Heterogeneous Networks. In *12th Annual Mediterranean Ad Hoc Networking Workshop (MED-HOC-NET)*, pages 82–88, 2013.
- [52] Mai-anh Phan, René Rembarz, and Sabine Sories. A Capacity Analysis for the Transmission of Event and Cooperative Awareness Messages in LTE Networks. In *18th ITS World Congress*, pages 1–12, 2011.
- [53] Maria Kihl, Kaan Bur, Pradyumna Mahanta, and Erik Coelingh. 3GPP LTE downlink scheduling strategies in vehicle-to-infrastructure communications for traffic safety applications. In *IEEE Symposium on Computers and Communications*, pages 448–453, 2012.
- [54] Broadband coverage in Europe 2014 - Mapping progress towards the coverage objectives of the Digital Agenda. Technical report, 2015.
- [55] Luca Delgrossi and Tao Zhang. *Vehicle Safety Communications - Protocols, Security, and Privacy*. 2012.

- [56] André-Luc Beylotand and Labiod Houda. *Vehicular Networks - Models and Algorithms*. 2013.
- [57] Giuseppe Araniti, Claudia Campolo, Massimo Condoluci, Antonio Iera, and Antonella Molinaro. LTE for vehicular networking: A survey. *IEEE Communications Magazine*, 51(5):148–157, 2013.
- [58] Jonathan Rodriguez. *Fundamentals of 5G Mobile Networks*, volume 53. John Wiley & Sons, 2015.
- [59] Zeeshan Hameed Mir and Fethi Filali. LTE and IEEE 802.11p for vehicular networking: a performance evaluation. *EURASIP Journal on Wireless Communications and Networking*, 11(89):1–15, 2014.
- [60] Tarik Taleb and Abderrahim Benslimane. Design guidelines for a network architecture integrating VANET with 3G & beyond networks. In *IEEE Global Telecommunications Conference (Globecom)*, 2010.
- [61] Abderrahim Benslimane, Tarik Taleb, and Rajarajan Sivaraj. Dynamic clustering-based adaptive mobile gateway management in integrated VANET 3G heterogeneous wireless networks. *IEEE Journal on Selected Areas in Communications*, 29(3):559–570, 2011.
- [62] Guillaume Rémy, Sidi Mohammed Senouci, François Jan, and Yvon Gourhant. LTE4V2X: LTE for a centralized VANET organization. *IEEE Global Telecommunications Conference (Globecom)*, pages 0–5, 2011.
- [63] Seyhan Ucar, Sinem Coleri Ergen, and Ozgur Ozkasap. Multihop-Cluster-Based IEEE 802.11p and LTE Hybrid Architecture for VANET Safety Message Dissemination. *IEEE Transactions on Vehicular Technology*, 65(4):2621–2636, 2016.
- [64] Afif Osseiran, Federico Boccardi, Volker Braun, Katsutoshi Kusume, Patrick Marsch, Michal Maternia, Olav Queseth, Malte Schellmann, Hans Schotten, Hidekazu Taoka, Hugo Tullberg, Mikko A. Uusitalo, Bogdan Timus, and Mikael Fallgren. Scenarios for 5G mobile and wireless communications: The vision of the METIS project. *IEEE Communications Magazine*, 52(5):26–35, 2014.
- [65] Klaus Doppler, Mika Rinne, Carl Wijting, Cássio B. Ribeiro, and Klaus Hug. Device-to-device communication as an underlay to LTE-advanced networks. *IEEE Communications Magazine*, 47(12):42–49, 2009.
- [66] Gábor Fodor, Erik Dahlman, Gunnar Mildh, Stefan Parkvall, Norbert Reider, György Miklós, and Zoltán Turányi. Design aspects of network assisted device-to-device communications. *IEEE Communications Magazine*, 50(3):170–177, 2012.
- [67] Laurent Gallo and Jérôme Harri. Short paper: A LTE-direct broadcast mechanism for periodic vehicular safety communications. In *IEEE Vehicular Networking Conference (VNC)*, pages 166–169, 2013.
- [68] Abdelmajid Khelil and David Soldani. On the suitability of Device-to-Device communications for road traffic safety. In *2014 IEEE World Forum on Internet of Things (WF-IoT)*, pages 224–229, 2014.

- [69] R Jain and K K Ramakrishnan. Congestion avoidance in computer networks with a connectionless network layer: concepts, goals and methodology. In [1988] *Proceedings. Computer Networking Symposium*, pages 134–143, 1988.
- [70] Ye Tian, Kai Xu, and N Ansari. TCP in wireless environments: problems and solutions. *IEEE Communications Magazine*, 43(3):S27—S32, 2005.
- [71] H Balakrishnan, V N Padmanabhan, S Seshan, and R H Katz. A comparison of mechanisms for improving TCP performance over wireless links. *IEEE/ACM Transactions on Networking*, 5(6):756–769, 1997.
- [72] George Xylomenos, George C Polyzos, Petri Mähönen, and Mika Saaranen. TCP Performance Issues over Wireless Links. *IEEE COMMUNICATIONS MAGAZINE*, 39(4):52–58, 2001.
- [73] Vaggelis G Douros and George C Polyzos. Review of some fundamental approaches for power control in wireless networks. *Computer Communications*, 34(13):1580–1592, 2011.
- [74] Mung Chiang, Prashanth Hande, Tian Lan, and Chee Wei Tan. Power Control in Wireless Cellular Networks. *Foundations and Trends® in Networking*, 2(4):381–533, 2008.
- [75] Ad Kamerman and Leo Monteban. WaveLAN {®}-II: A High-Performance Wireless LAN for the Unlicensed Band. *Bell Labs Technical Journal*, 2:118–133, 1997.
- [76] J Kim, S Kim, S Choi, and D Qiao. CARA: Collision-Aware Rate Adaptation for IEEE 802.11 WLANs. In *Proceedings IEEE INFOCOM 2006. 25TH IEEE International Conference on Computer Communications*, pages 1–11, 2006.
- [77] Sumit Rangwala, Apoorva Jindal, Ki-young Jang, Konstantinos Psounis, and Ramesh Govindan. Understanding Congestion Control in Multi-hop Wireless Mesh Networks. In *Proceedings of the 14th ACM international conference on Mobile computing and networking*, pages 291–302, 2008.
- [78] Saiid Biaz and Shaoen Wu. Rate Adaptation Algorithms for IEEE 802.11 Networks: A Survey and Comparison. In *2008 IEEE Symposium on Computers and Communications*, pages 130–136, 2008.
- [79] Daji Qiao, Sunghyun Choi, Amit Jain, Kang G Shin, and Ann Arbor. MiSer: An Optimal Low-Energy Transmission Strategy for IEEE 802.11a/h. In *Proceedings of the 9th annual international conference on Mobile computing and networking*, pages 161–175, 2003.
- [80] V P Mhatre, K Papagiannaki, and F Baccelli. Interference Mitigation Through Power Control in High Density 802.11 WLANs. *IEEE INFOCOM 2007 - 26th IEEE International Conference on Computer Communications*, pages 535–543, 2007.
- [81] Kishore Ramachandran, Ravi Kokku, Honghai Zhang, and Marco Gruteser. Symphony: Synchronous Two-Phase Rate and Power Control in 802.11 WLANs. *IEEE/ACM Transactions on Networking*, 18(4):1289–1302, 2010.

- [82] Jeongyeup Paek and Ramesh Govindan. RCRT: Rate-controlled Reliable Transport Protocol for Wireless Sensor Networks. *ACM Trans. Sen. Netw.*, 7(3), 2010.
- [83] Sumit Rangwala, Ramakrishna Gummadi, Ramesh Govindan, and Konstantinos Psounis. Interference-aware Fair Rate Control in Wireless Sensor Networks. *SIGCOMM Comput. Commun. Rev.*, 36(4):63–74, aug 2006.
- [84] Chieh-Yih Wan, Shane B Eisenman, and Andrew T Campbell. CODA: Congestion Detection and Avoidance in Sensor Networks. In *Proceedings of the 1st International Conference on Embedded Networked Sensor Systems, SenSys '03*, pages 266–279, New York, NY, USA, 2003. ACM.
- [85] Bret Hull, Kyle Jamieson, and Hari Balakrishnan. Mitigating Congestion in Wireless Sensor Networks. In *Proceedings of the 2Nd International Conference on Embedded Networked Sensor Systems, SenSys '04*, pages 134–147, New York, NY, USA, 2004. ACM.
- [86] Avinash Sridharan and Bhaskar Krishnamachari. Explicit and Precise Rate Control for Wireless Sensor Networks. In *Proceedings of the 7th ACM Conference on Embedded Networked Sensor Systems, SenSys '09*, pages 29–42, New York, NY, USA, 2009. ACM.
- [87] Swetha Narayanaswamy, Vikas Kawadia, R S Sreenivas, and P R Kumar. Power Control in Ad-Hoc Networks: Theory, Architecture, Algorithm and Implementation of the COMPOW Protocol. In *European Wireless Conference*, pages 156–162, 2002.
- [88] J Jeong, D Culler, and J H Oh. Empirical Analysis of Transmission Power Control Algorithms for Wireless Sensor Networks. In *2007 Fourth International Conference on Networked Sensing Systems*, pages 27–34, 2007.
- [89] Shan Lin, Jingbin Zhang, Gang Zhou, Lin Gu, John A Stankovic, and Tian He. ATPC: Adaptive Transmission Power Control for Wireless Sensor Networks. In *Proceedings of the 4th International Conference on Embedded Networked Sensor Systems, SenSys '06*, pages 223–236, New York, NY, USA, 2006. ACM.
- [90] Paolo Santi. Topology Control in Wireless Ad Hoc and Sensor Networks. *ACM Computing Surveys*, 37(2):164–194, 2005.
- [91] D Jiang, Q Chen, and L Delgrossi. Communication Density: A Channel Load Metric for Vehicular Communications Research. In *2007 IEEE International Conference on Mobile Adhoc and Sensor Systems*, pages 1–8, 2007.
- [92] Marc Torrent-Moreno. *Inter-vehicle communications: Achieving safety in a distributed wireless environment: Challenges, systems and protocols*. 2007.
- [93] Torsten Lorenzen. Experimental Analysis of the Channel Busy Time in Vehicular Ad-hoc Networks. In *The 25th International Conference on Computer Communication and Networks*, 2016.

- [94] Intelligent Transport Systems (ITS) - Decentralized Congestion Control Mechanisms for Intelligent Transport Systems operating in the 5 GHz range; Access layer part. Technical Specification ETSI TS 102 687 v1.1.1, The European Telecommunications Standards Institute, 2011.
- [95] Sofiane Zemouri, Soufiene Djahel, and John Murphy. Smart adaptation of beacons transmission rate and power for enhanced vehicular awareness in VANETs. In *17th International IEEE Conference on Intelligent Transportation Systems (ITSC)*, pages 739–746, 2014.
- [96] H Song and H S Lee. A survey on vehicle density estimation in vehicular safety communications and its challenging issues. In *16th International IEEE Conference on Intelligent Transportation Systems (ITSC 2013)*, pages 2427–2432, 2013.
- [97] T Darwish and K Abu Bakar. Traffic density estimation in vehicular ad hoc networks: A review. *Ad Hoc Networks*, 24(Part A):337–351, 2015.
- [98] M Sepulcre and J Gozalvez. Wireless Vehicular Adaptive Radio Resource Management Policies in Congested Channels. In *2007 4th International Symposium on Wireless Communication Systems*, pages 380–384, 2007.
- [99] Bengi Aygun, Mate Boban, and Alexander M Wyglinski. ECPR: Environment- and context-aware combined power and rate distributed congestion control for vehicular communications. *Computer Communications*, 93:3–16, 2016.
- [100] Miguel Sepulcre, Javier Gozalvez, Jerome Harri, and Hannes Hartenstein. Application-based congestion control policy for the communication channel in VANETs. *IEEE Communications Letters*, 14(10):951–953, 2010.
- [101] D B Rawat, D C Popescu, G Yan, and S Olariu. Enhancing VANET Performance by Joint Adaptation of Transmission Power and Contention Window Size. *IEEE Transactions on Parallel and Distributed Systems*, 22(9):1528–1535, sep 2011.
- [102] Larry L Peterson and Bruce S Davie. *Computer Networks, Fifth Edition: A Systems Approach*. Morgan Kaufmann Publishers Inc., San Francisco, CA, USA, 5th edition, 2011.
- [103] Dimitri Bertsekas and Robert Gallager. *Data Networks (2Nd Ed.)*. Prentice-Hall, Inc., Upper Saddle River, NJ, USA, 1992.
- [104] F P Kelly, A K Maulloo, and D K H Tan. Rate control for communication networks: shadow prices, proportional fairness and stability. *Journal of the Operational Research Society*, 49(3):237–252, 1998.
- [105] Jean-Yves Le Boudec. Rate adaptation, congestion control and fairness: A tutorial. Technical report, 2016.
- [106] Leonie Tessa Tielert, Erster Gutachter, Hartenstein Hannes, Zweiter Gutachter, and Marco Gruteser. *Rate-Adaptation Based Congestion Control for Vehicle Safety Communications*. PhD thesis, Karlsruher Instituts für Technologie (KIT), 2014.

- [107] Gaurav Bansal and John B Kenney. Achieving weighted-fairness in message rate-based congestion control for DSRC systems. In *2013 IEEE 5th International Symposium on Wireless Vehicular Communications (WiVeC)*, pages 1–5, 2013.
- [108] Marc Torrent-Moreno, Paolo Santi, and Hannes Hartenstein. Fair Sharing of Bandwidth in VANETs. *Proceedings of the 2nd ACM International Workshop on Vehicular Ad Hoc Networks (VANET)*, pages 49–58, 2005.
- [109] C L Huang, Y P Fallah, R Sengupta, and H Krishnan. Adaptive intervehicle communication control for cooperative safety systems. *IEEE Network*, 24(1):6–13, jan 2010.
- [110] Miguel Sepulcre, Javier Gozalvez, Onur Altintas, and Haris Kremo. Integration of congestion and awareness control in vehicular networks. *Ad Hoc Networks*, 37:29–43, 2016.
- [111] A Weinfield. Methods to reduce DSRC channel congestion and improve V2V communication reliability. *17th ITS World Congress*, pages 1–12, 2010.
- [112] Jun Yin, Xiaodong Xiadong Wang, Dharma Argawal, and D P Agrawal. Optimal packet size in error-prone channel for IEEE 802.11 distributed coordination function. In *2004 IEEE Wireless Communications and Networking Conference (IEEE Cat. No.04TH8733)*, volume 3, pages 1654–1659 Vol.3, 2004.
- [113] C. L. Robinson, L. Caminiti, D. Caveney, and Kenneth P. Laberteaux. Efficient Coordination and Transmission of Data for Cooperative Vehicular Safety Applications. In *Proceedings of the 3rd International Workshop on Vehicular Ad Hoc Networks*, volume 2006 of *VANET '06*, pages 10–19, New York, NY, USA, 2006. ACM.
- [114] C. L. Robinson, Derek Caveney, Lorenzo Caminiti, G. Baliga, Ken Laberteaux, and P. R. Kumar. Efficient Message Composition and Coding for Cooperative Vehicular Safety Applications. *IEEE Transactions on Vehicular Technology*, 56(6):3244–3255, nov 2007.
- [115] Michael Feiri, Jonathan Petit, and Frank Kargl. Evaluation of congestion-based certificate omission in VANETs. In *2012 IEEE Vehicular Networking Conference (VNC)*, pages 101–108, nov 2012.
- [116] Giorgio Calandriello, Panos Papadimitratos, Jean Pierre Hubaux, and Antonio Lioy. On the Performance of Secure Vehicular Communication Systems. *IEEE Transactions on Dependable and Secure Computing*, 8(6):898–912, nov 2011.
- [117] Elmar Schoch and Frank Kargl. On the Efficiency of Secure Beaconing in VANETs. In *Proceedings of the Third ACM Conference on Wireless Network Security, WiSec '10*, pages 111–116, New York, NY, USA, 2010. ACM.
- [118] Fan Bai, Daniel D. Stancil, and Hariharan Krishnan. Toward Understanding Characteristics of Dedicated Short Range Communications (DSRC) from a Perspective of Vehicular Network Engineers. In *Proceedings of the Sixteenth Annual International Conference on Mobile Computing and Networking, MobiCom '10*, pages 329–340, New York, NY, USA, 2010. ACM.

- [119] J A Fernandez, K Borries, L Cheng, B V K Vijaya Kumar, D D Stancil, and F Bai. Performance of the 802.11p Physical Layer in Vehicle-to-Vehicle Environments. *IEEE Transactions on Vehicular Technology*, 61(1):3–14, jan 2012.
- [120] S Yang, H Kim, and S Kuk. Less is more: need to simplify ETSI distributed congestion control algorithm. *Electronics Letters*, 50(4):279–281, 2014.
- [121] C B Math, A Ozgur, S H de Groot, and H Li. Data Rate Based Congestion Control in V2V Communication for Traffic Safety Applications. In *2015 IEEE Symposium on Communications and Vehicular Technology in the Benelux (SCVT)*, pages 1–6, nov 2015.
- [122] C Belagal Math, H Li, S Heemstra de Groot, and I G Niemegeers. V2X Application-Reliability Analysis of Data-Rate and Message-Rate Congestion Control Algorithms. *IEEE Communications Letters*, 21(6):1285–1288, 2017.
- [123] Y Yao, X Chen, L Rao, X Liu, and X Zhou. LORA: Loss Differentiation Rate Adaptation Scheme for Vehicle-to-Vehicle Safety Communications. *IEEE Transactions on Vehicular Technology*, 66(3):2499–2512, 2017.
- [124] Lars Wischhof and Hermann Rohling. Congestion control in vehicular ad hoc networks. In *IEEE International Conference on Vehicular Electronics and Safety, 2005.*, pages 58–63, 2005.
- [125] G Bianchi. Performance analysis of the IEEE 802.11 distributed coordination function. *IEEE Journal on Selected Areas in Communications*, 18(3):535–547, 2000.
- [126] Rene Reinders, Martijn Van Eenennaam, Georgios Karagiannis, and Geert Heijenk. Contention window analysis for beaconing in VANETs. In *2011 7th International Wireless Communications and Mobile Computing Conference*, pages 1481–1487, 2011.
- [127] Nathan Balon and Jinhua Guo. Increasing Broadcast Reliability in Vehicular Ad Hoc Networks. In *Proceedings of the 3rd International Workshop on Vehicular Ad Hoc Networks*, volume 2006 of *VANET '06*, pages 104–105, New York, NY, USA, 2006. ACM.
- [128] Y Mertens, M Wellens, and P Mahonen. Simulation-Based Performance Evaluation of Enhanced Broadcast Schemes for IEEE 802.11-Based Vehicular Networks. In *VTC Spring 2008 - IEEE Vehicular Technology Conference*, pages 3042–3046, 2008.
- [129] Razvan Stanica, Emmanuel Chaput, and André L. Beylot. Broadcast communication in Vehicular Ad-Hoc Network safety applications. In *2011 IEEE Consumer Communications and Networking Conference (CCNC)*, pages 462–466, jan 2011.
- [130] Razvan Stanica, Emmanuel Chaput, and André L. Beylot. Local density estimation for contention window adaptation in vehicular networks. In *2011 IEEE 22nd International Symposium on Personal, Indoor and Mobile Radio Communications*, pages 730–734, sep 2011.

- [131] C W Hsu, C H Hsu, and H R Tseng. MAC Channel Congestion Control Mechanism in IEEE 802.11p/WAVE Vehicle Networks. In *2011 IEEE Vehicular Technology Conference (VTC Fall)*, pages 1–5, sep 2011.
- [132] Arturo Gomez, Gladys Diaz, Khaled Boussetta, Nadjib Achir, and Abdelhak Farsi. Adaptive Contention Window for Zone-Based Dissemination of Vehicular Traffic. In *5th IEEE International Conference on Advanced Infocomm Technology, ICAIT 2012*, pages 330–339, Paris, 2013.
- [133] Danda B. Rawat, Gongjun Yan, Dimitrie C. Popescu, Michele C. Weigle, and Stephan Olariu. Dynamic Adaptation of Joint Transmission Power and Contention Window in VANET. In *2009 IEEE 70th Vehicular Technology Conference Fall*, pages 1–5, sep 2009.
- [134] Haitao Zhao, Aiqian Du, Hongbo Zhu, Dapeng Li, and Nanjie Liu. A self-adaptive back-off optimization scheme based on beacons probability prediction for vehicle Ad-Hoc networks. *China Communications*, 13(12):132–138, 2016.
- [135] Razvan Stanica, Emmanuel Chaput, and André L. Beylot. Enhancements of IEEE 802.11p Protocol for Access Control on a VANET Control Channel. In *2011 IEEE International Conference on Communications (ICC)*, pages 1–5, 2011.
- [136] Yan-Jing Wu, Tzu-Hsuan Yen, and Li-jia Chen. A Modified Backoff Algorithm with Dynamical Adjustment on Contention Window in VANETs. *Recent Advances in Telecommunications and Circuit Design*, pages 139–146, 2013.
- [137] Bernhard Kloiber, J Härri, Thomas Strang, Stephan Sand, Jerome Harri, Thomas Strang, Stephan Sand, J Härri, Thomas Strang, and Stephan Sand. Bigger is better #x2014; Combining contention window adaptation with geo-based backoff generation in DSRC networks. In *2014 International Conference on Connected Vehicles and Expo (ICCVE)*, pages 227–233, nov 2014.
- [138] Yanfei Lu, Jianmin Ren, Jin Qian, Meng Han, Yan Huo, and Tao Jing. Predictive Contention Window-Based Broadcast Collision Mitigation Strategy for VANET. In *2016 IEEE International Conferences on Big Data and Cloud Computing (BD-Cloud), Social Computing and Networking (SocialCom), Sustainable Computing and Communications (SustainCom) (BDCloud-SocialCom-SustainCom)*, pages 209–215, 2016.
- [139] Yunpeng Zang, Lothar Stibor, Xi Cheng, Hans-Jürgen Reumerman, Arthur Paruzel, and Andre Barroso. Congestion control in wireless networks for vehicular safety applications. In *Proceedings of the 8th European Wireless Conference*, volume 7, page 1, 2007.
- [140] Sarah Sharafkandi, Gaurav Bansal, John B. Kenney, and David H.C. Du. Using EDCA to improve Vehicle Safety Messaging. *2012 IEEE Vehicular Networking Conference (VNC)*, pages 70–77, 2012.
- [141] Deepak Puthal, Zeeshan Hameed Mir, Fethi Filali, and Hamid Menouar. Cross-layer architecture for congestion control in Vehicular Ad-hoc Networks. In *2013 International Conference on Connected Vehicles and Expo (ICCVE)*, pages 887–892, 2013.

- [142] Stephan Eichler and Christoph Schroth. A Multi-Layer Approach for Improving the Scalability of Vehicular Ad-Hoc Networks. In *Communication in Distributed Systems - 15. ITG/GI Symposium*, pages 1–12, feb 2007.
- [143] Tarik Taleb, Keisuke Ooi, and Kazuo Hashimoto. An Efficient Collision Avoidance Strategy for ITS systems. In *2008 IEEE Wireless Communications and Networking Conference*, pages 2212–2217, 2008.
- [144] Robert Karl Schmidt, Tim Leinmüller, Bert Böddeker, and Günter Schäfer. Adapting the wireless carrier sensing for VANETs. In *6th International Workshop on Intelligent Transportation (WIT)*, 2010.
- [145] R Stanica, E Chaput, and A L Beylot. Physical Carrier Sense in Vehicular Ad-Hoc Networks. In *2011 IEEE Eighth International Conference on Mobile Ad-Hoc and Sensor Systems*, pages 580–589, 2011.
- [146] Jason a. Fuemmeler, Nitin H Vaidya, and Venugopal V Veeravalli. Selecting Transmit Powers and Carrier Sense Thresholds in CSMA Protocols for Wireless Ad Hoc Networks. In *Proceedings of the 2Nd Annual International Workshop on Wireless Internet*, number October in WICON '06, New York, NY, USA, 2006. ACM.
- [147] Robert K Schmidt, Achim Brakemeier, Tim Leinmüller, Frank Kargl, and Günter Schäfer. Advanced Carrier Sensing to Resolve Local Channel Congestion. In *Proceedings of the Eighth ACM International Workshop on Vehicular Inter-networking, VANET '11*, pages 11–20, New York, NY, USA, 2011. ACM.
- [148] Razvan Stanica, Emmanuel Chaput, and André L. Beylot. Congestion control in CSMA-based vehicular networks: Do not forget the carrier sensing. In *2012 9th Annual IEEE Communications Society Conference on Sensor, Mesh and Ad Hoc Communications and Networks (SECON)*, volume 1, pages 650–658, 2012.
- [149] Giuseppe Caizzzone, Paolo Giacomazzi, Luigi Musumeci, Giacomo Verticale, and Milano Dei. A power control algorithm with high channel availability for vehicular ad hoc networks. In *IEEE International Conference on Communications, 2005. ICC 2005. 2005*, volume 5, pages 3171–3176 Vol. 5, 2005.
- [150] M Artimy. Local Density Estimation and Dynamic Transmission-Range Assignment in Vehicular Ad Hoc Networks. *IEEE Transactions on Intelligent Transportation Systems*, 8(3):400–412, sep 2007.
- [151] X Guan, R Sengupta, H Krishnan, and F Bai. A Feedback-Based Power Control Algorithm Design for VANET. In *2007 Mobile Networking for Vehicular Environments*, pages 67–72, 2007.
- [152] C Chigan and J Li. A Delay-Bounded Dynamic Interactive Power Control Algorithm for VANETs. In *2007 IEEE International Conference on Communications*, pages 5849–5855, 2007.
- [153] Lin Cheng and Rahul Shakya. VANET adaptive power control from realistic propagation and traffic modeling. In *2010 IEEE Radio and Wireless Symposium (RWS)*, pages 665–668, jan 2010.

- [154] Bernhard Kloiber, J Härrri, Thomas Strang, Jerome Harri, Thomas Strang, J Härrri, and Thomas Strang. Dice the TX power #x2014; Improving Awareness Quality in VANETs by random transmit power selection. In *2012 IEEE Vehicular Networking Conference (VNC)*, pages 56–63, nov 2012.
- [155] K Okamoto and S Ishihara. Highly reliable data distribution scheme for location information in vehicular networks using cyclic beacon transmission power patterns. In *2013 IEEE Vehicular Networking Conference*, pages 55–62, 2013.
- [156] Marc Torrent-Moreno, Paolo Santi, and Hannes Hartenstein. Distributed Fair Transmit Power Adjustment for Vehicular Ad Hoc Networks. In *2006 3rd Annual IEEE Communications Society on Sensor and Ad Hoc Communications and Networks*, volume 2, pages 479–488, sep 2006.
- [157] M Torrent-Moreno, J Mittag, P Santi, and H Hartenstein. Vehicle-to-Vehicle Communication: Fair Transmit Power Control for Safety-Critical Information. *Vehicular Technology, IEEE Transactions on*, 58(7):3684–3703, sep 2009.
- [158] Jens Mittag, Felix Schmidt-Eisenlohr, Moritz Killat, Jérôme Härrri, and Hannes Hartenstein. Analysis and Design of Effective and Low-overhead Transmission Power Control for VANETs. In *Proceedings of the Fifth ACM International Workshop on VehiculAr Inter-NETworking, VANET '08*, pages 39–48, New York, NY, USA, 2008. ACM.
- [159] H Lu and C Poellabauer. Balancing broadcast reliability and transmission range in VANETs. In *2010 IEEE Vehicular Networking Conference*, pages 247–254, 2010.
- [160] L Yang, J Guo, and Y Wu. Channel Adaptive One Hop Broadcasting for VANETs. In *2008 11th International IEEE Conference on Intelligent Transportation Systems*, pages 369–374, 2008.
- [161] G Lei, F Liu, P Wang, X Wang, and N Wang. Power Adjustment Based Congestion Control in Vehicular Ad-hoc Networks. In *2014 4th International Conference on Artificial Intelligence with Applications in Engineering and Technology*, pages 280–285, 2014.
- [162] N Nasiriani, Y P Fallah, and H Krishnan. Stability analysis of congestion control schemes in vehicular ad-hoc networks. In *2013 IEEE 10th Consumer Communications and Networking Conference (CCNC)*, pages 358–363, jan 2013.
- [163] Y P Fallah, N Nasiriani, and H Krishnan. Stable and Fair Power Control in Vehicle Safety Networks. *IEEE Transactions on Vehicular Technology*, 65(3):1662–1675, 2016.
- [164] Syed Adeel Ali Shah, Ejaz Ahmed, Feng Xia, Ahmad Karim, Muhammad Ahsan Qureshi, Ihsan Ali, and Rafidah MD D Noor. Coverage Differentiation Based Adaptive Tx-Power for Congestion and Awareness Control in VANETs. *Mobile Networks and Applications*, pages 1–12, 2016.

- [165] E Egea-Lopez, J J Alcaraz, J Vales-Alonso, A Festag, and J Garcia-Haro. Statistical Beaconing Congestion Control for Vehicular Networks. *IEEE Transactions on Vehicular Technology*, 62(9):4162–4181, nov 2013.
- [166] E Egea-Lopez. Fair distributed Congestion Control with transmit power for vehicular networks. In *2016 IEEE 17th International Symposium on A World of Wireless, Mobile and Multimedia Networks (WoWMoM)*, pages 1–6, 2016.
- [167] J Gozalvez and M Sepulcre. Opportunistic technique for efficient wireless vehicular communications. *IEEE Vehicular Technology Magazine*, 2(4):33–39, 2007.
- [168] M Sepulcre, J Gozalvez, J Harri, and H Hartenstein. Contextual Communications Congestion Control for Cooperative Vehicular Networks. *IEEE Transactions on Wireless Communications*, 10(2):385–389, 2011.
- [169] A A K Jeng, R H Jan, C Chen, and T C Chiang. Efficient Broadcast Mechanism for Cooperative Collision Avoidance Using Power Control. In *2009 10th International Symposium on Pervasive Systems, Algorithms, and Networks*, pages 266–271, 2009.
- [170] M A Javed and J Y Khan. A Cooperative Safety Zone Approach to Enhance the Performance of VANET Applications. In *2013 IEEE 77th Vehicular Technology Conference (VTC Spring)*, pages 1–5, 2013.
- [171] Mohammad Reza Jabbarpour Sattari, Rafidah Md Noor, Saied Ghahremani, Mohammad Reza, Jabbarpour Sattari, Rafidah Md Noor, and Saied Ghahremani. Dynamic congestion control algorithm for vehicular ad hoc networks. *International Journal of Software Engineering and Its Applications*, 7(3):95–108, 2013.
- [172] Mohammad Reza Jabbarpour, Rafidah Md Noor, Rashid Hafeez Khokhar, Chih-Heng Heng Ke, Rafidah Md Noor, Rashid Hafeez Khokhar, Chih-Heng Heng Ke, Rafidah Md Noor, Rashid Hafeez Khokhar, and Chih-Heng Heng Ke. Cross-layer congestion control model for urban vehicular environments. *Journal of Network and Computer Applications*, 44:1–16, 2014.
- [173] Torsten Lorenzen. Performance Analysis of the Functional Interaction of Awareness Control and DCC in VANETs. In *IEEE 84th Vehicular Technology Conference*, pages 0–6, 2016.
- [174] J He, H h. Chen, T M Chen, and W Cheng. Adaptive congestion control for DSRC vehicle networks. *IEEE Communications Letters*, 14(2):127–129, 2010.
- [175] W Guan, J He, L Bai, and Z Tang. Adaptive Rate Control of Dedicated Short Range Communications Based Vehicle Networks for Road Safety Applications. In *2011 IEEE 73rd Vehicular Technology Conference (VTC Spring)*, pages 1–5, 2011.
- [176] Humeng Lv, Xuemei Ye, Li An, and Yuan Wang. Distributed Beacon Frequency Control Algorithm for VANETs (DBFC). In *2012 Second International Conference on Intelligent System Design and Engineering Application*, pages 243–246, jan 2012.

- [177] B Kim, I Kang, and H Kim. Resolving the Unfairness of Distributed Rate Control in the IEEE WAVE Safety Messaging. *IEEE Transactions on Vehicular Technology*, 63(5):2284–2297, jun 2014.
- [178] Le Zhang and Shahrokh Valaee. Adapting to the Driving Context in Congestion Control for Vehicular Networks. In *Proceedings of the Fourth ACM International Symposium on Development and Analysis of Intelligent Vehicular Networks and Applications, DIVANet '14*, pages 67–71, New York, NY, USA, 2014. ACM.
- [179] J Kenney, D Jiang, G Bansal, and T Tielert. Controlling Channel Congestion using CAM Message Generation Rate. In *5th ETSI ITS Workshop*, pages 1–15, 2013.
- [180] K Ogura, J Katto, and M Takai. BRAEVE: Stable and adaptive BSM rate control over IEEE802.11p vehicular networks. In *2013 IEEE 10th Consumer Communications and Networking Conference (CCNC)*, pages 745–748, jan 2013.
- [181] Gaurav Bansal, Hongsheng Lu, John B Kenney, and Christian Poellabauer. EMBARC: Error Model Based Adaptive Rate Control for Vehicle-to-vehicle Communications. In *Proceeding of the Tenth ACM International Workshop on Vehicular Inter-networking, Systems, and Applications, VANET '13*, pages 41–50, New York, NY, USA, 2013. ACM.
- [182] Bin Cheng, A Rostami, M Gruteser, Hongsheng Lu, J B Kenney, and G Bansal. Evolution of vehicular congestion control without degrading legacy vehicle performance. In *2016 IEEE 17th International Symposium on A World of Wireless, Mobile and Multimedia Networks (WoWMoM)*, pages 1–6, 2016.
- [183] Esteban Egea-Lopez and Pablo Pavon-Mariño. Distributed and Fair Beaconing Congestion Control Schemes for Vehicular Networks. 15(12):1–11, 2014.
- [184] E Egea-Lopez and P Pavon-Mariño. Distributed and Fair Beaconing Rate Adaptation for Congestion Control in Vehicular Networks. *IEEE Transactions on Mobile Computing*, 15(12):3028–3041, 2016.
- [185] C Thaina, K N Nakorn, and K Rojviboonchai. A study of adaptive beacon transmission on Vehicular Ad-Hoc Networks. In *2011 IEEE 13th International Conference on Communication Technology*, pages 597–602, sep 2011.
- [186] Yongtae Park and Hyogon Kim. Application-level frequency control of periodic safety messages in the IEEE WAVE. *IEEE Transactions on Vehicular Technology*, 61(4):1854–1862, 2012.
- [187] Haiyue Piao, Yongtae Park, Byungjo Kim, and Hyogon Kim. Safety beaconing rate control based on vehicle counting in WAVE. In *2015 IEEE Intelligent Vehicles Symposium (IV)*, pages 1361–1366, 2015.
- [188] N Chaabouni, A Hafid, and P K Sahu. A collision-based beacon rate adaptation scheme(CBA) for VANETs. In *2013 IEEE International Conference on Advanced Networks and Telecommunications Systems (ANTS)*, pages 1–6, 2013.

- [189] C Sommer, S Joerer, M Segata, O K Tonguz, R L Cigno, and F Dressler. How Shadowing Hurts Vehicular Communications and How Dynamic Beaconing Can Help. *IEEE Transactions on Mobile Computing*, 14(7):1411–1421, 2015.
- [190] Fuxin Zhang, Guozhen Tan, Chao Yu, Nan Ding, Caixia Song, and Mingjian Liu. Fair Transmission Rate Adjustment in Cooperative Vehicle Safety Systems Based on Multi-Agent Model Predictive Control. *IEEE Transactions on Vehicular Technology*, 66(7):6115–6129, 2017.
- [191] C Sommer, O K Tonguz, and F Dressler. Traffic information systems: efficient message dissemination via adaptive beaconing. *IEEE Communications Magazine*, 49(5):173–179, 2011.
- [192] Linying Liu, Xinhong Wang, Chao Wang, and Fuqiang Liu. An efficient beacon rate adaptation scheme for vehicular networks. In *2013 International Conference on Wireless Communications and Signal Processing*, pages 1–6, 2013.
- [193] C L Huang, Y P Fallah, R Sengupta, and H Krishnan. Intervehicle Transmission Rate Control for Cooperative Active Safety System. *IEEE Transactions on Intelligent Transportation Systems*, 12(3):645–658, sep 2011.
- [194] S Rezaei, R Sengupta, and H Krishnan. Reducing the Communication Required By DSRC-Based Vehicle Safety Systems. In *2007 IEEE Intelligent Transportation Systems Conference*, pages 361–366, sep 2007.
- [195] Hoa-Hung Nguyen and Han-You Jeong. Adaptive beacon rate control algorithm for vehicular ad-hoc networks. In *2013 Fifth International Conference on Ubiquitous and Future Networks (ICUFN)*, pages 652–653, 2013.
- [196] M A Javed and J Y Khan. Performance analysis of a time headway based rate control algorithm for VANET safety applications. In *2013, 7th International Conference on Signal Processing and Communication Systems (ICSPCS)*, pages 1–6, 2013.
- [197] M Segata, F Dressler, and R Lo Cigno. Jerk Beaconing: A dynamic approach to platooning. In *2015 IEEE Vehicular Networking Conference (VNC)*, pages 135–142, 2015.
- [198] Kayhan Zrar Ghafoor, Kamalrulnizam Abu Bakar, Martijn van Eenennaam, Rashid Hafeez Khokhar, and Alberto J Gonzalez. A fuzzy logic approach to beaconing for vehicular ad hoc networks. *Telecommunication Systems*, 52(1):139–149, jan 2013.
- [199] N Wang, G Lei, X Wang, P Wang, and F Liu. A Beacon Rate Control Scheme Based on Fuzzy Logic for Vehicular Ad-Hoc Networks. In *2014 4th International Conference on Artificial Intelligence with Applications in Engineering and Technology*, pages 286–291, 2014.
- [200] Seyed Ahmad Soleymani, Abdul Hanan Abdullah, Mohammad Hossein Anisi, Ayman Altameem, Wan Haslina Hasan, Shidrokh Goudarzi, Satria Mandala, Zaidi Bin Razak, and Noorzaily Mohamed Noor. BRAIN-F: Beacon Rate

- Adaption Based on Fuzzy Logic in Vehicular Ad Hoc Network. *International Journal of Fuzzy Systems*, 19(2):301–315, apr 2017.
- [201] Michele Drigo, Wenhui Zhang, Roberto Baldessari, Long Le, Andreas Festag, and Michele Zorzi. Distributed Rate Control Algorithm for VANETs (DRCV). In *Proceedings of the Sixth ACM International Workshop on Vehicular InterNetworking, VANET '09*, pages 119–120, New York, NY, USA, 2009. ACM.
- [202] S Joerer, B Bloessl, M Segata, C Sommer, R L Cigno, A Jamalipour, and F Dressler. Enabling Situation Awareness at Intersections for IVC Congestion Control Mechanisms. *IEEE Transactions on Mobile Computing*, 15(7):1674–1685, 2016.
- [203] Sanjit Kaul, Marco Gruteser, Vinuth Rai, and John Kenney. Minimizing age of information in vehicular networks. In *8th Annual IEEE Communications Society Conference on Sensor, Mesh and Ad Hoc Communications and Networks (SECON)*, pages 350–358, 2011.
- [204] Roberto Baldessari, Damiano Scanferla, Long Le, Wenhui Zhang, and Andreas Festag. Joining forces for vanets: A combined transmit power and rate control algorithm. In *6th international workshop on intelligent transportation (WIT)*, 2010.
- [205] L Le, R Baldessari, P Salvador, A Festag, and W Zhang. Performance Evaluation of Beacon Congestion Control Algorithms for VANETs. In *2011 IEEE Global Telecommunications Conference - GLOBECOM 2011*, pages 1–6, 2011.
- [206] Tessa Tielert, Daniel Jiang, Hannes Hartenstein, and Luca Delgrossi. Joint Power/Rate Congestion Control Optimizing Packet Reception in Vehicle Safety Communications. In *Proceeding of the Tenth ACM International Workshop on Vehicular Inter-networking, Systems, and Applications, VANET '13*, pages 51–60, New York, NY, USA, 2013. ACM.
- [207] Hongsheng Lu, Gaurav Bansal, and John Kenney. A Joint Rate-Power Control Algorithm for Vehicular Safety Communications. In *22nd ITS World Congress*, 2015.
- [208] Jubin Jose, Chong Li, Xinzhou Wu, Lei Ying, and Kai Zhu. Distributed Rate and Power Control in Vehicular Networks. *CoRR*, abs/1511.0, 2015.
- [209] Esteban Egea-Lopez and Pablo Pavon-Mariño. Fair Congestion Control in Vehicular Networks with Beaconing Rate Adaptation at Multiple Transmit Powers. *IEEE Transactions on Vehicular Technology*, 65(6):3888–3903, 2016.
- [210] A Vesco, R Scopigno, C Casetti, and C.-F. Chiasserini. Investigating the effectiveness of decentralized congestion control in vehicular networks. In *Globecom Workshops (GC Wkshps), 2013 IEEE*, pages 1314–1319, 2013.
- [211] Seungho Kuk and Hyogon Kim. Preventing unfairness in the ETSI distributed congestion control. *IEEE Communications Letters*, 18(7):1222–1225, 2014.
- [212] A Alonso Gómez, C F Mecklenbräuker, Arrate Alonso Gomez, and Christoph F. Mecklenbrauker. Dependability of Decentralized Congestion Control for

- Varying VANET Density. *IEEE Transactions on Vehicular Technology*, 65(11):9153–9167, nov 2016.
- [213] Intelligent Transport Systems (ITS); Cross Layer DCC Management Entity for operation in the ITS G5A and ITS G5B medium; Report on Cross layer DCC algorithms and performance evaluation. Technical Report ETSI TR 101 612 v 1.1.1, 2014.
- [214] Intelligent Transport Systems (ITS); Cross Layer DCC Management Entity for operation in the ITS G5A and ITS G5B medium; Validation set-up and results. Technical Report ESTI TR 101 613 v1.1.1, 2015.
- [215] Intelligent Transport Systems (ITS); Cross Layer DCC Management Entity for operation in the ITS G5A and ITS G5B medium. Technical Report ETSI TS 103 175 V1.1.1, 2015.
- [216] M A Javed and J Y Khan. Performance analysis of an adaptive rate-range control algorithm for VANET safety applications. In *Computing, Networking and Communications (ICNC), 2014 International Conference on*, pages 418–423, feb 2014.
- [217] M Sepulcre, J Gozalvez, O Altintas, and H Kremo. Adaptive beaconing for congestion and awareness control in vehicular networks. In *2014 IEEE Vehicular Networking Conference (VNC)*, pages 81–88, 2014.
- [218] Matthias Sander Frigau. Fair Decentralized Congestion and Awareness Control for Vehicular Networks. In *2015 IEEE 21st International Conference on Parallel and Distributed Systems (ICPADS)*, volume 2016-Janua, pages 172–180, 2015.
- [219] Jin Qian, Tao Jing, Yan Huo, Hui Li, Liran Ma, and Yanfei Lu. *An Adaptive Beaconing Scheme Based on Traffic Environment Parameters Prediction in VANETs*, pages 524–535. Springer International Publishing, Cham, 2016.
- [220] Jens Mittag, Florian Thomas, Jérôme Härri, and Hannes Hartenstein. A Comparison of Single- and Multi-hop Beaconing in VANETs. In *Proceedings of the 6th ACM International Workshop on Vehicular Inter-NETworking (VANET)*, 2009.
- [221] Khalid Abdel Hafeez, Lian Zhao, Zaiyi Liao, and Bobby Ngok-Wah W Ma. A New Broadcast Protocol for Vehicular Ad Hoc Networks Safety Applications. In *2010 IEEE Global Telecommunications Conference GLOBECOM 2010*, pages 1–5, 2010.
- [222] Torsten Lorenzen and Hugues Tchouankem. Evaluation of an awareness control algorithm for VANETs based on ETSI EN 302 637-2 V1.3.2. In *Communication Workshop (ICCW), 2015 IEEE International Conference on*, pages 2458–2464, 2015.
- [223] Torsten Lorenzen. SWeRC: Self-Weighted Semi-Cooperative DSRC Congestion Control based on LIMERIC. In *IEEE 86th Vehicular Technology Conference*, Toronto, 2017.

- [224] Hugues Tchouankem. *Radio shadowing in vehicle-to-vehicle communication at urban intersections : a measurement and simulation-based evaluation*. PhD thesis, Leibniz Universität Hannover, 2016.
- [225] David Eckhoff, Nikoletta Sofra, and Reinhard German. A performance study of cooperative awareness in ETSI ITS G5 and IEEE WAVE. In *10th Annual Conference on Wireless On-Demand Network Systems and Services (WONS)*, pages 196–200, 2013.
- [226] Birgit Kull. DCC performance analysis. Technical Specification C2C 697 002 v 1.1.0, 2014.
- [227] Tamer ElBatt, Siddhartha K. Goel, Gavin Holland, Hariharan Krishnan, and Jayendra Parikh. Cooperative collision warning using dedicated short range wireless communications. In *Proceedings of the 3rd international workshop on Vehicular ad hoc networks (VANET)*, page 1, 2006.
- [228] Qi Chen, Daniel Jiang, and Luca Delgrossi. IEEE 1609.4 DSRC Multi-Channel Operations and Its Implications on Vehicle Safety Communications. In *IEEE Vehicular Networking Conference (VNC)*, pages 1–8, 2009.
- [229] Henrik Schumacher. *Netzlastabhängige Dienstgütebewertung in Fahrzeug-zu-Fahrzeug-Kommunikationsnetzen*. PhD thesis, Leibniz Universität Hannover, 2016.
- [230] Bernhard Kloiber, CR Garcia, Jérôme Härri, and Thomas Strang. Update delay: A new information-centric metric for a combined communication and application level reliability evaluation of cam based safety applications. In *ITS World Congress*, number October, pages 1–9, 2012.
- [231] Fan Bai and Hariharan Krishnan. Reliability analysis of DSRC wireless communication for vehicle safety applications. In *IEEE Intelligent Transportation Systems Conference (ITSC'06)*, pages 355–362, 2006.
- [232] N An, T Gaugel, and H Hartenstein. VANET: Is 95% probability of packet reception safe? In *11th International Conference on ITS Telecommunications (ITST)*, pages 113–119, aug 2011.
- [233] H Lu and C Poellabauer. Analysis of application-specific broadcast reliability for vehicle safety communications. In *Proceedings of the Eighth ACM international workshop on Vehicular inter-networking*, pages 67–72, 2011.
- [234] Francesca Martelli, M. Elena Renda, Giovanni Resta, and Paolo Santi. A measurement-based study of beaconing performance in IEEE 802.11p vehicular networks. In *IEEE INFOCOM*, pages 1503–1511, 2012.
- [235] Xue Yang, Jie Liu, Feng Zhao, and N.H. Vaidya. A vehicle-to-vehicle communication protocol for cooperative collision warning. In *The First Annual International Conference on Mobile and Ubiquitous Systems: Networking and Services (MOBIQUITOUS)*, pages 114–123, 2004.
- [236] Henrik Zöller and Wolfgang Hugemann. *Zur Problematik der Bremsreaktionszeit im Straßenverkehr*. Deutscher Psychologen Verlag, 1999.

- [237] Tetiana Zinchenko, Hugues Tchouankem, Lars Wolf, and André Leschke. Reliability Analysis of Vehicle-to-vehicle Applications Based on Real World Measurements. In *Proceeding of the Tenth ACM International Workshop on Vehicular Inter-networking, Systems, and Applications*, pages 11–20, 2013.
- [238] Julia Werneke, Andro Kleen, and Mark Vollrath. Perfect Timing. *Human Factors: The Journal of the Human Factors and Ergonomics Society*, 56(2):249–259, 2014.
- [239] Susann Winkler, Julia Werneke, and Mark Vollrath. Timing of early warning stages in a multi stage collision warning system: Drivers' evaluation depending on situational influences. *Transportation Research Part F: Traffic Psychology and Behaviour*, 36:57–68, 2016.
- [240] Henrik Schumacher, Hugues Tchouankem, Jörg Nuckelt, Thomas Kürner, Tetiana Zinchenko, André Leschke, and Lars Wolf. Vehicle-to-Vehicle IEEE 802.11p performance measurements at urban intersections. In *IEEE International Conference on Communications*, pages 7131–7135, Ottawa, 2012.
- [241] Intelligent Transport Systems (ITS); European profile standard for the physical and medium access control layer of Intelligent Transport Systems operating in the 5 GHz frequency band. Technical Report ETSI EN 302 663 v.1.1.0, 2009.
- [242] Sheldon M Ross. *Introduction to Probability Models*. Elsevier, 10 edition, 2010.

PUBLICATIONS

- [1] T. Lorenzen. SWeRC: Self-Weighted Semi-Cooperative DSRC Congestion Control based on LIMERIC. In *IEEE 86th Vehicular Technology Conference*, Toronto, 2017.
- [2] M. T. Garrosi, M. Kalac, and T. Lorenzen. Geo-routing in urban Vehicular Ad-hoc Networks: A literature review. In *2017 International Conference on Computing, Networking and Communications (ICNC)*, pages 865–871, 2017.
- [3] T. Lorenzen and M. T. Garrosi. Achieving Global Fairness at Urban Intersections Using Cooperative DSRC Congestion Control. In *Proceedings of the First ACM International Workshop on Smart, Autonomous, and Connected Vehicular Systems and Services at ACM MobiCom'16, CarSys '16*, pages 52–59, New York, NY, USA, 2016.
- [4] T. Lorenzen. Performance Analysis of the Functional Interaction of Awareness Control and DCC in VANETs. In *IEEE 84th Vehicular Technology Conference*, 2016.
- [5] T. Lorenzen. Experimental Analysis of the Channel Busy Time in Vehicular Ad-hoc Networks. In *The 25th International Conference on Computer Communication and Networks*, 2016.
- [6] H. Tchouankem and T. Lorenzen. Measurement-based evaluation of interference in Vehicular Ad-Hoc Networks at urban intersections. In *2015 IEEE International Conference on Communication Workshop (ICCW)*, pages 2381–2386, 2015.
- [7] T. Lorenzen and H. Tchouankem. Evaluation of an awareness control algorithm for VANETs based on ETSI EN 302 637-2 V1.3.2. In *2015 IEEE International Conference on Communication Workshop (ICCW)*, pages 2458–2464, 2015.

SCIENTIFIC CAREER

Name	Torsten Lorenzen
Date of birth	30.10.1988
Working Experience	
since 01/2014	Research assistant and PhD student at Institute of Communications Technology at Leibniz Universität Hannover Research in the field of Vehicle-to-X Communication Doctoral Candidate of the Research Training Group "SocialCars" – a DFG funded research project
12/2011 – 02/2013	Student assistant at Institute of Microelectronic Systems at Leibniz Universität Hannover
Teaching Experience	
since 04/2014	Lab exercise on "Networks and Protocols"
since 01/2014	Supervision of several B.Sc. and M.Sc. theses
Education	
10/2008 – 11/2013	Studies: Computer Science at Leibniz Universität Hannover Master thesis at Institute of Communications Technology at Leibniz Universität Hannover <i>"Auswirkung von Paketskollisionen auf Verkehrssicherheitsanwendungen in der Fahrzeug-Fahrzeug-Kommunikation"</i>